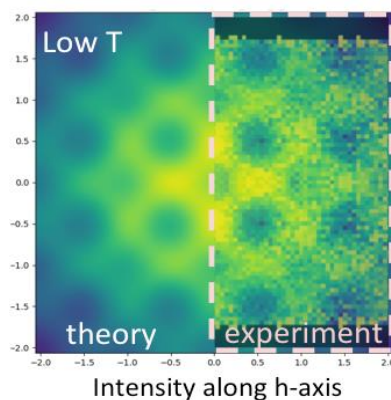
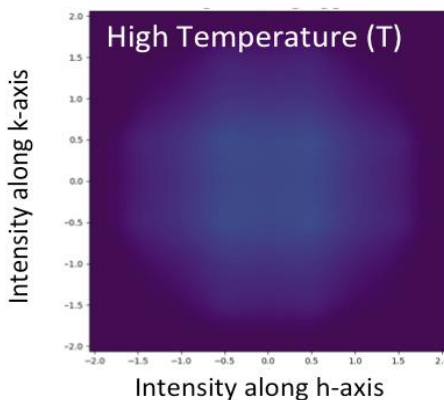
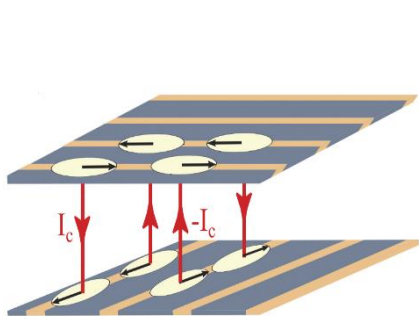
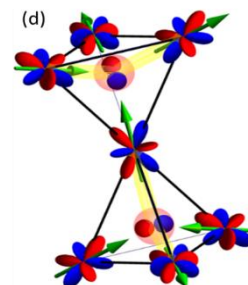
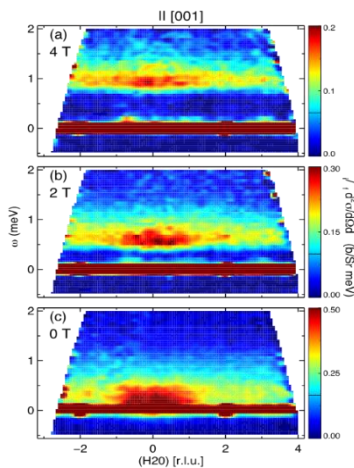
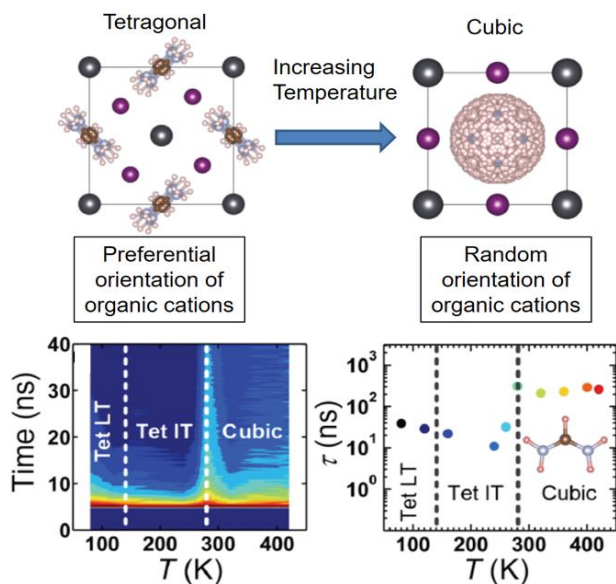


Neutron Scattering Principal Investigators' Meeting

July 1–3, 2019

Gaithersburg Marriott Washingtonian Center
Gaithersburg, Maryland



Office of Basic Energy Sciences
Division of Materials Sciences and Engineering



U.S. DEPARTMENT OF
ENERGY

Office of
Science

On the Cover

Top Left: Atomic structure of organic-inorganic perovskite was determined by neutron and x-ray diffraction. A tetragonal structure (top left) transitions to a cubic structure (top right) upon heating. Black and purple spheres represent lead and iodine atoms, respectively. Also shown in the top figures are the positively charged organic molecules (cations) with different rotational degrees of freedom (preferential or random) derived from first principles calculations. The cations in the cubic structure have more rotational freedom than in the tetragonal structure. Photoluminescence measurements (bottom left) and lifetimes (bottom right) as a function of temperature and structure are shown. The higher lifetime (τ) of the photo-excited charge carriers in the cubic phase correlates well with the higher rotational freedom (random orientation) available for the cations. *Image courtesy of Seunghun Lee, University of Virginia.*

Top Right: An elusive state of matter called a “quantum spin liquid” may actually be enhanced rather than suppressed by disorder. In $\text{Pr}_2\text{Zr}_2\text{O}_7$, rare earth ions with magnetic moments (green arrows in right image) occupy a lattice of corner-sharing tetrahedra. While the crystalline lattice frustrates conventional magnetism, weak disorder apparently promotes the rare spin liquid state. This is indicated by neutron scattering data (left) acquired near the absolute zero temperature. The signature of a “quantum spin liquid” is the persistence of intensity for $\omega > 0$ at low temperature. The variation in intensity with increasing magnetic field (bottom to top) indicates weak disorder can prevent spin freezing and preserve a spin liquid. *Image courtesy of Collin Broholm, Johns Hopkins University.*

Bottom Left: Scientists discovered hidden superconducting flow of electrons in a layered copper-oxide material. Copper-oxide compounds can exhibit superconductivity at higher temperatures than traditional superconductors. One particular copper-oxide material is known to have striped phases (regions with different electronic properties, colored with light orange above). It was hypothesized that a 90-degree rotation of the stripes between the adjacent atomic layers causes a suppression of the bulk superconductivity to low temperature. What has not been categorically demonstrated until now is whether electrons can be manipulated to tunnel coherently between the adjacent layers at higher temperatures. The present study, for the first time, demonstrates that such tunneling can indeed be induced. In the schematic, the black arrows correspond to a superconducting state confined within the striped regions. Electrons from neighboring stripes can tunnel along the directions shown in the red arrows, but the currents tend to cancel out. By driving the electrons with high-intensity light, a high-frequency reflected signal has been detected, characteristic of 3-D superconductivity that is otherwise hidden. *Image courtesy of Srivats Rajasekaran, Max Planck Institute, Hamburg.*

Bottom Right: Scientists validated decades-old prediction of a crossover from random (left) to coherent (right) electronic excitations upon cooling a single crystal of a cerium palladium compound. This remarkable achievement was only possible with advances in both neutron scattering tools and theory. Image on the left shows the theoretical intensity at higher temperature where the electron excitations are random (dark blue). The image on the right with highs and lows in intensity (yellow to blue) corresponds to low temperature. The theoretical (left half) and inelastic neutron scattering data (right half) are overlaid for quantitative comparison. The strong variation in intensity at low temperature is due to the emergence of a coherent wave-like behavior of electronic excitations. *Image courtesy of Argonne National Laboratory.*

This document was produced under contract number DE-SC0014664 between the U.S. Department of Energy and Oak Ridge Associated Universities.

The research grants and contracts described in this document are supported by the U.S. DOE Office of Science, Office of Basic Energy Sciences, Materials Sciences and Engineering Division.

Foreword

This volume comprises the scientific content of the 2019 Neutron Scattering Principal Investigators' (PI) Meeting sponsored by the Division of Materials Sciences and Engineering (MSED) in the Office of Basic Energy Sciences (BES) of the U.S. Department of Energy (DOE). This meeting on July 1–3, 2019, Gaithersburg Marriott Washingtonian Center, Gaithersburg, Maryland, is the sixth in the series, covering the projects funded by the Neutron Scattering Program. BES MSED has a long tradition of supporting a comprehensive neutron scattering program in recognition of the high impact neutron scattering and spectroscopy tools have in discovery and use-inspired research.

The MSED Neutron Scattering Core Research Activity (CRA) supports basic research on the fundamental interactions of neutrons with matter to achieve an understanding of the atomic, electronic, and magnetic structures and excitations of materials and their relationship to materials' properties. Major emphasis is on the application of neutron scattering and spectroscopy for materials research, primarily at BES-supported user facilities. Development of next-generation instrumentation concepts, innovative optics for time-of-flight instruments and application of polarized neutrons are distinct aspects of this activity. The increasing complexity of DOE mission-relevant materials for various energy applications requires sophisticated scattering and computational tools to investigate the structure and dynamics at relevant length and time scales. Additionally, neutrons allow access to the behavior of matter in extreme environments such as high temperature, pressure and magnetic field. A continuing theme of this program is the integration of material synthesis, neutron scattering measurements and computational modeling as this is vital to obtain controlled samples for experiments and modeling for an in-depth understanding of the structure and dynamics of materials and their relationship to macroscopic properties.

The purpose of the BES biennial principal investigators' meetings is to bring together all of the researchers funded by the Neutron Scattering Program at BES-MSED on a periodic basis to facilitate the discussion of new results and research highlights by PIs, to nucleate new ideas and collaborations among participants, and to identify new research opportunities. The meetings also serve MSED to assess the state of the program, to chart new research directions and to identify programmatic needs.

We thank all the meeting participants for their active contributions in sharing their ideas and research accomplishments. We wish to thank Teresa Crockett in MSED and Linda Severs at the Oak Ridge Institute for Science and Education (ORISE) for their outstanding work in all aspects of the meeting organization.

Thiyaga P. Thiyagarajan
MSED, BES, Office of Science
U.S. Department of Energy

Table of Contents

Agenda	ix
Poster List	xv
 Oral Abstracts	
Elucidation and Modulation of Ligand-Driven Segregation in Multicomponent Hybrid Particles for Dynamic Assembly of Nanostructures <i>Michael R. Bockstaller, Krzysztof Matyjaszewski, and Alamgir Karim</i>	3
Institute for Quantum Matter <i>C. Broholm, N. P. Armitage, R. J. Cava, N. Drichko, S. M. Koohpayeh, Yi Li, T. M. McQueen, S. Nakatsuji, P. Nikolic, and O. Tchernyshyov</i>	7
Nonreciprocal Effects in Non-centrosymmetric Magnets: Neutron and Optical Studies <i>S.-W. Cheong, V. Kiryukhin, and A. Sirenko</i>	18
Understanding Quantum Matter Beyond the Unit Cell <i>A. D. Christianson, A. F. May, D. S. Parker, and D. Mandrus</i>	25
Using Neutron as a Probe to Study Magnetic Excitations in Strongly Correlated Electron Materials <i>Pengcheng Dai</i>	30
Quasiparticle Couplings in Transport of Heat, Charge, and Spin for Novel Energy Materials <i>Olivier Delaire</i>	35
LaCNS: Building Neutron Scattering Infrastructure in Louisiana for Advanced Materials <i>J. F. DiTusa, D. Zhang, R. Jin, J. Zhang, W. A. Shelton, V. T. John, R. Kumar, Z. Q. Mao, E. Nesterov, E. W. Plummer, S. W. Rick, G. J. Schneider, D. P. Young, I. Vekhter, J.W. Sun, W. Xei, J. A. Dorman, B. Bharti, and M. Khonsari</i>	40
Equilibrium and Non-Equilibrium Vortex and Skyrmion Lattices <i>Morten R. Eskildsen</i>	51
Inelastic Neutron Scattering Studies of Phonon Thermodynamics and Thermophysical Properties of Materials <i>Brent Fultz</i>	56
University of Minnesota Center for Quantum Materials (CQM) <i>Martin Greven, Andrey Chubukov, Rafael Fernandes, Bharat Jalan, and Chris Leighton</i>	61

Understanding the Structure and Dynamics of Conjugated Polymers by Advancing Deuteration Chemistry and Neutron Scattering <i>Xiaodan Gu and Jason Azoulay</i>	68
Rheo-structural Spectroscopy: Fingerprinting the In Situ Response of Fluids to Arbitrary Flow <i>Matthew E. Helgeson</i>	73
Neutron Studies of Hybrid Excitations <i>R. P. Hermann, M. E. Manley, R. S. Fishman, and L. R. Lindsay</i>	77
Role of Organic Cations in Organic-Inorganic Perovskite Solar Cells <i>Seung-Hun Lee and Joshua Choi</i>	83
Scattering and Spectroscopic Studies of Quantum Materials <i>Young Lee, Hongchen Jiang, and Jiajia Wen</i>	86
Rational Design of Ion-Containing Nanostructured Ternary Polymer Blends <i>T. P. Lodge and F. S. Bates</i>	90
The Physics of Exotic Magnetoresistive Systems <i>Despina Louca</i>	96
Controlling Quantum Coherence in Frustrated Spin-Orbit Magnets <i>Martin Mourigal</i>	101
Measurement and Modeling of Organic Semiconductor Structure and Dynamics <i>Adam J. Moulé</i>	106
Engineered Protein Nanostructures for Advanced Functional Materials <i>Bradley D. Olsen</i>	111
Discovering Toroidal Materials with Spherical Neutron Polarimetry <i>Efrain E. Rodriguez</i>	117
Neutron and X-ray Scattering Studies of Complex Phenomena in Bulk Materials and Heterostructures of Strongly Correlated Systems <i>S. Rosenkranz, O. Chmaissem, R. Osborn, D. Phelan, and S. G. E. te Velthuis</i>	120
Study of Two-Dimensional Magnetic and Antiferromagnetic Lattice: From Fundamental Understanding to Novel Platform for Spintronics Research <i>Deepak K. Singh</i>	126
Neutron and X-Ray Studies of Spin and Charge Manipulation in Magnetic Nanostructures <i>Sunil K Sinha and Eric Fullerton</i>	130

Neutron Scattering Studies of Unconventional Superconductors <i>John M. Tranquada, Genda D. Gu, Cedomir Petrovic, and Igor A. Zaliznyak</i>	135
Orbitally Active NaMO₂ as a Platform for Novel Magnetism and Entangled Electronic States <i>Stephen D. Wilson</i>	147
Searching for the Universality of Collective Excitations in Liquids At and Away From Equilibrium <i>Yang Zhang</i>	151
 Poster Abstracts	
Investigation of Short-Range Ordering in Transition Metal Compounds by Diffuse Scattering <i>Jared M. Allred</i>	157
Characterizing Magnetic Quantum Materials by Neutron Scattering <i>Huibo Cao</i>	160
<i>In Operando</i> Neutron Diffraction Study of Phase Transitions in Si Electrode Morphologies Using a Novel Electrochemical Cell <i>K. S. Ravi Chandran</i>	167
Early Career: Flow-Through Neutron Reflectometry - An In Operando Sample Environment for Active Polymer Interface Studies <i>Steven C. DeCaluwe</i>	172
University of Minnesota Center for Quantum Materials (CQM): Superconductivity and Normal-State Transport in SrTiO₃ <i>Rafael Fernandes, Martin Greven, Bharat Jalan, and Chris Leighton</i>	176
University of Minnesota Center for Quantum Materials (CQM): Unusual Emergence of Superconductivity in Oxides <i>Martin Greven, Rafael Fernandes, Bharat Jalan, and Chris Leighton</i>	179
Long-Range Antiferromagnetic Order in an Entropy Stabilized Rocksalt Oxide <i>Raphaël P. Hermann</i>	182
Field-Induced Quantum Spin Liquid in the Kitaev-Heisenberg Model and Its Relation to Alpha-RuCl₃ <i>Hong-Chen Jiang, Yi-Fan Jiang, Thomas P. Devereaux, Chang-Yan Wang, Biao Huang, and Yuan-Ming Lu</i>	184

Novel Quantum Phenomena in Geometrically Frustrated Magnets Near the Metal-Insulator Phase Boundary <i>Xianglin Ke</i>	185
University of Minnesota Center for Quantum Materials (CQM): Oxygen-Vacancy-Based Control of Perovskite Oxides <i>C. Leighton, R. Fernandes, and M. Greven</i>	188
Phason Fast Propagation and Damping in Ferroelectric Materials <i>Michael E. Manley</i>	192
Relating Local Disorder and Short-Range Correlations to Material Properties using Single Crystal Diffuse Scattering <i>M.J. Krogstad, R. Osborn, D. Phelan, S.G.E. te Velthuis, O. Chmaissem, and S. Rosenkranz</i>	194
Exploiting Small Signatures: Quantifying Nanoscale Structure and Behavior <i>Katharine Page</i>	199
Ionic Polymers Under Dynamic Conditions: Shear and Electrical Field Response <i>Dvora Perahia</i>	206
Quantum Materials for Energy Science <i>C. Petrovic, I Zaliznyak, Genda Gu, and J. M. Tranquada</i>	210
Inelastic Neutron and X-ray Scattering Investigation of Electron-Phonon Effects in Quantum Materials <i>Dmitry Reznik</i>	214
National School on Neutron and X-ray Scattering <i>Stephan Rosenkranz, Bianca Haberl, Katharine Page, Brian H. Toby, Uta Ruett, and Michael Manley</i>	217
Non-Equilibrium Effects in Quantum Magnets <i>Kate A. Ross</i>	220
Fundamental Understanding of the Morphology and Dynamics of Bottlebrush Polymers <i>Gerald J. Schneider</i>	223
Intertwined Density Waves and Superconductivity in Cuprate High Temperature Superconductors <i>Jiajia Wen and Young Lee</i>	227
Polymer Conformations and Chain Dynamics under 1D and 2D Rigid Confinement <i>Karen I. Winey and Robert A. Riggleman</i>	228

Author Index	235
Participant List	239

AGENDA

2019 DOE/BES/MSED Neutron Scattering Program PI Meeting
Gaithersburg Marriott Washingtonian Center, Gaithersburg, MD

July 1–3, 2019

Meeting Chair: P. Thiyagarajan (Thiyaga), Office of Basic Energy Sciences, Program Manager

MONDAY, JULY 1, 2019

7:00 – 8:15 am *****Breakfast*****

8:15 – 8:45 am James Horwitz, Team Lead, DOE/BES/MSED
BES/MSED Update and Outlook

8:45 – 9:00 am P. Thiyagarajan (Thiyaga), Program Manager, Neutron Scattering
Welcome and Introductory Remarks

Session I **Chair: Eric Fullerton (University of California, San Diego)**

9:00 – 9:40 am Collin Broholm, Johns Hopkins University (*INVITED TALK*)
Institute for Quantum Matter (IQM)

9:40 – 10:10 am Pengcheng Dai, Rice University
*Using Neutron as a Probe to Study Magnetic Excitations in Strongly Correlated
Electron Materials*

10:10 – 10:35 am Martin Mourigal, Georgia Tech
Controlling Quantum Coherence in Frustrated Spin-Orbit Magnets

10:35 – 10:50 am *****Break*****

Session II **Chair: Suzanne te Velthuis (Argonne National Laboratory)**

10:50 – 11:20 am Martin Greven, University of Minnesota
University of Minnesota Center for Quantum Materials (CQM)

11:20 – 11:45 am Despina Louca, University of Virginia
The Physics of Exotic Magnetoresistive Systems

11:45 am – 12:15 pm Andrew Christianson, Oak Ridge National Laboratory
Understanding Quantum Matter Beyond the Unit Cell

- 12:15 pm
Session III *****Working Lunch** (Discussion on the scientific talks)*******
Chair: Karen Winey (University of Pennsylvania)
- 1:30 – 2:00 pm Timothy Lodge, University of Minnesota
Rational Design of Ion-Containing Nanostructured Ternary Polymer Blends
- 2:00 – 2:30 pm Michael Bockstaller, Carnegie Mellon University
Elucidation and Modulation of Ligand-Driven Segregation in Multicomponent Hybrid Particles for Dynamic Assembly of Nanostructures
- 2:30 – 3:00 pm John DiTusa, Louisiana State University
LaCNS: Building Neutron Scattering Infrastructure in Louisiana for Advanced Materials
- 3:00 – 3:15 pm *****Break*****
- 3:15 – 4:30 pm **Panel Discussion I**
Advanced Sample Environment and Equipment Needs for Neutron Scattering Research
Chair: Kate Ross (Colorado State University)
Panel Members: Kate Page (Oak Ridge National Laboratory),
Alamgir Karim (University of Houston), Olivier Delaire (Duke University)
- 4:30 – 5:00 pm *****Poster introductions** (2 minutes per poster): **Session I*****
- 5:00 – 6:45 pm ******* Poster Session I *******
- 6:45 pm *****Working Dinner** (Scientific Highlights of the Day: Discussion and input from attendees)*******

TUESDAY, JULY 2, 2019

- 7:00 – 8:15 am *****Breakfast*****
- Session IV** **Chair: Cedomir Petrovic (Brookhaven National Laboratory)**
- 8:15 – 8:45 am Young Lee, SLAC National Accelerator Laboratory
Scattering and Spectroscopic Studies of Quantum Materials
- 8:45 – 9:10 am Brent Fultz, Caltech
Inelastic Neutron Scattering Studies of Phonon Thermodynamics and Thermophysical Properties of Materials
- 9:10 – 9:35 am Olivier Delaire, Duke University
Quasiparticle Couplings in Transport of Heat, Charge, and Spin for Novel Energy Materials

9:35 – 10:05 am Sang Cheong, Rutgers University
Nonreciprocal Effects in Non-centrosymmetric Magnets: Neutron and Optical Studies

10:05 – 10:20 am *****Break*****

Session V Chair: Valery Kiryukhin (Rutgers University)

10:20 – 10:50 am Stephan Rosenkranz, Argonne National Laboratory
Neutron and X-ray Scattering Studies of Complex Phenomena in Bulk Materials and Heterostructures of Strongly Correlated Systems

10:50 – 11:15 am Yang Zhang, University of Illinois
Searching for the Universality of Collective Excitations in Liquids at and Away from Equilibrium

11:15 – 11:45 am Raphael Hermann, Oak Ridge National laboratory
Neutron Studies of Hybrid Excitations

11:45 am -12:15 pm Seunghun Lee, University of Virginia
Role of Organic Cations in Organic-Inorganic Perovskite Solar Cells

12:15 pm *****Working Lunch** (Discussion on the scientific talks)***

Session VI Chair: Frank Bates (University of Minnesota)

1:20 – 1:45 pm Adam Moule, University of California Davis
Measurement and Modeling of Molecular Dopant Structure and Dynamics

1:45 – 2:10 pm Matthew E. Helgeson, University of California Santa Barbara
Rheo-structural Spectroscopy: Fingerprinting the In Situ Response of Fluids to Arbitrary Flow

2:10 – 2:35 pm Bradley Olsen, MIT
Engineered Protein Nanostructures for Advanced Functional Materials

2:35 – 2:50 pm *****Break*****

Session VII Chair: Michael Manley (Oak Ridge National Laboratory)

2:50 – 3:20 pm John Tranquada, Brookhaven National Laboratory
Neutron Scattering Studies of Unconventional Superconductors

- 3:20 – 3:50 pm Sunil Sinha, University of California San Diego
Neutron and X-Ray Studies of Spin and Charge Manipulation in Magnetic Nanostructures
- 3:50 – 4:15 pm Stephen Wilson, University of California Santa Barbara
Orbitally Active NaMO₂ as a Platform for Novel Magnetism and Entangled Electronic States
- Panel Discussion II**
- 4:15 – 5:15 pm **Machine Learning & Data Science Approaches for Neutron Scattering Research**
Chair: Yang Zhang (UIUC)
Panel Members: Adam Moule (UC Davis), Matthew Helgeson (UCSB), Hong-Chen Jiang (SLAC), Andrew May (ORNL)
- 5:15 – 5:45 pm *****Poster introductions (2 minutes per poster): Session II*****
- 5:45 – 7:15 pm ******* Poster Session II *******
- 7:15 pm *****Working Dinner** (Scientific Highlights of the Day: Discussion and input from attendees)***

WEDNESDAY, JULY 3, 2019

- 7:00 – 8:15 am *****Breakfast*****
- 8:15 – 9:00 am **Chairs report on the results from the 2 Panel Discussions**
- Session VIII** **Chair: Chris Leighton (University of Minnesota)**
- 9:00 – 9:25 am Morten Eskildsen, University of Notre Dame
Equilibrium and Non-Equilibrium Vortex and Skyrmion Lattices
- 9:25 – 9:50 am Deepak Singh, University of Missouri
Study of Two-Dimensional Magnetic and Antiferromagnetic Lattice: From Fundamental Understanding to Novel Platform for Spintronics Research
- 9:50 – 10:05 am *****Break*****
- 10:05 – 10:30 am Efrain Rodriguez, University of Maryland
Discovering Toroidal Materials with Spherical Neutron Polarimetry

- 10:30 – 10:55 am Xiaodan Gu, The University of Southern Mississippi
*Understanding the Structure and Dynamics of Conjugated Polymers by
Advancing Deuteration Chemistry and Neutron Scattering*
- 10:55 – 11:15 am P. Thiyagarajan (Thiyaga), Program Manager, NS/BES
Discussions and Concluding Remarks
- 11:15 am ***** Adjourn *****

**2019 DOE/BES/MSED Neutron Scattering
PI Meeting**

LIST OF POSTER PRESENTATIONS
ODD numbers on July 1 and EVEN numbers on July 2, 2019

Number	PI Name	Institution	Title
1	Ray Osborn	Argonne National Laboratory	Relating local disorder and short-range correlations to materials properties using single crystal diffuse scattering
2	Suzanne te Velthuis	Argonne National Laboratory	Neutron and x-ray scattering studies of complex phenomena in heterostructures
3	Huibo Cao	Oak Ridge National Laboratory	Characterizing magnetic quantum materials by neutron scattering
4	Andrew May	Oak Ridge National Laboratory	Understanding quantum matter beyond the unit cell
5	K.S. Ravi Chandran	University of Utah	In operando neutron diffraction study of phase transitions in Si electrode morphologies using a novel electrochemical cell
6	Chris Leighton	University of Minnesota	University of Minnesota Center for Quantum Materials (CQM): Oxygen-vacancy-based control of perovskite oxides
7	Rafael Fernandes	University of Minnesota	University of Minnesota Center for Quantum Materials (CQM): Superconductivity and normal-state transport in SrTiO ₃
8	Katherine Page	Oak Ridge National Laboratory	Exploiting small signatures: Quantifying nanoscale structure and behavior
9	Igor Zaliznyak	Brookhaven National Laboratory	Neutron scattering studies of unconventional superconductors
10	Dan Phelan	Argonne National Laboratory	Neutron and x-ray scattering studies of complex phenomena in bulk compounds
11	Gerald Schneider	Louisiana State University	Fundamental understanding of the morphology and dynamics of bottlebrush polymers
12	Martin Greven	University of Minnesota	University of Minnesota Center for Quantum Materials (CQM): Unusual emergence of superconductivity in oxides
13	Dmitry Reznik	University of Colorado, Boulder	Inelastic neutron and x-ray scattering investigation of electron-phonon effects in quantum materials
14	Stephan Rosenkranz	Argonne National Laboratory	National School on Neutron and X-ray Scattering
15	Michael Manley	Oak Ridge National Laboratory	Phason fast propagation and damping in ferroelectric materials

16	Dvora Perahia	Clemson University	Ionic polymers under dynamic conditions: Shear and electrical field response
17	Cedomir Petrovic	Brookhaven National Laboratory	Quantum materials for energy science
18	Raphael Hermann	Oak Ridge National Laboratory	Long-range antiferromagnetic order in an entropy stabilized rocksalt oxide
19	Kate Ross	Colorado State University	Nonequilibrium effects in quantum magnets
20	Jiajia Wen	SLAC National Laboratory	Intertwined density waves and superconductivity in cuprate high temperature superconductors
21	Hong-Chen Jiang	SLAC National Laboratory	Field-induced quantum spin liquid in the Kitaev-Heisenberg model and its relation to α - RuCl_3
22	Xianglin Ke	Michigan State University	Novel quantum phenomena in geometrically frustrated magnets near the metal-insulator phase boundary
23	Jared Allred	The University of Alabama	Investigation of short-range ordering in transition metal compounds by diffuse scattering
24	Steven DeCaluwe	Colorado School of Mines	Early Career: Flow-through neutron reflectometry – An in operando sample environment for active polymer interface studies
25	Karen Winey	University of Pennsylvania	Polymer conformations and chain dynamics under 1D and 2D rigid confinement
26	Seungun Lee	University of Virginia	Structure, dynamics and photoluminescence of a two-dimensional photovoltaic perovskite
27	John DiTusa	Louisiana State University	LaCNS: Building neutron scattering infrastructure in Louisiana for advanced materials
28	Sang Cheong	Rutgers University	Non-reciprocal effects in non- centrosymmetric magnets: Neutron and optical studies
29	Sunil Sinha	University of California San Diego	Structure and dynamics of frustrated spin systems

***Oral
Abstracts***

Elucidation and Modulation of Ligand-Driven Segregation in Multicomponent Hybrid Particles for Dynamic Assembly of Nanostructures

Michael. R. Bockstaller, Department of Materials Science and Engineering, Carnegie Mellon University, 5000 Forbes Ave., Pittsburgh, 15213 PA

Krzysztof Matyjaszewski, Chemistry Department, Carnegie Mellon University, 4400 Fifth Ave., Pittsburgh, PA 15213

Alamgir Karim, Department of Chemical and Biomolecular Engineering, University of Houston, 4726 Calhoun Road, Houston, TX 77204-4004

Program Scope

The unique physical properties of nanocrystalline materials with controlled size and shape have rendered inorganic nanocrystals and their assembly structures an important platform to realize technological breakthroughs in areas ranging from sustainable energy technologies to magnetic storage or medical diagnostics. However, while synthetic methodologies have significantly advanced, the processing of nanoparticles into functional material structures remains a challenge. Consider, for instance, the fabrication of multicomponent nanoparticle (thin) films in which different particle species are to be organized into uniform and micron sized domain structures that are deliberately shaped to optimize performance. The fabrication of this type of ‘microstructured multicomponent nanomaterial system’ presents a pervasive challenge in technology areas ranging from functional coatings to photovoltaics or solid-state lighting. This project builds upon recent advances in polymer and particle science that promise transformative progress in the high-throughput fabrication of micro-structured multicomponent particulate films. First, advances in surface-initiated controlled radical polymerization have extended the range of possible ligand compositions to encompass polymer chains. This enables tailoring of the interactions between particle constituents by the deliberate design of the structure and composition of polymeric ligands [1]. Second, research revealed that tuning these interactions enables the autonomous organization of multicomponent particle mixtures (in which distinct particles are tethered with different polymer types) into monotype domain structures in a process similar to phase separating polymer blends [2]. Third, topographic confinement in athermal homopolymer/particle brush blend systems has been shown to enable the entropy-driven organization of particles into deliberately shaped array structures [3].

Building on these prior advancements, it is the fundamental objective of this project to test the hypothesis that ligand-interactions and topographic constraints can be harnessed to induce segregation processes in mixed nanoparticle systems that enable the reversible organization of particles into deliberately shaped uniform domain microstructures. In particular, the proposed research will (1) elucidate the conditions for ligand-interactions to facilitate *enthalpy-driven* phase separation of mixed particle brush systems in which the particle constituents are tethered with polymers of distinct chemical composition; (2) establish the thermodynamics and kinetics of enthalpy-driven phase separation processes in binary particle brush mixtures using concurrent

electron imaging and neutron scattering analysis; (3) test the hypothesis that the connectivity between particle and polymer constituents gives rise to an anomalous growth behavior that eventually transforms into regular diffusion-controlled growth; (4) evaluate the role of pattern-induced confinement and interactions on the *entropy-driven* particle segregation in binary blends of brush particles that exhibit tethers of distinct characteristic size; and (5) demonstrate the reversible organization of particles into deliberately shaped monotype domain structures by using confinement-induced segregation in binary asymmetric particle brush LCST blend systems near the critical temperature. Small and ultra-small angle neutron scattering (SANS/USANS) experiments are proposed to elucidate the mechanism and kinetics of the phase separation process of particle brush blend systems as a systematic function of brush architecture and quench depth. To enable neutron scattering analysis, brush particle blend systems are designed such that polymer tethers are matched to the distinct respective particle cores. This approach should enable the analysis of early-state phase separation through neutron scattering techniques that would otherwise be impractical due to the scattering of particle cores.

Recent Progress

At Carnegie Mellon University, the emphasis during the first year of project performance was on the development of synthetic routes towards contrast-matched poly(methyl methacrylate) (PMMA) and poly(styrene-*r*-acrylonitrile) (PSAN) tethered silica particles and the development of synthetic routes towards organosilica particles with distinct SLD. Experiments at the University of Houston were focused on the elucidation of the influence of spatial confinement on the properties of brush particles and the development of a process methodology (Direct Immersion Annealing, DIA) that enables the order-of-magnitude speed-up of phase separation processes in particle brush blends.

To avoid ‘parasitic’ scattering from particle cores, partially deuterated polymers are to be used such as to minimize SLD contrast between a particle core and its tethers. Different brush particles will be designed with distinct respective SLD so that scattering will arise in mixtures of distinct brush particle systems. Because phase separation requires the heating of brush particle blends to temperatures above the LCST (approx. 150 deg C for PMMA/PSAN tethered systems) brush materials are required to remain stable upto annealing temperatures. The constraint of thermal stability limits the choice of core compositions to silica chemistries. Thus an important objective during the first year has been to develop synthetic routes towards silica particles with different SLD. A more versatile approach was found to be the synthesis of *organosilica* particles which are formed by condensation of organic-modified tri-alkoxysilane. By variation of the Deuterium content of the *organo* moiety, the SLD of particles can be varied by substantial amounts. Furthermore, suitable choice of the organic functionality allows the preparation of smaller particle sizes (within the range of 2-5 nm) that exhibit superior diffusion kinetics and are thus

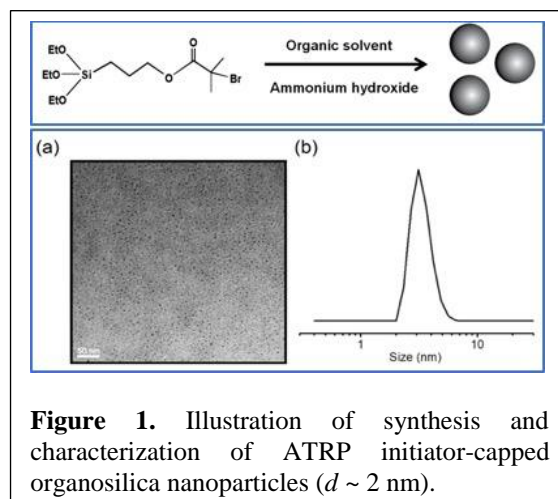


Figure 1. Illustration of synthesis and characterization of ATRP initiator-capped organosilica nanoparticles ($d \sim 2$ nm).

more conducive to in-situ annealing/scattering experiments. The approach is illustrated in Figure 1.

One important challenge in designing brush particle systems with tethers that are SLD matched to the core is that the SLD of the particle core is unknown. This is because the density of silica (and other nanoparticle compositions) is sensitive to the synthetic process and varies significantly from the corresponding bulk value of materials. For example, in the case of silica nanoparticles, densities in the range of 1.7 to 2.4 g/cm³ have been reported depending on the process that was used. To overcome this challenge, we propose to infer the particle density from the respective SLD that is determined via neutron transmission experiments. In a first step, SANS experiments on particle brush films (in which the SLD of tethers is systematically varied via controlled deuteration) are performed to determine ligand compositions that give rise to least scattering. Since the density of polymer ligands in the solid state can be assumed to correspond to the bulk density, this ‘minimum scattering condition’ allows determination of the SLD of the particle core. From the SLD of the particle core, the mass density can be calculated since the elemental composition is known. The process will be illustrated below. For commercial silica particles used in our study, a mass density of 1.78 g/cm³ was determined using this methodology, in excellent agreement with literature values. Representative SANS spectra and the determination of minimum contrast condition for the various film samples are shown in Figure 2.

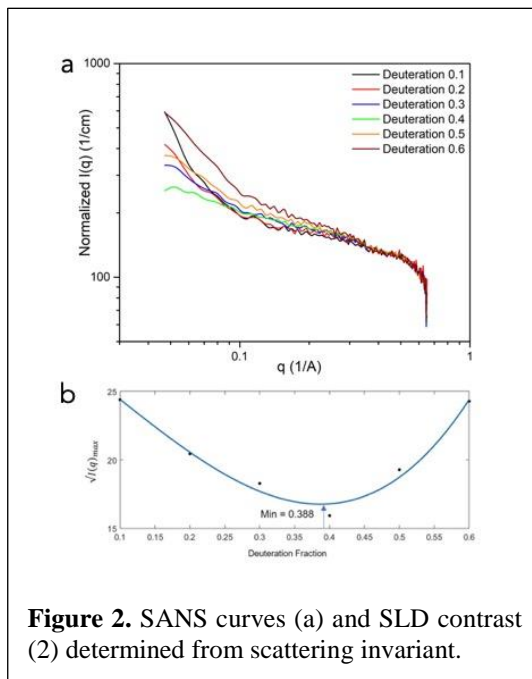


Figure 2. SANS curves (a) and SLD contrast (2) determined from scattering invariant.

Concurrent to the synthesis of brush particle systems, the relaxation behavior of topographically patterned particle brush/polymer blends was evaluated to assess the stability of topographically patterned films during film annealing conditions. Understanding the relaxation behavior of brush particle films is a prerequisite for the proposed application of topographic confinement to induce segregation in brush particle blends. The broader technological motivation for these experiments is that polymer films provide a versatile platform in which complex functional relief patterns can be thermally imprinted with a resolution down to few nanometers. However, a

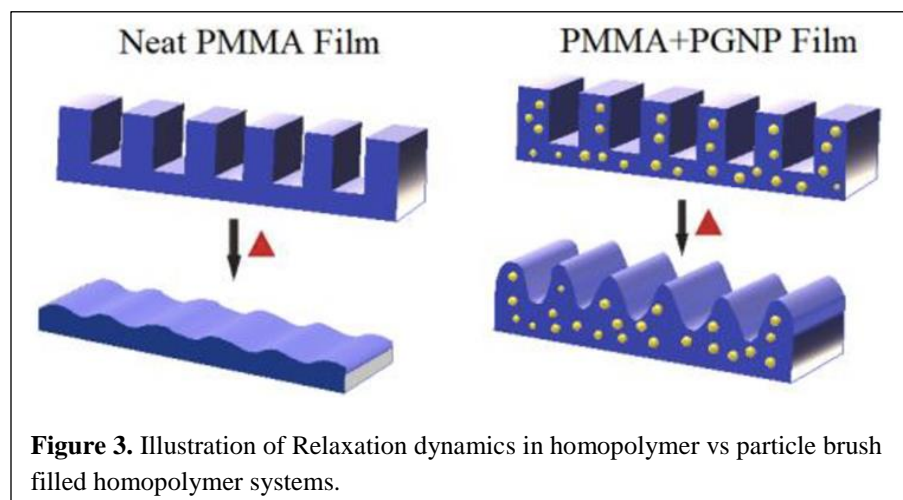


Figure 3. Illustration of Relaxation dynamics in homopolymer vs particle brush filled homopolymer systems.

practical limitation of this method is the tendency for the imprinted patterns to relax (“slump”), leading to loss of pattern fidelity over time. While increasing the temperature above glass transition temperature (T_g) accelerates the slumping kinetics of neat films, we found that the addition of polymer-grafted nanoparticles (PGNP) can greatly enhance the thermal stability of these patterns. Specifically, increasing the concentration of poly(methyl methacrylate) (PMMA) grafted titanium dioxide (TiO_2) nanoparticles in the composite films did slow down film relaxation dynamics, leading to enhanced pattern stability for the tested temperature range. Figure 3 illustrates the effect of brush particle addition to the relaxation behavior of patterned polymer thin films. Interestingly, slumping relaxation time is found to obey an entropy–enthalpy compensation (EEC) relationship with varying PGNP concentration, similar to recently observed relaxation of strain-induced wrinkling in glassy polymer films having variable film thickness. The compensation temperature, T_{comp} was found to be in the vicinity of the bulk T_g of PMMA. Our results suggest a common origin of EEC relaxation in patterned polymer thin films and nanocomposites.

Future Plans

Next steps will entail (a) the characterization of SLD and density of organosilica particles, (b) synthesis of PMMA- and PSAN tethered organosilica with appropriate degree of deuteration, (c) characterization of phase separation mechanism in blends of organosilica brush particle blends using SANS, (d) SANS/USANS/NR characterization of phase separation under DIA conditions both at NIST and Oak Ridge National Laboratory.

References

- [1] Hui, C. M.; Pietrasik, J.; Schmitt, M.; Mahoney, C.; Choi, J.; Bockstaller, M. R.; Matyjaszewski, K. Surface-initiated polymerization as an enabling tool for multifunctional (nano-) engineered hybrid materials. *Chemistry of Materials*, **2014**, *26*, 745-762.
- [2] M. Schmitt, J. Zhang, J. Lee, B. Lee, X. Ning, R. Zhang, A. Karim, R. F. Davis, K. Matyjaszewski, M. R. Bockstaller. Polymer ligand-induced autonomous sorting and reversible phase separation in binary particle blends. *Sci. Adv.*, **2016**, *2*, e1601484.
- [3] R. Zhang, B. Lee, C. M. Stafford, J. F. Douglas, A. V. Dobrynin, M. R. Bockstaller, A. Karim. Entropy-driven segregation of polymer-grafted nanoparticles under confinement. *PNAS*, **2017**, *114*, 2462-2467.

Publications

1. Bhadauriya, S., Wang, X., Pitliya, P., Zhang, J., Raghavan, D., Bockstaller, M., Stafford, C., Douglas, J., Karim, A. Tuning the Relaxation of Nano-Patterned Polymer Films with Polymer-Grafted Nanoparticles: Observation of Entropy-Enthalpy Compensation, *Nano Letters*, **2018**, *18* (12), 7441–7447.
2. Bongjoon Lee, Markus Bleuel, Adrian Zhao, David Ott, Ilhem F. Hakem, and Michael R. Bockstaller Kinetics and Energetics of Solute Segregation in Granular Block Copolymer Microstructures. *Macromolecules* **2018**, *51*, 10285–10296.

Institute for Quantum Matter

C. Broholm^{1,2,3,6}, N.P. Armitage¹, R.J. Cava⁴, N. Drichko¹, S. M. Koohpayeh¹, Yi Li¹, T.M. McQueen^{1,5,6}, S. Nakatsuji^{7,1}, P. Nikolic^{8,1}, and O. Tchernyshyov¹

¹Department of Physics and Astronomy, Johns Hopkins University, Baltimore, MD 21218

²NIST Center for Neutron Research, NIST, Gaithersburg, MD 20899

³Quantum Condensed Matter Division, ORNL, Oak Ridge, TN 37831

⁴Department of Chemistry, Princeton University, Princeton, NJ 08544

⁵Department of Chemistry, Johns Hopkins University, Baltimore, MD 21218

⁶Dept. of Materials Science & Engineering, Johns Hopkins University, Baltimore, MD 21218

⁷Institute for Solid State Physics, University of Tokyo, Kashiwa 277-8581, Japan

⁸School of Physics, Astronomy and Computational Sciences, George Mason University, Fairfax, Virginia 22030, USA

Program Scope

The Institute for Quantum Matter is a team of scientists spanning the materials by design triad of synthesis, characterization, and theory, to create, probe, and understand new forms of quantum matter with the potential for transformative impacts in energy and information technologies. Rather than having phase transitions and static magnetic order parameters, IQM explores materials where quantum fluctuations prevail and electronic topology impacts physical properties.

Recent Progress

Referring the reader to the IQM publication list for additional results and details (below and at <https://iqm.jhu.edu/publications/papers/>), here we present a synopsis of scientific progress at the Institute for Quantum Matter achieved since the last MSED meeting in December 2016.

The quest for a quantum spin liquid: New materials with the potential to exhibit spin liquid physics were discovered. These include a family of trimer-based materials [9,33] exemplified by $\text{Ba}_4\text{NbRu}_3\text{O}_{12}$ based on triangular planes of elongated Ru_3O_{12} trimers oriented perpendicular to the plane. Despite a Curie-Weiss temperature of -155 K, there is no conventional magnetic ordering, only two broad maxima in the specific heat (9 K and 45 K). An anomaly in the DC susceptibility at 4 K indicates spin freezing.

In three dimensions, NiRh_2O_4 realizes the spin-1 model on a diamond lattice [34]. Despite dominant antiferromagnetic interactions with $Q_{\text{CW}} = -11.3(7)\text{K}$, no phase transition to long-range magnetic order is observed by specific heat measurements down to $T = 0.1\text{ K}$. The material thus is a candidate to realize a theoretically predicted quantum spin liquid and topological paramagnet phases.

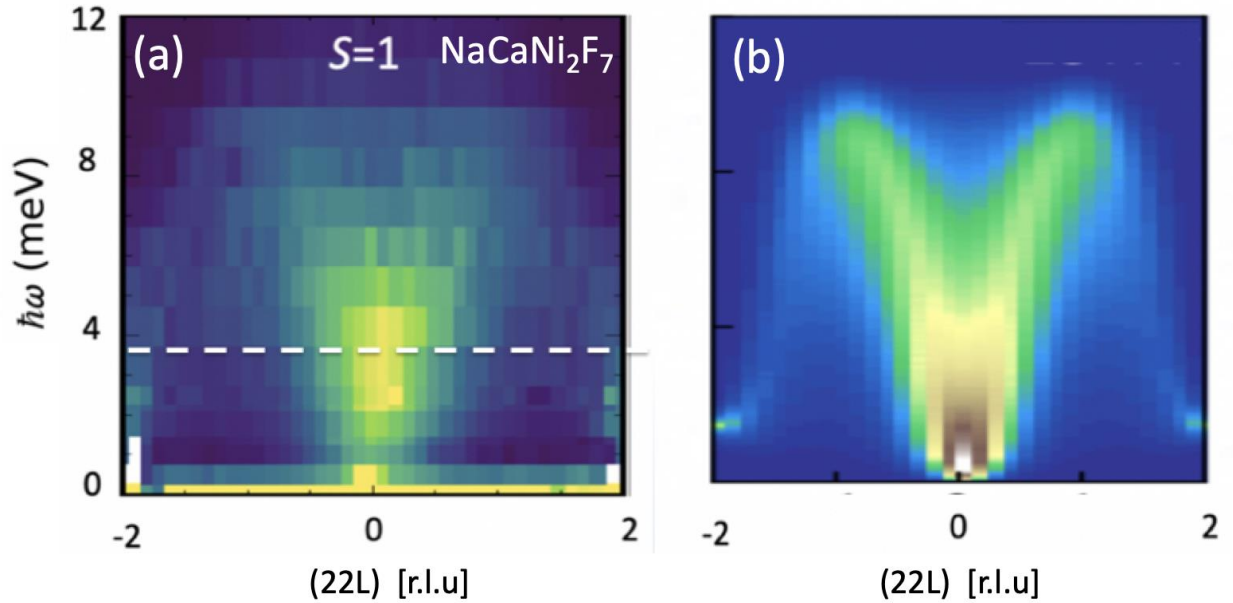


Figure 1. (a) Magnetic neutron scattering cross section measured for the Heisenberg pyrochlore antiferromagnet NaCaNi₂F₇ showing a broad continuum with a finite energy maximum (dashed line) in the intensity at an energy that corresponds to the nearest neighbor antiferromagnetic exchange constant [13]. (b) Classical spin wave calculation of magnetic excitations from a short range ordered state generated by Monte Carlo simulations. The spin Hamiltonian was that determined by measurements of the equal time spin correlation function for NaCaNi₂F₇. In contrast to the spin-1 experimental case the intensity for the classical calculation is maximum at the lowest energy [8].

A broad continuum of scattering was documented in NaCaNi₂F₇, which was shown to realize the nearest neighbor Heisenberg antiferromagnet on the pyrochlore lattice [13]. A possible explanation for the continuum was presented in the form of spin wave excitations from the highly degenerate manifold of low energy spin configurations [8]. A pseudo-gap in the experimental excitation spectrum with a characteristic energy similar to the nearest neighbor exchange constant is however, not reproduced in spin wave theory nor is it present for the isotropic spin-5/2 system NaCaMn₂F₇ [65]. This admits the intriguing possibility that the pseudo-gap arises from quantum fluctuations.

The quantum magnetism of highly anisotropic rare-earth based pyrochlore systems with ferromagnetic interactions was examined in Yb₂Ti₂O₇ and Pr₂Zr₂O₇. A novel travelling solvent floating zone method was used to create the first single crystals of Yb₂Ti₂O₇ with a sharp peak in the specific heat at the phase transition to ferromagnetic ordering [59]. A detailed specific heat and neutron scattering study revealed a reentrant phase diagram for fields applied along the three-fold axis, that is not accounted for by classical Monte Carlo simulations [47]. For Pr₂Zr₂O₇, which is a non-Kramers quantum spin ice candidate, we found evidence that a random transverse field with complex structural origin [30] may help to induce a spin-liquid-like state [64].

Raman scattering and heat capacity measurements were used to obtain evidence for emergent charge degrees of freedom and a quantum electrical dipole liquid in a molecule-based Mott insulator κ -(BEDT-TTF)₂Hg(SCN)₂Br [28].

Exact theoretical models of spin liquids provide crucial existence proofs and insights that motivate the ongoing search for experimental model systems. At IQM an exactly solvable 2D model of a quantum spin liquid with Abelian anyons was presented and analyzed. It consists of spins 1/2 on a triangular lattice with a six-body interaction. The model has four bosons and three fermions and a topological degeneracy of 64 on a torus. Elementary excitations are boson-fermion pairs that come in 12 distinct flavors [61].

Topology and Interactions: SmB₆ continues to attract attention as a compound where topology and strong electronic correlations produce unique electronic properties. IQM provided evidence for a Kondo-like screening of defect-induced local moments both through thermomagnetic [35] and circular magnetic dichroism measurements [12]. The THz optical conductivity of SmB₆ was shown to possess distinct regimes of either dominant free carrier or localized response contributions [27]. Raman spectroscopy was used to demonstrate that the hybridization gap in SmB₆ is very sensitive to Sm vacancies. For Sm deficiency above 1% the gap fills in with impurity states and low temperature heat capacity is greatly enhanced.

In a Weyl semimetal, the non-trivial Berry phase near a node yields a magnetic monopole in k space so the phase of a Cooper-pair wavefunction $\Delta(\mathbf{k})$ is no longer globally defined. This implies that a superconducting gap, if present, must be classified in terms of monopole harmonic functions rather than spherical harmonics. This never-before-realized, and topological, superconducting state is denoted a “monopole” superconductor [40]. A concrete approach to design, synthesize, and characterize materials that harbor this new state of matter has been developed. A number of material candidates have been identified, and specific experiments using microwaves, Raman, and neutron scattering to detect this unique state of matter are proposed. The pursuit of topological superconductivity in general and monopole superconductivity in particular is now one of the four thrusts of the IQM-EFRC (see below).

A simple model of a domain wall in a thin-film ferromagnet was derived. A domain wall is represented as a nonreciprocal string, on which transverse waves propagate with different speeds in opposite directions. The model has three parameters: mass density, tension, and a gyroscopic constant quantifying the nonreciprocity. The unusual dynamics of a nonreciprocal string in finite geometry was discussed. It agrees well with numerically simulated motion of a ferromagnetic domain wall in a strip of constant width.

A comprehensive review of Weyl and Dirac semimetals in three-dimensional solids was coauthored by IQM PI Peter Armitage, with E. J. Mele, and A. Vishwanath [42]. The paper provides the scientific background for the axion insulator and the topological magnetism thrusts of the IQM-EFRC (see below).

Future Plans

IQM began the transition to become an Energy Frontier Research Center (EFRC) in the fall of 2018. We have defined four specific quantum states of matter that we seek to realize and explore with an eye towards applications in energy and information technologies:

The Quantum Spin Liquid: By combining chemistry with physical insight, IQM seeks to form an extreme quantum mechanical version of a magnet: The quantum spin liquid supports exotic emergent quasi-particles that could form the basis for quantum computing.

The Axion Insulator: IQM seeks to form an “axion insulator” that responds magnetically to an electric field and electrically to a magnetic field within a quantum material. The strength of this effect is expected to be large and quantized. The axion insulator could become a unique new component in the engineering toolbox.

Topological Magnetism: Magnetism can qualitatively change the geometrical (topological) character of the electronic wave function of electrons that conduct electricity in solids. Such topological magnets exhibit exotic electronic transport properties and unique sensitivity to magnetic fields. The anomalous Hall effect and related quantum transport properties in development at IQM may be utilized for energy harvesting and ultra-high-density information storage.

Topological Superconductivity: When electrons with a topologically non-trivial wave function are the basis for superconductivity, the corresponding BCS wave function is profoundly impacted. IQM seeks to realize topological superconductivity because it constitutes a fundamentally new state of matter with unique and potentially useful physical properties.

Publications

- 1 “**Spin phases of the helimagnetic insulator Cu_2OSeO_3 probed by magnon heat conduction,**” N. Prasai, A. Akopyan, B. A. Trump, G. G. Marcus, S. X. Huang, T. M. McQueen and J. L. Cohn, Phys. Rev. B. 99, 020403(R) (2019).
- 2 “**Anisotropic spin fluctuations in detwinned FeSe,**” T. Chen, Y. Chen, A. Kreisel, X. Lu, A. Schneidewind, Y. Qiu, J. T. Park, T. G. Perring, J. R. Stewart, H. Cao, R. Zhang, Yu Li, Y. Rong, Y. Wei, B. M. Andersen, P. J. Hirschfeld, C. Broholm and P. Dai, Nature Materials, 10.1038 (2019).
- 3 “**Magnetic interactions and spin dynamics in the bond-disordered pyrochlore fluoride $\text{NaCaCo}_2\text{F}_7$,**” J. Zeisner, S. A. Bräuninger, L. Opherden, R. Sarkar, D. I. Gorbunov, J. W. Krizan, T. Herrmannsdörfer, R. J. Cava, J. Wosnitza, B. Büchner, H.-H. Klauss, and V. Kataev, Phys. Rev. B 99, 155104, (2019).

- 4 **“Resonating quantum three-coloring wave functions for the kagome quantum antiferromagnet,”** H.J. Changlani, S. Pujari, Chia-Min Chung, and B.K. Clark, Phys. Rev. B **99**, 104433, (2019).
- 5 **“Crystal growth, crystal structure and anisotropic magnetic properties of $\text{KBaR}(\text{BO}_3)_2$ ($R = \text{Y, Gd, Tb, Dy, Ho, Tm, Yb}$ and Lu) triangular lattice materials,”** S. Guo, T. Kong, F. Alex Cevallos, K. Stolze, and R.J.Cava, Journal of Magnetism and Magnetic Materials, **476**, Pages 104-110, (2019).
- 6 **“Locating the Missing Superconducting Electrons in the Overdoped Cuprates $\text{La}_{2-x}\text{Sr}_x\text{CuO}_4$,”** F. Mahmood, X. He, I. Božović, and N. P. Armitage, Phys. Rev. Lett. **122**, 027003, (2019).
- 7 **“A spin glass state in $\text{Ba}_3\text{TiRu}_2\text{O}_9$ ”** L. T. Nguyen and R.J. Cava, Journal of Magnetism and Magnetic Materials, **476**, Pages 334-336, (2019).
- 8 **“Dynamical Structure Factor of the Three-Dimensional Quantum Spin Liquid Candidate $\text{NaCaNi}_2\text{F}_7$,”** S. Zhang, H. J. Changlani, K. W. Plumb, O. Tchernyshyov, and R. Moessner, Phys. Rev. Lett. **122**, 167203, (2019).
- 9 **“Trimers of MnO_6 octahedra and ferrimagnetism of $\text{Ba}_4\text{NbMn}_3\text{O}_{12}$,”** L. T. Nguyen, T. Kong, and R. J. Cava, Materials Research Express, **6** (5), (2019).
- 10 **“Magnetic Excitations of the Classical Spin Liquid MgCr_2O_4 ,”** X. Bai, J. A. M. Paddison, E. Kapit, S. M. Koohpayeh, J.-J. Wen, S. E. Dutton, A. T. Savici, A. I. Kolesnikov, G. E. Granroth, C. L. Broholm, J. T. Chalker, and M. Mourigal, Phys. Rev. Lett. **122**, 097201, (2019).
- 11 **“From two-dimensional spin vortex crystal to three-dimensional Neel order in the Mott insulator $\text{Sr}_2\text{F}_2(\text{Fe}_{1-x}\text{Mn}_x)(2)\text{OS}_2$,”** Bayliff, K. W., Wu, S., Loganathan, V., Zhao, L. L., Wang, J. K., Nevidomskyy, A. H., Broholm, C., Huang, C-L, Morosan, E., Phys. Rev. B. **99** (2), 024412 (2019).
- 12 **“Magnetic dichroism in the Kondo insulator SmB_6 ,”** Fuhrman, W. T., Leiner, J. C., Freeland, J. W., van Veenendaal, M., Koohpayeh, S. M. Phelan, W. A., McQueen, T. M., Broholm, C., Phys. Rev. B. **99** (2), 020401 (2019).
- 13 **“Continuum of quantum fluctuations in a three-dimensional $S=1$ Heisenberg magnet,”** W. Plumb, H. J. Changlani, A. Scheie, S. Zhang, J.W. Krizan, J. A. Rodriguez-Rivera, Y. Qiu, B. Winn, R. J. Cava, C. L. Broholm, Nature Physics **15** (1):54, 10.1038 (2019).

- 14 **“Comparison of the magnetic properties of $\text{Mn}_3\text{Fe}_2\text{Si}_3\text{O}_{12}$ as a crystalline garnet and as a glass,”** Cevallos, F. A., Cava, R. J., Journal of Magnetism and Magnetic Materials **469**, 510-514 (2019).
- 15 **“Field-dependent heat transport in the Kondo insulator SmB_6 : phonons scattered by magnetic impurities”**, M-E. Boulanger, F. Laliberté, M. Dion, S. Badoux, N. Doiron-Leyraud, W. A. Phelan, S. M. Koohpayeh, W. T. Fuhrman, J. R. Chamorro, T. M. McQueen, X. F. Wang, Y. Nakajima, T. Metz, J. Paglione, and L. Taillefer, Phys. Rev. B **97**, 245141 (2018).
- 16 **“Magnetic properties of lithium-containing rare earth garnets $\text{Li}_3\text{RE}_3\text{Te}_2\text{O}_{12}$ (RE = Y, Pr, Nd, Sm-Lu),”** Cevallos, F. A., Guo, S., Cava, R. J., Materials Research Express, **5** (12), 126106 (2018).
- 17 **“Scaling and data collapse from local moments in frustrated disordered quantum spin systems,”** Kimchi, I., Sheckelton, J.P., McQueen, T. M., and Lee, Patrick A., Nature Communications **9**, 4367 (2018).
- 18 **“ μSR study of spin freezing and persistent spin dynamics in $\text{NaCaNi}_2\text{F}_7$,”** Cai, Y., Wilson, M. N., Hallas, A. M., Liu, L., Frandsen, B. A., Dunsiger, S. R., Krizan, J. W., Cava, R. J., Rubel, O., Uemura, Y. J., and Luke, G. M., Journal of Physics-Condensed Matter **30** (38), 385802 (2018).
- 19 **“Energy-momentum tensor of a ferromagnet,”** S. Dasgupta and O. Tchernyshyov, Phys. Rev. B, **98**, 224401 (2018).
- 20 **“Exact results on itinerant ferromagnetism and the 15-puzzle problem,”** E. Bobrow, K. Stubis, Y. Li, Phys. Rev. B, **98**, 10.1103 (2018).
- 21 **“Crystal field levels and magnetic anisotropy in the kagome compounds $\text{Nd}_3\text{Sb}_3\text{Mg}_2\text{O}_{14}$, $\text{Nd}_3\text{Sb}_3\text{Zn}_2\text{O}_{14}$, and $\text{Pr}_3\text{Sb}_3\text{Mg}_2\text{O}_{14}$,”** Scheie, A., Sanders, M., Krizan, J., Christianson, A. D., Garlea, V. O., Cava, R. J., Broholm, C., Phys. Rev. B, **98**, 134401 (2018).
- 22 **“Ferromagnetic domain wall as a nonreciprocal string,”** O. Tchernyshyov and S. Zhang, Phys. Rev. B, **98**, 104411 (2018).
- 23 **“The pyrochlore $\text{Ho}_2\text{Ti}_2\text{O}_7$: Synthesis, crystal growth, and stoichiometry,”** A. Ghasemi, A. Scheie, J. Kindervater, and S. M. Koohpayeh, Journal of Crystal Growth **500**, 38-43 (2018).
- 24 **“Hierarchy of Exchange Interactions in the Triangular-Lattice Spin-Liquid YbMgGaO_4 ,”** X. Zhang, F. Mahmood, M. Daum, Z. Dun, J. A. M. Paddison, N. J. Laurita, T. Hong, H. Zhou, N. P. Armitage, and M. Mourigal, Phys. Rev. X **8**, 031001(2018).

- 25 **“Inertial effects in systems with magnetic charge,”** N. P. Armitage, B-Condensed Matter, **536**, 10.1016, Pages 353-358 (2018).
- 26 **“An Effect of Sm Vacancies on the Hybridization Gap in Topological Kondo Insulator Candidate SmB₆,”** M.E. Valentine, S. M. Koohpayeh, W.A Phelan, T.M. McQueen, P.F.S. Rosa, Z. Fisk, and N. Drichko, , Physica B-Condensed Matter, **536**, 10.1016, Pages 60-63 (2018).
- 27 **“Impurities or a Neutral Fermi surface? A Further Examination of the Low-Energy ac Optical Conductivity of SmB₆,”** N. J. Laurita, C. M. Morris, S. M. Koohpayeh, W.A. Phelan, W. A., T. M. McQueen, and N. P. Armitage, Physica B-Condensed Matter, **536**, 10.1016, Pages 78-84 (2018).
- 28 **“Evidence for Quantum Dipole Liquid State in an Organic Quasi-Two-Dimensional Material,”** N. Hassan, S. Cunningham, M. Mourigal, E. I. Zhilyaeva, S. A. Torunova, R. N. Lyubovskaya, J. A. Schlueter, and N. Drichko, Science, **360**, 6393, pp. 1101-1104 (2018).
- 29 **“From Real Materials to Model Hamiltonians With Density Matrix Downfolding,”** H. Zheng, H. J. Changlani, K. T. Williams, B. Busemeyer, and L. K. Wagner, Frontiers in Physics (2018).
- 30 **“Universal Geometric Frustration in Pyrochlores,”** B. A. Trump, S. M. Koohpayeh, K. J. T. Livi, J. Wen, K. E. Arpino, Q. M. Ramasse, R. Brydson, M. Feygenson, H. Takeda, M. Takigawa, K. Kimura, S. Nakatsuji, C. L. Broholm, T. M. McQueen, accepted for publication in Nature Communications, 10.1038 (2018).
- 31 **“Lattice-mediated magnetic order melting in TbMnO₃,”** E. Baldini, T. Kubacka, B. P. P. Mallett, C. Ma, S. M. Koohpayeh, Y. Zhu, C. Bernhard, S. L. Johnson, and F. Carbone, Phys. Rev. B, **97**, 125149 (2018).
- 32 **“Stability of the Nagaoka-type ferromagnetic state in a t_{2g} orbital system on a cubic lattice,”** E. Bobrow and Y. Li, Phys. Rev. B, **97**, 155132 (2018).
- 33 **“A Geometrically Frustrated Trimer-Based Mott Insulator,”** L. T. Nguyen, T. Halloran, W. Xie, T. Kong, C. L. Broholm, and R. J. Cava, Phys. Rev. Materials **2**, 054414 (2018).
- 34 **“Frustrated spin one on a diamond lattice in NiRh₂O₄,”** J. R. Chamorro, L. Ge, J. Flynn, M. A. Subramanian, M. Mourigal, and T. M. McQueen, Phys. Rev. Materials **2**, 034404 “Editors’ Suggestion,” (2018). “
- 35 **“Screened moments and extrinsic in-gap states in samarium hexaboride,”** W.T. Fuhrman, J.R. Chamorro, P. A. Alekseev, J.-M. Mignot, T. Keller, J.A. Rodriguez-Rivera,

- Y. Qiu, P. Nikolic, T.M. McQueen, and C.L. Broholm, Nature Communications, **9**, 1539 (2018).
- 36 **“Nonuniform carrier density in Cd₃As₂ evidenced by optical spectroscopy,”** I. Crassee, E. Martino, C. C. Homes, O. Caha, J. Novak, P. Tuckmantel, M. Haki, A. Nateprov, E. Arushanov, Q. D. Gibson, R. J. Cava, S. M. Koohpayeh, K. E. Arpino, T. M. McQueen, M. Orlita, and A. Akrap, Phys. Rev. B, **97**, 125204 (2018).
- 37 **“Macroscopically Degenerate Exactly Solvable Point in the Spin-1/2 Kagome Quantum Antiferromagnet,”** H. J. Changlani, D. Kochkov, K. Kumar, B. K. Clark, and E. Fradkin, Phys. Rev. Lett. **120**, 117202 (2018).
- 38 **“Multi-q mesoscale magnetism in CeAuSb₂,”** G. G. Marcus, D.-J. Kim, J. A. Tutmaher, J. A. Rodriguez-Rivera, J. O. Birk, C. Niedermeyer, H. Lee, Z. Fisk, and C. Broholm, Phys. Rev. Lett. **120**, 097201 (2018).
- 39 **“Viscous dynamics of vortices in a ferromagnetic film,”** D. Reitz, A. Ghosh, and O. Tchernyshyov, Phys. Rev. B, **97**, 054424 (2018).
- 40 **“Topological Nodal Cooper Pairing in Doped Weyl Metals,”** Y. Li and F. D. M. Haldane, Phys. Rev. Lett., **120**, 067003 (2018).
- 41 **“Large magneto-optical Kerr effect and imaging of magnetic octupole domains in an antiferromagnetic metal,”** T. Higo, H. Man, D. B. Gopman, L. Wu, T. Koretsune, O. M. J. van ’t Erve, Y. P. Kabanov, D. Rees, Y. Li, M.-T. Suzuki, S. Patankar, M. Ikhlas, C. L. Chien, R. Arita, R. t D. Shull, J. Orenstein & S. Nakatsuji, Nature Photonics **12**, 73–78 (2018).
- 42 **“Weyl and Dirac semimetals in three-dimensional solids,”** N. P. Armitage, E. J. Mele, and A. Vishwanath, Rev. of Modern Phys., **90**, 015001 (2018).
- 43 **“Induced quadrupolar singlet ground state of praseodymium in a modulated pyrochlore,”** J. van Duijn, K. H. Kim, N. Hur, D. T. Adroja, F. Bridges, A. Daoud-Aladine, F. Fernandez-Alonso, R. Ruiz-Bustos, J. Wen, V. Kearney, Q. Z. Huang, S.-W. Cheong, S. Nakatsuji, C. Broholm, and T. G. Perring, Phys. Rev. B, **96**, 094409 (2018).
- 44 **“Real-space investigation of short-range magnetic correlations in fluoride pyrochlores NaCaCo₂F₇ and NaSrCo₂F₇ with magnetic pair distribution function analysis,”** B. A. Frandsen, K. A. Ross, J. W. Krizan, G. J. Nilsen, A. R. Wildes, R. J. Cava, R. J. Birgeneau, and S. J. L. Billinge, Phys. Rev. Materials **1**, 074412 (2017).
- 45 **“Spin freezing in the disordered pyrochlore magnet NaCaCo₂F₇: NMR studies and Monte Carlo simulations,”** R. Sarkar, J. W. Krizan, F. Bruckner, E. C. Andrade, S. Rachel, M. Vojta, R. J. Cava, and H. H. Klauss, Phys. Rev. B **96**, 235117 (2017).

- 46 **“Asymmetric Splitting of an Antiferromagnetic Resonance via Quartic Exchange Interactions in Multiferroic Hexagonal HoMnO_3 ,”** N. J. Laurita, Y. Luo, R. W. Hu, M. X. Wu, S. W. Cheong, O. Tchernyshyov, and N. P. Armitage, *Phys. Rev. Lett.* **119**, 227601 (2017).
- 47 **“Reentrant Phase Diagram of $\text{Yb}_2\text{Ti}_2\text{O}_7$ in a $\langle 111 \rangle$ Magnetic Field,”** A. Scheie, J. Kindervater, S. Saeubert, C. Duvina, C. Pfleiderer, H.J., Changlani, S. Zhang, L. Harriger, K. Arpino, S. M. Koochpayeh, O. Tchernyshyov, and C. Broholm, *Phys.Rev. Lett.* **119**, 127201 (2017).
- 48 **“Optical investigation of the strong spin-orbit-coupled magnetic semimetal YbMnBi_2 ,”** D. Chaudhuri, B. Cheng, A. Yaresko, Q. D. Gibson, R. J. Cava, and N. P. Armitage, *Phys. Rev. B* **96**, 075151 (2017).
- 49 **“Gyrotropic elastic response of skyrmion crystals to current-induced tensions,”** H. Ochoa, S. K. Kim, O. Tchernyshyov, and Y. Tserkovnyak, *Phys. Rev. B* **96**, 020410 (2017).
- 50 **“High-Pressure Study of Perovskites and Postperovskites in the $(\text{Mg,Fe})\text{GeO}_3$ System,”** C. V. Stan, R. Dutta, R. J. Cava, V. B. Prakapenka, and T. S. Duffy, *Inorganic Chem.* **56**, Issue 14, p. 8026-8035 (2017).
- 51 **“Dynamic pathway of the photoinduced phase transition of TbMnO_3 ,”** E. Bothschafter, E. Abreu, L. Rettig, T. Kubacka, S. Parchenko, M. Porer, C. Dornes, Y. W. Windsor, M. Ramakrishnan, A. Alberca, S. Manz, J. Saari, S. M. Koochpayeh, M. Fiebig, T. Forrest, P. Werner, S. S. Dhesi, S. L. Johnson, and U. Staub, *Phys. Rev. B* **96**, 184414; arXiv:1705.10136.
- 52 **“Low-energy magnon dynamics and magneto-optics of the skyrmionic Mott insulator Cu_2OSeO_3 ,”** N. J. Laurita, G. G. Marcus, B. A. Trump, J. Kindervater, M. B. Stone, T. M. McQueen, C. L. Broholm, and N. P. Armitage, *Phys. Rev. B* **95**, 235155 (2017); arXiv:1704.04228.
- 53 **“Gauge fields and related forces in antiferromagnetic soliton physics,”** S. Dasgupta, S.K. Kim, and O. Tchernyshyov, *Phys. Rev. B* **95**, 220407 (2017); arXiv:1701.05137.
- 54 **“Gapped excitations in the high-pressure antiferromagnetic phase of URu_2Si_2 ,”** T.J. Williams, H. Barath, Z. Yamani, J.A. Rodriguez-Riviera, J.B. Leão, J.D. Garrett, G.M. Luke, W.J.L. Buyers, and C. Broholm, *Phys. Rev. B* **95**, 195171 (2017); arXiv:1607.00967.
- 55 **“Interface-induced phenomena in magnetism,”** Hellman, F., Hoffmann, A., Tserkovnyak, Y., Beach, G. S. D., Fullerton, E. E., Leighton, C., MacDonald, A. H., Ralph, D. C., Arena, D.

- A., Dürr, H. A., Fischer, P., Grollier, J., Heremans, J. P., Jungwirth, T., Kimel, A. V., Koopmans, B., Krivorotov, I. N., May, S. J., Petford-Long, A. K., Rondinelli, J. M., Samarth, N., Schuller, I. K., Slavin, A. N., Stiles, M. D., Tchernyshyov, O., Thiaville, A., Zink, B. L., Rev. Mod. Phys. **89**, 025006 (2017); [arXiv:1607.00439](#).
- 56 **“Statistics of fractionalized excitations through threshold spectroscopy,”** S. C. Morampudi, A. M. Turner, F. Pollmann, and F. Wilczek, Phys. Rev. Lett. **118**, 227201 (2017); [arXiv:1608.05700](#).
- 57 **“Annihilation of domain walls in a ferromagnetic wire,”** A. Ghosh, K.S. Huang, and O. Tchernyshyov, Phys. Rev. B **95**, 180408 (2017); [arXiv:1702.02248](#).
- 58 **“Magnetism in the K_{Ba}RE(BO₃)₂ (RE = Sm, Eu, Gd, Tb, Dy, Ho, Er, Tm, Yb, Lu) series: materials with a triangular rare earth lattice,”** M. B. Sanders, F. A. Cevallos, and R. J. Cava, Mat. Res. Express **4**, 036102 (2017); [arXiv:1611.08548](#).
- 59 **“Impact of stoichiometry of Yb₂Ti₂O₇ on its physical properties,”** K. E. Arpino, B. A. Trump, A. O. Scheie, T. M. McQueen, and S. M. Koohpayeh, Phys. Rev. B **95**, 094407 (2017); [arXiv:1701.08821](#).
- 60 **“Single-ion properties of the $S_{\text{eff}} = 1/2$ XY antiferromagnetic pyrochlores Na A' Co₂F₇ ($A' = \text{Ca}^{2+}, \text{Sr}^{2+}$),”** K. A. Ross, J. M. Brown, R. J. Cava, J. W. Krizan, S. E. Nagler, J. A. Rodriguez-Rivera, and M. B. Stone, Phys. Rev. B **95**, 144414 (2017); [arXiv:1703.07468](#).
- 61 **“Quantum spin liquid with 7 elementary particles,”** H. Wang, H.J. Changlani, Y. Wan, and O. Tchernyshyov, Phys. Rev. B **95**, 144425 (2017); [arXiv:1702.01359](#).
- 62 **“Rearrangement of van der Waals stacking and formation of a singlet state at $T=90$ K in a cluster magnet,”** J.P. Sheckelton, K.W. Plumb, B.A. Trump, C.L. Broholm, and T.M. McQueen, Inorg. Chem. Front. **4**, 481-490 (2017).
- 63 **“Spin excitations and the Fermi surface of superconducting FeS,”** H. Man, J. Guo, R. Zhang, R. Schönemann, Z. Yin, M. Fu, M. B. Stone, Q. Huang, Y. Song, W. Wang, D. J. Singh, F. Lochner, T. Hickel, I. Eremin, L. Harriger, J. W. Lynn, C. Broholm, L. Balicas, Q. Si, and P. Dai, npj Quant. Mater. **2**, 1383 (2017).
- 64 **“Disordered route to the Coulomb quantum spin liquid: Random transverse fields on spin ice in Pr₂Zr₂O₇,”** J. J. Wen, S. M. Koohpayeh, K. A. Ross, B. A. Trump, T. M. McQueen, K. Kimura, S. Nakatsuji, Y. Qiu, D. M. Pajerowski, J. R. D. Copley, and C. L. Broholm, Phys. Rev. Lett. **118**, 107206 (2017); [arXiv:1609.08551](#).

65 **“NaSrMn₂F₇, NaCaFe₂F₇, and NaSrFe₂F₇: novel single crystal pyrochlore antiferromagnets,”** M.B. Sanders, J.W. Krizan, K.W. Plumb, T.M. McQueen, and R.J. Cava, *J. Phys.: Condens. Matter* **29**, 045801 (2017). [arXiv:1608.02907](https://arxiv.org/abs/1608.02907).

Non-reciprocal effects in non-centrosymmetric magnets: neutron and optical studies

S.-W. Cheong (Rutgers Univ.), V. Kiryukhin (Rutgers Univ.), and A. Sirenko (NJIT)

Program Scope

Effects lacking symmetry under the exchange of source and detector are called non-reciprocal. They are well-known in optics, but can occur for any (quasi)particles, including neutrons, spin waves etc. Numerous possible applications for these effects are in all-optics computing, quantum cryptography, and spintronics. While the non-reciprocal effects involving magnetic (spin-waves) and mixed (electromagnons) quasiparticles are important for both fundamental and applied science, they are not studied as well as those for photons. Neutron scattering is an ideal probe for magnetic excitations, capable of measuring their spectra with an unprecedented level of details. A team from Rutgers University and NJIT is engaged in a collaborative effort to understand non-reciprocal effects utilizing inelastic neutron scattering, advanced crystal growth, and optical spectroscopy. This Project focuses on studies of polar magnets, magnets with structural chirality, and ferroaxial magnets. Among these compounds are toroidal magnets, a spin liquid, and unconventional magnetoelectrics. In these systems, combination of absent inversion, time-reversal, and mirror symmetries leads to non-reciprocal effects revealed, for example, in non-equivalent magnon/electromagnon spectra for the opposite directions of the particle propagation, and as directional dichroism (difference in the light absorption) in the far-infrared optical spectra. The high-quality monodomain single crystals synthesized under this Project are crucial for the studies of nonreciprocal and magnetoelectric effects. Spectroscopic studies include utilization of vortex beams, which we recently developed as a new probe of orbital magnetism in matter. Combined neutron and optical studies should reveal the physical mechanisms responsible for the exotic nonreciprocal properties in low-symmetry materials, and help identify prospective quantum materials for novel computational techniques.

Recent Progress

High-quality single crystals of several low-symmetry magnets, including TbInO_3 , $(\text{Fe,Mn,Co,Ni,Zn})_2\text{Mo}_3\text{O}_8$, $\text{Ba}_3\text{NbFe}_3\text{Si}_2\text{O}_{14}$, $\text{Dy}_3\text{Fe}_5\text{O}_{12}$, Ni_3TeO_6 , and BaCoSiO_4 were grown using various methods, including the new laser-diode-heated floating zone (LFZ) technique. The prospective functional properties of these and other compounds have been studied using laboratory probes, neutron scattering, and optical spectroscopy. Since the last PI Meeting, 29 papers have been published. Below, we highlight the inelastic neutron scattering (INS) experiments resulting in the discovery of spin-liquid-like state in the nearly-triangular lattice

antiferromagnet TbInO_3 [1,2], and the observation of nonreciprocal spin waves in $\text{Ba}_3\text{NbFe}_3\text{Si}_2\text{O}_{14}$ [3]. Our project also involves significant technique development activities. Improvements to the synthesis of the single-domain samples using the LFZ technique are introduced on a regular basis, and new growth protocols are developed. Large monodomain BiFeO_3 and $\text{Ba}_3\text{NbFe}_3\text{Si}_2\text{O}_{14}$ samples recently obtained by this technique serve as good examples. We are also excited to report the development of two new experimental tools designed to investigate complex magnets, such as the ones we study. The first is a new approach for the imaging of antiferromagnetic domains using magnetic diffraction of coherent x-rays [4], and the second is creation of THz optical vortex beams and their utilization as a new probe of orbital magnetism in matter [5].

TbInO_3 is a layered antiferromagnet exhibiting a nearly triangular lattice of Tb^{3+} non-Kramers ions. Both the polycrystalline [1] and single crystal [2] samples have been studied. We observe strong evidence of the spin-liquid behavior. It includes absence of any long-range order at the temperatures two orders of magnitude smaller than the major interaction energy, as well as a very broad, gapless, nondispersing diffuse inelastic magnetic signal centered at the Brillouin zone boundary of the triangular lattice, see Fig 1. The data taken in the polycrystals were interpreted as suggesting an emergent honeycomb lattice. Later study of single crystals has indicated that the low-energy physics is better approximated by the properties of the frustrated triangular lattice instead. Our results emphasize that the systems with even numbers of the electrons in the magnetic ions (such as Tb^{3+}) provide a fruitful ground for the search of the spin-liquid behavior, in addition to the more standard compounds containing the Kramers doublets. Importantly to this Project, TbInO_3 is a polar magnet with the symmetry admitting non-reciprocal effects in an applied magnetic field, independent of any magnetic order or lack thereof. Thus, this system presents a unique opportunity: investigation of potential non-reciprocal effects in a spin liquid compound. We have made significant progress towards the synthesis of the required single-domain TbInO_3 samples. Studies of TbInO_3 in the context of non-reciprocal effects is one of the new future research directions of this Project.

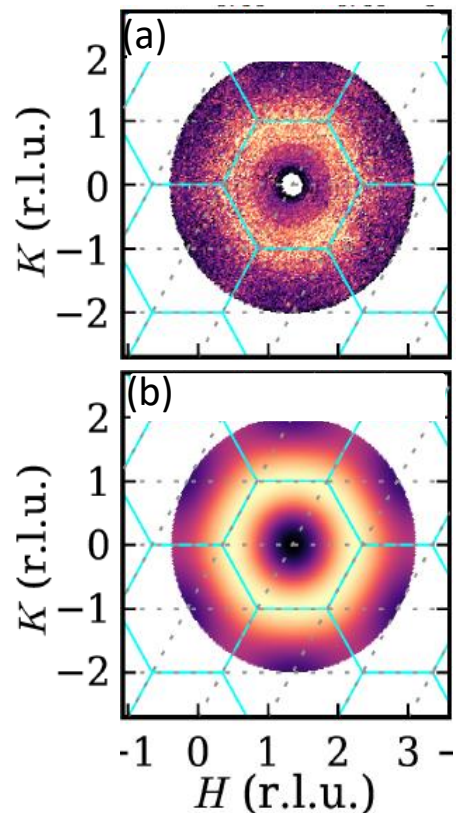


Fig. 1. (a) INS pattern for $E=0.8$ meV and $T=1.5$ K in TbInO_3 . Blue lines show the zone boundaries for the triangular lattice, H and K are indices for the actual unit cell. (b) Theoretical calculation for the uncorrelated valence bonds model consistent with the triangular lattice description of the magnetism.[2]

$\text{Ba}_3\text{NbFe}_3\text{Si}_2\text{O}_{14}$ (iron langasite) is structurally and magnetically chiral with the magnetic helicity induced through competing symmetric exchange interactions. We have grown large single crystals in the monodomain state for *both* the nuclear *and* the magnetic structures. Using neutron scattering, we show that the spin-waves display directional anisotropy, i.e. they are nonreciprocal.[3] On applying a time reversal symmetry breaking magnetic field along the c -axis, the spin wave energies differ when the sign is reversed for either the momentum transfer Q or applied magnetic field H . When the field is applied within the crystallographic ab -plane, the spin wave dispersion is directionally isotropic and symmetric in $\pm H$. However, a directional anisotropy is observed in the spin wave intensity. Directional anisotropy can therefore occur in the absence of spin-orbit coupling. These results illustrate how spin waves can be controlled in materials when the constraints from Kramer's theorem and inversion symmetry are relaxed.

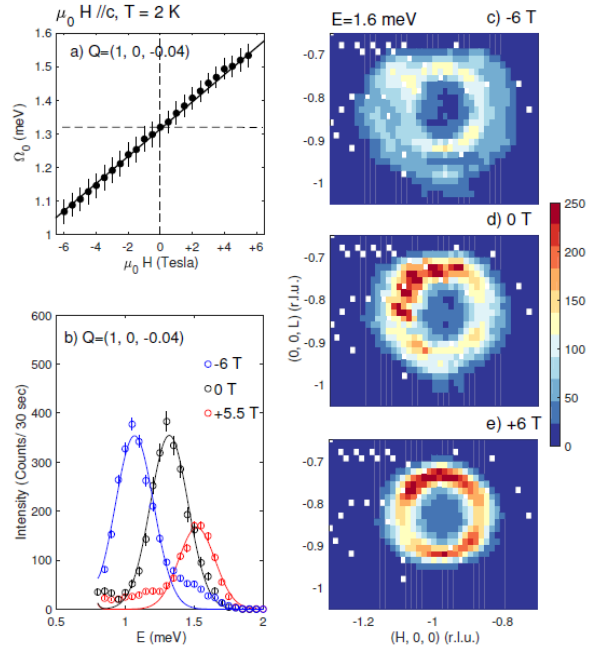


Fig. 2. (a) Linear scaling of $Q=(1,0,0)$ magnon showing a nonreciprocal behavior in $\text{Ba}_3\text{NbFe}_3\text{Si}_2\text{O}_{14}$. In a reciprocal system, the magnon energy does not change when the field changes its sign. (b) Representative constant momentum scans. (c-e) display constant $E=1.6$ meV cuts at 6, 0, and -6 tesla with a fixed final energy of $E_f=2.5$ meV.[3]

Imaging antiferromagnetic (AFM) domains is a nontrivial task. For some domain types, such as antiphase AFM domains in collinear magnets, there are no practical approaches. We have invented a new imaging technique for AFM domains which is applicable to many domain types, including the antiphase domains.[4] It is based on magnetic diffraction of coherent soft x-rays. The images are obtained in a single exposure, and don't require any algorithmic processing. Fig. 3 shows an AFM antiphase domain pattern measured in a collinear antiferromagnet $\text{Fe}_2\text{Mo}_3\text{O}_8$. The technique is fast, making possible collecting real-time movies of the domain evolution on the sub-second scale. Single-domain samples play a critical role for our Project, and this imaging technique will be used to characterize the relevant samples.

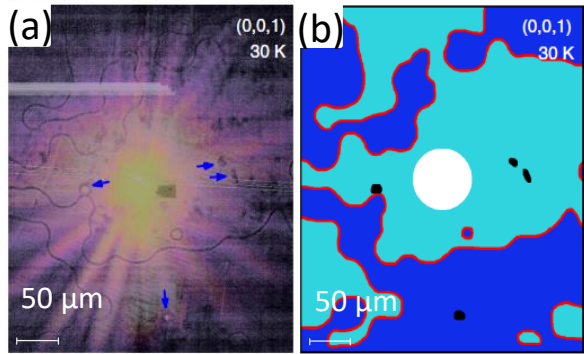


Fig. 3. (a) Detector image showing the AFM antiphase domain boundaries on the surface of bulk $\text{Fe}_2\text{Mo}_3\text{O}_8$ as dark lines. (b) The corresponding AFM domain pattern.[4]

In a circularly-polarized beam, the photons carry spin angular momentum of 1. Vortex beams can carry a large *orbital* angular momentum l , providing a complementary probe with many advantages. The selection rules, in particular, are modified for the vortex beams, increasing the range of the accessible materials. The interaction strength may be increased too. We present the first demonstration of THz vortex photon beam spectroscopy as a probe of magnetism in matter.[5] We have observed a strong dichroic signal for the vortex beams carrying $l=\pm 1$ in the ferrimagnetic $\text{Dy}_3\text{Fe}_5\text{O}_{12}$, see Fig 4. The observed effect is larger than the regular circular dichroism, demonstrating the new probe's potential. In this Project, we utilize the THz photon beams to study the magnetic state of the ions, as well as the magnetic excitations at low q , complementing the INS experiments.

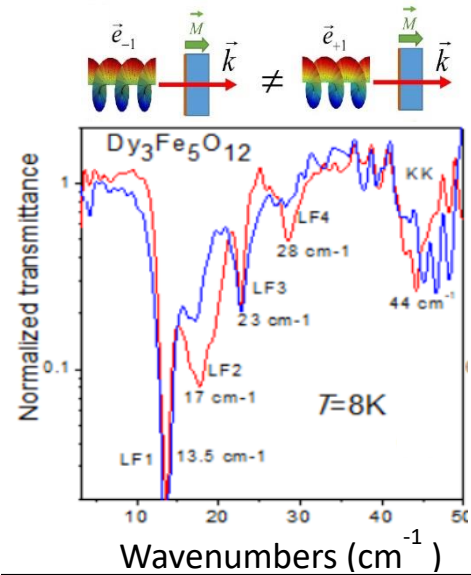


Fig. 4. Normalized transmittance spectra for two orthogonal vortex beams $l=+1$ (red) and $l=-1$ (blue) in $\text{Dy}_3\text{Fe}_5\text{O}_{12}$. [5]

Future Plans

Inelastic neutron scattering studies of the reduced-symmetry compounds with expected non-reciprocal spin-wave effects: $M_2\text{Mo}_3\text{O}_8$, monodomain TbInO_3 , hex- $(RE)(\text{Mn},\text{Fe})\text{O}_3$, BaCoSiO_4 , and Ni_3TeO_6 . Continuing sample-growth optimization. Monitoring of the most promising excitations for the INS studies by optical spectroscopy. Continuing development of the vortex-beam spectroscopy of magnetic materials using the listed systems as test subjects.

References

- [1] L. Clark et al, “Two-dimensional spin liquid behaviour in the triangular-honeycomb antiferromagnet TbInO_3 ”, *Nature Physics* **15**, 262–268 (2019).
- [2] M. G. Kim et al, “Spin-Liquid-Like State in the Triangular Lattice Antiferromagnet TbInO_3 ”, submitted, under review. Preprint arXiv:1812.01121.
- [3] C. Stock et al., “Spin-wave directional anisotropies in $\text{Ba}_3\text{NbFe}_3\text{Si}_2\text{O}_{14}$ without antisymmetric exchange”, submitted, under review (2019).
- [4] M. G. Kim et al, “Imaging antiferromagnetic antiphase domain boundaries using magnetic Bragg diffraction phase contrast”, *Nature Communications* **9**, article number: 5013 (2018).
- [5] A. A. Sirenko et al, "Terahertz vortex beam as a spectroscopic probe of magnetic excitations", *Phys. Rev. Lett.* **122**, (accepted May 9th, 2019).

Publications

- [1] P. Bowlan, S. A. Trugman, X. Wang, Y. M. Dai, S.-W. Cheong, E. D. Bauer, A. J. Taylor, D. A. Yarotski, and R. P. Prasankumar, “*Directly probing spin dynamics in insulating antiferromagnets using ultrashort terahertz pulses*”, Phys. Rev. B **94**, 184429 (2016).
- [2] Junjie Li, Wei-Guo Yin, Lijun Wu, Pengfei Zhu, Tatianna Konstantinova, Jing Tao, Junjie Yang, Sang-Wook Cheong, Fabrizio Carbone, James A Misewich, John P Hill, Xijie Wang, Robert J Cava & Yimei Zhu, “*Dichotomy in ultrafast atomic dynamics as direct evidence of polaron formation in manganites*”, npj Quantum Materials **1**, Article number: 16026 (2016).
- [3] S. H. Bukhari, Th. Kain, M. Schiebl, A. Shuvaev, Anna Pimenov, A. M. Kuzmenko, X. Wang, S.-W. Cheong, J. Ahmad, and A. Pimenov, “*Magnetoelectric phase diagrams of multiferroic $GdMn_2O_5$* ”, Phys. Rev. B **94**, 174446 (2016).
- [4] Y. W. Windsor, Yoshikazu Tanaka, V. Scagnoli, M. Garganourakis, R. A. de Souza, M. Medarde, S.-W. Cheong, and U. Staub, “*Ferromagnetic and antiferromagnetic orders of a phase-separated manganite probed throughout the B-T phase diagram*”, Phys. Rev. B **94**, 214412 (2016).
- [5] Thuc T. Mai, C. Svoboda, M. T. Warren, T.-H. Jang, J. Brangham, Y. H. Jeong, S.-W. Cheong, and R. Valdés Aguilar, “*Terahertz spin-orbital excitations in the paramagnetic state of multiferroic $Sr_2FeSi_2O_7$* ”, Phys. Rev. B **94**, 224416 (2016).
- [6] C. Stock, E. E. Rodriguez, N. Lee, F. Demmel, P. Fouquet, M. Laver, Ch. Niedermayer, Y. Su, K. Nemkovski, M. A. Green, J. A. Rodriguez-Rivera, J. W. Kim, L. Zhang, and S.-W. Cheong, “*Orphan Spins in the $S=5/2$ Antiferromagnet $CaFe_2O_4$* ”, Phys. Rev. Lett. **119**, 257204 (2017).
- [7] N. J. Laurita, Yi Luo, Rongwei Hu, Meixia Wu, S. W. Cheong, O. Tchernyshyov, and N. P. Armitage, “*Asymmetric Splitting of an Antiferromagnetic Resonance via Quartic Exchange Interactions in Multiferroic Hexagonal $HoMnO_3$* ”, Phys. Rev. Lett. **119**, 227601 (2017).
- [8] K. N. Boldyrev, T. N. Stanislavchuk, A. A. Sirenko, D. Kamenskyi, L. N. Bezmaternykh, and M. N. Popova, “*Bifurcations of Coupled Electron-Phonon Modes in an Antiferromagnet Subjected to a Magnetic Field*”, Phys. Rev. Lett. **118**, 167203 (2017).
- [9] T.N. Stanislavchuk, Y Wang, SW. Cheong, A.A. Sirenko, “*Far-IR magnetospectroscopy of magnons and electromagnons in $TbFeO_3$ single crystals at low temperatures*”, Phys. Rev. B **95** (5), 054427 (2017).
- [10] R Nirmala, Kwang-Hyun Jang Hasung Sim, Hwanbeom Cho, Junghwan Lee, Nam-Geun Yang, Seongsu Lee, R M Ibberson, K Kakurai, M Matsuda, “*Spin glass behavior in frustrated quantum spin system $CuAl_2O_4$ with a possible orbital liquid state*”, Journal of Physics: Condensed Matter **29**, 13LT01 (2017).

- [11] J. van Duijn, K. H. Kim, N. Hur, R. Ruiz-Bustos, D. T. Adroja, F. Bridges, A. Daoud-Aladine, F. Fernandez-Alonso, J. J. Wen, V. Kearney, Q. Z. Huang, S.-W. Cheong, T. G. Perring, and C. Broholm, “*Induced quadrupolar singlet ground state of praseodymium in a modulated pyrochlore*”, Phys. Rev. B **96**, 094409 (2017).
- [12] T. N. Stanislavchuk, D. S. Middlemiss, J. S. Syzdek, Y. Janssen, R. Basistyy, A. A. Sirenko, P. G. Khalifah, C. P. Grey, and R. Kostecki, “*Infrared-active optical phonons in LiFePO₄ single crystals*”, J. Appl. Phys. **122**, 045107 (2017).
- [13] Xiang-Bai Chen, Peng-Cheng Guo, Nguyen Thi Huyen, Seung Kim, In-Sang Yang, Xueyun Wang, and Sang-Wook Cheong “*Spin wave and spin flip in hexagonal LuMnO₃ single crystal*”, Appl. Phys. Lett. **110**, 122405 (2017).
- [14] Shukai Yu, Bin Gao, Jae Wook Kim, Sang-Wook Cheong, Michael K. L. Man, Julien Madéo, Keshav M. Dani, and Diyar Talbayev, “*High-Temperature Terahertz Optical Diode Effect without Magnetic Order in Polar FeZnMo₃O₈*”, Phys. Rev. Lett. **120**, 037601 (2018).
- [15] Peng Chen , Brian S. Holinsworth, Kenneth R. O’Neal, Xuan Luo, Craig V. Topping, Sang W. Cheong, John Singleton, Eun S. Choi, and Janice L. Musfeldt, “*Frustration and Glasslike Character in RIn_{1-x}Mn_xO₃ (R = Tb, Dy, Gd)*”, Inorg Chem., **57**(20):12501-12508 (2018).
- [16] J. C. Leiner, Taehun Kim, Kiso Park, Joosung Oh, T. G. Perring, H. C. Walker, X. Xu, Y. Wang, S.-W. Cheong, and Je-Geun Park, “*Magnetic excitations in the bulk multiferroic two-dimensional triangular lattice antiferromagnet (Lu,Sc)FeO₃*”, Phys. Rev. B **98**, 134412 (2018).
- [17] Qian Li, Mengmeng Yang, Cheng Gong, Rajesh V. Chopdekar, Alpha T. N’Diaye, John Turner, Gong Chen, Andreas Scholl, Pdraic Shafer , Elke Arenholz, Andreas K. Schmid, Sheng Wang, Kai Liu, Nan Gao, Alemayehu S. Admasu, Sang-Wook Cheong, Chanyong Hwang, Jia Li, Feng Wang, Xiang Zhang , and Ziqiang Qiu, ”*Patterning-Induced Ferromagnetism of Fe₃GeTe₂ van der Waals Materials beyond Room Temperature*”, Nano Lett., **18** (9), 5974–5980 (2018).
- [18] Elijah E. Gordon, Xiyue Cheng, Jaewook Kim, Sang-Wook Cheong, Shuiquan Deng , and Myung-Hwan Whangbo,” *Nonequivalent Spin Exchanges of the Hexagonal Spin Lattice Affecting the Low-Temperature Magnetic Properties of RInO₃ (R = Gd, Tb, Dy): Importance of Spin–Orbit Coupling for Spin Exchanges between Rare-Earth Cations with Nonzero Orbital Moments*”, Inorg Chem., **57**(15):9260-9265 (2018).
- [19] Xiixin Ding, Yi-Sheng Chai, Fedor Balakirev, Marcelo Jaime, Hee Taek Yi, Sang-Wook Cheong, Young Sun, and Vivien Zapf, “*Measurement of the angle dependence of magnetostriction in pulsed magnetic fields using a piezoelectric strain gauge*”, Rev. Sci. Instr. **89**, 085109 (2018).

- [20] Benjamin H. Savitzky, Ismail El Baggari, Colin B. Clement, Emily Waite, Berit H. Goodge, David J. Baek, John, P. Sheckelton, Christopher Pasco, Hari Nair, Nathaniel J. Schreiber, Jason Hoffman, Alemayehu S. Admasu, Jaewook Kim, Sang-Wook Cheong, Anand Bhattacharya, Darrell G. Schlomei, Tyrel M. McQueen, Robert Hovden, Lena F. Kourkoutis, “*Image registration of low signal-to-noise cryo-STEM data*”, *Ultramicroscopy* **191**, 56-65 (2018).
- [21] Yanbin Li, Yazhong Wang, Wenjie Tan, Wenbo Wang, Junjie Zhang, Jae Wook Kim, Sang-Wook Cheong and Xutang Tao, “*Laser floating zone growth of improper geometric ferroelectric GdInO₃ single crystals with Z6 topological defects*”, *J. Mater. Chem. C* **6**, 7024-7029 (2018).
- [22] Jae Wook Kim, E. D. Mun, X. Ding, A. Hansen, M. Jaime, N. Harrison, H. T. Yi, Y. Chai, Y. Sun, S. W. Cheong, and V. S. Zapf, “*Metastable states in the frustrated triangular compounds Ca₃Co_{2-x}Mn_xO₆ and Ca₃Co₂O₆*”, *Phys. Rev. B* **98**, 024407 (2018).
- [23] Sang-Wook Cheong, Diyar Talbayev, Valery Kiryukhin and Avadh Saxena, “*Broken symmetries, non-reciprocity, and multiferroicity*”, *npj Quantum Materials* **3**, 19 (2018).
- [24] J. C. Leiner, Joosung Oh, A. I. Kolesnikov, M. B. Stone, Manh Duc Le, E. P. Kenny, B. J. Powell, M. Mourigal, E. E. Gordon, M.-H. Whangbo, J.-W. Kim, S.-W. Cheong, and Je-Geun Park, “*Magnetic excitations of the Cu²⁺ quantum spin chain in Sr₃CuPtO₆*”, *Phys. Rev. B* **97**, 104426 (2018).
- [25] Hasung Sim, Jaehong Jeong, Haeri Kim, S-W Cheong and Je-Geun Park, ” *Studies on the high-temperature ferroelectric transition of multiferroic hexagonal manganite RMnO₃*”, *J. Phys. Condens. Matter.* **30**(10):105601 (2018).
- [26] M. G. Kim, H. Miao, B. Gao, S.-W. Cheong, C. Mazzoli, A. Barbour, W. Hu, S.B. Wilkins, I.K. Robinson, M.P.M. Dean, V. Kiryukhin, “*Imaging antiferromagnetic antiphase domain boundaries using magnetic Bragg diffraction phase contrast*”, *Nature Communications* **9**, article number: 5013 (2018).
- [27] L. Clark, Lucy, G. Sala, D. D. Maharaj, M. B. Stone, K. S. Knight, M. T. F. Telling, X. Wang, X. Xu, J. Kim, Y. Li, Yanbin, S.-W. Cheong, B. D. Gaulin, “*Two-dimensional spin liquid behaviour in the triangular-honeycomb antiferromagnet TbInO₃*”, *Nature Physics* **15**, 262–268 (2019).
- [28] Sang-Wook Cheong, “*Topological domains/domain walls and broken symmetries in multiferroics*”, *National Science Review*, nwz015 (2019). <https://doi.org/10.1093/nsr/nwz015>
- [29] A. A. Sirenko, P. Marsik, C. Bernhard, T. N. Stanislavchuk, V. Kiryukhin, and S. -W. Cheong, “*Terahertz vortex beam as a spectroscopic probe of magnetic excitations*”, *Phys. Rev. Lett.* **122**, (Accepted May 9th, 2019).

Understanding Quantum Matter Beyond the Unit Cell

A. D. Christianson, Materials Science & Technology Division, Oak Ridge National Laboratory, Oak Ridge, TN 37831.

A. F. May, Materials Science & Technology Division, Oak Ridge National Laboratory, Oak Ridge, TN 37831.

D. S. Parker, Materials Science & Technology Division, Oak Ridge National Laboratory, Oak Ridge, TN 37831.

D. Mandrus, Materials Science & Technology Division, Oak Ridge National Laboratory, Oak Ridge, TN 37831; Department of Physics & Astronomy, University of Tennessee, Knoxville, TN 37996; Department of Material Science & Engineering, University of Tennessee, Knoxville, TN 37996.

Program Scope

There has been increasing interest in novel quantum materials where strong electronic correlations, frustration, and spin-orbit coupling are intertwined with topological considerations. This project seeks to advance our understand of such systems, with an emphasis on utilizing neutron scattering to probe complex behaviors. The Overarching Goal of this project is to achieve understanding of quantum matter beyond the unit cell with focus on how topology, competing interactions, and frustration intertwine to produce new collective quantum states of matter. To achieve this goal, the specific aims of the project are: (1) To elucidate the properties of novel spin textures, especially those that possess an internal chiral degree of freedom; (2) To understand how spin-orbit coupling alters the hierarchy of energy scales to stabilize novel magnetic ground states that are strongly coupled to electronic structure; and (3) To determine conditions under which the spin excitation spectra of noncollinear quantum magnets and quantum paramagnets contain topologically-nontrivial character. These topics are pursued by combining materials synthesis and characterization and theory with experimental studies using neutron scattering techniques. Principal outcomes of this work will be the development of physical models that describe how quantum magnetism influences macroscopic behavior and clear guidelines for identifying and/or manipulating systems to produce specific, non-classical behaviors.

Recent Progress

I. Novel spin order in transition metal dihalides

Transition metal dihalides exhibit interesting magnetic properties as a consequence of geometric frustration due to triangular nets of magnetic ions as well as competing nearest neighbor and longer-range exchange interactions [1]. Here we focus on NiBr_2 , which undergoes a transition to commensurate magnetic order at 46 K and subsequently undergoes a transition to incommensurate magnetic order below 20 K. The low temperature magnetic structure is helimagnetic with in-plane

magnetic moments. As a consequence of these magnetic properties, NiBr₂ has been predicted to be a candidate for the realization of novel spin textures [2]. To explore the possibility of interesting spin textures in NiBr₂ derived materials, we have studied how the physical properties of NiBr₂ are tuned through chemical substitution and applied magnetic field. Our studies of the Ni_{1-x}Co_xBr₂ pseudo-binary materials represent the first complete substitutional series from one end member (NiBr₂) to the other (CoBr₂) in this family of materials. Cobalt-doping suppresses the commensurate transition whereas the incommensurate transition temperature initially increases slightly and is then suppressed and disappears around x=0.6. A structural transition from the CdCl₂ to the CdI₂ structure occurs near x=0.6-0.7. Neutron diffraction studies of single crystals reveal that the hexagonal pattern of the incommensurate spots in NiBr₂ transforms to a ring of magnetic scattering with cobalt doping, which may be due to the predicted impurity nucleated vortex lattice[2].

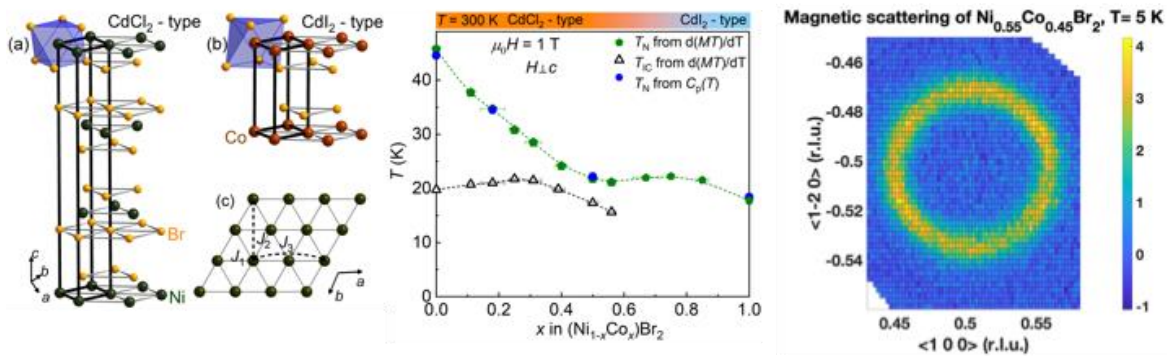


Figure 1. (Left) Crystal Structure of Ni_{1-x}Co_xBr₂. (Middle) Phase diagram of Ni_{1-x}Co_xBr₂. (Right) Neutron diffraction around near (0 1 0.5) shows the developing ring of magnetic scattering with Cobalt doping.

II. Breathing Pyrochlores Lattice Materials

Breathing pyrochlore lattice materials have recently been recognized as containing a novel structural motif to study quantum magnetism. Compelling examples are the enhanced stability of the quantum spin ice state [3] and a topologically nontrivial magnon band crossing termed a “Weyl magnon”, which is a bosonic analog of a Weyl fermion [4] that would be associated with magnon arc surface states. Breathing pyrochlore lattices are a variation of the pyrochlore lattice where the size of the tetrahedra alternates so that large and small tetrahedra yield a hierarchy of exchange interactions. To explore the novel physics hosted by this structural motif we have studied several examples of materials that contain a breathing pyrochlore sublattice. Here we focus on our studies of the family of breathing pyrochlores derived from Cr containing spinels.

A breathing pyrochlore lattice of Cr tetrahedra can be realized through substitution of inequivalent cations on the A-site of a spinel such as ACr₂X₄ where X is a chalcogen and the Cr sublattice forms a pyrochlore lattice. When the substituted cations are ordered, the Cr pyrochlore sublattice is altered to an arrangement of larger and smaller tetrahedra on a corner sharing network. The

resulting breathing pyrochlore lattice breaks inversion symmetry and is described by the space group $F\bar{4}3m$. In this family of materials, the size difference between the large and small tetrahedra is less than 10 %. Surprisingly, this modest difference leads to rather dramatic differences in the interactions within the large and small tetrahedra.

We have studied $\text{LiGaCr}_4\text{S}_8$, which has lengths in the large and small tetrahedra of $3.394(2)$ Å and $3.655(2)$ Å, respectively. Interestingly, we have found that $\text{LiGaCr}_4\text{S}_8$ is the first example of a breathing pyrochlore material which exhibits a region of negative thermal expansion. The magnetic behavior is also unusual, and we have found that magnetic correlations are apparent in neutron scattering data well above 100 K, consistent with theoretical calculations finding a large energy scale associated with magnetism. No long range order is observed, however, a broad transition at 12 K is observed in thermodynamic properties such as the magnetic susceptibility and specific heat. There is a corresponding increase in the static correlations and structure emerges in the spin excitation spectrum. However, no sharp phase transition is observed. We have modelled the elastic diffuse scattering with a Heisenberg Hamiltonian with two exchange interactions [5]. From this we determine that the exchange interactions within the small tetrahedra are antiferromagnetic while the interactions within the large tetrahedra are ferromagnetic. This work shows that dramatic changes in the exchange interactions should be expected for modest changes in the relative sizes of the small and large tetrahedra in Cr-based breathing pyrochlore materials.

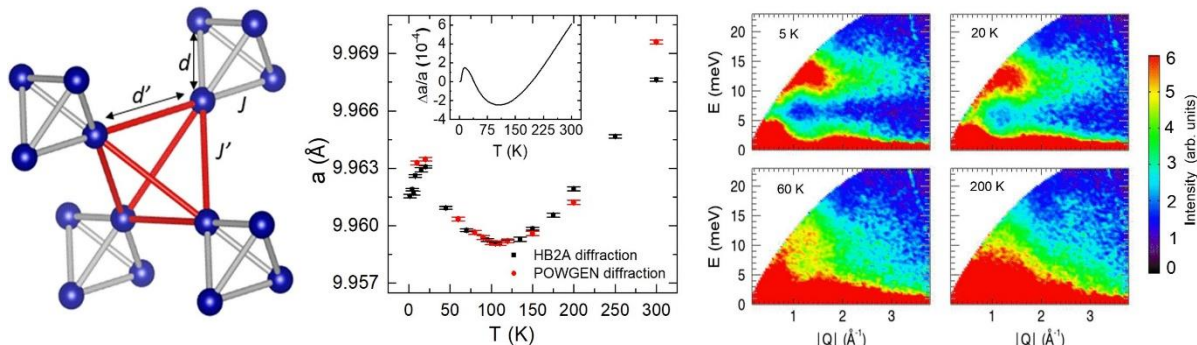


Figure 2. (Left) Breathing pyrochlore structure. $J(J')$ and $d(d')$ denote the nearest (next nearest) neighbor exchange and distances respectively. (Middle) Lattice parameter of $\text{LiGaCr}_4\text{S}_8$ as a function of temperature showing a region of negative thermal expansion from 100 to 10 K. (Right) Inelastic neutron scattering spectrum for $\text{LiGaCr}_4\text{S}_8$.

III. Topological Magnons

The Shastry-Sutherland lattice provides an important platform to study quantum magnetism [6] and has recently been shown to host nontrivial topological properties in the spin excitation spectrum [7]. $\text{BaNd}_2\text{ZnO}_5$ crystallizes in a layered tetragonal structure where the Nd^{3+} ions occupy well separated layers with a Shastry-Sutherland lattice geometry. Our studies of the crystal field

excitation spectrum indicate that the ground state magnetic order grows from a well-isolated Kramers doublet with a first excited state at 8 meV. Specific heat measurements indicate magnetic order at 1.6 K. Using neutron diffraction, we have determined that the magnetic structure is a two- Q structure that contains ferromagnetic dimers rather than the antiferromagnetic dimers in the canonical Shastry-Sutherland model. The spin Hamiltonian has been extracted from fits to the low energy excitation spectrum determined from inelastic neutron scattering measurements. The resulting Hamiltonian indicates that application of a magnetic field in combination with the Dzyaloshinskii-Moriya interaction will result in magnon bands with finite Chern number. This work shows that materials with a Shastry-Sutherland structural motif are a rich source for topological phenomena.

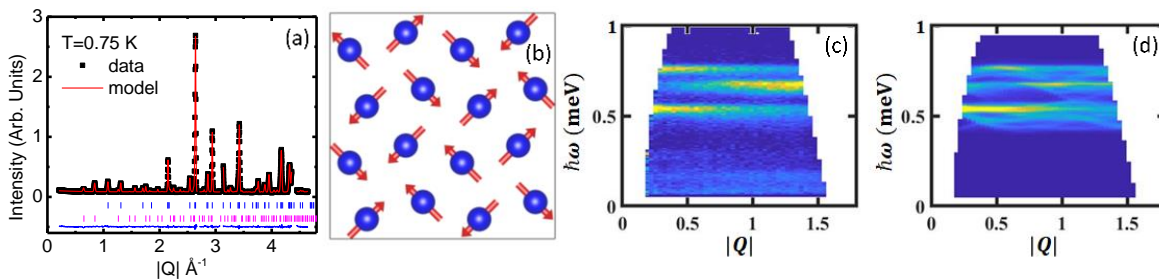


Figure 3. Neutron scattering data and models for $\text{BaNd}_2\text{ZnO}_5$. (a) Neutron diffraction pattern, (b) Magnetic structure of a Shastry-Sutherland layer. (c) Inelastic neutron scattering data at $T = 1.6$ K and (d) Model calculation of excitation spectra.

Future Plans

- Continue investigations of lattice geometries that have the potential for realizations of nontrivial magnon topologies.
- Investigate additional materials for the formation of novel spin textures in both insulating and metallic systems including both centrosymmetric and non-centrosymmetric unit cells.
- Study frustrated magnetism, particularly $5d$, $4d$, and $4f$ systems where strong spin-orbit coupling plays an important role.

References

- [1] M. A. McGuire, *Crystals* **7**, 121 (2017).
- [2] S.-Z. Lin, *et al.*, *Phys. Rev. Lett.* **116**, 187202 (2016).
- [3] L. Savary, *et al.*, *Phys. Rev. B* **94**, 075146 (2016).
- [4] F. Li, *et al.*, *Nature Communications* **7**, 12691 (2016).
- [5] O. Benton and N. Shannon, *J. Phys. Soc. Japan* **84**, 104710 (2015).
- [6] B. S. Shastry and B. Sutherland, *Physica (Amsterdam)* **108B**, 1069 (1981).
- [7] P. A. McClarty, *et al.*, *Nature Physics* **13**, pages 736–741 (2017).

Publications

- [7] Binod K. Rai, Andrew D. Christianson, David Mandrus, and Andrew F. May, “Influence of cobalt substitution on the magnetism of NiBr₂”, *Phys. Rev. Materials* **3**, 034005 (2019).
- [6] L. S. Wu, S. E. Nikitin, Z. Wang, W. Zhu, C. D. Batista, A. M. Tsvelik, A. M. Samarakoon, D. A. Tennant, M. Brando, L. Vasylechko, M. Frontzek, A. T. Savici, G. Sala, G. Ehlers, A. D. Christianson, M. D. Lumsden, and A. Podlesnyak, “Tomonaga-Luttinger Liquid Behavior and Spinon Confinement in YbAlO₃”, *Nature Comm.* **10**, 698 (2019).
- [5] J. G. Rau, L. S. Wu, A. F. May, A. E. Taylor, I-Lin Liu, J. Higgins, N. P. Butch, K. A. Ross, H. S. Nair, M. D. Lumsden, M. J. P. Gingras, and A. D. Christianson, “Behavior of the breathing pyrochlore lattice Ba₃Yb₂Zn₅O₁₁ in applied magnetic field”, *J. Phys.: Condens. Matter* **30**, 455801 (2018).
- [4] A. E. Taylor, R. Morrow, M. D. Lumsden, S. Calder, M. H. Upton, A. I. Kolesnikov, M. B. Stone, R. S. Fishman, A. Paramakanti, P. M. Woodward, A. D. Christianson, “Origin of magnetic excitation gap in double perovskite Sr₂FeOsO₆”, *Phys. Rev. B* **98**, 214422 (2018).
- [3] G. Sala, M. B. Stone, B. K. Rai, A. F. May, C. R. Dela Cruz, H. Suriya Arachchige, G. Ehlers, V. R. Fanelli, V. O. Garlea, M. D. Lumsden, D. Mandrus, and A. D. Christianson, “Physical properties of the trigonal binary compound Nd₂O₃”, *Phys. Rev. Materials* **2**, 114407 (2018). Selected as an Editor’s Suggestion.
- [2] Arun Paramakanti, David J. Singh, Bo Yuan, Young-June Kim, Andrew D. Christianson, “Spin-orbit coupled systems in the “atomic” limit: rhenates, osmates, iridates”, *Phys. Rev. B* **97**, 235119 (2018).
- [1] G. Pokharel, A. F. May, D. S. Parker, S. Calder, G. Ehlers, A. Huq, S. A. J. Kimber, H. S. Arachchige, L. Poudel, M. A. McGuire, D. Mandrus, A. D. Christianson, “Negative thermal expansion and magnetoelastic coupling in the breathing pyrochlore lattice material LiGaCr₄S₈”, *Phys. Rev. B* **97**, 134117 (2018).

**USING NEUTRON AS A PROBE TO STUDY MAGNETIC EXCITATIONS IN
STRONGLY CORRELATED ELECTRON MATERIALS**

**Professor Pengcheng Dai
Department of Physics and Astronomy**

**Rice University
Houston, Texas 77005**

<http://pdai.phys.rice.edu>

Phone: 865-607-8067, E-mail: pdai@rice.edu or pdai.utk@gmail.com

**DOE/Office of Science Program Office: Neutron Scattering
DOE/Office of Science Program Manager Contact: P. Thiyagarajan
Phone: (301) 903-9706, e-mail: p.thiyagarajan@science.doe.gov
DOE Grant Number: DE-SC00012311
Report covering period: 01/01/2017 till 06/01/2019**

Research Scope:

Understanding the interplay between magnetism and superconductivity continues to be a “hot” topic in modern condensed matter physics. The discovery of high-temperature superconductivity in iron-based materials in 2008 provided an unique opportunity to compare and contrast these materials with traditional high- T_c copper oxide superconductors. Neutron scattering plays an important role in determining the dynamical spin properties in these materials. This proposal is a continuation of A previous DOE supported proposal. Our primary research is divided into three parts: (1) An advanced materials synthesis program that grows high-quality large single crystals of quantum materials; (2) Transport, magnetic susceptibility, and heat capacity measurements to establish the basic physical properties of quantum materials, and investigating uniaxial strain-induced changes in transport and magnetic properties of quantum materials utilizing a specially designed uniaxial pressure device; and (3) A neutron scattering program utilizing the most innovative, sophisticated neutron scattering facilities worldwide to study the magnetic properties of quantum materials.

This report summarizes the progress we have made over the past 12 months from March 2018 till March 2019. Overall, we continue to carry out extensive neutron scattering experiments on Fe-based materials, focusing on understanding their magnetic properties. We have also investigated spin excitations in detwinned FeSe, the paper describing this result is published by Nature Materials. We are also starting a new direction in searching for new quantum spin liquid materials. Our first paper reporting discovery of quantum spin liquid candidate $Ce_2Zr_2O_7$ is accepted by Nature Physics.

In addition, our materials laboratory at Rice allowed us to grow new iron-based superconductors. Because neutron scattering typically demands a large amount of samples, by growing these materials in our own laboratory, we can now pursue neutron scattering experiments over the entire electronic phase diagram, focusing on regions of interests. The material synthesis laboratory at Rice was established mostly with the

support of DOE funding, and Welch foundation provided partial funding for our materials efforts at Rice. This not only allowed us to carry out neutron scattering experiments, but also permit us to provide samples to other US/International collaborators for studying these materials. Our papers are cited on average about 800 times per year. Over the past year, we have made significant progress in our understanding of the magnetic properties in Fe-based superconductors. In the following, we summarize key research progress made over the past 12 month.

Recent progress:

Dynamic Spin-Lattice Coupling and Nematic Fluctuations in NaFeAs

We use inelastic neutron scattering to study acoustic phonons and spin excitations in single crystals of NaFeAs, a parent compound of iron-pnictide superconductors. NaFeAs exhibits a tetragonal-to-orthorhombic structural transition at $T_s \approx 58$ K and a collinear antiferromagnetic order at $T_N \approx 45$ K. While longitudinal and out-of-plane transverse acoustic phonons behave as expected, the in-plane transverse acoustic phonons reveal considerable

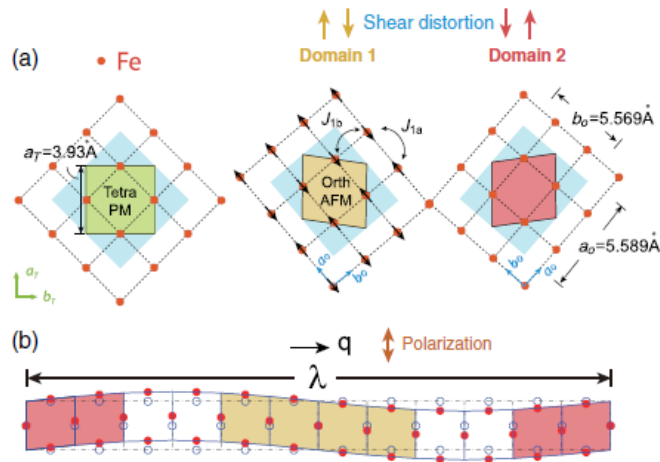


Fig. 1 Acoustic phonons relevant to the spin-lattice coupling in NaFeAs. We have discovered a new spin-lattice coupling mechanism for iron based superconductors.

softening on cooling to T_s and then harden on approaching T_N before saturating below T_N . In addition, we find that spin-spin correlation lengths of low-energy magnetic excitations within the FeAs layer and along the c axis increase dramatically below T_s and show a weak anomaly across T_N . These results suggest that the electronic nematic phase present in the paramagnetic tetragonal phase is closely associated with dynamic spin-lattice coupling, possibly arising from the one-phonon-two-magnon mechanism. [Summary paper: Y. Li et al., Phys. Rev. X 8, 021056 (2018).]

Local orthorhombic lattice distortions in the paramagnetic tetragonal phase of superconducting NaFe_{1-x}Ni_xAs

Understanding the interplay between nematicity, magnetism and superconductivity is pivotal for elucidating the physics of iron-based superconductors. Here we use neutron scattering to probe magnetic and nematic orders throughout the phase diagram of NaFe_{1-x}Ni_xAs, finding that while both static antiferromagnetic and nematic orders compete with superconductivity, the onset temperatures for these two orders remain well

separated approaching the putative quantum critical points. We uncover local orthorhombic distortions that persist well above the tetragonal-to-orthorhombic structural transition temperature T_s in underdoped samples and extend well into the overdoped regime that exhibits neither magnetic nor structural phase transitions. These unexpected local orthorhombic distortions display Curie–Weiss temperature dependence and become suppressed below the superconducting transition temperature T_c , suggesting that they result from the large nematic susceptibility near optimal superconductivity. Our results account for observations of rotational symmetry breaking above T_s , and attest to the presence of significant nematic fluctuations near optimal superconductivity. [Summary papers: *Nat. Comm.* **9**, 3128 (2018).]

Anisotropic spin fluctuations in detwinned FeSe

Superconductivity in FeSe emerges from a nematic phase that breaks four-fold rotational symmetry in the iron plane. This phase may arise from orbital ordering, spin fluctuations or hidden magnetic quadrupolar order. Here we use inelastic neutron scattering on a mosaic of single crystals of FeSe, detwinned by mounting on a BaFe_2As_2 substrate to demonstrate that spin excitations are most intense at the antiferromagnetic wave vectors $Q_{\text{AF}} = (\pm 1, 0)$ at low energies $E = 6\text{--}11$ meV in the normal state. This two-fold (C_2) anisotropy is reduced at lower energies, 3–5 meV, indicating a gapped four-fold (C_4) mode. In the superconducting state, however, the strong nematic anisotropy is again reflected in the spin resonance ($E = 3.6$ meV) at Q_{AF} with incommensurate scattering around 5–6 meV. Our results highlight the extreme electronic anisotropy of the nematic phase of FeSe and are consistent with a highly anisotropic superconducting gap driven by spin fluctuations. [Summary papers: *Nature Materials* <https://doi.org/10.1038/s41563-019-0369-5> (2019).]

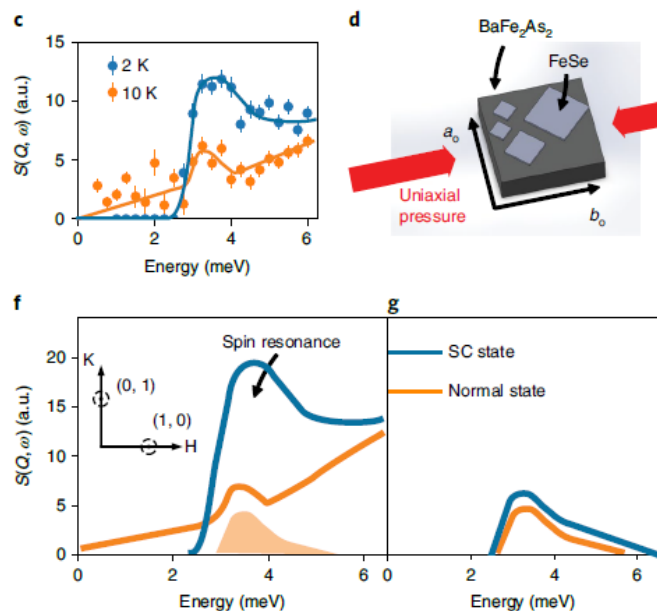


Fig. 2 Energy dependence of the spin excitations below and above T_c in detwinned FeSe.

Experimental signatures of a three-dimensional quantum spin liquid in effective spin-1/2 $\text{Ce}_2\text{Zr}_2\text{O}_7$ pyrochlore

A quantum spin liquid (QSL) is a state of matter where unpaired electrons' spins, although being entangled, do not show magnetic order even at the zero-temperature. Their realization is a long-sought goal in condensed matter physics. Although neutron scattering experiments on the two-dimensional (2D) spin-1/2 kagome-lattice $\text{ZnCu}_3(\text{OD})_6\text{Cl}_2$ and triangular lattice YbMgGaO_4 have found evidence for the hallmark of a QSL at very low temperature - a continuum of magnetic excitations, the presence of magnetic and nonmagnetic site chemical disorder complicates the interpretation of the data. Recently, the three-dimensional (3D) Ce^{3+} pyrochlore lattice $\text{Ce}_2\text{Sn}_2\text{O}_7$ has been suggested as a clean, effective spin-1/2 QSL candidate, but the evidence of a spin excitation continuum is still missing. Here we use

thermodynamic, muon spin relaxation (μSR), and neutron scattering experiments on single crystals of $\text{Ce}_2\text{Zr}_2\text{O}_7$, a compound isostructural to $\text{Ce}_2\text{Sn}_2\text{O}_7$, to demonstrate the absence of magnetic ordering and the presence of a spin excitation continuum at 35 mK. With no evidence of oxygen deficiency and magnetic/nonmagnetic ion disorder seen by neutron diffraction and diffuse scattering measurements, $\text{Ce}_2\text{Zr}_2\text{O}_7$ may be a 3D pyrochlore lattice QSL material with minimum magnetic and nonmagnetic chemical disorder. [Summary papers: *Nature Physics: in the press* (2019).]

Future plans:

In the upcoming funding period, we will continue to work on iron based superconductors with a focus on FeSe and RbFe_2As_2 family of materials. One unresolved issue is the role of electronic nematic phase to the microscopic origin of superconductivity. We will also move a part of our focus away from iron based superconductors and move to frustrated materials. For initial experiment, we will focus on $\text{Ce}_2\text{Zr}_2\text{O}_7$ family of materials. In addition to pure $\text{Ce}_2\text{Zr}_2\text{O}_7$, we will grow $\text{Ce}_2\text{Zr}_{2-x}\text{Ce}_x\text{O}_7$ and $\text{Ce}_{2-x}\text{Zr}_x\text{Zr}_2\text{O}_7$ to test how magnetic and nonmagnetic impurities will affect the observed spin excitation continuum. We will grow and test other classes of spin frustrated materials, focusing on most honeycomb lattice materials. This will be the new scheme for our renew efforts at DOE next year.

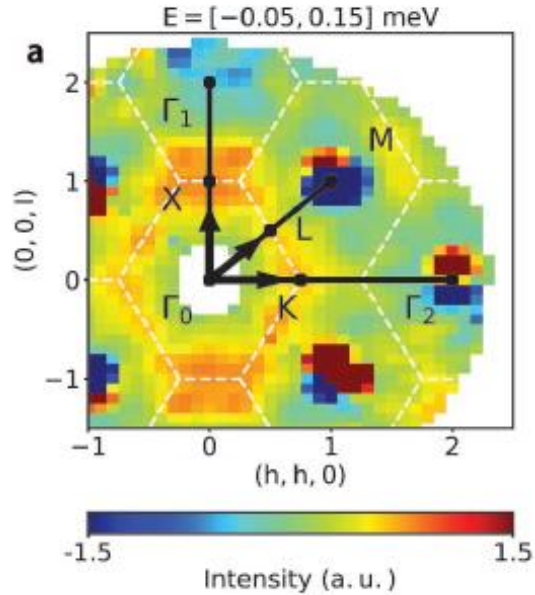


Fig. 3 Summary of spin excitation continuum seen near the elastic line of $\text{Ce}_2\text{Zr}_2\text{O}_7$ at 35 mK.

Journal publications from January 2017 till June 2019:

1. G. T. Tan et al. Phys. Rev. B 95, 054501 (2017).
2. Haoran Man et al., npj Quantum Materials 2, 14 (2017).
3. Zhi-Guo Chen et al., Phys. Rev. Lett. 119, 096401 (2017).
4. Weiyi Wang et al., Phys. Rev. B 95, 094519 (2017).
5. W. J. Gannon et al., Phys. Rev. B 96, 041111(R) (2017).
6. Haoran Man et al., Phys. Rev. B 96, 100406(R) (2017).
7. Yu Song et al., Phys. Rev. B 96, 184512 (2017).
8. A. Charnukha et al., Phys. Rev. B 96, 195121 (2017).
9. Yu Song et al., Phys. Rev. B 97, 024519 (2018).
10. J. Pellicairi et al., Sci. Rep. 7, 8003 (2017).
11. Yu Li et al. Phys. Rev. X 8, 021056 (2018).
12. Z. H. Liu et al, App. Phys. Lett. 112, 232602 (2018).
13. S. C. Cheung et al., Phys. Rev. B 97, 224508 (2018).
14. W. Y. Wang et al., Nat. Comm. 9, 3128 (2018).
15. Y. Song et al., Phys. Rev. B 98, 064507 (2018).
16. W.L. Zhang et al., Phys. Rev. B 98, 094512 (2018).
17. S. J. Zhang et al., Phys. Rev. B 98, 224507 (2018).
18. B. K. Rai et al., Phys. Rev. X 8, 041047 (2018).
19. B. K. Rai et al., Phys. Rev. B 99, 085120 (2019).
20. Y.Z. Xin et al. Phys. Rev. B 99, 155114 (2019).
21. C.W. Chen et al. Phys. Rev. B 99, 144423 (2019).
22. T. Chen et al., Nature Materials, <https://www.nature.com/articles/s41563-019-0369-5> (2019).
23. B. Gao et al. Nature Physics (in press)

Quasiparticle Couplings in Transport of Heat, Charge, and Spin for Novel Energy Materials

Olivier Delaire

Mechanical Engineering and Materials Science & Physics, Duke University, Durham, NC

Program Scope

This program focuses on elucidating the couplings between microscopic degrees-of-freedom of atomic vibrations, spins, and electrons, which underpin heat, charge, and spin transport in novel energy materials. Understanding the microscopic processes involved in the transport and conversion of energy from the atomic-scale to the meso-scale is critical for the development of next-generation materials for energy sustainability. At a microscopic level, these couplings result from anharmonic phonon-phonon interactions, and interaction of phonons with electrons or spin degrees of freedom, which can lead to hybrid excitations. This project investigates these quasiparticle interactions, how hybrid quasiparticles form or break down, and their consequences on transport properties. We use state-of-the-art neutron and x-ray scattering techniques, optical spectroscopy, synthesis and transport measurements, and first-principles computer simulations.

Recent Progress

Momentum-resolved observations of the phonon instability driving geometric improper ferroelectricity in yttrium manganite: We investigated the detailed mechanism of the improper ferroelectric (FE) transition in the archetypal improper ferroelectric (and multiferroic) YMnO_3 [1,2]. We obtained direct experimental and theoretical evidence of an unstable zone-boundary (K-point) phonon driven FE transition and its coupling to a zone-center polar mode, leading to a gradual increase in polarization [1,3]. We tracked the condensation of a precursor phonon instability at the zone-boundary, acting as primary order parameter, and resulting in the formation of a trimerized unit cell at the FE transition temperature, $T_{\text{FE}} \sim 1260$ K. Our detailed study explains the unusual T-dependence of the polarization [3], based on the strongly T-dependent lattice dynamics and coupling strength of anharmonically coupled zone-boundary unstable phonon and zone-center stable, polar distortions. This microscopic picture differs from proper FE with second-order phase transitions. Our results demonstrate how experimental measurements of atomic structure and lattice dynamics combined with first-principles simulations including anharmonic effects provide a comprehensive

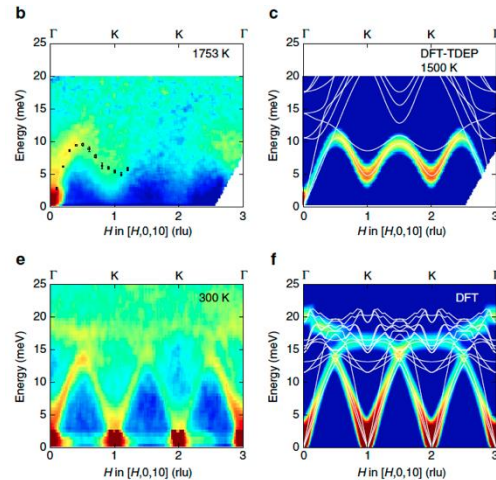


Fig. 1 Dynamics and condensation of the K3 distortion across ferroelectric transition in YMnO_3 . Phonon $\chi''(\mathbf{Q}, E)$ along $[H,0,10]$ measured at $T = 1753\text{K}$ (b) and 300K (e) are compared with $\chi''(\mathbf{Q}, E)$ intensity calculated from DFT for 1500K (c) and 0K (f) (white lines in are the calculated dispersions). [Pub6]

understanding of lattice instabilities driving novel ferroelectric transitions. This study was published in Nature Communications [Pub6].

Atomic dynamics in CuCrSe₂ across its superionic transition: We performed neutron and x-ray

scattering studies combined with first-principles calculations of the superionic compound CuCrSe₂. Our results showed that long-wavelength acoustic phonons capable of heat conduction remain largely intact in the superionic phase, whereas specific phonon quasiparticles for low-energy optical branches, dominated by motions of Cu ions, break down as a result of anharmonicity and disorder. Our measurements investigated both oscillatory

atomic vibrations (phonons) and relaxational atomic dynamics characteristic of diffusive hopping. Anharmonicity introduces a damping mechanism for phonon states, via phonon-phonon interactions, and characteristic broadening of phonon spectral functions, increasing with temperature. INS and IXS measurements proved highly complementary for studying phonons in this compound. QENS probed the dynamics of ion diffusion (~GHz), complementing our measurements of THz lattice dynamics with INS and IXS, as shown in Fig. 2. Further, we analyzed our INS and QENS data by performing ab initio MD simulations, which provide detailed insights into the complex atomic dynamics and its evolution across the superionic transition. This study was published in Nature Physics [pub1].

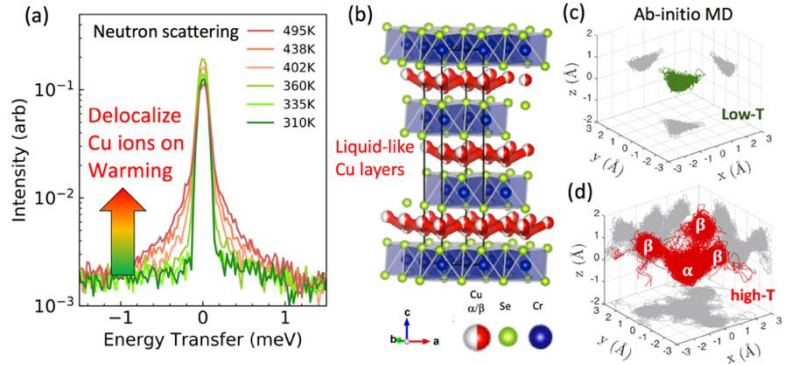


Fig. 2 (a) Quasi-elastic neutron scattering signal showing delocalization of Cu ions with increasing temperature. (b) Layered structure of CuCrSe₂, showing liquid-like Cu layers in superionic phase above 365K. (c,d) Ab-initio MD calculations of Cu ion trajectory, showing hopping across α and β sites at high T (adapted from [pub1]).

Phonons in VO₂ across the metal-insulator transition:

Following on our previous INS and IXS investigations of phonons in VO₂ [4], we performed x-ray scattering measurements (including ultrafast time-resolved diffuse x-ray scattering at LCLS) and first-principles simulations of phonons in VO₂, focusing on both the thermal transport properties and the mechanism of the photo-induced phase transitions. The thermal transport studies showed little change in thermal conductivity across the metal-insulator transition, resulting in a significant deviation from the Wiedemann-Franz law in the metallic phase [pub10]. The

LCLS diffuse x-ray scattering measurements and ab-initio MD simulations revealed an ultrafast (<150 fs) disruption and disordering of V dimers upon photoexcitation, with a lack of coherence

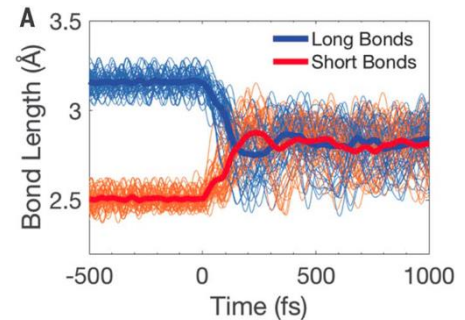
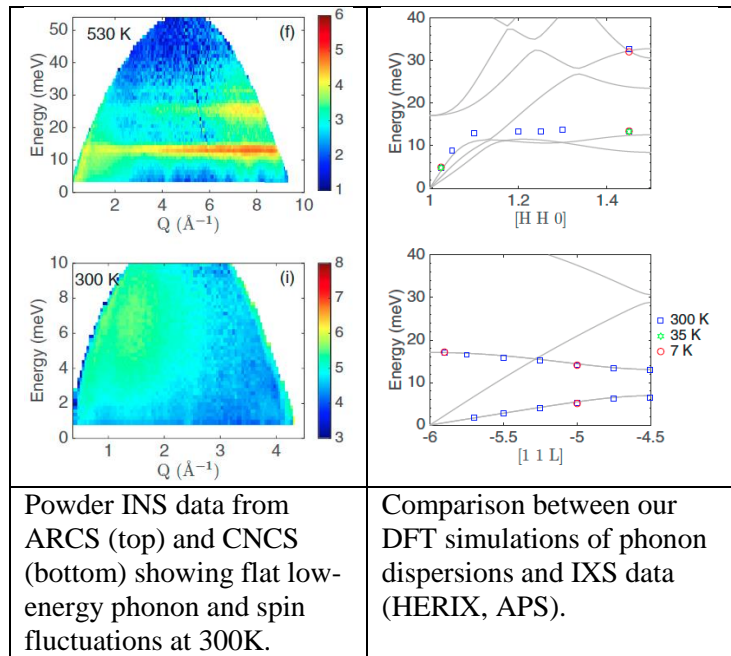


Fig. 3 Time evolution of V-V dimer bond lengths in photoexcited VO₂ predicted with AIMD (laser pulse at t=0fs). [pub4].

across unit cells, manifested via a broad diffuse signature, and rationalized via the ultrafast change in bonding as seen in our AIMD simulations (Fig. 3). These studies on VO₂ have led to two manuscripts published in Science [pubs 4,10].

Lattice dynamics, thermal transport, and coupling to magnetic fluctuations in delafossite multiferroic CuCrO₂: Understanding the interplay of phonons and spin dynamics is critical to the development of novel multiferroics, and for controlling thermal transport in spin-caloritronics. While the spin excitations have been mapped with neutron scattering in multiferroic CuCrO₂, no phonon dispersion measurements have been previously reported [5-8]. We have performed momentum-resolved studies of the phonon dispersions and density of states (DOS) in CuCrO₂ using INS and IXS. In addition, transport measurements have revealed a strong coupling between phonons and spin-fluctuations in this geometrically frustrated structure (antiferromagnetic triangular lattice). The determination of dispersions and their behavior as function of temperature was key to isolate the respective contributions of phonons and spin fluctuations to thermal transport. We found little effect of magnetic ordering at T_N=24K on the phonon energies, despite the elastic signature reported from ultrasound measurements. On the other hand, our INS data clearly revealed spin fluctuations persisting above 300K, and our modeling of thermal conductivity showed that phonons are strongly scattered by these spin fluctuations. We performed first-principles simulations of phonon dispersions and DOS with density functional theory (DFT), and found very good agreement with our measurements. Published in Phys. Rev. B [Pub9].



Neutron and x-ray scattering study of phonon dispersion and diffuse scattering in (Na,Bi)TiO₃-xBaTiO₃ single crystals near the morphotropic phase boundary: Neutron and x-ray scattering measurements were performed on (Na_{1/2}Bi_{1/2})TiO₃-x at%BaTiO₃ (NBT-xBT) single crystals (x = 4, 5, 6.5, and 7.5) across the morphotropic phase boundary (MPB), as a function of both composition and temperature, and probing both structural and dynamical aspects. In addition to the known diffuse scattering pattern near the G points, our measurements revealed new, faint superlattice peaks, as well as an extensive diffuse scattering network, revealing a short-range ordering of polar nanoregions (PNR) with a static stacking morphology. In samples with compositions closest to the MPB, our INS investigations of the phonon dynamics showed two

unusual features in the acoustic phonon branches, between the superlattice points, and between the superlattice points and M/R points, respectively. These elements are not present in the other compositions away from the MPB, which suggests that these features may be related to the tilt modes coupling behavior near the MPB. A manuscript was published in Phys. Rev. B [Pub11].

Future Plans

This Early Career Award project will come to a close in 2019. A new project “Neutron scattering studies of phonon anharmonicity and coupling with spin and charge degrees of freedom” will focus on the following areas of research. A first thrust will focus on structural transitions associated with soft-modes, especially in ferroelectric and multiferroics. This thrust focuses on the mechanism of the instabilities based on the anharmonic lattice dynamics, their origins in terms of electronic structure, and coupling with magnetic degrees of freedom. In particular, we will investigate SrTiO₃, EuTiO₃, and RMnO₃ compounds. A second thrust will investigate how phonons and magnons both contribute to thermal transport, and how transport can be rationalized based on a full microscopic characterization of phonon/magnon dispersions and linewidths with INS/IXS. Further, the coupling between spin and lattice, and scattering between phonons and magnons will also be modeled based on first-principles simulations. In particular, we will perform investigations of MnO, yttrium-iron garnet (YIG), and FeS, for which our preliminary experimental data and simulations show interesting effects.

References

- [1] Fennie, C. J. & Rabe, K. M., Phys. Rev. B 72, 100103(R) (2005).
- [2] Spaldin, N. A. & Fiebig, M., Science 309, 391–392 (2005).
- [3] M. Lilienblum et al., Nat. Phys. 11, 1070–1073 (2015).
- [4] J. D. Budai, J. W. Hong, M. E. Manley, E. D. Specht, C. W. Li, J. Z. Tischler, D. Abernathy, A. H. Said, B. M. Leu, L. A. Boatner, R. J. McQueeney, and O. Delaire, Nature 515, 535 (2014).
- [5] M. Poirier, *et. al.* Phys. Rev. B. 81, 104411 (2010).
- [6] K. Kimura, *et. al.* Phys. Rev. Lett. 103, 107201 (2009).
- [7] O. Aktas, *et. al.* J. Phys. Condens. Matter 24, 036003 (2012).
- [8] T. Okuda, *et. al.* J. Phys. Soc. Japan, 82, 014706 (2013).

Publications

- [pub1] J. L. Niedziela, D. Bansal, A. F. May, J. Ding, T. Lanigan-Atkins, G. Ehlers, D. L. Abernathy, A. Said & O. Delaire, “Selective Breakdown of Phonon Quasiparticles across Superionic Transition in CuCrSe₂”, Nature Physics, 15, 73–78 (2019).
- [pub2] J.C. Leiner, H.O. Jeschke, R. Valenti, S. Zhang, A.T. Savici, J. Lin, M.B. Stone, M.D. Lumsden, J. Hong, O. Delaire, W. Bao, C.L. Broholm, “Frustrated magnetism in Mott insulating (V_{1-x}Cr_x)₂O₃”, Physical Review X 9, 011035 (2019).

[pub3] Jiawang Hong and Olivier Delaire “Electronic Instability and Anharmonicity in SnSe”, *Materials Today Physics*, *in press* (2019).

[pub4] S. Wall*†, S. Yang,* L. Vidas, M. Chollet, M. Glowia, M. Kozina, T. Katayama, T. Henighan, M. Jiang, T. A. Miller, D. A. Reis, L. Boatner, O. Delaire† and Mariano Trigo†, “Ultrafast disordering of vanadium dimers in photoexcited VO₂”, *Science* 362, pp. 572-576 (2018) (* equal contrib., † co-corresponding authors).

[pub5] K. Liu, S. Lee, S. Yang, O. Delaire, J. Wu, “Recent progress on physics and applications of vanadium dioxide”, *Materials Today*, 1369, 7021 (2018).

[pub6] D. Bansal, J. L. Niedziela, R. Sinclair, V. O. Garlea, D. L. Abernathy, S. Chi, Y. Ren, H. Zhou, and O. Delaire, “Momentum-resolved observations of the phonon instability driving geometric improper ferroelectricity in yttrium manganite”, *Nature Communications* 9, 15 (2018).

[pub7] P. Jain, D. Bansal, G. Sharma, A. Bhattacharya, B. Ingale, O. Delaire, and R. Chatterjee, “Observation of low temperature metastable states in complex CaMn₇O₁₂”, *J. Phys.: Condens. Matter* 30, 075801 (2018).

[pub8] S. Muy, J. C. Bachman, L. Giordano, H.-H. Chang, D. L. Abernathy, D. Bansal, O. Delaire, S. Hori, R. Kanno, F. Maglia, S. Lupart, P. Lamp, and Y. Shao-Horn, “Tuning mobility and stability of lithium ion conductors based on lattice dynamics”, *Energy Environ. Sci.* **11**, 850 (2018).

[pub9] D. Bansal, J. L. Niedziela, A. F. May, A. Said, G. Ehlers, D. L. Abernathy, A. Huq, M. Kirkham, H. Zhou, and O. Delaire, “Lattice dynamics and thermal transport in multiferroic CuCrO₂”, *Phys. Rev. B* **95**, 054306 (2017).

[pub10] S. Lee, K. Hippalgaonkar, F. Yang, J. Hong, C. Ko, J. Suh, K. Liu, K. Wang, J. J. Urban, X. Zhang, C. Dames, S. A. Hartnoll, O. Delaire†, J. Wu†, “Anomalously low electronic thermal conductivity in metallic vanadium dioxide”, *Science*, 355 (6323): 371 (2017).

[pub11] C. Luo, D. Bansal, J. Li, D. Viehland, B. Winn, Y. Ren, X. Li, H. Luo, and O. Delaire, “Neutron and x-ray scattering study of phonon dispersion and diffuse scattering in (Na,Bi)TiO₃-xBaTiO₃ single crystals near the morphotropic phase boundary”, *Phys. Rev. B* 96, 174108 (2017).

[pub12] S. Mukhopadhyay, D. Bansal, O. Delaire, D. Perrodin, E. Bourret-Courchesne, D. J. Singh, and L. Lindsay, “The curious case of cuprous chloride: Giant thermal resistance and anharmonic quasiparticle spectra driven by dispersion nesting”, *Phys. Rev. B* 96, 100301(R) (2017).

LaCNS: Building Neutron Scattering Infrastructure in Louisiana for Advanced Materials

J. F. DiTusa¹ (ditusa@phys.lsu.edu), D. Zhang², R. Jin¹, J. Zhang¹, W. A. Shelton³, V. T. John⁴, R. Kumar², Z. Q. Mao⁵, E. Nesterov², E. W. Plummer¹, S. W. Rick⁶, G. J. Schneider², D. P. Young¹, I. Vekhter¹, J.W. Sun⁵, W. Xei², J. A. Dorman³, B. Bharti³, M. Khonsari⁷

¹*Department of Physics and Astronomy, Louisiana State University, Baton Rouge, LA 70803*

²*Department of Chemistry, Louisiana State University, Baton Rouge, LA 70803*

³*Department of Chemical Engineering, Louisiana State University, Baton Rouge, LA 70803*

⁴*Dept. of Chem. and Biomolecular Engineering, Tulane University, New Orleans, LA 70118*

⁵*Department of Physics and Engineering Physics, Tulane University, New Orleans, LA 70118*

⁶*Department of Chemistry, University of New Orleans, New Orleans, LA 70148*

⁷*Louisiana Board of Regents, Baton Rouge, LA 70821*

Program Scope: This DOE EPSCoR / LA Board of Regents program aims to build neutron scattering infrastructure capable of treating both soft and hard materials. Our objectives include: discovery of the coupling of degrees of freedom that determine the emergent properties of complex materials, training of talented students in synthesis and neutron scattering techniques who will become the next generation of neutron users; and building a base of users of SNS and HFIR.

The scientific focus of this program is explore emergent complex materials with guided-design of materials in mind. Our goal is to tune dominant couplings to enhance critical properties in order to derive new functionality. In the hard materials we focus on non-centrosymmetric and chiral magnetic materials where topologically non-trivial magnetic structures can be found, complex Dirac systems and Dirac materials where magnetic ordering likely leads to the formation of Weyl semimetal states, and transition metal oxides where the coupling of electronic, magnetic, phononic, and orbital degrees of freedom lead to novel behaviors. In the soft materials we explore the role of secondary interactions in determining the structural and dynamic properties of polymeric systems.

Recent Progress

I include examples of projects that demonstrate the progress we have recently achieved. These include investigations of electronic and magnetic topological materials and the investigation of tunable charged soft colloids where we make use of peptoid amphiphiles as a model system.

According to electronic structure calculations [1], PdSb₂ (Pyrite-type structure (space group $Pa\bar{3}$)) is a candidate for hosting 6-fold-degenerate exotic fermions with a degeneracy stabilized by the non-symmorphic symmetry. Unlike linearly dispersing Dirac and Weyl bands, the electronic structure of PdSb₂ displays a quadratic dispersion at the 6-fold degenerate R point [Fig. 1b]. For the first time, we have grown crystals and characterized the physical properties of PdSb₂. We find metallic behavior with indications of a Fermi-liquid ground state. Surprisingly, an unusually large

transverse magneto-resistance is found that obeys Kohler's law indicating that a single band dominates the charge transport. To directly probe the electronic structure of PdSb₂, we have measured the de Haas-van Alphen (dHvA) effect apparent in our magnetization measurements in fields as low as 3 T [Fig. 1a, c, d]. The result is the identification of a single band having a dHvA frequency of 102 T, and a mass of $m^* = 0.045m_0$ (m_0 is free electron mass). A Landau fan diagram is constructed for this frequency yielding a non-trivial Berry phase of $\Phi_{\text{Berry}} = 0.58 \cdot 2\pi \sim 1.16\pi$, suggesting a topological nontrivial electronic structure. Remarkably, we discovered a superconducting transition for pressures, $p > 41$ GPa. Our discovery of nearly massless electrons with nontrivial Berry phase and superconductivity in PdSb₂ offers a unique system for investigating metals with unusual topology [2].

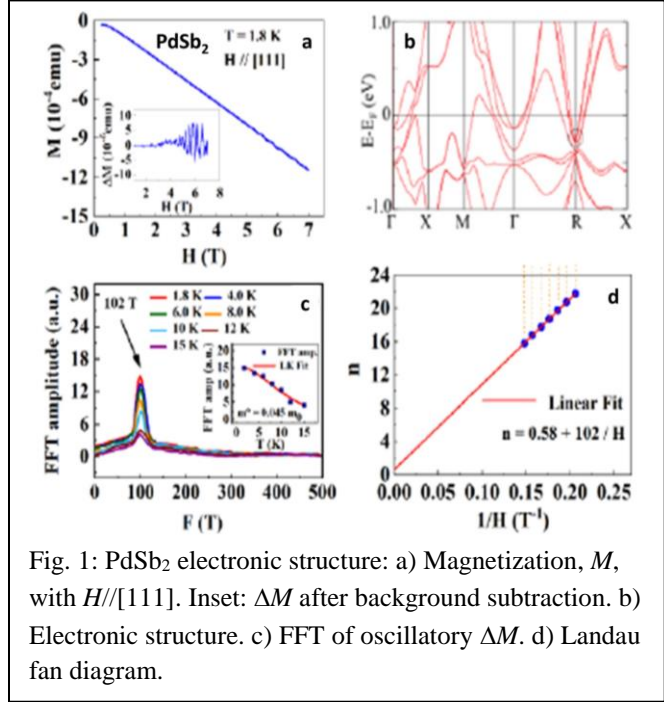


Fig. 1: PdSb₂ electronic structure: a) Magnetization, M , with $H//[111]$. Inset: ΔM after background subtraction. b) Electronic structure. c) FFT of oscillatory ΔM . d) Landau fan diagram.

We have synthesized high quality crystals and explored the magnetic, thermodynamic, and charge transport properties of Mn_{1/3}NbS₂, which forms in a chiral hexagonal structure (space group $P6_322$) [inset of Fig. 2d]. The motivation comes from the recent discovery of a magnetic soliton lattice in isostructural Cr_{1/3}NbS₂[3]. Mn_{1/3}NbS₂ displays a magnetic transition at $T_C = 45$ K with a highly anisotropic magnetization and a significant magnetic entropy surviving to $T \ll T_C$ unlike what was observed in Cr_{1/3}NbS₂ [4]. Small angle neutron scattering (SANS) [Fig. 2a] and neutron diffraction revealed a disordered helical state with a small wave-vector, q , parallel to the hexagonal c -axis with magnetic moments lying in the ab -plane. This long period helical state is confirmed by preliminary Lorentz Force TEM (LTEM) [Fig. 2c] taken at 12 K, which also displays variations in the period. The LTEM contrast is found only below 25 K indicating significant disorder or dynamics for $T > 0.5T_C$. The ac magnetic susceptibility [Fig. 2 b and d] displays significant low field structure for $T < T_C$, including a sharply peaked imaginary

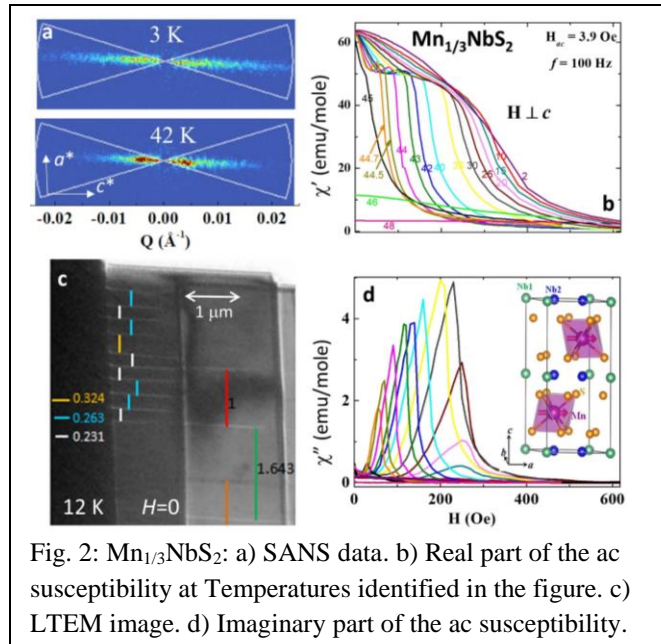


Fig. 2: Mn_{1/3}NbS₂: a) SANS data. b) Real part of the ac susceptibility at Temperatures identified in the figure. c) LTEM image. d) Imaginary part of the ac susceptibility.

component which subsides at low T . In addition, we observe significant temperature variation in the SANS data over the same range of T . These data reveal a much richer, and perhaps more dynamic, magnetic behavior in $\text{Mn}_{1/3}\text{NbS}_2$ than was discovered in $\text{Cr}_{1/3}\text{NbS}_2$ [5].

Non-covalent interactions play important roles in the structure and dynamics of complex soft matter. Understanding the contribution and coupling effects of these interactions in the structural outcome is important towards the development of design rules for advanced soft materials with tailorable properties. Here, we investigated how sequence-encoded electrostatic interactions

influence the solution structure of ionic peptoid amphiphiles in water. The peptoids are a model system due to our ability to control precisely the monomer sequence and discrete chain length. In addition, the absence of hydrogen bonding and secondary structures render it possible to reveal unambiguously the effects of sequence-encoded charge-charge interactions on the structure. Specifically, we have designed and synthesized a series of amphiphilic peptoid diblock

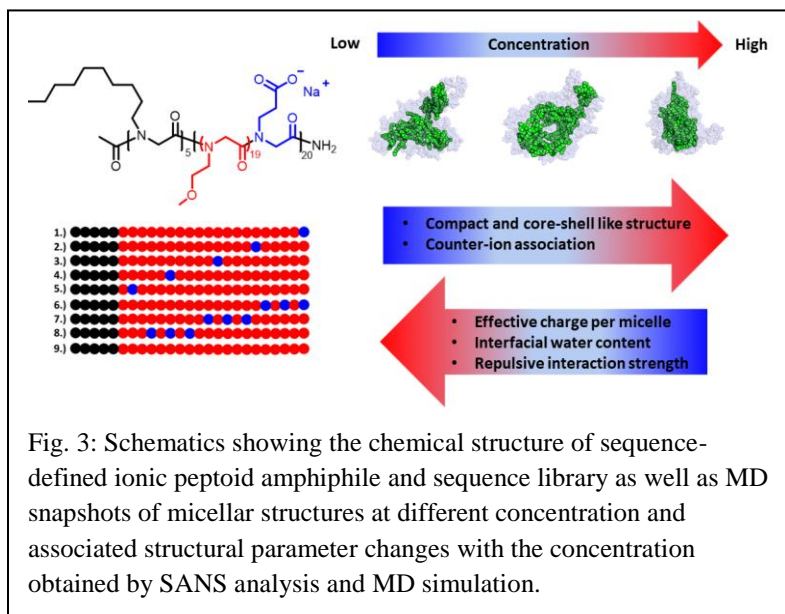


Fig. 3: Schematics showing the chemical structure of sequence-defined ionic peptoid amphiphile and sequence library as well as MD snapshots of micellar structures at different concentration and associated structural parameter changes with the concentration obtained by SANS analysis and MD simulation.

copolymer comprised of 5 hydrophobic monomer and 20 hydrophilic monomers (Fig. 3). Out of the 20 hydrophilic monomers, 1 or 3 monomers bear negatively charged carboxyl sidechains whereas the remaining 19 or 17 have polar and charge-neutral oligomeric ethylene glycol sidechains. Their solution self-assembly in aqueous solution was investigated by a combination of CryoTEM, DLS, SANS methods and MD simulations. Under dilute conditions at pH=9, the peptoid amphiphiles form micelles whose structures are strongly dependent on the position and number of charged monomers in the chain [6]. The structural parameters of the micelles (e.g., aggregation number, micellar size, R_g , interfacial areal density per chain, etc.) are correlated to the position of the charged groups by scaling relationships. MD simulation and SANS analysis both revealed an inward mass relocation as the charged monomers are positioned increasingly close to the hydrophobic segment along the chain. MD simulations have revealed the preferential location of the charged monomers on the micellar surface to maximize their solvation resulting in a systematic deviation of the micelles from a classical spherical and core-shell like structure [7]. Increasing concentration results in the micelles steadily approaching a more compact core-shell like structure. In addition, increasing concentration results in the reduction of interfacial water content, increased counter-ion association, and decreased repulsive potentials. These results have highlighted the potential to control the structures of ionic molecular assemblies or possibly other ionic soft matters by judiciously positioning the charged monomers along the

chain without changing the chemical composition, adding a new tool for the design of ionic soft materials for advanced applications.

Future Plans

We will continue to develop a neutron-centric program in Louisiana in hard and soft materials. Several seed projects headed by assistant professors are funded and we continue to hire young scientists that make use of neutrons in their research. The hard matter program now focuses on quantum materials including topological electronic and magnetic systems. Areas of emphasis include the synthesis and exploration of materials that are thought to host free fermionic excitations with no high-energy counterparts due to the symmetry of their crystal structures. We will explore the consequences of these particle types on the electronic structure and physical properties. Our effort to identify and characterize magnetic Weyl systems will be expanded to make use of chemical substitutions to stimulate magnetic ordering. In addition, the exploration of chiral and non-centrosymmetric magnetic materials will be extended to materials from other crystal families to explore the variety of spin textures that can be discovered and controlled. For the polypeptoid research, we will be developing methods for the investigation of polymer synthesis at the neutron beam line; Lab-on-an Instrument. That is, we will work to create a chemistry lab on the neutron instruments to investigate reaction-driven self-assembly in complex fluids. The goal is to explore the structural and dynamic evolution of hierarchical self-assembly resulting from the complex interplay between secondary (non-covalent) interactions and primary (covalent) interactions in a reactive system. The complex nature of the multi-length-scale experimental system requires a combined approach: synthesis of well-characterized model systems, neutron scattering to identify the structural features, and simulations to suggest which interactions determine the morphology.

References

- [1] B. Bradlyn, J. Cano, Z. Wang, M. G. Vergniory, C. Felser, R. J. Cava, and B. A. Bernevig, *Science* **353**, aaf5037 (2016).
- [2] R. Chapai, Y. Jia, W. A. Shelton, R. Nepal, M. Saghayezhian, J. F. DiTusa, E. W. Plummer, and R. Jin, *Phys. Rev. B (Rapid Comm.)* **99**, 161110 (2019).
- [3] Y. Togawa, T. Koyama, K. Takayanagi, S. Mori, Y. Kousaka, J. Akimitsu, S. Nishihara, K. Inoue, A. S. Ovchinnikov, and J. Kishine, *Phys. Rev. Lett.* **108**, 107202 (2012).
- [4] N. J. Ghimire, M. A. McGuire, D. S. Parker, B. Sipos, S. Tang, J.-Q. Yan, B. C. Sales, and D. Mandrus, *Phys. Rev. B* **87**, 104403 (2013).
- [5] S. K. Karna, F. N. Womack, R. Chapai, D. P. Young, M. Marshall, Weiwei Xie, D. Graf, Yan Wu, Huibo Cao, L. DeBeer-Schmitt, P. W. Adams, R. Jin, and J. F. DiTusa, Submitted (2019).
- [6] G. L. Sternhagen, S. Gupta, Y. Zhang, V. John, G. Schneider, D. Zhang, *J. Am. Chem. Soc.* **140**, 4100-4109 (2018).
- [7] P. Du, S. W. Rick, R. Kumar, *Physical Chemistry Chemical Physics* **20**, 23386 (2018).

Publications (January 2017 – present)

- 1) Berardo E, Kaplan F, Bhaskaran-Nair K, Shelton WA, van Setten MJ, Kowalski K, Zwijnenburg M. Benchmarking the fundamental electronic properties of small TiO₂ nanoclusters by GW and Coupled Cluster Theory calculations. *J Chem Theory Comp* **13**(8), 3814-3828 (2017).
- 2) Brooks AJ, Ge J, Kirka MM, Dehoff RR, Bilheux HZ, Kardjilov N, Manke I, Butler LG. Porosity detection in electron beam-melted Ti₆Al₄V using high-resolution neutron imaging and grating-based interferometry. *Prog Addit Manuf* **2**, 125 (2017).
- 3) Brooks AJ, Knapp GL, Yuan J, Lowery CG, Pan M, Cadigan BE, Gueo S, Hussey DS, Butler LG. Neutron Imaging of Laser Melted SS316 Test Objects with Spatially Resolved Small Angle Neutron Scattering. *J. Imaging* **3**(4), 58 (2017).
- 4) Cao G, Xie W, Phelan WA, DiTusa JF, Jin R. Electrical anisotropy and coexistence of structural transitions and superconductivity in IrTe₂. *Phys Rev B* **95**, 035148 (2017).
- 5) Chen C, Kim J, Yang Y, Cao G, Jin R, Plummer EW. Surface phases of the transition-metal dichalcogenide IrTe₂. *Phys Rev B* **95**, 094118 (2017).
- 6) Dhital C, DeBeer-Schmitt L, Zhang Q, Xie W, Young DP, DiTusa JF. Exploring the origins of the Dzyaloshinskii-Moriya interaction in MnSi. *Phys Rev B* **96**, 214425 (2017).
- 7) Dhital C, Khan MA, Saghayezhian M, Phelan WA, Young DP, Jin RY, DiTusa JF. Effect of negative chemical pressure on the prototypical itinerant magnet MnSi. *Phys Rev B* **95**, 024407 (2017).
- 8) Diao Z, Lee HN, Chisholm MF, Jin R. Thermoelectric properties of Bi₂Sr₂Co₂O_y thin films and single crystals. *Physica B: Cond Matt* **511**, 42-46 (2017).
- 9) Du P, Li A, Li X, Zhang Y, Do C, He L, Rick SW, John V, Kumar R, Zhang D. Aggregation of cyclic polypeptoids bearing zwitterionic end-groups with attractive dipole-dipole and solvophobic interactions: A study by small-angle neutron scattering and molecular dynamics simulation. *Phys Chem Chem Phys* **19**(22), 14388-14400 (2017).
- 10) Gyawali G, Sternfield S, Kumar R, Rick SW. Coarse-Grained Models of Aqueous and Pure Liquid Alkanes. *J Chem Theory Comput* **13**(8), 3846–3853 (2017).
- 11) Halwidl D, Mayr-Schmölzer W, Fobes D, Peng J, Mao Z, Schmid M, Mittendorfer F, Redinger J, Diebold U. Ordered hydroxyls on Ca₃Ru₂O₇(001). *Nat Commun* **8**, 23 (2017).
- 12) He J, Zhang Y, Wen L, Yang Y, Liu J, Wu Y, Lian H, Xing H, Wang S, Mao Z, Liu Y. Band dependence of charge density wave in quasi-one-dimensional Ta₂NiSe₇ probed by orbital magnetoresistance. *Appl Phys Lett* **111**, 052405 (2017).
- 13) Liu JY, Hu J, Zhang Q, Graf D, Cao HB, Radmanesh SMA, Adams DJ, Zhu YL, Cheng GF, Liu X, Phelan WA, Wei J, Jaime M, Balakirev F, Tennant DA, DiTusa JF, Chiorescu I, Spinu L, Mao ZQ. A magnetic topological semimetal Sr_{1-y}Mn_{1-z}Sb₂ (y, z < 0.1). *Nature Materials* **16**, 905-910 (2017).
- 14) Liu JY, Hu J, Graf D, Zou T, Zhu M, Shi Y, Che S, Radmanesh SMA, Lau CN, Spinu L, Cao H, Ke X, Mao ZQ. Unusual interlayer quantum transport behavior caused by the zeroth Landau level in YbMnBi₂. *Nat Commun* **8**, 646 (2017).

- 15) Pan J, Karki A, Plummer EW, Jin R. Doping effect on the physical properties of $\text{Ca}_{10}\text{Pt}_3\text{As}_8(\text{Fe}_2\text{As}_2)_5$ single crystals. *J Phys: Condens Matter* **29**, 485702 (2017).
- 16) Patterson MC, DiTusa MF, McFerrin CA, Kurtz RL, Hall RW, Poliakoff ED, Sprunger PT. Formation of environmentally persistent free radicals (EPFRs) on ZnO at room temperature: Implications for the fundamental model of EPFR generation. *Chem Phys Lett* **670**, 5-10 (2017).
- 17) Peng J, Gu MQ, Gu XM, Zhou GT, Gao XY, Liu JY, Xu WF, Liu GQ, Ke X, Zhang L, Han H, Qu Z, Fu DW, Cai HL, Zhang FM, Mao ZQ, Wu XS. Mott transition controlled by lattice-orbital coupling in 3d-metal-doped double-layer ruthenates. *Phys Rev B* **96**, 205105 (2017).
- 18) Rivero P, Meunier V, Shelton WA. Half-metallic ferromagnetism in $\text{Sr}_3\text{Ru}_2\text{O}_7$. *Phys Rev B* **95**, 195106 (2017).
- 19) Rivero P, Jin R, Chen C, Meunier V, Plummer EW, Shelton WA. Predicting hidden bulk phases from surface phases in bilayered $\text{Sr}_3\text{Ru}_2\text{O}_7$. *Scientific Reports* **7**, 10265 (2017).
- 20) Vinokurov V, Stavitskaya A, Ivanov E, Shrestha L, Ariga K, Darrat Y, Lvov Y. Formation of metal clusters in halloysite clay nanotubes. *Sci Tech Adv Mat* **18**(1), 147-151 (2017).
- 21) Wang H, Luo J, Lou W, Ortmann JE, Mao ZQ, Liu Y, Wei J. Probing chiral superconductivity in Sr_2RuO_4 underneath the surface by point contact measurements. *New J Phys* **19**, 053001 (2017).
- 22) Weber CP, Berggren BS, Masten MG, Ogloza TC, Deckoff-Jones S, Madeo J, Man MKL, Dani KM, Zhao L, Chen G, Liu J, Mao Z, Schoop LM, Lotsch BV, Parkin SSP, Ali M. Similar ultrafast dynamics of several dissimilar Dirac and Weyl semimetals. *J App Phys* **122**, 223102 (2017).
- 23) Xuan S, Gupta S, Li X, Bleuel M, Schneider GJ, Zhang D. Synthesis and Characterization of Well-defined PEGylated Polypeptoids as Protein-resistant Polymers. *Biomacromolecules* **18**, 951-964 (2017).
- 24) Zhang Q, Ye F, Tian W, Cao H, Chi S, Hu B, Diao Z, Tennant DA, Jin R, Zhang J, Plummer W. Manganese-induced magnetic symmetry breaking and its correlation with the metal-insulator transition in bilayered $\text{Sr}_3(\text{Ru}_{1-x}\text{Mn}_x)_2\text{O}_7$. *Phys Rev B* **95**, 220403(R) (2017).
- 25) Zhang Y, Xuan S, Owoseni O, Omarova M, Li X, Saito M, He J, McPherson G, Raghavan S, Zhang D, John V. Amphiphilic Polypeptoids Serve as the Connective Glue to Transform Liposomes into Multilamellar Structures with Closely Spaced Bilayers. *Langmuir* **33**, 2780-2789 (2017).
- 26) Zhu M, Peng J, Hong T, Prokes K, Zou T, Mao ZQ, Ke XL. Field-induced metastability of the modulation wave vector in a magnetic soliton lattice. *Phys Rev B* **95**, 134429 (2017).

- 27) Zhu M, Peng J, Tian W, Hong T, Mao ZQ, Ke X. Tuning the competing phases of bilayer ruthenate $\text{Ca}_3\text{Ru}_2\text{O}_7$ via dilute Mn impurities and magnetic field. *Phys Rev B* **95**, 144426 (2017).
- 28) Zhu M, Shanavas KV, Wang Y, Zou T, Sun WF, Tian W, Garlea VO, Podlesnyak A, Matsuda M, Stone MB, Keavney D, Mao ZQ, Singh DJ, Ke X. Non-Fermi surface nesting driven commensurate magnetic ordering in Fe-doped Sr_2RuO_4 . *Phys Rev B* **95**, 054413 (2017).
- 29) Zhu M, Wang Y, Li PG, Ge JJ, Tian W, Keavney D, Mao ZQ, Ke X. Tipping the magnetic instability in paramagnetic $\text{Sr}_3\text{Ru}_2\text{O}_7$ by Fe impurities. *Phys Rev B* **95**, 174430 (2017).
- 30) Zou T, Lee CC, Tian W, Cao HB, Zhu M, Qian B, dela Cruz CR, Ku W, Mao ZQ, Ke X. G-type magnetic order in ferropnictide $\text{Cu}_x\text{Fe}_{1-y}\text{As}$ induced by hole doping on As sites. *Phys Rev B* **95**, 054414 (2017).
- 31) Ban WJ, Xu B, Li WH, Wang Y, Ge JJ, Li PG, Yang R, Da YM, Mao ZQ, Xiao H. Revealing the pseudogap in $\text{Sr}_3(\text{Ru}_{0.985}\text{Fe}_{0.015})_2\text{O}_7$ by optical spectroscopy. *Phys Rev B* **98**, 205111 (2018).
- 32) Brooks AJ, Hussey DS, Yao H, Haghshenas A, Yuan J, LaManna JM, Jacobson DL, Lowery CG, Kardjilov N, Guo S, Khonsari MM, Butler LG. Neutron interferometry detection of early crack formation caused by bending fatigue in additively manufactured SS316 dogbones. *Materials & Design* **140**(15), 420-430 (2018).
- 33) Carnicom EM, Strychalska-Nowak J, Wisniewski P, Kaczorowski D, Xie W, Klimczuk T, Cava RJ. Superconductivity in the superhard boride $\text{WB}_{4.2}$. *Supercond Sci Tech* **31**, 115005 (2018).
- 34) Chan BA, Xuan S, Li A, Simpson JM, Sternhagen GL, Yu T, Darvish OA, Jiang N, Zhang D. Polypeptoid polymers: Synthesis, characterization, and properties. *Biopolymers* **109**(1), 23070 (2018).
- 35) Chatterjee S, Karam TE, Rosu C, Wang CH, Youm SG, Li X, Do C, Losovyj Y, Russo PS, Haber LH, Nesterov EE. Silica-Conjugated Polymer Hybrid Fluorescent Nanoparticles: Preparation by Surface-Initiated Polymerization and Spectroscopic Studies. *J Phys Chem C* **122**, 6963-6975 (2018).
- 36) Chen JH, Saleheen AU, Karna SK, Young DP, Dubenko I, Ali N, Stadler S. Tuning martensitic transitions in $(\text{MnNiSi})_{0.65}(\text{Fe}_2\text{Ge})_{0.35}$ through heat treatment and hydrostatic pressure. *J Appl Phys* **124**, 203903 (2018).
- 37) Du P, Rick SW, Kumar R. Towards a coarse-grained model of the peptoid backbone: the case of N,N- dimethylacetamide. *Phys Chem Chem Phys* **20**, 23386-23396 (2018).
- 38) Gupta S, Bleuel M, Schneider GJ. A New Ultrasonic Transducer Sample Cell for In Situ Small-Angle Scattering Experiments. *Review of Scientific Instruments* **89**, 015111-1-7 (2018).

- 39) Gupta S, De Mel J, Perera R, Zolnierczuk P, Bleuel M, Faraone A, Schneider G. Dynamics of Phospholipid Membranes beyond Thermal Undulations. *J Phys Chem Lett* **9**, 2956-2960 (2018).
- 40) Lee JG, Porter V, Shelton WA, Bharti B. Magnetic Field-Driven Convection for Directed Surface Patterning of Colloids. *Langmuir* **34**(50), 15416-15424 (2018).
- 41) Lei SM, Gu MQ, Pugtgioni D, Stone G, Peng J, Ge JJ, Wang Y, Wang BM, Yuan YK, Wang K, Mao ZQ, Rondinelli JM, Gopalan V. Observation of Quasi-Two-Dimensional Polar Domains and Ferroelastic Switching in a Metal, $\text{Ca}_3\text{Ru}_2\text{O}_7$. *Nano Lett* **18**(5), 3088-3095 (2018).
- 42) Nepal R, Zhang Q, Dai S, Tian W, Nagler SE, Jin R. Structural and magnetic transitions in spinel FeMn_2O_4 single crystals. *Phys Rev B* **97**, 024410 (2018).
- 43) Novak E, Jalarvo N, Gupta S, Hong K, Forster S, Egami T, Ohl M. Dynamics in the Plastic Crystalline Phases of Cyclohexanol and Cyclooctanol Studied by Quasielastic Neutron Scattering. *J Phys Chem B* **122**(23), 6296-6304 (2018).
- 44) Owoseni O, Zhang Y, Omarova M, Li X, Lal J, McPherson G, Raghavan S, Bose A, John V. Microstructural Characteristics of Surfactant Assembly into a Gel-like Mesophase for Application as an Oil Spill Dispersant. *J Colloid Interface Sci* **524**, 279-288 (2018).
- 45) Peng J, Gu XM, Zhou GT, Wang W, Liu JY, Wang Y, Mao ZQ, Wu XS, Dong S. Electron mass enhancement and magnetic phase separation near the Mott transition in double-layer ruthenates. *Front Phys* **13**, 137108 (2018).
- 46) Rivero P, Meunier V, Shelton W. Revealing out-of-equilibrium hidden phases in $\text{Sr}_3\text{Ru}_2\text{O}_7$ by applying stress. *Phys Rev B* **97**, 134116 (2018).
- 47) Siwakoti P, Guo HW, Wang Z, Zhu YM, Fittipaldi R, Vecchione A, Wang Y, Mao ZQ, Zhang JD. Coherent growth of oxide films on a cleaved layered metal oxide substrate. *Phys Rev Matls* **2**, 104407 (2018).
- 48) Sternhagen GL, Gupta S, Zhang Y, John V, Schneider GH, Zhang D. Solution Self-Assemblies of Sequence-Defined Ionic Peptoid Block Copolymers. *J Am Chem Soc* **140**(11), 4100-4109 (2018).
- 49) Weber CP, Masten MG, Ogloza TC, Berggren BS, Man MKL, Dani KM, Liu JY, Mao ZQ, Klug DD, Adeleke AA, Yao YS. Using coherent phonons for ultrafast control of the Dirac node of SrMnSb_2 . *Phys Rev B* **98**, 155155 (2018).
- 50) Wu Y, Ning Z, Cao H, Cao G, Benavides KA, McCandless GT, Jin R, Chan JY, Shelton WA, DiTusa JF. Spin density wave instability in a ferromagnet. *Scientific Reports* **8**, 5225 (2018).
- 51) Xiao H, Hu T, Liu TW, Zhu YL, Li PG, Mu G, Su J, Li K, Mao ZQ. Superconductivity in the half-Heusler compound TbPdBi . *Phys Rev B* **97**, 224511 (2018).
- 52) Xing H, Wen L, Shen C, He J, Cai X, Peng J, Wang S, Tian M, Xu Z-A, Ku W, Mao Z, Liu Y. Existence of electron and hole pockets and partial gap opening in the correlated semimetal $\text{Ca}_3\text{Ru}_2\text{O}_7$. *Phys Rev B* **97**, 041113(R) (2018).

- 53) Zhou Y, Xing L, Finkelstein G, Gui X, Marshall M, Dera P, Jin R, Xie W. Cr_{2.37}Ga₃Se₈: A Quasi-Two-Dimensional Magnetic Semiconductor. *Inorg Chem* **57**, 14298-14303 (2018).
- 54) Zhu M, Li PG, Wang Y, Cao HB, Tian W, Zhang HD, Phelan BD, Mao ZQ, Ke X, Temperature- and field-driven spin reorientations in triple-layer ruthenate Sr₄Ru₃O₁₀. *Scientific Reports* **8**, 3914 (2018).
- 55) Zhu M, Hong T, Peng J, Zou T, Mao ZQ, Ke X, Field-induced magnetic phase transitions and memory effect in bilayer ruthenate Ca₃Ru₂O₇ with Fe substitution. *J Phys Cond Matter* **30**, 075802 (2018).
- 56) Chapai R, Jia Y, Shelton WA, Nepal R, Saghayezhian M, DiTusa JF, Plummer EW, Jin C, Jin R. Fermions and bosons in nonsymmorphic PdSb₂ with sixfold degeneracy. *Phys Rev B* **99**, 161110(R) (2019).
- 57) Dhital C, DeBeer-Schmitt L, Young DP, DiTusa JF. Unpinning the skyrmion lattice in MnSi: Effect of substitutional disorder. *Phys Rev B* **99**, 024428 (2019).
- 58) Gui X, Finkelstein G, Graf DE, Wei K, Zhang D, Baumbach RE, Dera P, Xie W. Enhanced Néel Temperature in EuSnP. *Dalton Trans* **48**, 5327-5334 (2019).
- 59) Khan MA, Graf DE, Browne D, Vekhter I, DiTusa JF, Phelan WA, Young DP. Quantum oscillations and a non-trivial Berry phase in the noncentrosymmetric topological superconductor candidate BiPd. *Phys Rev B* **99**, 02050y(R) (2019).
- 60) Meissner J, Wu Y, Jestin J, Shelton WA, Findenegg GH, Bharti B. pH-Induced reorientation of cytochrome c on silica nanoparticles. *Soft Matter* **15**(3), 350-354 (2019).
- 61) Stone G, Puggioni D, Lei SM, Gu MQ, Wang K, Wang Y, Ge JJ, Lu XZ, Mao ZQ, Rondinelli JM, Gopalan V. Atomic and electronic structure of domain walls in a polar metal. *Phys Rev B* **99**, 014105 (2019).
- 62) Wu Y, Ma Y, He L, Rother G, Shelton WA, Bharti B. Directed Pore Uptake and Phase Separation of Surfactant Solutions Under Confinement. *J Phys Chem C* **123**(15), 9957-9966 (2019).
- 63) Xu XL, Peng J, Zhang JP, Ma ZW, Chen C, Han JB, Liu BJ, Lin LF, Wu XS, Mao ZQ, Qu Z, Sheng ZG. Optical spectroscopy study of Ca₃(Ru_{0.91}Mn_{0.09})₂O₇ single crystal in high magnetic fields. *Sci Bull* **64**, 20-25 (2019).
- 64) Yuan YK, Kissin P, Puggioni D, Cremin K, Lei SM, Wang Y, Mao ZQ, Rondinelli JM, Averitt RD, Gopalan V. Ultrafast quasiparticle dynamics in the correlated semimetal Ca₃Ru₂O₇. *Phys Rev B* **99**, 155111 (2019).
- 65) Zhang Q, Cao G, Ye F, Cao H, Matsuda M, Tennant DA, Chi S, Nagle SE, Shelton WA, Jin R, Plummer EW, Zhang J. Anomalous magnetic behavior of Ba₂CoO₄ with isolated CoO₄ tetrahedra. *Phys Rev B* **99**, 094416 (2019).
- 66) Zhang Q, Diao Z, Cao H, Saleheen A, Chapai R, Gong D, Stadler S, Jin R. Structure-Property Relationship in Layered BaMn₂Sb₂ and Ba₂Mn₃Sb₂O₂. *Phys Rev B* (accepted).

- 67) Zou T, Peng J, Gottschalk M, Zhang PP, Mao ZQ, Ke X. Insulator-metal transition induced by electric voltage in a ruthenate Mott insulator. *J Phys: Condens Matter* **31**, 195602 (2019).
- 68) Chandrasiria I, Abebe DG, Gupta S, Williams JSD, Rieger WD, Simms BL, Noh Y, Payne ME, Fortenberry A, Smith A, Lee B, Grayson S, Schneider GJ, Watkins DL. Synthesis and Characterization of PAMAM-Polylactide “Janus-type” Linear-Dendritic Hybrids. *Journal of Polymer Science, Part A: Polymer Chemistry* (2019).
<https://doi.org/10.1002/pola.29409>
- 69) Gupta S, De Mel J, Schneider GJ. Dynamics of Liposomes in the Fluid Phase. *Current Opinion in Colloid & Interface Science* <https://doi.org/10.1016/j.cocis.2019.05.003> (2019).
- 70) J. Lee, A. M. Brooks, W. A. Shelton, K. M. Bishop, B. Bharti, “Directed Propulsion of Spherical Particles Along Three Dimensional Helical Trajectories”, *Nat. Commun.*, DOI: 10.1038/s41467-019-10579-1 (2019).
- 71) Y. Guo, J. A. Belgodere, Y. Ma, J. P. Jung, B. Bharti, “Directed Printing and Reconfiguration of Thermoresponsive Silica-pNIPAM Nanocomposites”, *Macromol. Rapid Commun.*, DOI: 10.1002/marc.201900191 (2019).

Papers Recently Submitted:

- 1) Cai X, Ying YA, Ortmann JE, Sun WF, Mao ZQ, Liu Y. Magnetoresistance oscillations and the half-flux-quantum state in spin-triplet superconductor Sr_2RuO_4 (*submitted 2019*).
- 2) Cao G, Zhang Q, Frontzek M, Xie W, Jin R. Correlation between Structure, Cr Vacancy, and Magnetism in Novel $\text{Cr}_{12-x}\text{Te}_{16}$ with $x \sim 2.65$, (*submitted 2019*).
- 3) Chiang C-H, Youm SG, Lu L, Arachchige NMK, Ankner JF, Strzalka J, Losovyj Y, Garno JC, Nesterov EE. Precision Synthesis of Conjugated Polymer Films by Surface-Confined Stepwise Sonogashira Coupling (*submitted 2019*)
- 4) Gupta S, Chatterjee S, Zolnierczuk P, Nesterov EE, Schneider GJ. Impact of Local Stiffness on Entropy Driven Microscopic Dynamics of Polymers (*submitted 2019*).
- 5) Gupta S, Schneider GJ. Modeling of Transient Trapping of Fatty Acid Tails in Phospholipids (*submitted 2019*).
- 6) Islam NN, Sharma A, Gyawali G, Kumar R, Rick SW. Coarse-grained models for constant pH simulations of carboxylic acids. (*submitted 2019*).
- 7) Karna S, Womack FN, Chapai R, Young DP, Marshall M, Xie W, Graf D, Wu Y, Cao H, DeBeer-Schmitt L, Adams PW, Jin R, DiTusa JF. Observation of a mesoscopic magnetic modulation in chiral $\text{Mn}_{1/3}\text{NbS}_2$ (*submitted 2019*).
- 8) Lee SH, Zhu Y, Wang Y, Miao L, Pillsbury T, Kempinger S, Graf D, Alem N, Chang C-Z, Samarth N, Mao Z. Spin scattering and noncollinear spin structure-induced intrinsic anomalous Hall effect in antiferromagnetic topological insulator MnBi_2Te_4 (*submitted 2019*).

- 9) Tan Y-T, Zhang T, Zou T, dos Santos AM, Hu J, Yao D-X, Mao ZQ, Ke X, Ku W. Unusually stronger quantum fluctuation with larger spins: Novel phenomena revealed by emergent magnetism in pressurized high-temperature superconductor FeSe (*submitted 2019*).
- 10) Ying YA, Zakrzewski BM, Cai X, Mills S, Yan X, Staley NE, Wang Z, Sun WF, Mao ZQ, Liu Y. “Sensitive Josephson junction detection of chiral edge currents in Sr₂RuO₄” Phys. Rev. Lett. (*submitted 2019*).
- 11) Zhang Q, Okamoto S, Stone MB, Liu J, Zhu Y, DiTusa JF, Mao ZQ, Tennant DA. Quasi-2D magnetism and origin of the Dirac semimetallic behavior in nonstoichiometric Sr_{1-y}Mn_{1-z}Sb₂ ($y, z < 0.1$) (*submitted 2019*).
- 12) Zhang Y, Heidari Z, Su Y, Yu T, Sunting X, Omarova M, Yucel A, Dash S, Zhang D, John V. Amphiphilic Polypeptoids Rupture Vesicle Bilayers to Form Peptoid-Lipid Rafts Effective in Enhancing Hydrophobic Drug Delivery (*submitted 2019*).

Equilibrium and Non-Equilibrium Vortex and Skyrmion Lattices

Morten R. Eskildsen, University of Notre Dame

Program Scope

The program is focused on the small-angle neutron scattering (SANS) studies of mesoscopic magnetic structures, specifically the vortex lattice (VL) in type-II superconductors and the skyrmion lattice (SkL) in chiral magnets in nonequilibrium conditions. The vortex studies has a dual focus: (i) Using the VL as a probe of the superconducting state in unconventional superconductors, and (ii) Studies of the structural transition kinetics and activated behavior in vortex matter. Similarly, the SkL studies has a dual objective: (i) Determination of the activation barrier for skyrmion formation/annihilation from hysteresis measurements, and (ii) using transport currents to access metastable SkL configurations. Both the VL and SkL studies are complemented by molecular dynamics simulations.

Recent Progress

Order parameter in the topological superconductor UPT_3 . To provide a direct test of broken time-reversal symmetry in the UPT_3 B phase, SANS measurements were carried out with $H \parallel c$ where the VL is especially sensitive to changes in the superconducting. The VL was prepared using one of two different field histories, illustrated in Fig. 1(a), to achieve states where the phase winding in the vortex cores is either parallel ($++$ or $--$) or anti-parallel ($+-$ or $-+$) to the global phase winding set by the direction of the applied field [1]. Figs. 1(b) and 1(c) show diffraction patterns illustrating the two main results: (i) a splitting of the VL Bragg peaks, indicating the presence of two triangular VL domain orientations rotated in opposite directions about the c -axis, and (ii) a different splitting for the two field histories providing direct evidence

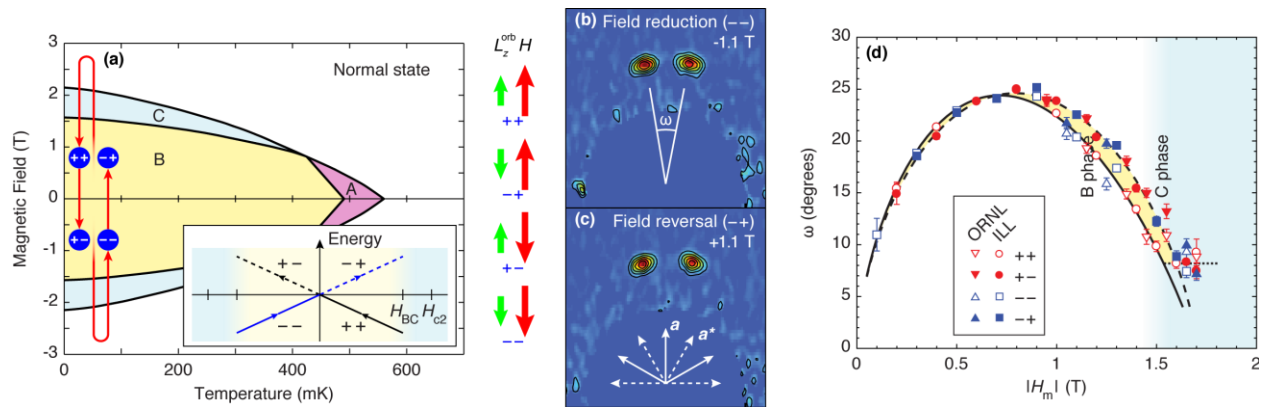


Fig. 1 Broken time reversal symmetry in UPT_3 . **(a)** Phase diagram showing the three superconducting phases. Inset shows energy of the superconducting condensate as a function of field history. **(b,c)** VL diffraction patterns following a field reduction and a field reversal. **(d)** Field dependence of the VL Bragg peak splitting.

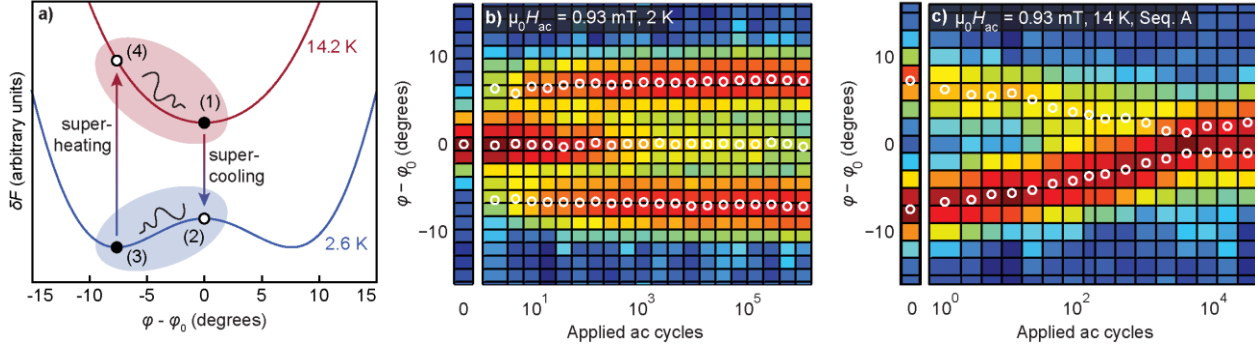


Fig. 2 MS to ES transition for supercooled and superheated VLs in MgB. **(a)** Schematic single domain VL free energy curves corresponding to the supercooled and superheated VL configurations. Solid (open) circles represent an ES (MS) VL. **(b)** Azimuthal intensity distribution versus the number of applied ac cycles for the supercooled VL. The left colorbar indicates the pristine MS VL. **(c)** Similar data for the superheated VL.

for an internal degree of freedom associated with the vortex cores. The field dependence of the VL splitting is shown in Fig. 1(d), where the difference between the two field histories is seen to vanish in the C phase. From this we infer that time-reversal symmetry is broken in the zero-field B phase, and that the c -axis is an axis of chiral symmetry.

Structural transition kinetics and activated behavior in the vortex lattice. The VL in MgB₂ can be driven into metastable states (MS) by cooling or heating across (equilibrium) phase transitions [2,3]. Using SANS we have studied the VL in this material, as it gradually transition from the MS to the equilibrium state (ES) due to successive applications of ac magnetic field cycles. Figs. 2(b) and 2(c) compares measurements sequences for a supercooled and superheated VL respectively. In the supercooled case ES domains that nucleate in their final orientations and grow at the expense of the MS domains, making the transition discontinuous. In comparison the VL in the superheated case rotate continuously towards the ES orientation. This difference is due to the qualitatively different single-domain free energy configuration, shown in Fig. 2(a).

The MS-ES transition can be analyzed in terms of an activated behavior. In this context the ac amplitude (H_{ac}) and cycle count (n) take the role of, respectively, the effective “temperature” and “time.” This allows a determination of the activation field (\tilde{H}) shown in Fig. 3, representing the barrier between MS and ES VL domain orientations [4,5]. Here, the “transition coordinate” for the supercooled case is the remaining metastable volume fraction (f_{MS}) and for the superheated case the VL peak splitting. Despite the qualitatively different nature of the

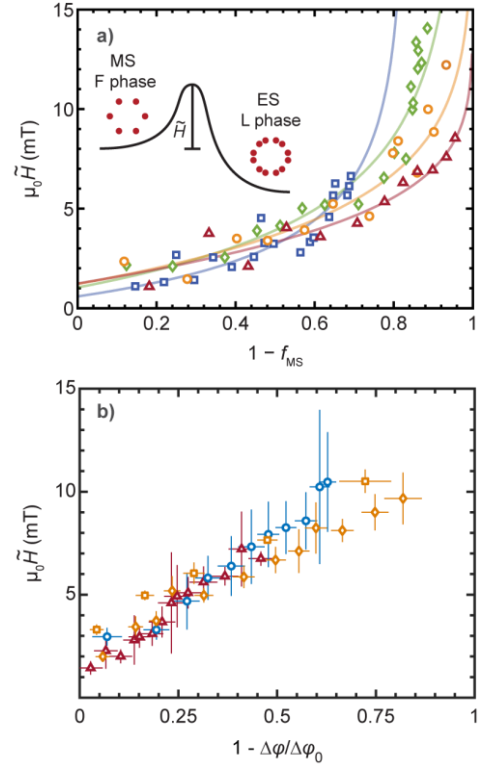


Fig. 3 Activation fields for the MS to ES transition in MgB₂ for a (a) supercooled VL and (b) superheated VL. Different symbols represent different ac field amplitudes.

transition, the activation field evolves in a similar way for both the supercooled and superheated VL. Notably \hat{H} increases as the transition progresses, equivalent to an aging of the VL. We note the similarity to isothermal martensitic phase transformations in maraging steel which are governed by domain formation and growth, and where an increasing activation energy has also been observed [6].

Activation barrier for SkL formation. The transition between the conical and SkL phases is discontinuous and therefore one where it is natural to expect a hysteretic behavior. Since these two phases are easily distinguishable in reciprocal space, SANS is an ideal technique to study the hysteresis associated with the creation or destruction of skyrmions. In Fig. 4 we show measurements of the scattered intensity from the SkL in MnSi, showing a small but measurable shift between increasing and decreasing magnetic fields. To model the observed hysteresis we have used an adapted Preisach model, from we may determine the activation barrier between the SkL and conical phases. This yields an activation barrier of ~ 1 mT.

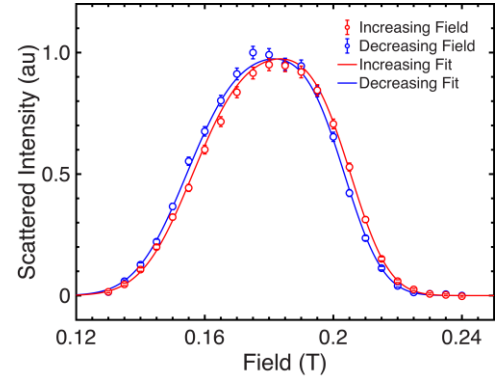


Fig. 4 Hysteresis of the SkL intensity in MnSi. Lines are a fits to an adapted Preisach model.

Future Plans

Presence or absence of vortex lattice metastability without domain boundaries. A main conclusion of our previous VL studies is that domain formation and interaction is responsible for the metastable phases observed experimentally in MgB₂ and also govern the transition kinetics. To better model the domain-dominated kinetics, further measurements will be undertaken in systems where domain formation is suppressed. This may be achieved by rotating the applied magnetic field away from the c -axis in a uniaxial superconductor, introducing a two-fold anisotropy which break the degeneracy and favor one VL domain orientation over another [7]. If the presence of domain boundaries is required to sustain the metastable states, the metastability will gradually become less pronounced and eventually cease to exist as the field rotation angle increases. Furthermore, the VL activation field (see Fig. 3) will be suppressed.

Kinetics and activated behavior for first order vortex lattice transitions. To fully understand metastability in vortex matter, it is important to study this in connection with discontinuous (first order) phase transitions which complement the continuous (second order) transitions previously studied in MgB₂. Non-magnetic members of the nickelborocarbide superconductors are known to undergo a discontinuous 90° rotation within a rhombic phase, as part of the transition from a triangular to square symmetry [8]. We will perform SANS studies of the VL in YNi₂B₂C, with an initial goal of establishing whether long-lived metastable states associated with the reorientation transition can be achieved. If these states are observed, we will

proceed with measurements of the transition kinetics, in analogy with our previous studies of MgB₂ discussed above.

An alternative approach to realizing metastable VL states in connection with a first order transition is the application of strain, which in recent years has emerged as a powerful “knob” to tune the Fermi surface of materials and thereby associated properties such as superconductivity. We have performed preliminary SANS measurements of in niobium, observing a change of the VL configuration at approximately 0.03% strain. These studies will be continued.

Manipulating the SkL by electric currents. While vortex motion may be induced by a change in the magnetic field, skyrmions typically require an electric current. A rotation of the SKL may be achieved by combining a uniform current density with a thermal gradient [9]. We will use a Corbino geometry, where a radial current produces an azimuthal Magnus force, and hence a torque on the SkL without requiring a thermal gradient. This approach presents several advantages: (i) the number of skyrmions entering and leaving the sample will be minimized, reducing complications or artifacts due to geometric barriers; (ii) the results will be easier to model since it does not require knowledge of an immeasurable temperature gradient; (iii) a lower current density will be required, since the Magnus force is directly working to rotate the lattice. At low currents the SkL is expected to rotate as one unit, with an angle versus current dependence that reflect the anisotropic interaction potential similar to the one shown in Fig. 2(a). At higher currents, a deformation or fracturing of the SkL is expected as the force on the skyrmions near the center will be greater than those on the perimeter. Finally, we may be able to observe a compression or expansion of the SkL depending on the direction of the current and the corresponding radial drag force. Together, we will be able to explore the strength and elastic properties of the SkL [10]. In the longer term, it may also be used to study the transition kinetics associated with metastable SkL phases, in analogy with the VL measurements discussed above.

In addition to the main projects outlined above, we will continue molecular dynamics simulations to complement our SANS studies of the VL and the SkL. This will provide real-space information, which is particularly valuable for understanding domain formation and growth in connection with structural transitions in these systems.

References

1. T. A. Tokuyasu, D. W. Hess, and J. A. Sauls, Phys. Rev. B **41**, 8891 (1990).
2. P. Das *et al.*, Phys. Rev. Lett. **108**, 167001 (2012).
3. C. Rastovski *et al.*, Phys. Rev. Lett. **111**, 107002 (2013).
4. E.R. Loudon *et al.*, Phys. Rev. B **99**, 060502(R) (2019).
5. E.R. Loudon *et al.*, Phys. Rev. B **99**, 144515 (2019).
6. D. San Martin *et al.*, Mater. Sci. Eng. A **527**, 5241 (2010).
7. M. Laver *et al.*, Phys. Rev. B **79**, 1174 (2009).
8. S. J. Levett, C. D. Dewhurst, and D. M. Paul, Phys. Rev. B **66**, 014515 (2002).
9. F. Jonietz *et al.*, Science **330**, 1645 (2010).
10. Y. Nii *et al.*, Phys. Rev. Lett. **113**, 267203 (2014).

Publications

1. S.J. Kuhn *et al.*, *Structure and Property Correlations in FeS*, *Physica C* **354**, 29-36 (2017).
2. M. Marziali Bermúdez *et al.*, *Metastability and hysteretic vortex pinning near the order-disorder transition in NbSe₂: Interplay between plastic and elastic energy barriers*, *Phys. Rev. B* **95**, 104505 (2017).
3. W.J. Gannon *et al.*, *Spin susceptibility of the topological superconductor UPt₃ from polarized neutron diffraction*, *Phys. Rev. B* **96**, 041111(R) (2017).
4. S.J. Kuhn *et al.*, *Anisotropy and multiband superconductivity in Sr₂RuO₄ determined by small-angle neutron scattering studies of the vortex lattice*, *Phys. Rev. B* **96**, 174507 (2017).
5. M.P. Smylie *et al.*, *Superconductivity, pairing symmetry, and disorder in the doped topological insulator Sn_{1-x}In_xTe for x ≥ 0.10*, *Phys. Rev. B* **97**, 024511 (2018).
6. M.W. Olszewski *et al.*, *Structural Transitions in Vortex Systems with Anisotropic Interactions*, *New J. Phys* **20**, 023005 (2018).
7. R. Brearton *et al.*, *Skyrmions in anisotropic magnetic fields: Strain and defect driven dynamics*, *MRS Advances*, 1-8 (2019). [10.1557/adv.2019.43](https://doi.org/10.1557/adv.2019.43)
8. E.R. Loudon *et al.*, *Structural Transition Kinetics and Activated Behavior in the Superconducting Vortex Lattice*, *Phys. Rev. B* **99**, 060502(R) (2019).
9. S. Mühlbauer *et al.*, *Magnetic small-angle neutron scattering*, *Rev. Mod. Phys.* **91**, 015004 (2019).
10. E.R. Loudon *et al.*, *Non-equilibrium structural phase transitions of the vortex lattice in MgB₂*, *Phys. Rev. B* **99**, 144515 (2019).
11. E.R. Loudon *et al.*, *Structural studies of metastable and equilibrium vortex lattice domains in MgB₂*, *New J. Phys.* **21**, 063003 (2019).
12. K.E. Avers *et al.*, *Vortex lattices and broken time reversal symmetry in the topological superconductor UPt₃*, [arXiv:1812.05690](https://arxiv.org/abs/1812.05690).

Inelastic Neutron Scattering Studies of Phonon Thermodynamics and Thermophysical Properties of Materials

**Brent Fultz, Rawn Professor of Materials Science and Applied Physics
California Institute of Technology, W. M. Keck Laboratory, Pasadena CA 91125 USA**

Program Scope

This program uses inelastic neutron scattering (INS) to measure thermal excitations in materials, especially atom vibrations (phonons), but also electron spins (magnons). Modern computational studies give the effects of electronic excitations, and help identify couplings between the different types of excitations at high temperatures. The primary effort is to measure accurately the phonon spectra and dispersions. Phonons are the most important thermal excitations for materials thermodynamics. They give the vibrational entropy, and show its importance to the Gibbs free energies of materials. Our experiments address cases where the vibrational entropy should be large and interesting. Measurements at high temperatures can show significant effects from anharmonicity and electron-phonon interactions. The work also focuses on the importance of vibrational dynamics for other thermophysical properties such as thermal expansion, and perhaps the temperature dependence of elastic constants.

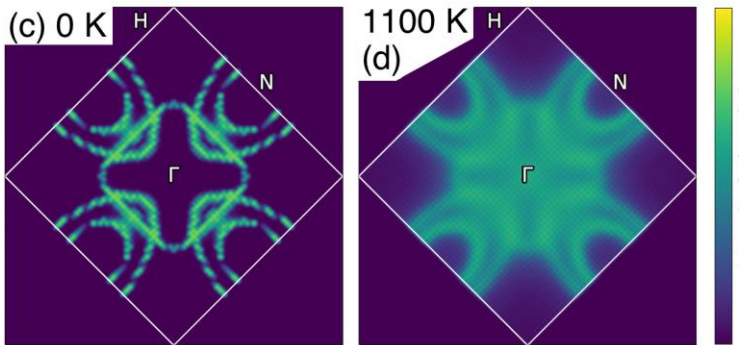
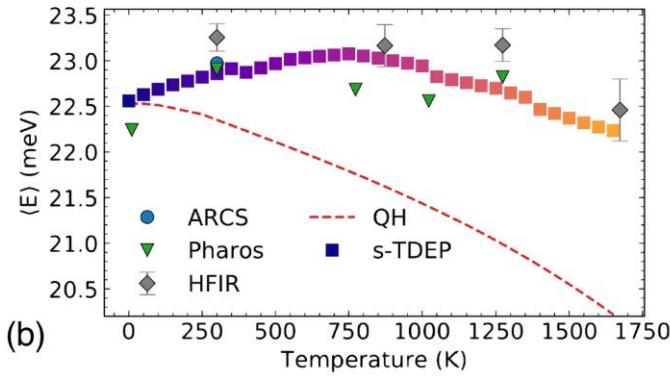
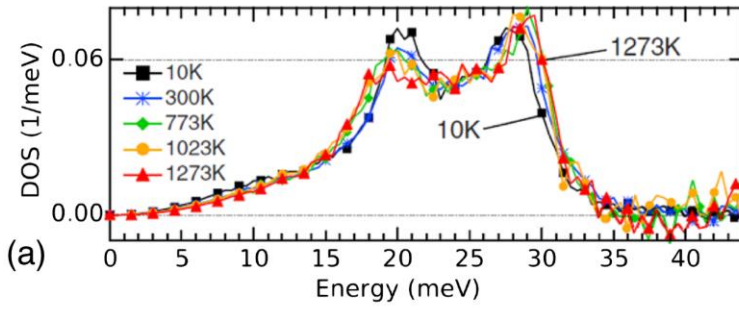
This is primarily an experimental investigation based on INS measurements performed at the Spallation Neutron Source, ORNL. In conjunction with computation, INS is the most powerful approach today for understanding the different contributions to the entropy of materials. Some of the experimental work involves obtaining accurate phonon densities of states (DOS) at different temperatures. With the development of single crystal techniques with chopper spectrometers such as ARCS, it is now possible to measure phonon excitations at all crystallographic directions and wavevectors in a crystal (its Brillouin zone). These new measurements offer a more detailed understanding of why phonon energies and lifetimes change with temperature, and are a highly efficient alternative to measuring phonon dispersions with triple axis spectrometers.

Computational methods similar to ab-initio molecular dynamics computations can account for large anharmonicities beyond the realm of phonon-phonon perturbation theory, and they also show how the electronic structure changes with temperature. At high temperatures there is a hierarchy of anharmonic effects, and with computational support they can be separated into quasiharmonic entropy, anharmonic entropy, and effects of electron-phonon interactions.

Recent Progress

1. Effects of Temperature on Electron-Phonon Interactions We interpreted neutron scattering measurements of the temperature dependence of the phonon DOS of bcc vanadium (Fig. 1a) using new first-principles calculations (Fig. 1b). Supercell calculations accounted for effects of

thermal atom displacements on electronic energies, and band unfolding was used to project the spectral weight of the electron states into the Brillouin zone of a standard bcc unit cell. These projections were used to generate the electronic structure around the Fermi surface of vanadium at elevated temperatures (Fig. 1c,d). We found, for the first time, that temperature caused an electronic topological transition (ETT, or Lifshitz transition) near the Γ point (new intensity at the center of Fig. 1d). However, the large thermal smearing of electron state energies from the



atomic disorder and the Fermi-Dirac distribution reduced the importance of this ETT for electron-phonon interactions. The phonon dispersions showed thermal stiffening of their Kohn anomalies near the Γ point, and of the longitudinal N phonon mode.

In short, the effects of the thermally-driven ETT are overcome by the thermal smearing of the Fermi surface, which reduces the density of phonon spanning vectors across the Fermi surface.

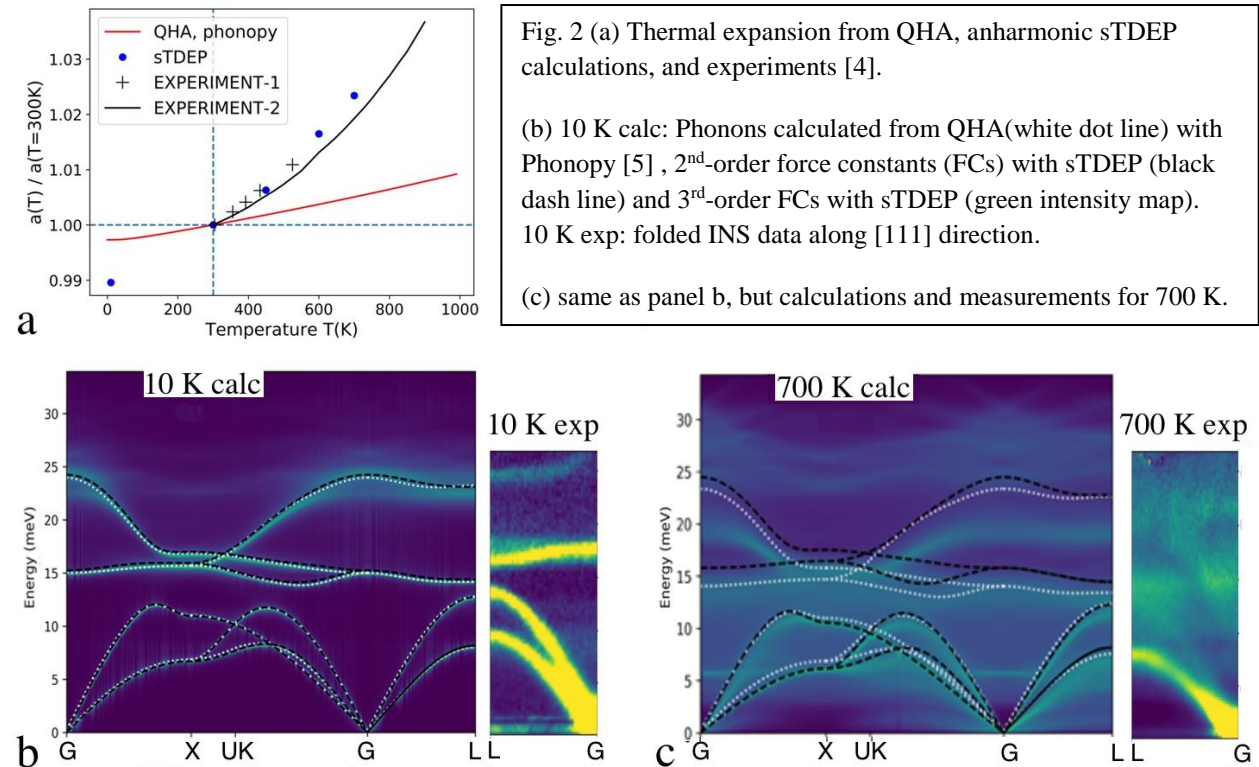
Fig. 1 (a) Experimental phonon DOS curves from bcc V at different temperatures [1]. (b) First moment phonon energies of experimental DOS curves from three neutron instruments, and our ab initio calculations (colored squares). Quasiharmonic calculations are dashed red curve. (c,d) (100) cuts through Fermi surfaces from supercell calculations and band unfolding. (c) 0 K and (d) 1100 K (indices are for simple cubic structure).

2. Phonon Anharmonicity and Thermal Expansion of NaBr

Thermal expansion is a fundamental thermophysical property that originates from a balance between phonon entropy (which increases as the material expands) and elastic energy (a penalty against expansion). The usual way to predict thermal expansion is based on the quasiharmonic approximation (QHA), which assumes a volume dependence of the phonon frequencies. Although a QHA theory of thermal expansion is logically self-consistent, it ignores pure anharmonicity, where phonon frequencies

depend on both temperature and volume. In our recent work on the thermal expansion of silicon, we found that the QHA gave the wrong sign for the temperature dependence of most of the phonons measured by inelastic neutron scattering. The QHA must therefore be physically incorrect, but it did predict correctly the thermal expansion (owing to a surprising cancellation of erroneous contributions from individual phonons). Convincing the materials physics community that the QHA is inappropriate for explaining thermal expansion requires a new example, and we have chosen NaBr.

Figure 2a shows that the QHA fails to predict the thermal expansion of NaBr. Anharmonic effects were included in our *ab initio* calculations (sTDEP [2,3]), which reproduced well the thermal expansion with temperature (Fig. 2a). Figure 2a shows that the large thermal expansion of NaBr depends on the pure anharmonicity. Figure 2b,c show how the LO phonon modes soften significantly with temperature, in both INS measurements and the full calculations. We are attempting to identify the types of phonon-phonon interactions that are responsible for these large changes in phonon spectral weight, and how they correlate to the thermal expansion of NaBr.



Future Plans

In earlier work we found that the thermal softening of phonons in transition metal alloys depended on the electronic density of states at the Fermi level [1]. In general, the greater the electronic density of states, the more effective the electronic screening of ion core displacements, and the softer are the phonon frequencies. In 2016 we reported a new phenomenon in FeTi, where temperature created a new feature at the Fermi surface (an electronic topological

transition, ETT) [3]. This ETT increased the electron-phonon interaction, and gave an anomalous temperature-dependence to the phonon energies. Very recently, for vanadium we found a new ETT that was driven by temperature, but other types of thermal broadening of the electronic energies largely cancelled its effects. The temperature dependence of the electron-phonon interaction remains of interest, but we need to decide on an experiment that will better separate these different effects.

In 2018 we showed that the thermal expansion of silicon is dominated by phonon anharmonicity, and at low temperatures the anharmonic leakage of the zero-point of optical modes causes negative thermal expansion. The materials physics community has a large investment in a more conventional quasiharmonic theory of the thermal expansion of silicon, and although this quasiharmonic theory makes highly inaccurate predictions of the temperature dependence of the phonons, it does give approximately the correct thermal expansion. We have therefore taken up the case of thermal expansion of NaBr, since it has a thermal expansion that cannot be predicted by the quasiharmonic theory. This work, discussed with Fig. 2, is coming along well. We need to plan another study to follow it.

A thermodynamic identity is $\partial^2 F / \partial V \partial T = \beta B$, where the mixed second derivative of free energy with respect to volume and temperature equals the thermal expansion coefficient times the isothermal bulk modulus. If the anharmonic leakage of zero point energy from optical modes alters the thermal expansion of NaBr, it should also affect the temperature dependence of its elastic constants. This is a new opportunity for modern experiments with inelastic neutron scattering, supported by modern computational methods, to give new insights into the equations of state of materials.

References

- [1] O. Delaire, M.G. Kresch, J.A. Munoz, M.S. Lucas, J.Y.Y. Lin, and B. Fultz, "Electron-Phonon Interactions and High-Temperature Thermodynamics of Vanadium and its Alloys", *Phys. Rev. B* **77**, 214112 (2008).
- [2] O. Hellman, P. Steneteg, I. A. Abrikosov, and S. I. Simak, "Temperature dependent effective potential method for accurate free energy calculations of solids," *Phys. Rev. B* **87**, 104111. (2013).
- [3] D.S. Kim, O. Hellman, J. Herriman, H.L. Smith, J.Y.Y. Lin, N. Shulumba, J.L. Niedziela, C.W. Li, D.L. Abernathy, and B. Fultz, " Nuclear quantum effect with pure anharmonicity and the anomalous thermal expansion of silicon," *Proc. Nat'l Acad. Sciences* **115**, 1992 (2018).
- [4] A. Rao, K. Narender, K. Rao and N. Krishna, "Thermophysical properties of NaCl, NaBr and NaF by γ -ray attenuation technique," *J. Mod. Phys.* **4**, 208 (2013).
- [5] A. Togo and I. Tanaka, "First principles phonon calculations in materials science," *Scr. Mater.* **108**, 1 (2015).

Publications

- H.L. Smith, C.W. Li, A. Hoff, G. Garrett, D.S. Kim, F.C. Yang, M.S. Lucas, T. Swan-Wood, J.Y.Y. Lin, M.B. Stone, D.L. Abernathy, M. Demetriou, and B. Fultz, "Separating the Configurational and Vibrational Entropy Contributions in Metallic Glasses," *Nature Physics* 13, 900 (2017).
- D.S. Kim, O. Hellman, J. Herriman, H.L. Smith, J.Y.Y. Lin, N. Shulumba, J.L. Niedziela, C.W. Li, D.L. Abernathy, and B. Fultz, "Nuclear quantum effect with pure anharmonicity and the anomalous thermal expansion of silicon," *Proc. Nat'l Acad. Sciences* 115, 1992 (2018). See also: C. Ash and J. Smith, "In Other Journals," *Science* 360, 167 (2018).
- Garrett E. Granroth, Ke An, Hillary L. Smith, Pamela Whitfield, Joerg C. Neufeind, Jooseop Lee, Wenduo Zhou, Vladislav N. Sedov, Peter F. Peterson, Andre Parizzi, Harley Skorpenske, Steven M. Hartman, Ashfia Huq and Douglas L. Abernathy, "Event-based processing of neutron scattering data at the Spallation Neutron Source," *J. Appl. Cryst.* 51, 616 (2018).
- Hillary L. Smith*, Yang Shen*, Dennis S. Kim, Fred C. Yang, C.P. Adams, Chen W. Li, D.L. Abernathy, M.B. Stone, and B. Fultz, "The temperature dependence of phonons in FeGe₂," *Phys. Rev. Mater.* 2, 103602 (2018).
- Fred Chae-Reem Yang, "High Temperature Electron-Phonon and Magnon-Phonon Interactions," Ph.D. in Materials Science, March 25, 2019.
- Fred C-R. Yang, O. Hellman, and B. Fultz, "The temperature dependence of electron-phonon interactions in vanadium," submitted to *Phys. Rev. B* in May 2019.

University of Minnesota Center for Quantum Materials (CQM)

Andrey Chubukov¹, Rafael Fernandes¹, Martin Greven¹, Bharat Jalan², Chris Leighton²

¹School of Physics and Astronomy, University of Minnesota

²Department of Chemical Engineering and Materials Science, University of Minnesota

Program Scope

The Center for Quantum Materials (CQM) at the University of Minnesota, established in 2016, is comprised of an inter-disciplinary team of five faculty and more than a dozen Ph.D. students and post-docs. The team investigates the physics and materials science of quantum materials, primarily complex oxides, a vast class of materials that embody many of the most fundamental questions regarding quantum behavior of interacting electrons. These materials are also relevant to important technologies, in data storage, spintronics, catalysis, fuel cells, *etc.* Their rich phase diagrams are manifestations of the interplay between electronic kinetic energy and interactions, resulting in myriad quantum states that can, in principle, be controlled experimentally. *The CQM vision is to substantially raise the understanding of quantum electronic phases and transitions in oxides, through investigation of exceptional quality materials.* Emphasis is placed on synergy between bulk crystal and epitaxial film approaches, application of cutting-edge neutron, X-ray, and other tools, and microscopic modeling.

Recent Progress

The primary recent CQM emphasis has been on model oxides from three representative families: perovskite titanates, cuprates, and perovskite cobaltites. Work on titanates has been a central focus, involving all CQM faculty. Major efforts were made to understand the foundational complex oxide SrTiO₃, including the nature of its structural phase transition [2], normal state behavior [24], and superconductivity [14,15,26], which have remained unresolved for over half a century. A related direction has been the study of rare-earth titanates as model Mott insulators with controllable spin-orbital structures, with focus on the antiferromagnetic-ferromagnetic (AF-FM) transition in Y_{1-x}La_xTiO₃. With respect to cuprates, the model system HgBa₂CuO_{4+δ}, and the overall temperature-doping phase diagram, have been specific foci [1,4,12,13,17,19,22,23,25-28,32,35]. CQM research has made significant advances, unraveling commonalities among oxide superconductors, the latter involving a natural extension to superconducting (SC) Sr₂RuO₄ [26]. In terms of cobaltites, CQM research has emphasized thin films and heterostructures, focusing on spin-state physics [7], magnetic and electronic inhomogeneity, and oxygen-vacancy-based control [5,6,16,18,20]. In addition to these main topics, CQM research included complex magnetic alloys, the magnetic mineral Fe₇S₈ [11], and

BaSnO₃ [9], the highest room temperature mobility perovskite oxide. Below, we describe a few examples of recent CQM progress; additional progress is highlighted in separate abstracts.

Examples of recent CQM progress – titanates. Beginning with SrTiO₃, *Leighton* shed new light on the nature of the antiferrodisplacive cubic-tetragonal transition by uncovering a key role for valence mismatch in the dependence of the transition temperature on substitution [2]. A quantitative relation between transition temperature and structure was unveiled, providing the first predictive capability [2]. The perplexing T^2 normal-state resistivity was then explored in doped SrTiO₃ via the first comprehensive study of electronic specific heat (*Leighton, Fernandes*) [24]. The well-known Kadowaki-Woods scaling was found to be qualitatively violated, pointing to the urgent need for new theoretical normal-state descriptions of SrTiO₃, potentially beyond the standard Fermi liquid picture.

Chubukov and *Fernandes* shed light on the nature of the SC state in SrTiO₃, which has remained elusive. In back-to-back papers, *Fernandes* addressed an important property of the SC dome, also observed in LaAlO₃/SrTiO₃ [14,15]. *Chubukov* and *Fernandes* further studied the origin of the attractive intra-band pairing interaction. In a related breakthrough, *Jalan* developed hybrid MBE of highly perfect, doped SrTiO₃ films, with the goal to utilize controlled doping in strain-engineered heterostructures to understand SC phase behavior vs. doping, disorder, strain, *etc.* Using Nd, *Jalan* also established controlled doping of SrTiO₃ films, discovered that they are indeed SC, and established the existence of a SC dome. Additionally, *Jalan* developed remote doping of SrTiO₃ using a nonpolar/polar heterostructure, discovering superconductivity.

Greven and *Leighton* also initiated neutron-based studies of bulk Y_{1-x}La_xTiO₃, in collaboration with ORNL and NIST. The phase behavior of the Mott-insulating rare-earth titanates RTiO₃ has long been debated, due to the variety of spin- and orbital-ordered states. In particular, an AF-FM transition occurs vs. R ion, as the Ti-O-Ti bond angle decreases. This transition also occurs in Y_{1-x}La_xTiO₃, where it can be studied quasi-continuously vs. x . Despite this opportunity, neutron scattering studies have been limited to the parent compounds YTiO₃ and LaTiO₃. We thus conducted an extensive study of Y_{1-x}La_xTiO₃ crystals up to $x = 0.3$. Fig. 1(a,b) shows the doping evolution of the T -dependence of the AF

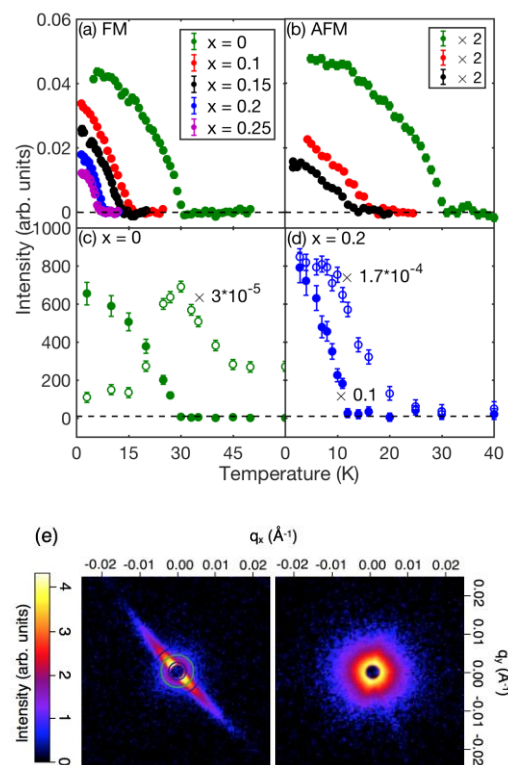


Figure 1: Doping evolution of the T dependence of (a) the 020 (FM) and (b) the 011 (G-type AF) Bragg intensity, normalized by the nuclear Bragg intensity. (c,d) Low- q (0.003\AA^{-1} , closed symbols) and high- q (0.1\AA^{-1} , open symbols) SANS intensity vs. temperature for (c) $x = 0$ and (d) $x = 0.2$. (e) Momentum space map of SANS intensity at $T = 3\text{ K}$ for $x = 0$ (left) and $x = 0.2$ (right).

(011) and FM (020) Bragg intensities. Although Y-rich compounds are predominantly FM, AF reflections show nonzero intensity due to spin canting. From the x dependence of the magnetic Bragg intensities we find strong suppression of the ordered magnetic moment with doping. These data were supplemented with SANS measurements (Fig. 1(c,d,e)), on $x = 0, 0.1, 0.2$ crystals. Importantly, magnetic inhomogeneities are seen at ~ 10 nm length scales, even in undoped YTiO_3 . The high- q (scattering wavevector) scattering (Fig. 1(c,d)) also suggests distinct changes in critical scattering as the magnetic crossover is approached in the $x = 0.2$ crystal. Moreover, a clear crossover from easy-axis to almost isotropic low T behavior is seen as x increases from 0 to 0.2 (Fig. 1(e)), correlating well with angle-dependent magnetometry. The destruction of FM order with x is thus accompanied by a dramatic decrease in magnetocrystalline anisotropy.

Examples of recent CQM progress – cuprates. Exploiting the unique CQM capability to grow sizable crystals of the model compound $\text{HgBa}_2\text{CuO}_{4+\delta}$, the single- CuO_2 -layer cuprate with the highest optimal T_c , *Greven* performed crystal growth [17], neutron [1,19], X-ray [4,35], transport [12,13,28,32], and nonlinear response [25,26] work, the latter with *Leighton* [26]. This enabled construction of a detailed phase diagram and led to numerous insights. For example, time-of-flight neutron work at the SNS yielded key insight into the AF response (Fig. 2; [1] and manuscript in preparation). The unusual Y-shaped AF excitation spectrum previously observed at moderate doping ($T_c \approx 71$ K), where charge order is prominent, was found to be even more robust at lower doping ($T_c \approx 55$ K), and hence to be unrelated to the charge-order instability. The Y-shaped (wine-glass) spectrum, rather than the X-shaped (hour-glass) excitations seen in structurally more complex cuprates, appear to be the underlying normal-state response of the cuprates. This insight is important, as SC pairing may be driven by AF correlations. The response is enhanced below the pseudogap (PG) temperature, indicating that AF correlations are affected by, but do not drive the PG formation. In the PG state, the cuprates exhibit unusual intra-unit-cell magnetism. Building on prior work, *Greven* performed polarized neutron diffraction measurements to determine the moment direction [19]. The observed angle of $70^\circ \pm 10^\circ$ away from the normal to the CuO_2 layers rules out purely planar loop currents and high-symmetry Dirac multipoles, two prominent proposals for the microscopic origin. However, the data are consistent with Dirac multipoles of lower symmetry or, alternatively, with a particular configuration of loop currents along the faces of the CuO_6 octahedra.

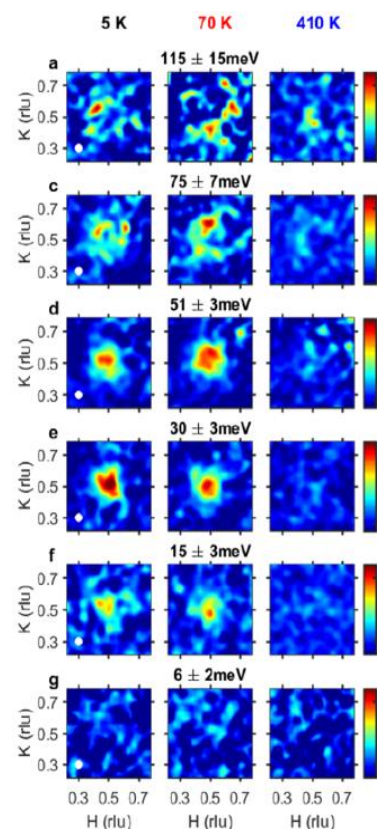


Figure 2: Neutron TOF data confirm Y-shaped magnetic response. Susceptibility in units of $\mu_B^2 \text{eV}^{-1} \text{f.u.}^{-1}$ at 5 K (left), 70 K (middle) and 410 K (right) for Hg_{1201} ($p \approx 0.064$, $T_c \approx 55$ K, $T \approx 400$ K). Data averaged within indicated energy ranges. White dots (left): FWHM resolution.

Examples of recent CQM progress – cobaltites. Emphasis has been placed on the use of tuning of oxygen vacancy (V_O) density and spatial ordering to control electronic and magnetic properties (*Leighton* and *Greven*). Examples include V_O -based control of thermal conductivity, which can be reduced to almost the amorphous limit even in highly epitaxial systems [5], and magnetic order and anisotropy [16]. Strain-based tuning of the orientation of long-range V_O ordering in $\text{La}_{1-x}\text{Sr}_x\text{CoO}_{3-\delta}$ is now under exquisite control, enabling *perpendicular* magnetic anisotropy [16]. Large perpendicular anisotropy (up to almost 10^7 erg/cm³, despite the absence of high Z elements) occurs under compressive strain, where the naturally-formed in-plane superlattice associated with V_O order plays the key role [16]. Other enhancements of anisotropic properties have been found under these conditions, including what may be the largest anisotropic magnetoresistance values recorded. Control of dead layers by this approach is currently being pursued. These methods are also being extended to other materials, such as BaSnO_3 , where V_O -based doping control has now been demonstrated [9]. Moreover, dynamical electrochemical control of V_O density and order is being explored by *Leighton*, *Greven*, and *Fernandes*. In CQM/MRSEC collaborative research, synchrotron X-ray diffraction (SXR) and polarized neutron reflectometry (PNR) are being used as powerful *operando* probes of electrolyte-gated perovskites [6,18,20]. Electrochemical control of Curie temperature in $\text{La}_{1-x}\text{Sr}_x\text{CoO}_{3-\delta}$ is now possible over a 220 K window (*via* V_O induction, verified by *operando* SXR and PNR) [6], while pure electrostatic gating has induced a record 150 K modulation of the Curie point [18]. The latter was verified directly by PNR at the SNS, on only 6 unit-cell-thick films.

The perplexing problem of FM in tensile-strained films of undoped LaCoO_3 is also under investigation. This has recently been tuned *via* chemical substitution [7], pointing to potential means to tune the spin gap, and thus approach the putative spin-state quantum critical point. CQM research has also discovered a majority carrier type inversion from p to n with tensile strain, revealing a previously unknown link to the existence of ferromagnetism (*Leighton*, *Biról*).

Future Plans

Building on the success of our synergistic approach, we will deepen our efforts to tackle important questions pertaining to these model systems, and expand our reach to other promising oxides. These include *bismuthates*, which display charge order and unconventional superconductivity, and *metallic delafossites*, which display record-breaking oxide conductivities, hydrodynamic electron flow, and possibly nontrivial electronic topology. We will emphasize a dual thin film/bulk crystal approach wherever feasible, model systems, neutron and X-ray investigations, and collaboration with experts in the use of complementary methods. Overarching questions are how such systems evolve from strongly-correlated insulators to weakly-correlated metals *via* interesting intermediate states, and the role of local *vs.* average structure in determining the myriad phases. A key cross-cutting aspect will be advancement and utilization of novel experimental approaches (hybrid MBE, plastic-deformation control, next-level diffuse scattering, nonlinear magnetic response, *etc.*), and state-of-the-art first-principles computation.

Publications

1. "Hourglass Dispersion and Resonance of Magnetic Excitations in the Superconducting State of the Single-Layer Cuprate $HgBa_2CuO_{4+\delta}$ ", M. K. Chan, Y. Tang, C. J. Dorow, J. Jeong, L. Mangin-Thro, M. J. Veit, Y. Ge, D. L. Abernathy, Y. Sidis, P. Bourges, and **M. Greven**, Phys. Rev. Lett. **117**, 277002 (2016).
2. "A unified view of the substitution-dependent antiferrodistortive phase transition in $SrTiO_3$ ", E. McCalla, J. Walter and **C. Leighton**, Chem. Mater. **28**, 7973 (2016).
3. "Interface-induced phenomena in magnetism", F. Hellman, A. Hoffmann, Y. Tserkovnyak, G.S.D. Beach, E.E. Fullerton, **C. Leighton**, A.H. MacDonald, D.C. Ralph, D.A. Arena, H.A. Durr, P. Fischer, J. Grollier, J.P. Heremans, T. Jungwirth, A.V. Kimel, B. Koopmans, I.N. Krivorotov, S.J. May, A.K. Petford-Long, J.M. Rondinelli, N. Samarth, I.K. Schuller, A.N. Slavin, M.D. Stiles, O. Tchernyshyov, A. Thiaville and B.L. Zink, Rev. Mod. Phys. **89**, 025006 (2017).
4. "Synchrotron x-ray scattering study of charge-density-wave order in $HgBa_2CuO_{4+\delta}$ ", W. Tabis, B. Yu, I. Bialo, M. Bluschke, T. Kolodziej, A. Kozłowski, E. Blackburn, K. Sen, E. M. Forgan, M. v. Zimmermann, Y. Tang, E. Weschke, B. Vignolle, M. Hepting, H. Gretarsson, R. Sutarto, F. He, M. Le Tacon, N. Barišić, G. Yu and **M. Greven**, Phys. Rev. B **96**, 134510 (2017).
5. "Glass-Like Through-Plane Thermal Conductivity Induced by Oxygen Vacancies in Nanoscale Epitaxial $La_{0.5}Sr_{0.5}CoO_{3-\delta}$ ", X. Wu, J. Walter, T. Feng, J. Zhu, H. Zheng, J.F. Mitchell, N. Biskup, M. Varela, X. Ruan, **C. Leighton** and X. Wang, Adv. Func. Mater. **27**, 1704233 (2017). (Cover Article)
6. "Ion-Gel-Gating-Induced Oxygen Vacancy Formation in Epitaxial $La_{0.5}Sr_{0.5}CoO_{3-\delta}$ Films from in operando X-ray and Neutron Scattering", J. Walter, G. Yu, B. Yu, A. Grutter, B. Kirby, J. Borchers, Z. Zhang, H. Zhou, T. Birol, **M. Greven**, and **C. Leighton**, Phys., Rev. Mater. **1**, 071403(R) (2017).
7. "Magnetism in epitaxial $PrCoO_3$ and $Pr_{0.7}Y_{0.3}CoO_3$ thin films", T.D. Sanders, U.S. Alaan, M.T. Gray, S. Bose, M. Taylor, M. Cabero, V. Mehta, M. Varela, **C. Leighton** and Y. Suzuki, J. Mag. Mag. Mat. **451**, 654-659 (2018).
8. "Interconversion of intrinsic defects in $SrTiO_3(001)$ ", S.A. Chambers, Y. Du, Z. Zhu, J. Wang, M.J. Wahila, L.F.J. Piper, A. Prakash, J. Yue, **B. Jalan**, S.R. Spurgeon, D.M. Kepaptsoglou, Q. M. Ramasse, and P.V. Sushko, Phys. Rev. B. **97**, 245204 (2018).
9. "Electrical transport, magnetic, and thermodynamic properties of La-, Pr- and Nd-doped $BaSnO_{3-d}$ single crystals", E. McCalla, D. Phelan, M.J. Krogstad, B. Dabrowski and **C. Leighton**, Phys. Rev. Materials **2**, 084601 (2018).
10. "Effects of Lifshitz transitions in ferromagnetic superconductors: the case of $URhGe$ ", Y. Sherkunov, **A. V. Chubukov**, and J. Betouras, Phys. Rev. Lett. **121**, 097001 (2018).
11. "Changes in physical properties of 4C pyrrhotite (Fe_7S_8) across the 32 K Besnus transition", M.W.R. Volk, E. McCalla, B. Voigt, M. Manno, **C. Leighton** and J.M. Feinberg, American Mineralogist **103**, 1674 (2018).
12. "Emergence of superconductivity in the cuprates via a universal percolation process", D. Pelc, M. Vučković, M. Grbić, M. Požek, G. Yu, T. Sasagawa, **M. Greven**, N. Barišić, Nat. Commun. **9**, 4327 (2018).
13. "Percolative nature of the direct current paraconductivity in the cuprate superconductors", P. Popčević, D. Pelc, Y. Tang, K. Velebit, Z. Anderson, V. Nagarajan, G. Yu, M. Požek, N. Barišić, **M. Greven**, npj Quantum Materials **3**, 42 (2018).
14. "Impact of disorder on the superconducting transition temperature near a Lifshitz transition", T. V. Trevisan, M. Schütt, and **R. M. Fernandes**, Phys. Rev. B **98**, 094514 (2018).
15. "Unconventional multi-band superconductivity in bulk $SrTiO_3$ and $LaAlO_3/SrTiO_3$ interfaces", T. V. Trevisan, M. Schütt, and **R. M. Fernandes**, Phys. Rev. Lett. **121**, 127002 (2018).

16. *Perpendicular magnetic anisotropy via strain-engineered oxygen vacancy ordering in epitaxial $\text{La}_{1-x}\text{Sr}_x\text{CoO}_3$* ", J. Walter, M. Cabero Piris, B. Yu, G. Yu, **M. Greven**, M. Varela, and **C. Leighton**, *Phys. Rev. Materials* **2**, 111404(R) (2018).
17. *"Growth and characterization of $\text{HgBa}_2\text{CaCu}_2\text{O}_{6+\delta}$ and $\text{HgBa}_2\text{Ca}_2\text{Cu}_3\text{O}_{8+\delta}$ crystals"*, L. Wang, X. Luo, J. Li, J. Zhen, M. Cheng, J. Freyermuth, Y. Tang, B. Yu, G. Yu, **M. Greven**, and Y. Li, *Phys. Rev. Materials* **2**, 123401 (2018).
18. *Giant electrostatic modification of magnetism via electrolyte-gate-induced cluster percolation in $\text{La}_{1-x}\text{Sr}_x\text{CoO}_{3-\delta}$* ", J. Walter, T. Charlton, H. Ambaye, M. R. Fitzsimmons, P. P. Orth, **R. M. Fernandes** and **C. Leighton**, *Phys. Rev. Materials* **2**, 111406(R) (2018).
19. *"Orientation of the intra-unit-cell magnetic moment in the high- T_c cuprate superconductor $\text{HgBa}_2\text{CuO}_{4+\delta}$ "*, Y. Tang, L. Mangin-Thro, A. Wildes, M. K. Chan, C. J. Dorow, J. Jeong, Y. Sidis, **M. Greven**, and P. Bourges, *Phys. Rev. B* **98**, 1214418 (2018).
20. *"Electrolyte-based control of functional materials: Electronics or ionics?"*, **C. Leighton**, *Nat. Mater.* **18**, 13 (2019).
21. *"Magnetic small-angle neutron scattering"*, S. Muhlbauer, A. Heinemann, M. Eskildsen, **C. Leighton**, E. Perigo, F. Bergner, S. Disch, S. Erokhin, D. Berkov and A. Michels, *Rev. Mod. Phys.* **91**, 015004 (2019).
22. *"Unusual behavior of cuprates explained by heterogeneous charge localization"*, D. Pelc, P. Popčević, G. Yu, M. Požek, **M. Greven**, N. Barišić, *Sci. Adv.* **5**, eaau4538 (2019).
23. *"Signatures of enhanced superconducting phase coherence through MID-IR excitation in optimally doped Y-Bi2212 "*, F. Giusti, A. Marciniak, F. Randi, G. Sparapassi, F. Boschini, H. Eisaki, **M. Greven**, A. Damascelli, A. Avella, and D. Fausti, *Phys. Rev. Lett.* **122**, 067002 (2019).
24. *Low temperature specific heat of doped SrTiO_3 : Doping dependence of the effective mass and Kadowaki-Woods scaling violation"*, E. McCalla, M. Navarro-Gastiasoro, G. Cassuto, **R. M. Fernandes**, and **C. Leighton**, *Phys. Rev. Materials* **3**, 022001(R) (2019).
25. *"Universal precursor of superconductivity in the cuprates"*, G. Yu, D.-D. Xia, D. Pelc, R.-H. He, N.-H. Kaneko, T. Sasagawa, Y. Li, X. Zhao, N. Barišić, A. Shekhter, and **M. Greven**, *Phys. Rev. B*, in press (2019); arXiv:1710.10957.
26. *Universal superconducting precursor regime in perovskite-based oxides"*, D. Pelc, Z. Anderson, B. Yu, **C. Leighton**, and **M. Greven**, *Nat. Commun.*, in press (2019); arXiv:1808.05763.
27. *"Diagonal nematicity in the pseudogap phase of $\text{HgBa}_2\text{CuO}_{4+\delta}$ "*, H. Murayama, Y. Sato, R. Kurihara, S. Kasahara, Y. Mizukami, Y. Kasahara, H. Uchiyama, A. Yamamoto, E.-G. Moon, J. Cai, J. Freyermuth, **M. Greven**, T. Shibauchi, and Y. Matsuda, in review with *Nat. Commun.*; arXiv:1805.00276.
28. *"Evidence for a universal Fermi-liquid scattering rate throughout the phase diagram of the copper-oxide superconductors"*, N. Barišić, M. K. Chan, M. J. Veit, C. J. Dorow, Y. Ge, Y. Tang, W. Tabis, G. Yu, X. Zhao, and **M. Greven**, submitted to *New. J. Phys.*
29. *"Hopping transport in $\text{SrTiO}_3/\text{Nd}_x\text{Ti}_{1-x}\text{O}_3/\text{SrTiO}_3$ heterostructures"*, L. R. Thoutam, J. Yue, P. Xu, and **B. Jalan**, submitted to *Phys. Rev. Materials*; arXiv:1811.11311.
30. *"Evidence for multiband superconductivity above the Paul limit in $\text{Nd}_x\text{Sr}_{1-x}\text{TiO}_3$ "*, Y. Ayino, J. Yue, X. Cai, T. Wang, **B. Jalan**, and V. Pribiag, submitted to *Phys. Rev. B*; arXiv:1812.02875.
31. *Phonon-mediated superconductivity in low carrier-density systems"*, M. N. Gastiasoro, **R. M. Fernandes**, and **A. V. Chubukov**, *Phys. Rev. B* **99**, 094524 (2019).
32. *"Resistivity phase diagram of the cuprates revisited"*, D. Pelc, M. J. Veit, M. K. Chan, G. Yu, N. Barišić, and **M. Greven**. Submitted to *npj Quantum Materials*; arXiv:1902.00529.

33. "*Superconductivity at small Fermi energy – the analysis beyond ladder approximation*", D. Phan and **A. V. Chubukov**. Submitted to Phys. Rev. B.
34. "*Disentangling spin-orbit coupling and local magnetism in a quasi-2D electron system*", X. Cai, Y. Ayino, J. Yue, P. Xu, **B. Jalan**, and V. Pribiag, submitted to Phys. Rev. Lett.
35. "*Unusual dynamic charge-density-wave correlations in $\text{HgBa}_2\text{CuO}_{4+\delta}$* ," B. Yu, W. Tabis, I. Bialo, F. Yakhou, N. Brookes, Z. Anderson, Y. Tang, G. Yu and **M. Greven**, submitted to Phys. Rev. X.

Understanding the Structure and Dynamics of Conjugated Polymers by Advancing Deuteration Chemistry and Neutron Scattering

Xiaodan Gu and Jason Azoulay, School of Polymer Science and Engineering, The University of Southern Mississippi

Program Scope

This program aims to understand the structure and dynamics of conjugated polymers (CPs) by new click based deuteration chemistry and neutron scattering. This project aims to: i) develop new methodologies to efficiently deuterate sidechains of CPs; ii) understand the role of dynamic and static disorder of the sidechains on backbone rigidity and how this impacts optical, mechanical and electronic properties; and iii) formulate design principles for next-generation CPs that are resilient to disorder through precise control of electronic structure through manipulating backbone and side chain structure. This project will provide new methodologies to quantitatively measure chain conformation of CPs, which is vital for further advancements, understanding underlying structure-function relationships that lead to emerging CPs, discovering new phenomena, improving device performance, and creating new energy-related technologies.

Recent Progress

This project started in September 2018. During the past 9 months, the team made the following progress regarding development CPs with deuterated sidechains and characterization of those CPs by neutrons.

Develop method to prepare deuterated conjugated polymers. The team prepared several CPs with deuterated sidechains. Two different routes for adding deuterated sidechain onto various CPs were used. The first route aims to use the click chemistry to add thiol-functionalized deuterated sidechains to the CP's backbone. We focused on the polyfluorene polymers as a starting point, which previously we had experience to synthesis. Parallely, another route was used to synthesize CPs with deuterated sidechains, starting from the monomer level. This bottom-up route focused on attaching deuterated functional sidechains to a conjugated monomer, then polymerizing the monomer. Both methods were performed in parallel to compare efficiency of deuteration of CPs. The bottom up synthesis route was performed by graduate student hosted full time at the CNMS, a user facility at ORNL, through approved user proposal.

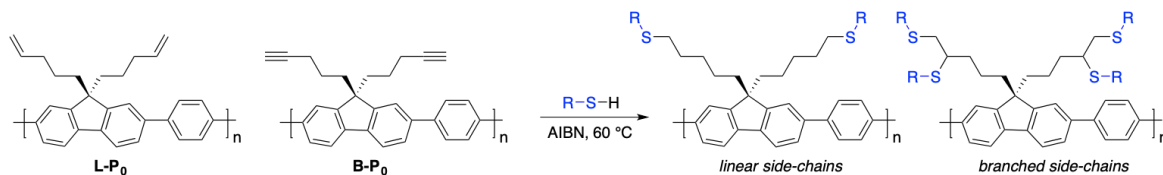


Figure 1. Scope of Thiol-X post-modification strategy on CPs providing linear and branched side-chains

In the first route to use click chemistry to prepare deuterated conjugated polymers, we accomplished the following synthesis work. The post-modification click-on methodology is highly efficient and allows the placement of various sidechains (different length, branching points, functionality) onto the same CP scaffold¹. By “clicking” the functionalities onto the CP after polymerization, batch-to-batch variation can be reduced between polymers with different side-chains, allowing for a more controlled assessment of structure-function-property relationships. Alkene and alkyne hydrothiolations, commonly referred to as thiol-ene and thiol-yne reactions respectively, or thiol-x chemistries collectively, have been widely utilized in the areas of material science, nanotechnology, and bioconjugation due to their fast reaction rates, high yields, functional group tolerance, and powerful thermodynamic driving force². By synthesizing polymer backbones with pendant reactive handles, and subsequently functionalizing the CPs through these approaches, the synthetic rigor to access a library of structurally diverse CPs is reduced dramatically. This post-modification approach is demonstrated in **Figure 1**, where pre-organized scaffolds with pendant alkene and alkyne functional groups are post-functionalized through thiol-ene and thiol-yne reactions respectively. Past progress involves controlling reaction conditions such as temperature, additives, catalyst, and stoichiometries to allow access to high molecular weight linear CPs with pendant olefins without the need of the organotin species required for the Stille reaction. We synthesized several PFO based polymers with deuterated sidechains using above approach. This approach will be further expanded to other D-A polymers.

We also synthesized deuterated poly(3-alkyl)thiophenes (P3AT), a well-known conjugated polymer, with various length of side chains using the bottom up approach³. This chemistry allows the incorporation of fully deuterated side chains, leaving no protic regions between the polymer backbone and deuterated side chains. Therefore, it allows simplified interpretation of fundamental structural properties such as persistence length,

dihedral angle, conjugation length, etc. P3ATs were synthesized by a modified GRIM method, as described in **Figure 2**. Briefly speaking, 3-bromothiophene and deuterated alkyl magnesium bromide participate in a Kumada reaction with Ni(dppp)Cl₂ catalyst to yield 3-alkylthiophene compounds⁴. After adding a bromide in the second position and fifth position by reacting with N-bromosuccinimide in a mixture solvent of chloroform and acetic acid, 2,5-dibromo-3-alkylthiophene monomers were obtained. The intermediate was reacted with Grignard reagent (isopropylmagnesium chloride) and Ni(dppp)Cl₂ catalyst to polymerize the monomers to form P3ATs with various length of deuterated sidechains. P3ATs (P3PT-d11, P3HT-d13, P3OT-d17, and P3DT-d21) were synthesized with close molecular weight (20 kg/mol) and low PDI (e.g.

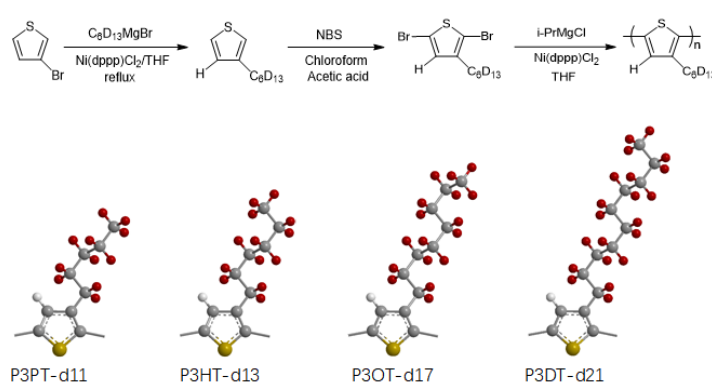


Figure 2. Synthesis of P3ATs with deuterated side-chains. Four deuterated conjugated polymers were prepared.

<1.05). High-resolution ^1H NMR and ^{13}C NMR spectroscopy were utilized to determine the chemical structure of the synthesized P3ATs. The results showed that side-chain deuterated P3ATs with various length of side chains were successfully synthesized. These polymers have very high regularities of over 97%.

Probe conjugated polymers backbone conformation by neutron scattering in contrast varied solvents. We first performed solution scattering for the non-deuterated CPs (P3AT, PFO and DPP CPs) in solvents to study the chain conformation. Take DPP polymers for example, we put backbone building blocks with different flexibility and examined their property (**Figure 3**) at two polymer concentrations (1mg/ml and 5mg/ml) and temperatures (room temperature and elevated temperature). We were able to develop an understanding for CP's chain conformation, which would lay a foundation for the following up experiments for measuring the backbone rigidity of those polymers in contrast matched solvent with sidechains. The preliminary results suggested that those DPP polymer has a rigid backbone compared to P3ATs. The Kuhn length for the DPP polymer was measured to be around 10nm, which is around two times higher than P3AT polymer⁵. The preliminary result indicated that those rigid backbone could be responsible to improved charge transfer property. We are in the process of comparing DPP polymers from the same family but with different sidechains to understand the effect of sidechain's influence on polymer's backbone rigidity⁶.

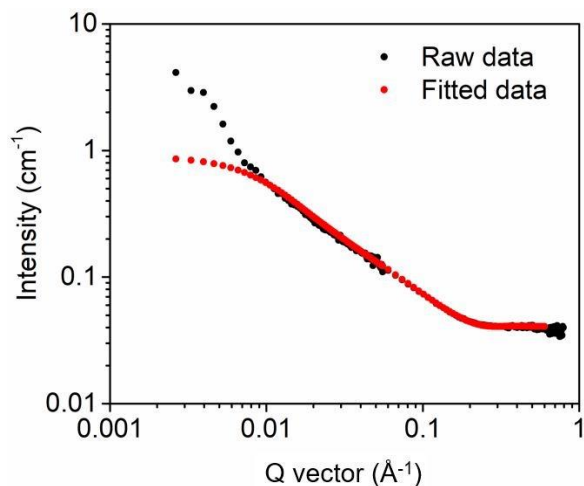


Figure 3. Neutron scattering raw curve (black dot) and fitted curve (red dot) for DPP-T polymer. A flexible cylinder model was used to fit the data using a q range from 0.008 \AA^{-1} to 0.9 \AA^{-1} due to the strong aggregation behavior shown at low q , the contour length and persistence length were fitted to be 216 \AA and 90 \AA , respectively.

Influence of the backbone rigidity on the physical property of CPs. The research team designed and synthesized 10 different DPP polymers and studied their thin film mechanical property. We found the backbone rigidity play a key role in determining the thin film mechanical property probed by our thin film tensile stage. Several works based on this new technique were published early this year in Advanced Electronic Materials [Publication 3], Advanced Materials [Publication 4], and Chemistry of Materials [Publication 5]. We also started to look into the effect of backbone rigidity on the crystallization of conjugated polymers [Publication 2]. Preliminary results suggested that the rigidity of the polymer also strongly influences the crystallization kinetics. The work to relate the backbone rigidity to the optical and electronic property of the CPs will start in year 2.

Future Plans

Following the successful preparation of several deuterated CPs, we will focus on the following tasks in near future.

1) We will further expand the deuterated chemistry by using both bottom-up and post-modification approaches to prepared CPs with deuterated sidechains. We will focus on several state-of-the-art donor-acceptor CPs such as DPP or Isoindigo polymers, which are widely used in organic electronic device and have superior performance than P3AT CPs.

2) We will continue to use neutron scattering to probe the chain conformation and backbone rigidity for CPs in solution. We will measure deuterated CPs in contrast-varied solvents to obtain scattering information originated from polymeric backbone and obtain degree of backbone rigidity. Along this line, we aim to establish collaboration with molecular dynamic (MD) simulation research group to compare the experimental results with simulations. We will also perform neutron spectroscopy to understand the heterogeneity of dynamics for a given polymer chain. We expect that understand the backbone dynamic potentially can provide new angle to under the charge transport phenomenon for organic electronic dynamics.

3) We will study the effect of the rigidity of polymer backbone on their physical, optical and electronic property. We plan to perform solution-based spectroscopy (UV-vis and fluorescence spectroscopy) on previous synthesis CPs with or without deuterated sidechains. We expect the rigidity of the polymer backbone would have an impact on their conjugated length and optical property. The electronic property of the polymeric thin film will also be measured in thin film transistor devices. We hypothesize that the rigid and planer polymer backbone could impact the charge transport property.

References

- (1) Hoyle, C. E.; Bowman, C. N. Thiol–Ene Click Chemistry. *Angew. Chem. Int. Ed.* **2010**, *49* (9), 1540–1573.
- (2) Smith, K. A.; Lin, Y.-H.; Dement, D. B.; Strzalka, J.; Darling, S. B.; Pickel, D. L.; Verduzco, R. Synthesis and Crystallinity of Conjugated Block Copolymers Prepared by Click Chemistry. *Macromolecules* **2013**, *46* (7), 2636–2645.
- (3) Shao, M.; Keum, J.; Chen, J.; He, Y.; Chen, W.; Browning, J. F.; Jakowski, J.; Sumpter, B. G.; Ivanov, I. N.; Ma, Y.-Z.; Rouleau, C. M.; Smith, S. C.; Geohegan, D. B.; Hong, K.; Xiao, K. The Isotopic Effects of Deuteration on Optoelectronic Properties of Conducting Polymers. *Nature Communications* **2014**, *5*, 3180EP—3111.
- (4) Osaka, I.; McCullough, R. D. Advances in Molecular Design and Synthesis of Regioregular Polythiophenes. *Acc. Chem. Res.* **2008**, *41* (9), 1202–1214.
- (5) McCulloch, B.; Ho, V.; Hoarfrost, M.; Stanley, C.; Do, C.; Heller, W. T.; Segalman, R. A. Polymer Chain Shape of Poly(3-Alkylthiophenes) in Solution Using Small-Angle Neutron Scattering. *Macromolecules* **2013**, *46* (5), 1899–1907.

- (6) Nielsen, C. B.; Turbiez, M.; McCulloch, I. Recent Advances in the Development of Semiconducting DPP-Containing Polymers for Transistor Applications. **2013**, *25* (13), 1859–1880.

Publications [from Sept 2018 to Jun 2019]

- (1) London, A. E.; Chen, H.; Sabuj, M. A.; Tropp, J.; Saghayezhian, M.; Eedugurala, N.; Zhang, B. A.; Liu, Y.; Gu, X.; Wong, B. M.; Rai, N.; Bowman, M. K.; Azoulay, J. D. A High-Spin Ground-State Donor-Acceptor Conjugated Polymer. *Sci Adv* 2019, *5* (5), eaav2336.
- (2) Qian, Z.; Cao, Z.; Galuska, L.; Zhang, S.; Xu, J.; Gu, X. Glass Transition Phenomenon for Conjugated Polymers. *Macromol. Chem. Phys.* 2019, *361*, 1900062–30.
- (3) Zhang, S.; Ocheje, M. U.; Huang, L.; Galuska, L.; Cao, Z.; Luo, S.; Cheng, Y.-H.; Ehlenberg, D.; Goodman, R. B.; Zhou, D.; Liu, Y.; Chiu, Y.-C.; Azoulay, J. D.; Rondeau-Gagné, S.; Gu, X. The Critical Role of Electron-Donating Thiophene Groups on the Mechanical and Thermal Properties of Donor-Acceptor Semiconducting Polymers. *Adv. Electron. Mater.* 2019, *26*, 1800899–11.
- (4) Yao, Z.-F.; Zheng, Y.-Q.; Li, Q. Y.; Lei, T.; Zhang, S.; Zou, L.; Liu, H. Y.; Dou, J.-H.; Lu, Y.; Wang, J.-Y.; Gu, X.; Pei, J. Wafer-Scale Fabrication of High-Performance N-Type Polymer Monolayer Transistors Using a Multi-Level Self-Assembly Strategy. *Adv. Mater.* 2018, *0* (0), 1806747–1806749.
- (5) Wang, G.-J. N.; Zheng, Y.; Zhang, S.; Kang, J.; Wu, H.-C.; Gasperini, A.; Zhang, H.; Gu, X.; Bao, Z. Tuning the Cross-Linker Crystallinity of a Stretchable Polymer Semiconductor. *Chem. Mater.* 2018, acs.chemmater.8b04314.

Rheo-structural spectroscopy: fingerprinting the *in situ* response of fluids to arbitrary flow

Matthew E. Helgeson, Dept. of Chemical Engineering, UC Santa Barbara

Program Scope

Small angle neutron and X-ray scattering (SANS/SAXS) are powerful tools for understanding and engineering flow-structure coupling during processing of complex fluids, such as polymeric liquids and colloidal suspensions. Although existing methods for *in situ* neutron scattering during flow have been successful in characterizing structure-processing-property relationships for fluids under shearing deformation, most industrial processes involve more complicated deformations including combinations of shearing, elongation, and rotation. The goal of this research program is to develop new tools for *in situ* SANS/SAXS measurements under fluid flows involving arbitrary, time-programmable deformation types, and apply these tools to study microstructural transformations in energy-relevant complex fluids including polymeric liquids and nanoparticle suspensions. This is achieved through three primary objectives to: (1) design and validate a fluidic four roll mill (FFoRM) device and associated methods that are optimized for SANS/SAXS and flow velocimetry measurements; (2) combine the FFoRM with modeling to develop and refine microscopically-informed rheological models for complex fluids in complex deformations; (3) understand how deformation type and nanoscale architecture impact a number of flow-induced structural transformations observed during processing of a range of complex fluids.

Recent Progress

In the previous reporting period, we successfully developed a FFoRM device capable of both flow visualization and *in situ* SANS measurements under programmable processing flow histories.[1] In the current period, we developed a general theory and computational workflow for simulating 2D SANS/SAXS patterns under flow. This powerful new tool has enabled a number of studies into detailed flow-structure coupling of orientable polymeric fluids including semiflexible polymers, cellulosic nanomaterials and surfactant micelles. We have also adapted the FFoRM-SANS device for SAXS imaging measurements, which enables high spatiotemporal resolution measurements to map the dynamic response of fluid structure to a range of programmed processing flows. These examples highlight the unique capabilities enabled by combining novel programmable flows within neutron and X-ray beams with advanced modeling.

Modeling 2D SANS/SAXS patterns of orientable fluids. Conventional analyses for anisotropic scattering from orientable microstructures in flow and other forcing fields has largely been limited to calculation of reduced scalar order parameters from raw scattering data that describe the average orientation and degree of alignment of the scattering anisotropy at a particular q -value or discrete range of q -space.[2] Such low-dimensionality parameterizations, though generally applicable, fail to provide direct mechanistic detail about flow-structure coupling. For example, they are incapable of separating anisotropic intra- and inter-particle correlations that encode information about single molecule dynamics and intermolecular interactions.

To gain deeper insight into the structures encoded by anisotropic scattering, we have developed a general theoretical framework and associated workflow for modeling 2D anisotropic scattering from orientable fluids (Figure 1, left panel). Two advances in scattering theory and analysis underlie the development of this powerful new tool. The first involves a general mathematical framework for describing the scattering from individual orientable particles relative to the scattering coordinate frame using a transformation matrix approach, enabling computationally efficient calculation of the scattering from particles with a prescribed 3D orientation probability distribution function (OPDF). The second involves a novel Bayesian inversion method that uses the former advance to provide a model-free “fit” of the 2D scattering pattern to a high-resolution 3D OPDF. This model-free approach allows for separation of the measured scattering into the contributions from the form factor, $P(\mathbf{q})$, which encodes the 3D OPDF, and the effective structure factor, $S_{\text{eff}}(\mathbf{q})$, which encodes interparticle interactions.

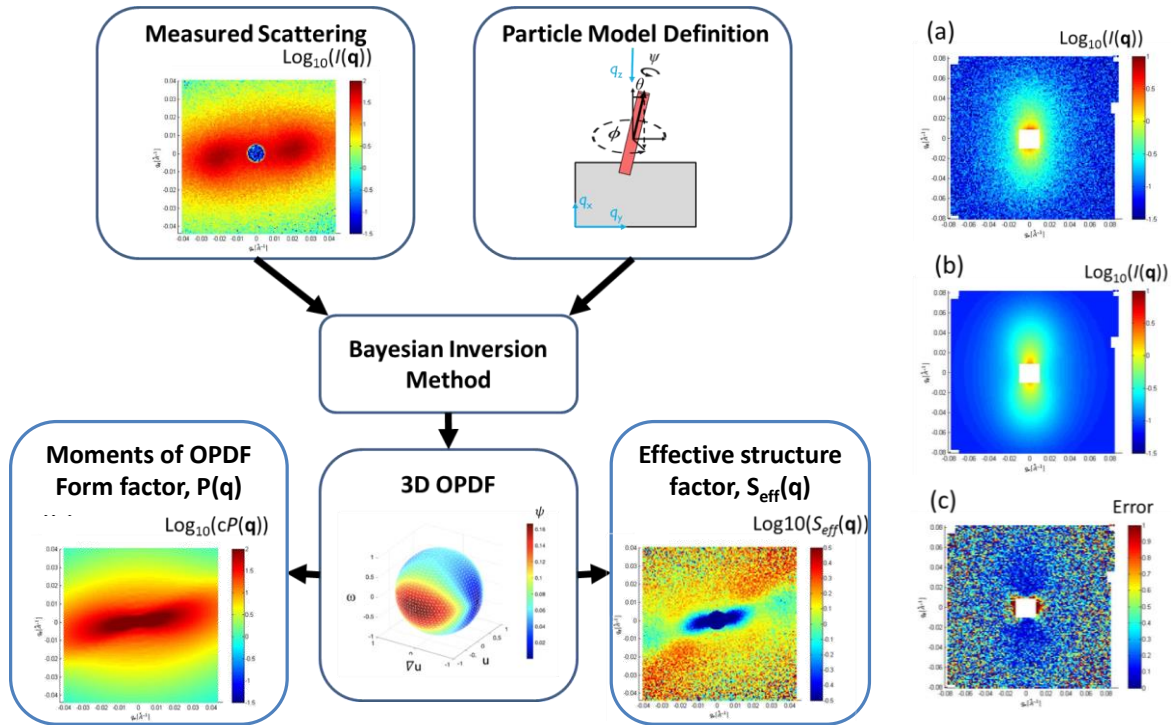


Figure 1. (Left panel) Workflow for our new framework to fit 2D SANS/SAXS patterns from oriented fluids, resulting in model-free estimations of the 3D orientation probability distribution function (OPDF) and effective structure factor, $S_{\text{eff}}(\mathbf{q})$. **(Right panel)** Model validation using parameter-free predictions of 2D SANS patterns from fd-virus solutions in shear flow. (a) Measured rheo-SANS spectra for the dilute fd-virus dispersion under shear flow ($\dot{\gamma} = 512 \text{ s}^{-1}$). (b) Model predicted SANS spectra for physical parameters chosen to match this fd-virus dispersion in shear flow ($\dot{\gamma} = 512 \text{ s}^{-1}$). (c) Error between the two spectra, where $\text{Error} = |I_{\text{measured}} - I_{\text{theory}}|/I_{\text{theory}}$.

Testing theories for rod-like polymers in flow. To test the framework described above as well as contemporary theories for rod-like polymers, we use flow-SANS measurements on dilute solutions of fd-virus, a model rigid rod-like polymer,[3] in shear flow (Fig. 1, right panel). The previously described Bayesian inversion method was used to estimate the 3D OPDF from 2D scattering patterns in the flow-vorticity plane (Fig. 1a). Independently, the Doi-Edwards-Kuzuu theory for the dynamics of Brownian rod-like suspensions [4] was used to predict the OPDF, and the resulting 2D scattering pattern (Fig. 1b). The results are in quantitative agreement over a range of shear rates (Figure 1c), validating both our modeling framework and the theory.

Understanding the role of interparticle forces on flow-induced ordering of orientable fluids.

Despite the accuracy of dilute theories for orientable particles in predicting flow-induced structure, theories for semi-dilute and concentrated systems have been largely untested due to the complicated coupling of flow with interparticle interactions. The measurement and analysis tools we have developed are ideally suited to addressing this challenge. As a model system, we choose to study rigid rod-like colloidal dispersions of cellulose nanocrystals (CNCs), which show liquid crystalline phases representative of many orientable particle and polymeric systems. Flow-SANS and flow-SAXS measurements (described below) were taken over a range of flow types spanning steady shear and elongation, as well as during transient changes in flow type. Our new modeling tools enable independent estimation of the interparticle form factor particle orientation and the anisotropic effective structure factor, $S_{\text{eff}}(\mathbf{q})$, which encodes information about interparticle interactions. To our knowledge, this is the first time the latter quantity has been directly accessible in SANS measurements. Representative results are shown in Fig. 1 (left panel). The anisotropic “peak” in $S_{\text{eff}}(\mathbf{q})$ suggests that CNCs exhibit both strong orientational and weak translational ordering due to the influence of interparticle interactions. The latter has not yet been predicted by any theory, and so our results call for new theories into the coupling of interparticle interactions and flow in the ordering of non-dilute rod-like systems.

Fingerprinting strain-dependent structural response in processing-like flows. The long-range objective of this project is to enable the “fingerprinting” of how fluid microstructure evolves in response to an arbitrary flow history meant to simulate an industrial process of interest. Achieving this grand vision requires scattering measurements with fine spatial ($<100 \mu\text{m}$) and temporal ($<1 \text{ s}$) resolution that are outside the achievable parameters of existing SANS instruments. To bridge this gap, we have adapted the FFORM-SANS device for SAXS measurements (Fig. 2a). The re-designed device also significantly increases the achievable deformation rates to $>1000 \text{ s}^{-1}$. Our first FFORM-SAXS imaging experiments on CNC suspensions show the power of this approach, in which the microstructure within a programmed flow in the FFORM can be mapped with high spatial ($\sim 10 \mu\text{m}$) and temporal ($\sim 100 \text{ ms}$) resolution (Figure 1b). In this way, the transient microstructure of a complex fluid can be mapped as it evolves in a Lagrangian frame during programmed changes in flow type and rate.

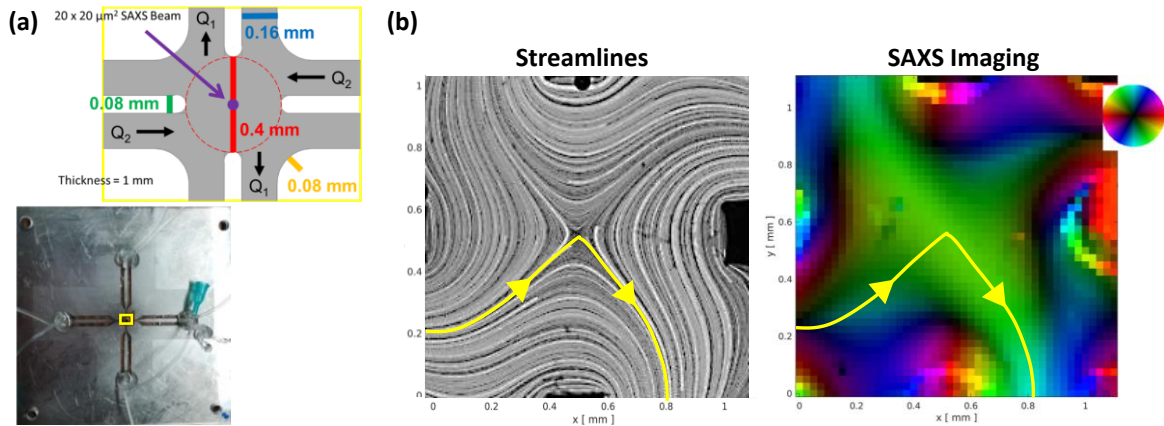


Figure 2. (a) Re-designed FFORM device for SAXS imaging measurements. Inset shows device dimensions and typical beam size. (b) Streamline image (left) and SAXS map (right) of a CNC suspension at a nominal rotational Peclet number of $Pe_r = 2$. In the SAXS image, each pixel represents an independently measured SAXS pattern. Pixel hue represents the direction of average orientation (see inset scale) and intensity represents the degree of alignment along the direction of average orientation. Yellow line indicates the inflow and outflow directions.

Future Plans

We plan to use our new modeling framework to highlight both the limitations of conventional low-dimensional parameterization of anisotropic scattering patterns and the deeper information gained through model-free estimation of the 3D OPDF and $S_{\text{eff}}(\mathbf{q})$. In particular, we plan to use $S_{\text{eff}}(\mathbf{q})$ to develop a theoretical model to describe the coupling of flow with interparticle interactions and the resulting effect on non-equilibrium particle dynamics, ultimately to develop a new rheological model for semi-dilute and concentrated rod-like systems. Further FFoRM-SAXS imaging experiments will be used to fingerprint the strain-dependent microstructural response of orientable particle and polymer solutions. Ultimately, we will demonstrate the utility of the our new integrated FFoRM-SAXS and modeling approaches by designing optimized flows for developing ordered morphologies, and testing them in model 3D printing flows. Each of these studies will be the subject of publications to be submitted in the next reporting period.

References

- [1] P.T. Corona *et al.*, Scientific Reports, 2018, 8(1):15559.
- [2] A.P.R. Eberle and L. Porcar. Current Opinion in Colloid & Interface Science, 2012, 17(1): 33-43.
- [3] M.P. Lettinga and J. K. G. Dhont, Journal of Physics: Condensed Matter, 2004, 16(38): S3929.
- [4] N.Y. Kuzuu and M. Doi, Polymer Journal, 1980, 12(12): 883.

Publications

P.T. Corona, N. Ruocco, K. Weigandt, L.G. Leal and M.E. Helgeson, “A fluidic four-roll mill for in situ neutron scattering under arbitrary two-dimensional deformations”, Scientific Reports, 2018, 8(1): 15559. [DOI: 10.1038/s41598-018-33514-8]

Neutron Studies of Hybrid Excitations

R. P. Hermann, M. E. Manley, R. S. Fishman, and L. R. Lindsay

Materials Science & Technology, Oak Ridge National Laboratory, Oak Ridge, TN

Program Scope

Our program is focused on understanding how hybridized atomic vibrations control energy transport and functionalities in energy materials. Understanding and controlling hybridized excitations that couple phonons with the charge or spin of electrons will provide critical knowledge needed to design new materials with tailored thermal transport and ionic mobility and to harness quantum fluctuations for advanced ferroic sensing. Simple theoretical descriptions of the behavior of individual electrons, spins, and phonons fail when strong coupling between these quasiparticles lead to hybrid excitations and we aim to understand and use these strong couplings to control thermal transport, diffusion and phase stability. This program evolved from our earlier program (FY16-FY18) that assessed the impact of dynamic instabilities and microstructure on energy materials. Our research primarily utilizes DOE neutron scattering facilities to assess the dynamical structure factor and integrates the scattering results with first-principle and model Hamiltonian calculations. Current research thrusts include investigations of emerging lattice dynamic modes through incommensurate periodicity and strong anharmonicity, spin-fluctuation-driven thermopower in magnetic semiconductors, the interplay of charge order, spins and phonons in mixed valence oxides, and the impact of chirality and topology on lattice dynamics and quantum fluctuations.

Recent Progress

Supersonic propagation of lattice energy by phasons in fresnoite. Using neutron scattering, we made the first observations of the supersonic propagation of pure lattice energy (heat) in the piezoelectric fresnoite ($\text{Ba}_2\text{TiSi}_2\text{O}_8$) [1]. Our results show that energy moves at surprisingly high speeds of up to 4.3 times the speed of sound in the form of phasons and contribute a substantial fraction, ~20%, of the thermal transport. Phasons are quasiparticles that arise from an incommensurate modulation [2-3] in the flexible framework structure of fresnoite. Supersonic phasons enhance thermal conductivity and channel lattice energy at speeds well beyond the limits of phonons.

Anharmonic localization of lattice vibrations in thermoelectric PbSe. We observed a novel nonlinear mechanism for stopping heat-carrying phonons in a perfect crystal of thermoelectric PbSe [4], see Fig. 1. A strategy for improving thermoelectric efficiency is to reduce the transport of heat without reducing the flow of electrons. The conventional materials science approach

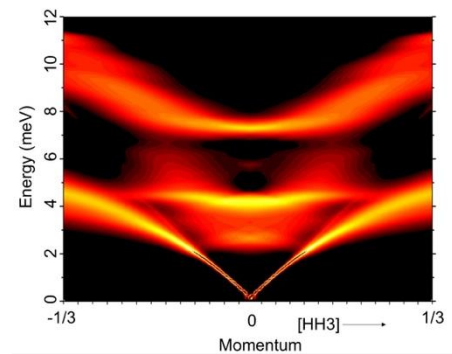


Fig 1. Calculated momentum resolved phonon spectrum of thermoelectric PbSe. Intrinsic localized modes, which halt transport of heat-carrying phonons, are the flat bands between the transverse optic phonon (top band) and the transverse acoustic phonons (lower “V” shaped band).

of introducing defects or nanostructures to reduce transport of heat in a crystal lattice suffers because such structures also tend to reduce electronic conductivity. Our research combines inelastic neutron and x-ray scattering with *ab initio* simulations to reveal a mechanism for halting vibrational energy that is intrinsic to the crystal. Isolated intrinsic local modes in perfect crystals were known to occur in nonlinear physics, but here nonlinear localization of a large fraction of an entire phonon mode was revealed for the first time and shown to play an important role in the transport properties of a thermoelectric material. This phonon stopping in a perfect crystal moves us closer to the theoretical ideal for a thermoelectric of a ‘phonon-glass electron-crystal.’

Phonons and magnons in antiferromagnetic semiconductor

MnTe. Employing a combination of density functional theory (DFT), first principles phonon transport, advanced synthesis techniques, and inelastic neutron scattering, we advanced a cohesive picture of the electronic, magnetic, vibrational and thermal transport properties of MnTe [5], a promising room temperature antiferromagnetic semiconductor of interest for spintronics and thermoelectrics applications. In particular, this work provided a physically justified Coulomb correlation for the Mn atoms and the various exchange interactions, new element-specific phonon density of states by combining inelastic neutron scattering with nuclear inelastic scattering, and provided evidence of negligible coupling of the vibrational and magnetic degrees of freedom, of critical importance for spintronic and thermoelectric applications. Utilizing neutron spectroscopy on Li-doped MnTe, at ARCS, SNS, above $T_N=307$ K, we have revealed slow long-range paramagnetic spin relaxation ($\tau\sim 30$ fs; $\xi\sim 2$ nm) that is temperature independent [6]. These measurements establish Li:MnTe as the first paramagnon drag based high-performance thermoelectric material, with $ZT=1$.

Normal modes of spin cycloids and helices. Although spin cycloids and helices are quite common in magnetic materials, remarkably little is known about their normal modes on a discrete lattice. Based on simple one-dimensional lattice models, we have numerically evaluated the normal modes of a spin cycloid or helix produced by either Dzyaloshinskii-Moriya (DM) or competing exchange (CE) interactions [7]. The normal modes depend on the type of interaction and the nearest-neighbor exchange, which can be antiferromagnetic (AF) or ferromagnetic (FM). In the AF/DM and FM/DM cases, there is only a single Goldstone mode; in the AF/CE and FM/CE cases, there are three. For FM exchange, the spin oscillations produced by non-Goldstone modes contain a mixture of tangential and transverse components. For the DM cases, we compare our numerical results with analytic results in the continuum limit and find excellent agreement. Materials that fall into the four cases are BiFeO₃ [8] and Ba₂CuGeO₇ [9] (AF/DM), MnSi [10] (FM/DM), MnWO₄ [11] and Ni₃V₂O₈ [12] (AF/CE), and Sr₃Fe₂O₇ [13] (FM/CE). Based on these results, we predicted the

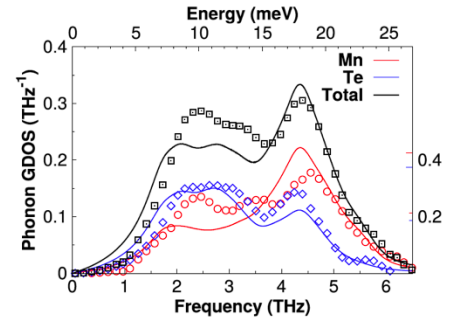


Fig 2. Measured (symbols) and calculated (curves) total and partial density of phonon states (DOS) of MnTe in the antiferromagnetic state. Mn and Te states normalized to red and blue ticks (right). Total DOS and Te DOS obtained by inelastic neutron scattering (ARCS, SNS) and nuclear inelastic scattering (ID18, ESRF), respectively.

observability of cycloidal modes by inelastic neutron scattering or THz spectroscopy in all four cases.

Future Plans

Phason dynamics in incommensurate relaxor ferroelectric $Sr_xBa_{1-x}Nb_2O_6$ and in fresnoite. In an inelastic neutron scattering spectrum phasons appear as gapless (or near gapless) excitations emerging from the incommensurate reflections in a way similar to the acoustic phonons emerging from the primary Bragg reflections. Phasons can have an intrinsic glass-like overdamping at long wavelengths [14] that originates with the viscosity of sliding the phase of an incommensurate modulation through the crystal [14]. Interestingly, glass-like overdamping also appears to be an essential feature of relaxor ferroelectrics [15]. In the relaxor ferroelectric $Sr_xBa_{1-x}Nb_2O_6$ [16], we will explore whether phason glass-like damping can play a similar role in incommensurate relaxor ferroelectrics, and, more specifically, whether coupling between the optical phonon and the phason introduces any relaxor like effects in these systems. Finding evidence for phason mediated relaxor ferroelectric behavior has the potential to open an exciting new research direction because, unlike with phonons, the glass-like properties of the phason are always present (coll. D. Phelan and B. Wang at ANL). In fresnoite, we will establish the phason lifetimes and the existence of a potential pinning gap, which requires much better energy resolution than provided by our HB3 and ARCS measurements.

Spin-phonon coupling and dynamics in charge ordered, entropy stabilized, and shape memory materials. We have established the long range magnetic structure of the entropy stabilized (MgCoNiCuZn)O rocksalt oxide[17], which also reveals the existence of well-defined spin waves that persist in the magnetically disordered phase and seem to couple to the lattice dynamics. We will develop a model for spin dynamics in the presence of disorder of the spins both in magnitude and the presence on non-magnetic cations. In mixed-valent $Sr_3Fe_2O_7$ [13] crystals grown by high-oxygen-pressure floating zone synthesis, we have obtain the first evidence of charge order superstructure peaks and will now explore the impact of the charge order on the spin dynamics and the lattice dynamics both by first principles calculations, Hamiltonian modelling[7] and inelastic neutron scattering. Furthermore, we will work to understand the observed phonon-magnon coupling in the shape memory material $Ni_{45}Co_5Mn_{36.6}In_{13.4}$ near a magnetic and structural phase transition [18].

Building insights into the impact of chirality and topology on lattice dynamics. Tellurium dioxide exhibits record negative linear compressibility, pressure driven phase transitions, and non-linear optical properties [19]. Chirality imposes topological quantum properties on materials [20] that we aim

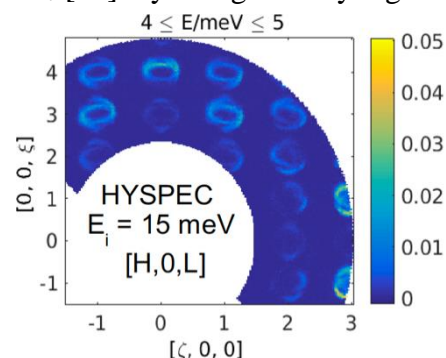


Fig 3. Constant energy cut of the scattering intensity in chiral TeO₂ at 295 K. Chirality leads to anomalous structure factors with ‘galaxy’ shaped phonon intensities that first principles calculations reproduce. A detailed explanation of the eigenvector mixing and mode width is still missing.

to reveal for the lattice dynamics. We are exploring chiral phonons in TeO₂ by combining dispersion relation and structure factor calculations with inelastic neutron scattering data in order to understand how chirality leads to specific phonon lifetime modifications and structure factors. The Bi-Sb system has recently attracted much attention both for novel devices [21], theoretically [22-24] and experimentally [25], including some debate about the origin of non-Ohmic behavior of transport [23,25]. Our collaborators (J. Heremans, Ohio State University) have established Bi_{0.89}Sb_{0.11} as a gold-standard composition for studying the transition from a topological insulator to Weyl semi-metal phase by application of moderate magnetic field of a few Tesla along the *c*-axis of the trigonal system, in a wide range of temperature (34-200 K). We will explore the impact of this topological transition and the Landau-level crossings on the lattice dynamics by means of inelastic neutron scattering.

References

- [1] M. E. Manley, *et al.*, *Nature Commun.* **9**, 1823 (2018).
- [2] P. Bak, J.von Boehm, *Phys. Rev. B* **21**, 5297–5308 (1980).
- [3] P. Bak, *Rep. Prog. Phys.* **45**, 587–629 (1981).
- [4] M. E. Manley, *et al.*, *Nature Commun.* **10**, 1928 (2019).
- [5] S. Mu, *et al.*, *Phys. Rev. Materials* **3**, 025403 (2019).
- [6] Y. Zheng, *et al.* “Paramagnon drag yields a high thermoelectric figure of merit in Li-doped MnTe,” *Science Advances*, *under review* (2019).
- [7] R.S. Fishman, T. Room, and R. de Sousa, *Phys. Rev. B* **99**, 064414 (2019).
- [8] I. Sosnowska and A.K. Zvezdin, *J. Magn. Magn. Mater.* **140-144**, 167 (1995).
- [9] A. Zheludev, *et al.*, *Phys. Rev. B* **54**, 15163 (1996).
- [10] P. Bak and M. H. Jensen, *J. Phys. C* **13**, L881 (1980).
- [11] A. H. Arkenbout, T. T. Palstra, T. Siegrist, and T. Kimura, *Phys. Rev. B* **74**, 184431 (2006).
- [12] G. Lawes, *et al.*, *Phys. Rev. Lett.* **95**, 087205 (2005).
- [13] J.-H. Kim, *et al.*, *Phys. Rev. Lett.* **113**, 147206 (2014).
- [14] A. Cano, A. P. Levanyuk, *Phys. Rev. Lett.* **93**, 245902 (2004).
- [15] T. Lookman, X. Ren (eds.), “Frustrated Materials and Ferroic Glasses,” *Springer Series in Materials Science*, vol. **275** (Springer, Cham, 2018).
- [16] W. Kleeman, *et al.*, *J. Adv. Diel.* **2**, 1241001 (2012).
- [17] J. Zhang, *et al.*, *Chemistry of Materials* **31**, 3705-3711 (2019).
- [18] P. J. Stonaha, *et al.*, *Phys. Rev. Lett.* **120**, 245701 (2018).
- [19] Cairns, A. B., *et al.*, *Phys. Chem. Chem. Phys.* **17**, 20449 (2015).
- [20] Chang, G., *et al.*, *Nature Materials* **17**, 978–985 (2018).
- [21] Zhi-Xue Xu, *et al.*, *Applied Physics Letters* **113**, 223504 (2018).
- [22] S. Singh *et al.*, *Phys Rev. B* **94**, 161116(R) (2016).
- [23] Yu-Hsin Su, *et al.*, *Phys. Rev. B* **97**, 155431 (2018).
- [24] P. Rinkel, *et al.*, *Phys. Rev. B* **99**, 144301 (2019).
- [25] D. Shin, *et al.*, *Nature Materials* **16**, 1096-1099 (2017).

Publications

‘Impact of Dynamic Instabilities and Microstructure on Energy Materials’ (FY16-FY18)

PI: J. D. Budai, M. E. Manley, R. P. Hermann, and O. Delaire

1. C. M. Berger, A. Mahmoud, R. P. Hermann, W. Braun, E. Yazhenskikh, Y. J. Sohn, N. H. Menzler, O. Guillon, M. Bram, “Calcium-Iron Oxide as Energy Storage Medium in Rechargeable Oxide Batteries,” *Journal of the American Ceramic Society* **99**, 4083 (2016).
2. K. S. Nemkovski, D. P. Kozlenko, P. A. Alekseev, J.-M. Mignot, A. P. Menushenkov, A. A. Yaroslavtsev, E. S. Clementyev, A. S. Ivanov, S. Rols, B. Klobes, R. P. Hermann, and A. V. Gribanov, “Europium mixed-valence, long-range magnetic order, and dynamic magnetic response in $\text{EuCu}_2(\text{Si}_x\text{Ge}_{1-x})_2$,” *Phys. Rev. B* **94**, 195101 (2016).
3. M. E. Manley, A. D. Christianson, R. Sahul, and D. L. Abernathy, “Phonon localization transition in relaxor ferroelectric PZN-5%PT,” *Appl. Phys. Lett.* **110**, 132901 (2017).
4. C. M. Malengreaux, S. L. Pirard, G. Leonard, J. G. Mahy, M. Herlitschke, B. Klobes, R. Hermann, B. Heinrichs, J. R. Bartlett, “Study of the photocatalytic activity of Fe^{3+} , Cr^{3+} , La^{3+} and Eu^{3+} single-doped and co-doped TiO_2 catalysts produced by aqueous sol-gel processing,” *J. All. Compounds* **691**, 726-738 (2017).
5. A. Jafari, I. Sergueev, D. Bessas, B. Klobes, B. S. Roschin, V. E. Asadchikov, P. Alexeev, J. Härtwig, A. I. Chumakov, H.-C. Wille, R. P. Hermann, “Rocking curve imaging of high quality sapphire crystals in backscattering geometry,” *J. Appl. Phys.* **121**, 44901 (2017).
6. T. Berlijn, P. C. Snijders, O. Delaire, H.-D. Zhou, T. A. Maier, H.-B. Cao, S.-X. Chi, M. Matsuda, Y. Wang, M. R. Koehler, P. R. C. Kent, and H. H. Weiering, “Itinerant Antiferromagnetism in RuO_2 ,” *Phys. Rev Lett.* **118**, 077201 (2017).
7. S. W. Lee, K. Hippalgaonkar, F. Yang, J. Hong, C. Ko, J. Suh, K. Liu, K. Wang, J. J. Urban, X. Zhang, C. Dames, S. A. Hartnoll, O. Delaire, and J. Wu, “Anomalously low electronic thermal conductivity in metallic vanadium dioxide,” *Science* **355**, 371-374 (2017).
8. Y. B. Zhang, J. D. Budai, J. Z. Tischler, W. Liu, R. Xu, E. R. Homer, A. Godfrey and D. Juul Jensen, “Boundary migration in a 3D deformed microstructure inside an opaque sample,” *Scientific Reports* **7**, 4423 (2017). doi:10.1038/s41598-017-04087-9.
9. M. E. Manley, D. L. Abernathy, and J. D. Budai, “Reply to ‘Phantom phonon localization in relaxors’,” *Nature Commun.* **8**, 1936 (2017).
10. G. Giampaoli, J. Li, R. P. Herman, J. K. Stalick, and M. A. Subramanian, “Tuning color through sulfur and fluorine substitutions in the defect tin (II, IV) niobate pyrochlores,” *Solid State Sciences* **81**, 32-42 (2018).
11. M. E. Manley, P. J. Stonaha, D. L. Abernathy, S. Chi, R. Sahul, R. P. Hermann, J. D. Budai, “Supersonic propagation of lattice energy by phasons in fresnoite,” *Nature Commun.* **9**, 1823 (2018).
12. P. J. Stonaha, I. Karaman, R. Arroyave, D. Salas, N. M. Bruno, M. F. Chisholm, S. Chi, D. L. Abernathy, Y. I. Chumlyakov, M. E. Manley, “Glassy phonon heralds strain glass state in a shape memory alloy,” *Phys. Rev. Lett.* **120**, 245701 (2018).
13. G. Svensson, L. Samain, J. J. Biendicho, A. Mahmoud, R. P. Hermann, S. Ya. Istomin and J. Grins, “Crystal Structure and Coordination of B-Cations in the Ruddlesden–Popper Phases $\text{Sr}_{3-x}\text{Pr}_x(\text{Fe}_{1.25}\text{Ni}_{0.75})\text{O}_7(0 < x < 0.4)$,” *Inorganics* **6**, 89 (2018).

‘Neutron Studies of Hybrid Excitations’ (FY19-FY21)

PI: R. P. Hermann, M. E. Manley, R. S. Fishman, and L. Lindsay

14. M. E. Manley, “Glassy phenomena and precursors in the lattice dynamics,” Chapter 4 in “Frustrated Materials and Ferroic Glasses,” Lookman T., Ren X. (eds), Springer Series in Materials Science, vol. 275, 101-117 (Springer, Cham, 2018).
15. D. Hobbis, R. P. Hermann, H. Wang, D. S. Parker, T. Pandey, J. Martin, K. Page, and G. S. Nolas, “Structural, Chemical, Electrical, and Thermal Properties of n-Type NbFeSb”, *Inorg. Chem.* **58**, 1826-1833 (2019).
16. S. Mu, R. P. Hermann, S. Gorsse, H. Zhao, M. E. Manley, R. S. Fishman, and L. Lindsay, “Phonons, magnons and lattice thermal transport in the antiferromagnetic semiconductor MnTe,” *Phys. Rev. Materials* **3**, 025403 (2019).
17. R. S. Fishman, T. Room, and R. de Sousa, “Normal Modes of a Spin Cycloid or Helix,” *Phys. Rev. B* **99**, 064414 (2019).
18. B. Klobes, J. deBoor, A. Alatas, M. Y. Hu, R. E. Simon, R. P. Hermann, “Lattice dynamics and elasticity in thermoelectric $\text{Mg}_2\text{Si}_{1-x}\text{Sn}_x$,” *Phys. Rev. Materials* **3**, 025404 (2019).
19. P.-C. Wei, S. Bhattacharya, Y.-F. Liu, F. Liu, Jian He, Y.-S. Tung, C.-C. Yang, C.-R. Hsing, D.-L. Nguyen, C.-M. Wei, M.-Y. Chou, Y.-C. Lai, T.-L. Hung, S.-Y. Guan, C.-S. Chang, R. P. Hermann, Y.-Y. Chen, A. M. Rao, “Thermoelectric figure-of-merit of a fully dense single crystalline SnSe,” *ACS Omega* **4**, 5442-5450 (2019).
20. M. E. Manley, D. L. Abernathy, A. D. Christianson, J. W. Lynn, “Response to Comment on “Giant electromechanical coupling of relaxor ferroelectrics controlled by polar nanoregion vibrations,”” *Science Advances* **5**, eaaw4367 (2019).
21. M. E. Manley, O. Hellman, N. Shulumba, J. W. Lynn, P. J. Stonaha, O. V. Garlea, A. Alatas, R. P. Hermann, J. D. Budai, A. F. May, B. C. Sales, A. J. Minnich, “Intrinsic anharmonic localization in thermoelectric PbSe,” *Nature Communications* **10**, 1928 (2019).
22. J. Zhang, J. Yan, S. Calder, Q. Zheng, M. A. McGuire, D. L. Abernathy, Y. Ren, S. H. Lapidus, K. Page, H. Zheng, J. W. Freeland, J. D. Budai, R. P. Hermann, “Long range antiferromagnetic order in a rocksalt high entropy oxide,” *Chemistry of Materials* **31**, 3705-3711 (2019).
23. A. F. May, D. Ovchinnikov, Q. Zheng, R. P. Hermann, S. Calder, B. Huang, Z. Fei, Y. Liu, X. Xu, and M. A. McGuire, “Ferromagnetism near room temperature in the cleavable van der Waals crystal Fe_5GeTe_2 ”, *ACS Nano* **13**, 4436-4442, (2019).
24. J. Moon, R. P. Hermann, M. E. Manley, A. Alatas, A. Said, A. J. Minnich, “Thermal acoustic excitations with atomic-scale wavelengths in amorphous silicon”, *Phys. Rev. Materials* **3**, 065601 (2019).

Role of Organic Cations in Organic-Inorganic Perovskite Solar Cells

Seung-Hun Lee (PI) and Joshua J. Choi (Co-PI)

University of Virginia

Program Scope

HOIPs are poised to revolutionize the field of optoelectronic materials with their phenomenal performance.^{1, 2} HOIPs are unique in that they combine low-cost solution processability with superb electronic quality that is comparable to, or surpasses, that of the state-of-the-art epitaxial grown semiconductors. Moreover, the crystal structure and optoelectronic properties of HOIPs are widely tunable by using different organic molecules and inorganic components. For instance, three-dimensional HOIPs such as methylammonium lead iodide ($\text{CH}_3\text{NH}_3\text{PbI}_3$) and formamidinium lead iodide ($\text{HC}(\text{NH}_2)_2\text{PbI}_3$) exhibit optoelectronic properties that are heavily dependent on the structure and dynamics of organic cations.^{3, 4}

In this program, the properties of hybrid organic-inorganic perovskites (HOIPs) are investigated at multiple length scales to achieve a full understanding of the microscopic mechanism of the photovoltaic effect. Specifically, this research program is testing the hypothesis that the structure and dynamics of organic cations and their associated electric multipoles cause screening and protection of charge carriers which results in long carrier lifetime and high solar cell efficiency. The experimental approach is to employ several complimentary techniques that can probe from atomic to macroscopic properties: molecular structure and dynamics at the microscopic level, charge transfer at the mesoscopic level, and the solar cell efficiency at the macroscopic level. Neutron diffraction and time-of-flight neutron scattering spectroscopy are used to characterize the structure and dynamics of organic cations. Optical spectroscopy, electrical transport measurements and solar cell fabrication and testing are employed to determine the impact of organic cations on the bulk properties and photovoltaic performance. Different organic cations, including methylammonium and formamidinium with different molecular symmetries and electric multipole moments are studied. These studies are revealing the microscopic origin of the high photovoltaic performance of HOIPs.

Recent Progress

Our research program discovered a mechanism for the higher carrier lifetime that is responsible for the superior HOIP solar cell performance.³ The mechanism involves screening of excited charge carriers by the rotating positively charged (cationic) organic molecules in the crystal. The extent of rotational freedom available for the cations determines the magnitude of the lifetime of the photo-excited charge carriers. By combining neutron scattering, high-performance computing, and optoelectronic measurements, the excited carrier lifetimes were found to dramatically increase whenever the system enters from a phase with a lower number of configurations of

rotating cations (called rotational entropy) to a phase with a higher value. The lifetime increases upon transition from a tetragonal with constrained orientation for the cation to a cubic phase with random orientation. The enhanced rotational entropy screens the charge carriers, thereby extending their lifetimes. This combination of optical measurements and neutron scattering results provides new understanding of the peculiarly long lifetime of charge carriers in these HOIPs, which is the key property that makes them promising for solar cells.

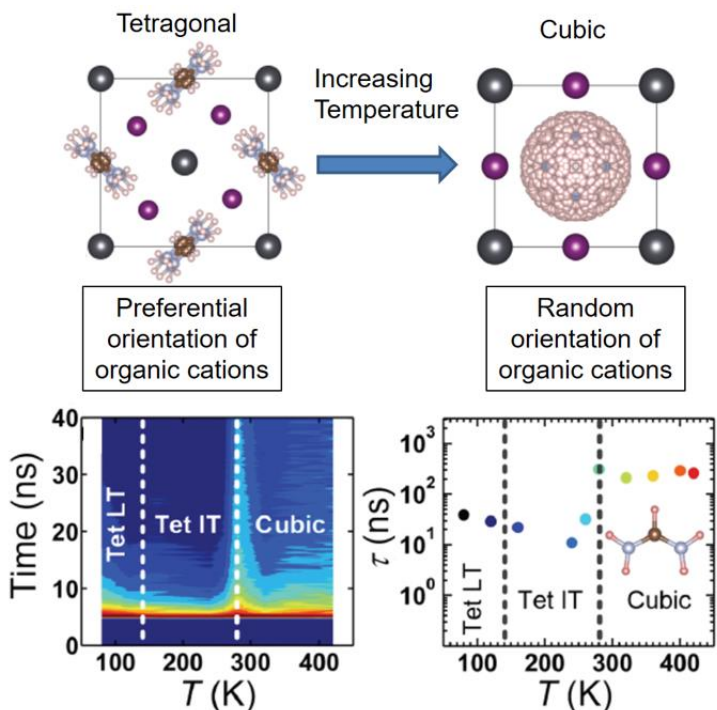


Figure 1. Atomic structure of hybrid organic-inorganic perovskite was determined by neutron and x-ray diffraction. A tetragonal structure (top left) transitions to a cubic structure (top right) upon heating. Black and purple spheres represent lead and iodine atoms, respectively. Also shown in the top figures are the positively charged organic molecules (cations) with different rotational degrees of freedom (preferential or random) derived from first principles calculations. The cations in the cubic structure have more rotational freedom than in the tetragonal structure. Photoluminescence measurements (bottom left) and lifetimes (bottom right) as a function of temperature and structure are shown. The higher lifetime (τ) of the photo-excited charge carriers in the cubic phase correlates well with the higher rotational freedom (random orientation) available for the cations.

Future Plans

Two-dimensional (2D) HOIPs with long chain organic cations are expected to have similarity to as well as distinctive differences from their 3D counterparts that we have studied so far. First, we expect that the long chain organic cations and the varying crystal environments on different parts of the molecule (ammonium head group and methyl group for example) will alter the rotational modes significantly compared to those of 3D HOIPs. Second, we hypothesize that a combination of the limited rotational motions and quantum confinement of 2D HOIPs will contribute to the enhanced formation of exciton and, consequently, shorter PL lifetime compared to the 3D HOIPs with dominant polaronic characteristics. Third, phonon contribution in 2D HOIPs will be more significant to electronic structure through electron-phonon coupling, compared to the rotational contribution. We hypothesize that hybrid phonon modes between organic cations and inorganic components will have a major contribution to electron-phonon coupling, and therefore significant differences in optoelectronic properties in 2D HOIPs with organic cations with different structure. To test this hypothesis, we will perform inelastic neutron scattering combined with DFT calculations and optoelectronic property measurements to identify the phonon modes with strong electron-phonon couplings.

References

1. E. H. Jung *et al.*, Efficient, stable and scalable perovskite solar cells using poly (3-hexylthiophene). *Nature* **567**, 511 (2019)
2. Brenner, T. M., Egger, D. A., Kronik, L., Hodes, G. and Cahen, D. Hybrid organic—inorganic perovskites: low-cost semiconductors with intriguing charge-transport properties. *Nature Reviews Materials* **1**, 15007 (2016).
3. Chen, T., Chen, W.-L., Foley, B. J., Lee, J., Ruff, J. P. C., Ko, J. Y. P., Brown, C. M., Harriger, L. W., Zhang, D., Park, C., Yoon, M., Chang, Y.-M., Choi, J. J. and Lee, S.-H. Origin of long lifetime of band-edge charge carriers in organic—inorganic lead iodide perovskites. *PNAS* **114**, 7519-7524 (2017).
4. Chen, T., Foley, B. J., Park, C., Brown, C. M., Harriger, L. W., Lee, J., Ruff, J., Yoon, M., Choi, J. J. and Lee, S.-H. Entropy-driven structural transition and kinetic trapping in formamidinium lead iodide perovskite. *Science Advances* **2**, e1601650 (2016)

Publications

1. T. Chen, W.-L. Chen, B. J. Foley, J. Lee, J. P. C. Ruff, J. Y. P. Ko, C. M. Brown, L. W. Harriger, D. Zhang, C. Park, M. Yoon, Y.-M. Chang, J. J. Choi, and S.-H. Lee “Origin of Long Lifetime of Band-Edge Charge Carriers in Organic-Inorganic Lead Iodide Perovskites” *Proceedings of the National Academy of Sciences*, 114, 7519-7524 (2017)
2. B. J. Foley, J. Girard, B. A. Sorenson, A. Z. Chen, J. S. Niezgoda, M. R. Alpert, A. F. Harper, D.-M. Smilgies, P. Clancy, W. A. Saidi, and J. J. Choi “Controlling Nucleation, Growth, and Orientation of Metal Halide Perovskite Thin Films with Rationally Selected Additives” *Journal of Materials Chemistry A*, 5, 113 - 123 (2017)
3. A. Z. Chen, B. J. Foley, J. H. Ma, M. R. Alpert, J. S. Niezgoda, and J. J. Choi “Crystallographic Orientation Propagation in Metal Halide Perovskite Thin Films” *Journal of Materials Chemistry A*, 5, 7796 – 7800 (2017)
4. A. Z. Chen, M. Shiu, J. H. Ma, M. R. Alpert, D. Zhang, B. J. Foley, D.-M. Smilgies, S.-H. Lee and J. J. Choi “Origin of vertical orientation in two-dimensional metal halide perovskites and its effect on photovoltaic performance” *Nature Communications*, 9, 1336 (2018)
5. B. J. Foley, S. A. Cuthriell, S. Yazdi, A. Z. Chen, S. M. Guthrie, X. Deng, G. Giri, S.-H. Lee, K. Xiao, B. Doughty, Y.-Z. Ma, J. J. Choi “Impact of Crystallographic Orientation Disorders on Electronic Heterogeneities in Metal Halide Perovskite Thin Films” *Nano Letters*, 18, 6271-6278 (2018)
6. A. Z. Chen, M. Shiu, X. Deng, M. Mahmoud, D. Zhang, B. J. Foley, S.-H. Lee, G. Giri, J. J. Choi “Understanding the Formation of Vertical Orientation in Two-dimensional Metal Halide Perovskite Thin Films” *Chemistry of Materials*, 31, 1336-1343 (2019)

Scattering and Spectroscopic Studies of Quantum Materials

Young Lee (SLAC National Accelerator Laboratory and Stanford University)

Hongchen Jiang (SLAC National Accelerator Laboratory)

Jiajia Wen (SLAC National Accelerator Laboratory)

Program Scope

We pursue research on quantum materials with a comprehensive effort involving complementary experiment (neutron and x-ray scattering, crystal growth, and thermodynamic measurements) and theory (numerical simulations). A focus of this effort is on creating and understanding new states of quantum magnetism, such as quantum spin liquids. Such systems have ground states with long-range quantum entanglement, which break the classical paradigm of local order parameters. Only a handful of such materials have been synthesized, and the most promising are based on low-dimensional frustrated lattices. Spin liquids are relevant to theories of high-Tc superconductivity and has possible applications in quantum information. Our expertise allows us to follow a clear path towards improved understanding: performing scattering and spectroscopic studies on crystals of real materials and comparing the results with theoretical calculations for these materials. In addition, the theory effort sheds light on possible competing orders, and guides our pursuit of scattering measurements to perform. We also study closely related phenomena such as topological magnon bands and intertwined order in cuprate superconductors.

Recent Progress

We have studied the new quantum magnets barlowite and Zn-barlowite, using neutron and x-ray scattering on single crystal and powder samples.[1] These are examples of $S=1/2$ kagome lattice materials, similar to herbertsmithite. In barlowite, we used magnetic neutron scattering on a co-aligned crystal sample to discover a new magnetically ordered ground state in a variant with a high-symmetry hexagonal crystal structure. Numerical studies were performed based on a Hamiltonian consistent with the crystal structure, and we find that a valence bond crystal state is competitive in energy. However, the spins between the kagome planes have a strong coupling to the kagome moments and eventually induce a "pinwheel $q=0$ " order. This system appears to intertwine aspects of both valence bond crystal order and spin order, indicating that these states are adjacent to the quantum spin liquid phase depending on the microscopic coupling parameters. We have also performed the first inelastic neutron scattering on single crystal samples of barlowite, measuring the excitations of the "pinwheel $q=0$ " magnetically ordered state.

We have grown new large single crystal samples of herbertsmithite, and we have performed inelastic neutron scattering measurements to conclusively determine the nature of the spin liquid state by measuring the excitations from 0.1 meV up to 50+ meV. In particular, we have used polarized and unpolarized measurements at HYSPEC to distinguish the spinon continuum at high energies from phonon scattering. Numerical calculation of the structure factor aid our understanding of the underlying physics of the Heisenberg kagome model. In addition, we have used numerical methods to systematically studied the ground state phase diagram of the Kitaev-Heisenberg model under magnetic field proposed to describe the physics of α -RuCl₃. [2]

We have performed resonant x-ray scattering studies of both La_{2-x}Sr_xCuO₄ and oxygen doped La₂CuO_{4+y} and found that the charge density wave order is closely coupled to the spin density wave order. [3] In La₂CuO_{4+y}, we have succeeded in varying the degree of dopant disorder in-situ during the soft x-ray resonant scattering experiment. We found that a higher degree of disorder enhances the charge density wave in a manner similar to the spin density wave.

Future Plans

We will perform elastic and inelastic neutron scattering measurements on barlowite crystals to study the evolution of the magnetic order under large applied fields. We also plan to perform resonant inelastic x-ray scattering on our kagome spin liquid crystals to discern the differences in the high-energy spin excitations between the quantum spin liquid and closely related $q=0$ ground states. In herbertsmithite, we plan to perform inelastic neutron scattering experiments in high magnetic fields to examine the correlations related to the closure of the spin-gap. Theoretical tools will be developed to help explore the phase space of new materials to target for synthesis, as well as aid in analysis of the data.

References

- [1] R.W. Smaha, W. He, J.P. Sheckelton, J.J. Wen, and Y.S. Lee, *Journal of Solid State Chemistry* 268, 123 (2018).
- [2] Yi-Fan Jiang, Thomas P. Devereaux, Hong-Chen Jiang, arXiv:1901.09131 (Phys. Rev. B, under review).
- [3] J.J. Wen, H. Huang, S.-J. Lee, H. Jang, J. Knight, Y. S. Lee, M. Fujita, K. M. Suzuki, S. Asano, S. A. Kivelson, C.-C. Kao, J.-S. Lee, arXiv:1810.10600 (Nature Communications, under review).

Publications

Observation of intertwined density-wave orders and superconductivity in $\text{La}_{2-x}\text{Sr}_x\text{CuO}_4$, J.J. Wen, H. Huang, S.-J. Lee, H. Jang, J. Knight, Y. S. Lee, M. Fujita, K. M. Suzuki, S. Asano, S. A. Kivelson, C.-C. Kao, J.-S. Lee, arXiv:1810.10600 (Nature Communications, under review).

Field induced quantum spin liquid with spinon Fermi surfaces in the Kitaev model, Hong-Chen Jiang, Chang-Yan Wang, Biao Huang, Yuan-Ming Lu, arXiv:1809.08247 (Phys. Rev. X, under review).

Field-induced quantum spin liquid in the Kitaev-Heisenberg model and its relation to $\alpha\text{-RuCl}_3$, Yi-Fan Jiang, Thomas P. Devereaux, Hong-Chen Jiang, arXiv:1901.09131 (Phys. Rev. B, under review).

Fermi surface reconstruction in electron-doped cuprates without antiferromagnetic long-range order, Junfeng He, Costel R. Rotundu, Mathias S. Scheurer, Yu He, Makoto Hashimoto, Ke-Jun Xu, Yao Wang, Edwin W. Huang, Tao Jia, Sudi Chen, Brian Moritz, Donghui Lu, Young S. Lee, Thomas P. Devereaux, and Zhi-xun Shen, PNAS 116, 3449 (2019).

Synthesis-Dependent Properties of Barlowite and Zn-Substituted Barlowite, R.W. Smaha, W. He, J.P. Sheckelton, J.J. Wen, and Y.S. Lee, *Journal of Solid State Chemistry* 268, 123 (2018).

Three-dimensional collective charge excitations in electron-doped copper oxide superconductors, M. Hepting, L. Chaix, E.W. Huang, R. Fumagalli, Y.Y. Peng, B. Moritz, K. Kummer, N.B. Brookes, W.C. Lee, M. Hashimoto, T. Sarkar, J.F. He, C.R. Rotundu, Y.S. Lee, R.L. Greene, L. Braicovich, G. Ghiringhelli, Z.X. Shen, T.P. Devereaux, W.S. Lee, Nature 563, 374 (2018).

Enhancement and destruction of spin-Peierls physics in a one-dimensional quantum magnet under pressure, C.R. Rotundu, J.J. Wen, W. He, Y. Choi, D. Haskel, Y.S. Lee, Phys. Rev. B 97, 054415 (2018).

^{139}La and ^{63}Cu NMR investigation of charge order in $\text{La}_2\text{CuO}_{4+y}$ ($T_c=42\text{ K}$), T. Imai and Y. S. Lee, Phys. Rev. B 97, 104506 (2018).

^{139}La NMR investigation of the charge and spin order in a $\text{La}_{1.885}\text{Sr}_{0.115}\text{CuO}_4$ single crystal, A. Arsenault, S.K. Tahahashi, T. Imai, W. He, Y. S. Lee, and M. Fujita, Phys. Rev. B 97, 064511 (2018).

Holon Wigner Crystal in a Lightly Doped Kagome Quantum Spin Liquid, Hong-Chen Jiang, T. Devereaux, S. A. Kivelson, Phys. Rev. Lett. 119, 067002 (2017)

Fractional charge and emergent mass hierarchy in diagonal two-leg t-J cylinders, Yi-Fan Jiang, Hong-Chen Jiang, Hong Yao, Steven A. Kivelson, Phys. Rev. B 95, 245105 (2017).

The phase transitions between $\text{Zn}\times\text{Zn}$ bosonic topological phases in 1+1 D, and a constraint on the central charge for the critical points between bosonic symmetry protected topological phases,

Lokman Tsui, Yen-Ta Huang, Hong-Chen Jiang, Dung-Hai Lee, Nuclear Physics, B 919, 470 (2017).

Ising orders in a magnetized Heisenberg chain subject to a uniform Dzyaloshinskii-Moriya interaction, Yang-Hao Chan, Wen Jin, Hong-Chen Jiang, Oleg A. Starykh, Phys. Rev. B 96, 214441 (2017).

Intertwined Order in a Frustrated 4-leg t - J Cylinder, John F. Dodaro, Hong-Chen Jiang, Steven A. Kivelson, Phys. Rev. B 95, 155116 (2017).

Disordered Route to the Coulomb Quantum Spin Liquid: Random Transverse Fields on Spin Ice in $\text{Pr}_2\text{Zr}_2\text{O}_7$, Jiajia Wen, S. M. Koohpayeh, K. A. Ross, B. A. Trump, T. M. McQueen, K. Kimura, S. Nakatsuji, Y. Qiu, D. M. Pajerowski, J. R. D. Copley, and C. L. Broholm, Phys. Rev. Lett, 118, 107206 (2017).

Strong ferromagnetic exchange interaction in the parent state of the superconductivity in BaFe_2S_3 , Meng Wang, S. J. Jin, Ming Yi, Yu Song, Hong-Chen Jiang, W. L. Zhang, H. Q. Luo, A. D. Christianson, E. Bourret-Courchesne, D. H. Lee, Dao-Xin Yao, R. J. Birgeneau, Phys. Rev. B 95, 060502 (2017).

Rational Design of Ion-Containing Nanostructured Ternary Polymer Blends

T. P. Lodge, F. S. Bates, Chemical Engineering & Materials Science, U. of Minnesota

Program Scope

A central challenge in next-generation materials is to develop a broadly applicable strategy to systematically tailor nanostructure, in order to simultaneously optimize two (or more) orthogonal properties. A prime example of this prevalent competition is to prepare polymeric membranes that exhibit both high transport for selected small molecules or ions, while concurrently exhibiting superior mechanical, thermal, and chemical robustness. Key to achieving this goal is to prepare a co-continuous nanostructure, whereby one domain is responsible for molecular or ionic transport, while the other imparts mechanical strength. We propose that ternary blends comprising A and B homopolymers, plus an A-B block copolymer surfactant, present a broadly tunable and widely applicable strategy to access predictable and functional co-continuous nanostructures (Fig. 1). We have previously pioneered the development of an equilibrium co-continuous but globally disordered structure, the polymeric bicontinuous microemulsion ($B\mu E$),¹⁻³ which is the initial target for ion-containing materials.

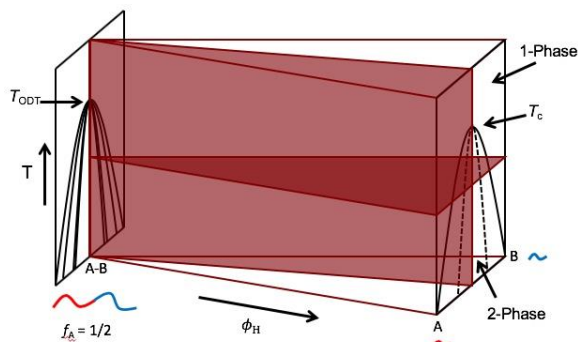


Fig. 1 A/B/A-B ternary blend phase prism. Shaded planes indicate an isopleth and an isothermal cut.

We approach this target through three parallel thrusts. The first concerns ternary blends plus added salt. By choosing a system in which the salt dissolves exclusively in the A (= PEO) domains, and maintaining the ratio of salt to PEO, the resulting “pseudo-ternary” blends are amenable to systematic study. We build on our recent discovery that such systems can exhibit highly conductive, bicontinuous phases.^{4,5} The second thrust encompasses ternary blends where polymer A is charged. Such systems have never been studied before, but recent theories offer provocative predictions about the phase behavior of both binary blends and diblock copolymers, which we can test *en route* to bicontinuous ternary phases.⁶⁻⁸ The third thrust targets a deeper understanding of the universal phase behavior of a ternary blend, near the predicted Lifshitz point (LP) anticipated by mean-field theory.⁹ Our previous work over two decades was predicated on the assumption that the $B\mu E$ occurs near the LP, where large amplitude fluctuations invalidate mean-field assumptions. However, more recently we have seen indications that the $B\mu E$ may be even more prevalent away from the LP, along a constant homopolymer concentration plane.¹⁰ This provocative result merits deeper investigation.

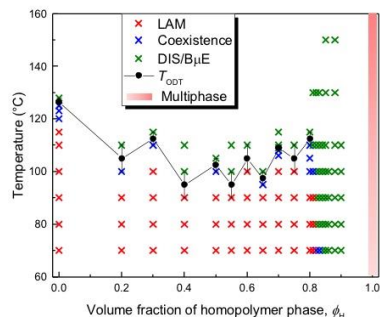


Fig. 2 PS/PEO/PS-PEO isopleth for $r = 0.03$.

Recent Progress: A/B/A-B plus salt

Diblocks of PS-PEO+salt have been extensively studied,¹¹⁻¹³ but not homopolymer blends of PS+PEO+salt; we found that addition of even tiny amounts of salt (1 LiTFSI per 100 PEO chains) could move the phase boundary by 100 °C; the diagram became extremely asymmetric, and the coexisting phase compositions did not follow the cloud point curve.¹⁴ A recent theory could describe these observations well.¹⁵ We have since studied the ternary blend carefully,

along the volumetrically symmetric isopleth (equal volumes of perdeuterated dPS (1kDa) and PEO (1.2 kDa) added to a symmetric dPS-PEO copolymer (5.2 kDa), with LiTFSI ($r = 0.03$). Phase identification relies on a combination of SANS, SAXS, and rheology, and an example is shown in Fig. 2. A well-defined B μ E is found over a remarkably wide range of homopolymer composition (*ca.* $\phi_H \approx 80$ -90%), compared to the neutral case, where a 1-3% range is typical. This result is both highly encouraging, and possibly surprising, given that the effective PS/PEO segregation strength clearly increases with r , which might be expected to disrupt the delicate balance of curvature that stabilizes a B μ E (note that this A+B+A-B combination is fully mixed in the absence of salt). Quantitative analysis of the SANS curves using the Teubner-Strey (T-S) structure factor ($I(q) = 1/(a_2 + c_1q^2 + c_2q^4)$), where $I(q)$ is the background-subtracted scattered intensity and a_2 , c_1 , and c_2 are composition-dependent coefficients of a Landau expansion of the free energy, Fig. 3a)¹⁶ yields evidence of an excellent B μ E (*i.e.*, the amphiphilicity factor $f = c_1/(4a_2c_2)^{1/2}$ is as low as -0.8 , with a 40 nm periodicity, Fig. 3b). Even doubling the amount of salt ($r = 0.06$) does not eliminate the B μ E (Fig. 3b).

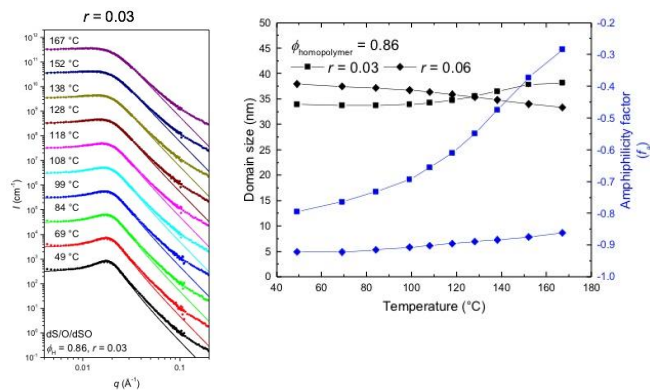


Fig. 3 (a) SANS vs. T for one blend, and (b) Teubner-Strey analysis for the same blend, plus one with $r = 0.06$.

We have chosen PEO as the ion-solvating polymer, as it is by far the most studied, and typically shows higher ionic conductivity than most, if not all, common polymers, especially for Li^+ . However, an underlying question that is still not resolved, is whether the presence of salt modifies the conformational statistics of PEO. For example, in the Wang model Li^+ is assumed to form physical crosslinks with a finite number of ether oxygens;¹⁵ other authors have invoked a “wrapping” of PEO around the cations, or other specific conformations.^{17, 18} An early study used SANS and a dPEO/PEO blend ($M \approx 25$ kDa) to explore this, by measuring R_g in the presence of LiI with $r \approx 0.06$.¹⁹ The authors reported a 10-15% contraction; MD simulations supported a model in which some chains were contracted by wrapping, and others were unperturbed. We have attempted to reproduce this result, while also extending the measurements to other M (22 kDa, 40 kDa, in collaboration with Dr. Kunlun Hong, CNMS, ORNL), salts (LiTFSI, LiClO_4), and r values (0 – 0.13), at 90 °C. Using random phase approximation analysis, we find surprisingly that R_g first increases with modest amounts of salt, before shrinking (see Fig. 4a). Equally interesting is the observation that the pure PEO is not Gaussian; the Kratky plots in Figure 4b suggest a fractal dimension above 2, or a slightly compressed chain. These results are quite sensitive to background subtraction, so further measurements are needed.

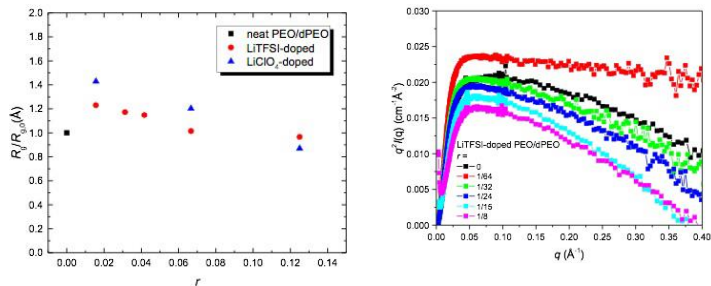


Fig. 4 (a) Normalized R_g for dPEO/PEO (40 kDa) with added salt; (b) Kratky plots show non-Gaussian behavior even with no salt.

reproduce this result, while also extending the measurements to other M (22 kDa, 40 kDa, in collaboration with Dr. Kunlun Hong, CNMS, ORNL), salts (LiTFSI, LiClO_4), and r values (0 – 0.13), at 90 °C. Using random phase approximation analysis, we find surprisingly that R_g first increases with modest amounts of salt, before shrinking (see Fig. 4a). Equally interesting is the observation that the pure PEO is not Gaussian; the Kratky plots in Figure 4b suggest a fractal dimension above 2, or a slightly compressed chain. These results are quite sensitive to background subtraction, so further measurements are needed.

A-B and A/B/A-B where A is charged

We have developed a highly tunable new system to study blends with a charged block; B is still PS, but A is poly[(oligo(ethylene glycol) methyl ether methacrylate)-*co*-oligo(ethylene

glycol) propyl sodium sulfonate methacrylate)] (POEGMA#), where # refers to the percentage of side groups with a pendant sulfonate (Fig. 5a). In this class of materials, even the pure A/B blend and the pure A-B diblock have not been studied systematically, although fascinating results are anticipated by theory.⁶ We prepared a series of compositionally symmetric diblocks

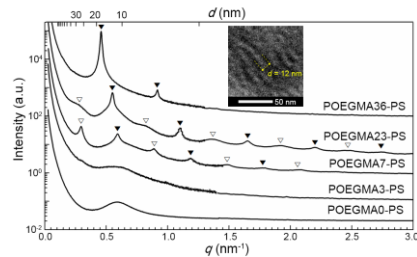
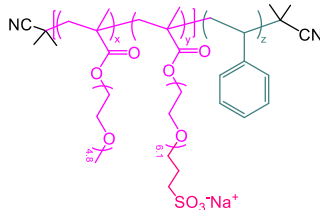


Fig. 5 (a) POEGMA#-PS system; (b) SAXS plots for POEGMA#-PS, showing the superlattice peaks (open triangles); $M \approx 20$ kDa.

(POEGMA#-PS) ($M \approx 20$ kDa) with varying charge fractions #, by RAFT polymerization followed by installation of the charged groups, and examined the bulk self-assembly. The uncharged polymer ($\# = 0$) is disordered, and at $\# = 36$, the sample is lamellar, as anticipated given the increased segregation strength and the compositional symmetry. Remarkably, at intermediate charge fractions ($5 < \# < 25$), an unprecedented superlattice structure appears (see SAXS patterns in Fig. 5b). The origins of this result remain to be elucidated, but possibly it reflects a competition between charge correlations (that might normally give rise to an “ionomer peak”) and the segregation of the two blocks. A first account of this work has just appeared.²⁰

We have since begun to map out the phase diagram of a model ternary polymer blend by adding homopolymers POEGMA23 ($M_n = 2.3$ kDa) and PS ($M_n = 2.5$ kDa) to POEGMA23-PS. The experimentally determined phase diagram along the volumetrically symmetric isopleth as a function of homopolymer volume fraction (ϕ_H) is presented in Fig. 6. Strikingly, the phase diagram largely mirrors those previously observed from neutral ternary blend systems, in that a narrow $B\mu E$ channel separates the ordered region on the block copolymer-rich side and macrophase-separated region on the homopolymer-rich side. Furthermore, T_{ODT} continuously decreases upon increasing the homopolymer

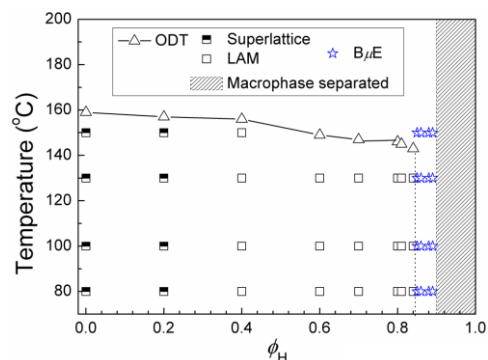


Fig. 6 Symmetric isopleth for PS/POEGMA23/POEGMA23-PS.

loading, due in part to an overall decrease in the average molecular weight of the components. The pure $B\mu E$ channel persists in the composition range $0.85 \leq \phi_H \leq 0.89$, which is close to the theoretical mean-field Lifshitz composition $\phi_{H,L} = 1/(1 + 2\alpha^2) = 0.89$, where $\alpha = (N_A N_B)^{1/2}/N_{AB}$. SANS and SAXS profiles of the representative blends containing $\phi_H = 0.85$ and 0.88 at 80°C , which produces the $B\mu E$ morphology, were fit using the T-S model. Although there is a substantial deviation at low- q due to an intensity upturn (as often observed from charged polymer systems such as ionomers and polyelectrolytes, presumably due to large-scale inhomogeneities in the distribution of charged species²¹), the shape near the scattering peak is in a good agreement with the T-S model. The amphiphilicity factor falls in the range $-1 < f_a \leq 0$, again revealing for the first time a well-defined charged polymer $B\mu E$.²²

Neutral A/B/A-B blends

In almost all previous studies of the ternary phase prism, the focus has been on the symmetric isopleth, *i.e.*, equal volumes ($\phi_A = \phi_B$) of equal molar volume homopolymers ($N_A = N_B$), with a symmetric diblock ($f_A=0.5$). However, even in the ideal case where such symmetries are realized precisely, conformational asymmetry confers an inherent bias for interfacial curvature toward the larger statistical segment block (PE). It is therefore of fundamental interest to explore phase

behavior off the symmetric isopleth, and in particular to see whether the region of $B\mu E$ might actually be wider than reported. To this end we previously developed a new system of PE/PCHE/PE-PCHE (prepared from hydrogenating anionically polymerized 1,4-polybutadiene and polystyrene). One key finding was a line of *congruent* order-disorder transitions, where the lamellar phase disordered directly, with no region of phase co-existence.¹⁰ Even though the symmetry conditions were met closely, the congruent isopleth was rich in PCHE ($\phi_{PCHE}/\phi_H \approx 0.6$). Furthermore, the critical point for the binary blend was similarly offset ($\phi_{PCHE,c} \approx 0.63$). To gain more insight into how the $B\mu E$ location is affected by the preferred interfacial curvature of the diblock copolymer monolayer, a compositionally asymmetric PCHE-PE block copolymer ($f_{PCHE} = 0.67$) was prepared, and the congruent condition was determined by optical transmittance as a function of temperature. A representative phase diagram at $\phi_H = 0.82$ is presented in Fig. 7a, showing that with this compositionally asymmetric copolymer, the congruent composition shifts to $\phi_{PCHE}/\phi_H \approx 0.43$. On the other hand, starting from the binary blend, the line of critical points (Scott line) does not move much with added copolymer, as expected (Fig. 7b); critical scattering along the Scott line was confirmed using SANS measurements as a function of temperature. In fact, it will not approach the line of congruent ODTs at all, eliminating any possibility of approaching LP-like behavior. This important result also reveals that copolymer asymmetry is a useful tool to modulate interfacial curvature, and, potentially, widen the regime of accessible $B\mu E$ s.

Future Plans

In the area of ternary blends plus salt, the discovery of a remarkably wide region of $B\mu E$ is unexpected. As we have both dPS and dPS-PEO, we can use isotopic blends to extract all three partial structure factors, and thus a deeper understanding of the interfacial packing.^{23,24,25} Guided by the neutral blend case, exploration of phase behavior off the symmetric isopleth is warranted. We will also pursue measurements of ionic conductivity and rheological properties. We will complete the SANS study of PEO conformations in the presence of salt, which requires very careful background subtraction and also attention to unexplained low- q scattering in pure PEO homopolymers. For the charged polymer systems, we will explore ternary polymer blends using PS-POEGMA# containing various charge fractions and different counter ions. In the pure diblock limit, we will explore the role of copolymer composition and molecular weight to provide the first systematic experimental study of the charged diblock phase portrait. In the neutral ternary blend limit, we will use SANS, optical transmittance, rheology, and TEM to study in detail the region of the phase prism where the $B\mu E$ is found, bounded by the lamellar (or other) ordered states and phase separation. This will provide the first quantitative mapping of the width of the $B\mu E$ channel in the homopolymer composition plane (*i.e.*, varying ϕ_{PCHE}/ϕ_H at fixed ϕ_H), as opposed to the previously emphasized total homopolymer content axis (*i.e.*, varying ϕ_H at fixed ϕ_{PCHE}/ϕ_H). These results will then feed back into explorations of phase behavior in the two charged systems. Publications describing (*i*) the wide $B\mu E$ window in the A+B+A-B+salt system, (*ii*) the conformation of PEO in the presence of salt, (*iii*) the discovery of a $B\mu E$ in charged polymer ternary blends, and (*iv*) the decoupling of congruency and criticality in neutral ternary blends, are currently in preparation.

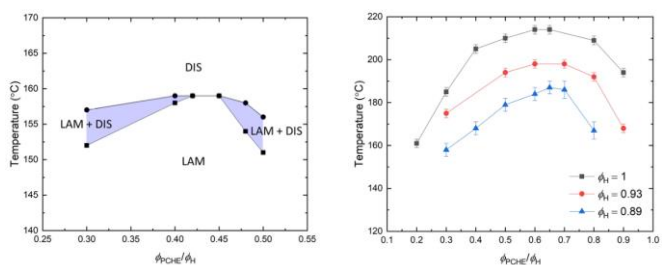


Fig. 7 (a) Phase slice for PE/PCHE/PE-PCHE at $\phi_H = 0.82$, showing congruent ODT near 0.43; (b) Phase slices near the binary blend limit, showing critical points near 0.65.

References

- ¹ Bates, F. S.; Maurer, W. W.; Lipic, P. M.; Hillmyer, M. A.; Almdal, K.; Mortensen, K.; Fredrickson, G. H.; Lodge, T. P. Polymeric Bicontinuous Microemulsions. *Phys. Rev. Lett.* **1997**, *79*, 849–852.
- ² Hillmyer, M.A.; Maurer, W.W.; Lodge, T.P.; Bates, F.S.; Almdal, K. Model Bicontinuous Microemulsions in Ternary Homopolymer/Block Copolymer Blends, *J. Phys. Chem. B.*, **1999**, *103*, 4814.
- ³ Zhou, N.; Bates, F.S; Lodge, T.P. Mesoporous Membrane Templated by a Polymer Bicontinuous Microemulsion, *Nano Letters*, **2006**, *6*, 2354–2357.
- ⁴ Irwin, M. T.; Hickey, R. J.; Xie, S.; Bates, F. S.; Lodge, T. P. Lithium salt-induced microstructure and ordering in diblock copolymer/homopolymer blends. *Macromolecules* **2016**, *49*, 4839–4849.
- ⁵ Irwin, M. T.; Hickey, R. J.; Xie, S.; So, S.; Bates, F. S.; Lodge, T. P. Structure–conductivity relationships in ordered and disordered salt-doped diblock copolymer/homopolymer blends. *Macromolecules* **2016**, *49*, 6928–6939.
- ⁶ Sing, C. E., Zwanikken, J. W.; Olvera de la Cruz, M. Electrostatic control of block copolymer morphology. *Nat. Mater.* **2014**, *13*, 694–698.
- ⁷ Nakamura, I.; Wang, Z.-G. Salt-doped block copolymers: ion distribution, domain spacing and effective parameter. *Soft Matter* **2012**, *8*, 356–9367.
- ⁸ Pryamitsyn, V. A., Kwon, H.-K., Zwanikken, J. W.; Olvera de la Cruz, M. Anomalous phase behavior of ionic polymer blends and ionic copolymers. *Macromolecules* **2017**, *50*, 5194–5207 (2017).
- ⁹ Broseta, D.; Fredrickson, G. H. Phase equilibria in copolymer/homopolymer ternary blends: Molecular weight effects. *J. Chem. Phys.* **1990**, *93*, 2927–2938.
- ¹⁰ Hickey, R. J.; Gillard, T. M.; Irwin, M. T.; Morse, D. C.; Lodge, T. P.; Bates, F. S. Phase Behavior of Diblock Copolymer–Homopolymer Ternary Blends: Congruent First-Order Lamellar–Disorder Transition. *Macromolecules* **2016**, *49*, 7928–7944.
- ¹¹ Teran, A. A.; Balsara, N. P. Thermodynamics of block copolymers with and without salt. *J. Phys. Chem. B* **2014**, *118*, 4–17.
- ¹² Wanakule, N. S.; Virgili, J. M.; Teran, A. A.; Wang, Z.-G.; Balsara, N. P. Thermodynamic properties of block copolymer electrolytes containing imidazolium and lithium salts. *Macromolecules* **2010**, *43*, 8282–8289.
- ¹³ Young, W.-S.; Epps, T. H., III. Salt doping in PEO-containing block copolymers: counterion and concentration effects. *Macromolecules* **2009**, *42*, 2672–2678.
- ¹⁴ Xie, S.; Lodge T.P. Phase Behavior of Binary Polymer Blends Doped with Salt, *Macromolecules*, **2018**, *51*, 266–274
- ¹⁵ Ren, C.-L.; Nakamura, I.; Wang, Z.-G. Effects of ion-induced cross-linking on the phase behavior in salt-doped polymer blends. *Macromolecules* **2016**, *49*, 425–431.
- ¹⁶ Teubner, M.; Strey, R. Origin of the Scattering Peak in Microemulsions. *J. Chem. Phys.* **1987**, *87*, 3195–3200.
- ¹⁷ MacGlashan, G.S.; Andreev, Y.G.; Bruce, P.G. Structure of the polymer electrolyte poly(ethylene oxide)₆:LiAsF₆, *Nature*, **1999**, *398*, 792–794.
- ¹⁸ Mao, G.; Saboungi, M.-L.; Price, D.L.; Armand, M.B.; Howells, W.S. Structure of Liquid PEO-LiTFSI Electrolyte, *Phys. Rev. Lett.* **2000**, *84*, 5536–5539.

- ¹⁹ Annis, B. K.; Kim, M. H.; Wignall, G. D.; Borodin, O.; Smith, G. D. A study of the influence of LiI on the chain conformations of poly(ethylene oxide) in the melt by small-angle neutron scattering and molecular dynamics simulations. *Macromolecules* **2000**, *33*, 7544-7548.
- ²⁰ Shim, J.; Bates, F. S.; Lodge, T. P. Superlattice by Charged Block Copolymer Self-Assembly. *Nat. Commun.* **2019**, *10*, 2108.
- ²¹ Seitz, M. E.; Chan, C. D.; Opper, K. L.; Baughman, T. W.; Wagener, K. B.; Winey, K. I. Nanoscale Morphology in Precisely Sequenced Poly(ethylene-co-acrylic acid) Zinc Ionomers. *J. Am. Chem. Soc.* **2010**, *132*, 8165–8174.
- ²² Morkved, T. L.; Stepanek, P.; Krishnan, K.; Bates, F. S.; Lodge, T. P. Static and Dynamic Scattering from Ternary Polymer Blends: Bicontinuous Microemulsions, Lifshitz Lines, and Amphiphilicity. *J. Chem. Phys.* **2001**, *114*, 7247–7259.
- ²³ Balsara, N. P.; Jonnalagadda, S. V.; Lin, C. C.; Han, C. C.; Krishnamoorti, R. Thermodynamic interactions and correlations in mixtures of two homopolymers and a block copolymer by small angle neutron scattering. *J. Chem. Phys.* **1993**, *99*, 10011-10020.
- ²⁴ Ruegg, M. L.; Reynolds, B. J.; Lin, M. Y.; Lohse, D. J.; Balsara, N. P. Microphase and Macrophase Separation in Multicomponent A/B/A–C Polymer Blends with Attractive and Repulsive Interactions. *Macromolecules* **2006**, *39*, 1125-1134.
- ²⁵ Lee, D. D.; Chen, S. H. Local geometry of surfactant monolayers in a ternary microemulsion system. *Phys. Rev. Lett.* **1994**, *73*, 106-109.

Publications

Xie, S.; Lodge, T. P. Phase behavior of binary polymer blends doped with salt. *Macromolecules* **2018**, *51*, 266-274.

Chen, Q.P.; Xie, S.; Foudazi, R.; Lodge, T.P.; Siepmann, J.I. Understanding the Molecular-Weight Dependence of χ and the Effect of Dispersity on the Polymer Blend Phase Diagram, *Macromolecules*, **2018**, *51*, 3774-3787. (*Experiments by Xie supported by DOE*).

Shim, J.; Bates, F. S.; Lodge, T. P. Superlattice by Charged Block Copolymer Self-Assembly. *Nat. Commun.* **2019**, *10*, 2108.

The Physics of Exotic Magnetoresistive Systems

Despina Louca, University of Virginia

Program Scope

The goal of this program is to understand the mechanism behind the anomalously large magnetoresistance (MR) observed under high magnetic fields in semiconductors, induced by the introduction of defects, application of tensile strain and doping. Several exemplary systems have been selected for the study that are of fundamental scientific interest as well as promising candidates for the next generation of MR devices. Two classes of emergent materials are currently under investigation: these are the three-dimensional antiferromagnetic (AFM) semiconductors, i.e. I-Mn-V compounds with Néel temperatures (T_N) above 300 K that are promising candidates for the next generation of AFM spintronics; and the quasi two-dimensional transition metal dichalcogenides (TMD) semiconductors with very versatile physical characteristics, fundamentally important for optoelectronic applications.

Recent Progress

Transition-metal dichalcogenides are hosts to exotic quantum states, with electronic features that are suitable for optoelectronic and quantum technologies (1,2). Their crystal structures consist of van der Waals-bound layers, where a change in the layer stacking can result in new properties such as superconductivity, recently observed in bilayer graphene with a “magic” twist angle (3), or transition to the Weyl semimetal state (4, 5) reported in the T_d phase of MoTe_2 and in the Kooi phase of $\text{Ge}_2\text{Sb}_2\text{Te}_5$. MoTe_2 is a prototype for understanding how stacking variations in layered materials can lead to exotic states of matter. Its crystal structure can be tuned by temperature and pressure between two phases; the topologically trivial $1T'$ phase, and the noncentrosymmetric T_d phase, the host of Weyl quasiparticles. The crystal symmetry is thus essential to predicting the emergence of topologically protected states.

The mechanism of the structural transition has been of particular interest in MoTe_2 , since Weyl quasiparticles are predicted in the low-temperature phase of the noncentrosymmetric orthorhombic T_d phase, protected by crystal symmetry. How the stacking pattern and disorder arise in MoTe_2 has implications on many other van der Waals-bound layered materials where stacking can be controlled reproducibly by temperature or pressure. The T_d phase can be thought of as having “AA” layer order, where “A” denotes an operation mapping one layer to the next. For T_d , this operation involves translation along the c axis by 0.5 lattice constants and reflections about the a and b directions. Though there are two layers per unit cell, the operation is the same for both layers. In contrast, the layer stacking of $1T'$ can be described by “AB”, where “B”

denotes an operation just like “A” but with an additional shift of about ± 0.15 lattice constants along the a direction, where the sign depends on whether the “B” is in an even or odd position in the layer sequence. To elucidate the nature of the transition mechanism across the phase boundary, we employed high-resolution single-crystal neutron diffraction and showed that the diffuse scattering that appears on cooling through the $1T'$ to T_d transition is consistent with random layer shifts, driving the transition from ABAB layer stacking in the $1T'$ phase to AAAA layer stacking in the T_d phase.

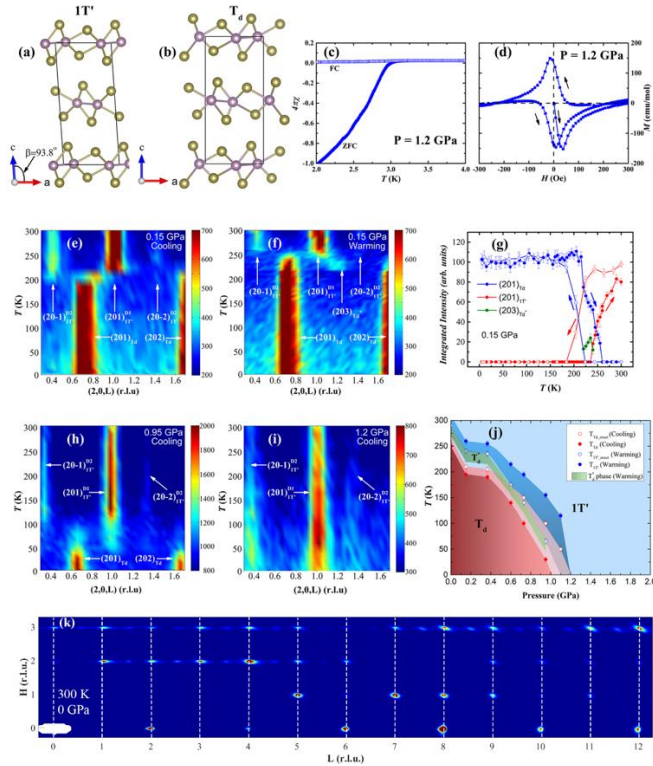
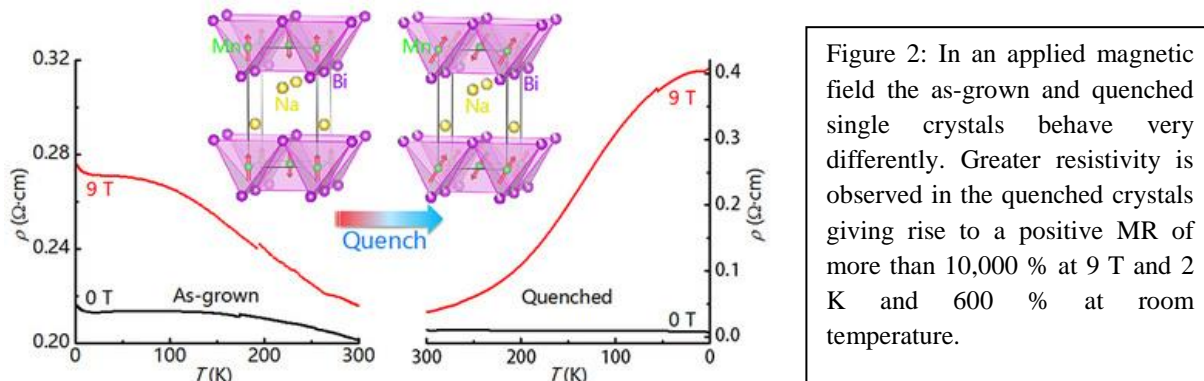


Figure 1: (a) Crystal structure of MoTe_2 in the $1T'$ and (b) T_d . (c) Superconducting shielding and Meissner fraction in $H = 20$ Oe at 1.2 GPa. (d) Magnetic hysteresis loop for MoTe_2 at 2 K and 1.2 GPa. (e, f) Contour map of the neutron scattering intensity across the $(2\ 0\ l)$ Bragg peak along the $[0\ 0\ 1]$ direction at 0.15 GPa. (g) Temperature dependence of the q integrated neutron scattering intensity for $(201)_{1T'}^{D1}$ peak (red squares), $(201)_{T_d}$ peak (blue circles) and $(201)_{T_d^*}$ (green circles). (h and i) Contour map of the neutron scattering intensity obtained by scanning across the $(2\ 0\ l)$ Bragg peak along the $[0\ 0\ 1]$ direction at 0.95 GPa on cooling (h) and at 1.2 GPa on cooling (i). (j) The phase diagram under pressure. (k) HOLL plot.

Moreover, MoTe_2 is a candidate topological superconductor (TSC) in the orthorhombic phase at ambient pressure (6). In the superconducting state, Fermi arcs are proposed to still exist even though the Weyl nodes are completely gapped out by the superconducting gap, and the onset of superconductivity can generate a quantum anomaly (7, 8). The application of pressure enhances the superconducting transition temperature from 0.25 to about 8 K (9) and extends the superconducting phase over a wide pressure range. Recent studies showed that while in the superconducting state, a phase transition occurs from the orthorhombic T_d to the monoclinic $1T'$ phase under pressure (10) with a large hysteresis region and coexistence of the two phases. A high-pressure muon-spin rotation study of superconductivity in MoTe_2 suggested that a topologically non-trivial s^{++} state likely exists in MoTe_2 at pressures up to 1.9 GPa (11). Key components to a TSC state are the crystal structure and band topology under pressure. Existing reports stop short of exploring the symmetry in the superconducting phase and no calculations exist on the electronic band structure under pressure. Using single crystal neutron diffraction, the *pressure-temperature* phase diagram is mapped out (Fig. 1), and combined with band

structure calculations, we elucidate the effects of pressure on the electronic band structure topology.

The emerging field of antiferromagnetic (AFM) spintronics aims at using room temperature AFM semiconductors to complement or replace ferromagnetic (FM) electrodes in hard drive read heads and magnetic random access memories (13, 14). Their resilience to external magnetic fields and the absence of stray fields make AFMs suitable for ultrafast, ultrahigh-density magnetic storage devices and AFM spin valves. AFM semiconductors can potentially integrate spintronics and microelectronic functionalities in a single material (15). New materials engineering holds the promise for realizing AFM spintronics. Three-dimensional AFM semiconductors of the I-Mn-V (with I = Li, Na, and K, and V = As, Sb, and Bi) class with Néel temperatures above 300 K are promising candidates for the next generation of AFM spintronics. Of this class, LiMnAs has been predicted to exhibit large spin orbit coupling induced magnetic anisotropy. Tetragonal phases of CuMnSb and CuMnAs are compatible with existing semiconducting technologies but show little magnetoresistance in bulk form. We recently reported that the narrow-gap NaMnBi semiconductor can exhibit a very large MR when defects are introduced in the crystal lattice. When quenched from high temperature, the MR increases thousand-fold, with the large increase observed upon cooling from room temperature to 2 K, and is not limited to the vicinity of the Neel transition temperature (Fig. 2). Quenching introduces vacancies on the Bi and Na sublattices, accompanied by reorientation of the AFM coupled spins which involves spin canting. Deviations of the local magnetization can propagate through magnons and may find use in information processing such as in magnonic devices.



At present, it is difficult to specify the microscopic origin of the large MR in NaMnBi. One possible mechanism may arise from spin fluctuations. It is known that enhanced spin fluctuations in antiferromagnets under a magnetic field can raise MR. This is related to the well-known GMR, originating from the suppression of spin fluctuation of ferromagnets by the stabilization of the ferromagnetic order under a magnetic field, which, on the other hand, does not stabilize the AFM order. NaMnBi may be useful as a single magnetic electrode in devices because it carries both magnetism and a very large magnetoresistance.

Future Plans

In the next year or so, we will continue the work on the dichalcogenides by doping W in MoTe₂. We will also investigate other systems such as TaS/Se₂, exhibiting similar characteristics. We will also continue to understand the origin of the huge MR in I-Mn-V, and continue to dope the system for better control of the defects.

References

1. Wang, Q. H. et al., *Nat. Nanotechnol.* **7**, 699 (2012).
2. Jariwala, D. et al., *ACS Nano* **8**, 1102 (2014).
3. Cao, Y. et al., *Nature* (London) **556**, 43 (2018).
4. Huang, L. et al., *Nat. Mater.* **15**, 1155 (2016).
5. Sun, Y. et al., *Phys. Rev. B* **92**, 161107(R) (2015).
6. Soluyanov, A. A. et al., *Nature* (London) **527**, 495 (2015).
7. Xu, S.-Y. et al., *Science* **7**, 613 (2015).
8. Qi, Y.-P. et al, *Nature Commun.* **7**, 11038 (2016).
9. Alidoust, M., Halterman, K. & Zyuzin, A. A, *Phys. Rev. B* **95**, 155124 (2017).
10. Wang, R., Hao, L., Wang, B. G. & Ting, C. S. *Physical Review B* **93**, 184511 (2016).
11. Heikes, C. et al, *Phys. Rev. Materials* **2**, 074202 (2018).
12. Guguchia, Z. et al, *Nature Commun.* **8**, 1082 (2017).
13. Máca, F. et al., *J. Magn. Magn. Mater.* **324**, 1606 (2012).
14. Marti, X. et al., *Nat. Mater.* **13**, 367 (2014).
15. Jungwirth, T. et al., *Phys. Rev. B* **83**, 035321 (2011).

Publications

“Emergence of topologically protected states in MoTe₂ Weyl semimetal with layer stacking order”, J. A. Schneeloch, C. Duan, J. Yang, J. Liu, X. Wang, and D. Louca, accepted Phys. Rev. B. Rapid Comm. (2019).

“Appearance of a new phase across the Td-IT’ phase boundary in Weyl semimetal Mo_{1-x}W_xTe₂”, Y. Tao, J. A. Schneeloch, C. Duan, M. Matsuda, S. E. Dissanayake, A. Aczel, J. A. Fernandez-Baca, and D. Louca, submitted to Phys. Rev. B. Rapid Comm. (2019).

“Electronic band tuning under pressure in MoTe₂ Weyl semimetal”, S. Dissanayake, C. Duan, J. Yang, J. Liu, M. Matsuda, C. Yue, J. A. Schneeloch, J. C. Y. Teo, and D. Louca, submitted to NPJ Quantum Materials (2019).

“Local trigonal modes and the suppression of the charge density wave in TiSe_{2-x}Te_x”, A. Wegner, D. Louca, and J. Yang, accepted to Phys. Rev. B (2019).

“Fe vacancy order and domain distribution in A_xFe_{2-y}Se₂”, C. Duan and D. Louca, *J. Supercond. Novel Magn.* **31**, 757 (2018).

“Evidence for pseudo Jahn-Teller distortions in the charge density wave phase of TiSe₂”, A. Wagner, J. Zhao, K. Wijayarathne, J. Li, J. Yang, A. A. Anikin, G. Karapetrov, D. Louca and U. Chatterjee, submitted to Phys. Rev. Lett. (2018).

“A Monte-Carlo Study on the Coupling of Magnetism and Ferroelectricity in the Hexagonal Multiferroic $RMnO_3$ ”, C. Duan, G.-W. Chern and D. Louca, *Cond. Matter* **3**(4), 28 (2018).

“Appearance of superconductivity at the vacancy order-disorder boundary in $K_xFe_{2-y}Se_2$ ”, C. Duan, J. Yang, Y. Ren, S. M. Thomas and D. Louca, *Phys. Rev. B* **97**, 184502 (2018).

“Defect-driven extreme magnetoresistance in an I-Mn-V semiconductor”, J. Yang, A. Wegner, C. M. Brown, and D. Louca”, *Appl. Phys. Lett.* **113**, 122105 (2018).

“Bismuth defects create the largest magnetoresistance seen in an I-Mn-V semiconductor”, AIP Scilight <https://aip.scitation.org/doi/10.1063/1.5058147>.

“Elastic and electronic tuning of magnetoresistance in $MoTe_2$ ”, J. Yang, J. Colen, J. Liu, M. C. Nguyen, G.-W. Chern, and D. Louca, *Science Advances* **3**, No. 12, eaao4949 (2017).

“Particle-hole asymmetry and orbital selectivity of the charge density wave energy gap in $2H-TaS_2$ ”, J. Zhao, J. Wijayarathne, A. Butler, V. Karlapati, J. Yang, C. D. Maliakas, D. Y. Chung, D. Louca, M. G. Kanatzidis, J. van Wezel, U. Chatterjee, *Phys. Rev. B* **96**, 125103 (2017).

“The magnetic structure of NiS_2 ”, S. Yano, C.-W. Wang, J. S. Gardner, A. J. Studer, D. Louca, submitted to *Physica B* (2017).

Controlling quantum coherence in frustrated spin-orbit magnets

Martin Mourigal, Georgia Institute of Technology, Atlanta, GA

Program Scope

Magnetism originates from the quantized nature of electrons' magnetic moments (spins). Atomic-scale interactions between spins can lead to exotic quantum coherence and entanglement effects. In typical magnets, however, quantum entanglement is very short-ranged and collective phenomena such as broken-symmetry phases and their excitations are semi classical in nature. It is a central challenge to discover or design magnetic materials in which entanglement extends beyond the angstrom scale. Such quantum magnets promise applications in spintronics, energy materials or quantum computing. Many forms of highly-entangled magnetic matter, called quantum spin-liquids, have been predicted by theory and successfully classified according to their non-local (topological) properties. Distinctively, they host excitations with fractional quantum numbers, leading to a continuous (rather than sharp) excitation spectrum in spectroscopic experiments. The quest to detect these excitations in actual materials, and thus discover quantum spin-liquids, is extremely active with inelastic neutron scattering at the forefront.

The working hypothesis of this program is that the detection of a continuous excitation spectrum at low temperatures is a *necessary but not sufficient* condition to the positive detection of a quantum spin-liquid. Intrinsic effects, such as non-linear spin dynamics or the presence of classical degeneracies, or extrinsic materials perturbations, such as chemical heterogeneities, none of which are generally well-understood, may generate continuous excitation spectra in absence of quantum entanglement. This program seeks to understand the latter effects to advance neutron scattering in its quest to identify the fabric of genuine quantum correlations in materials. The program uses a combination of neutron scattering experiments (primarily at ORNL), materials synthesis, and high-fidelity modeling to amplifying the depth and breadth of our understanding of quantum phases and excitations in insulating magnets. In terms of target materials, focus is on geometrically-frustrated rare-earth and transition-metal magnets with kagome, pyrochlore and other geometrically frustrated structures for which spin-orbital effects endow spins with controllable quantum properties.

The program, established in 2018, has three goals: **(Goal I)** – Study frustrated spin-orbit materials as a central platform to design and interrogate model Hamiltonians; **(Goal II)** – Develop local and cloud material synthesis efforts at Georgia Tech to gain control on the structure and properties of crystalline materials under investigation; **(Goal III)** – Pair time-of-flight neutron spectroscopy and realistic simulations to reveal the development (or absence thereof) of quantum coherence in real magnets.

Recent Progress

Highlight I: Nature of excitations in a classical spin-liquid MgCr_2O_4

We performed a comprehensive inelastic neutron-scattering study of the frustrated pyrochlore antiferromagnet MgCr_2O_4 in its cooperative paramagnetic regime, using the SEQUOIA spectrometer at ORNL and crystals grown at Johns Hopkins' IQM. At 20 K, MgCr_2O_4 is above its ordering temperature of 13 K but well below the Weiss constant of $|\sim 400 \text{ K}|$, such that its $S=3/2$ spins are highly correlated. The ground-state of the pyrochlore Heisenberg antiferromagnet is known to be a degenerate manifold of spatially disordered (yet correlated) spin configurations [1]. Theoretical analysis of the energy-integrated response (diffuse scattering)

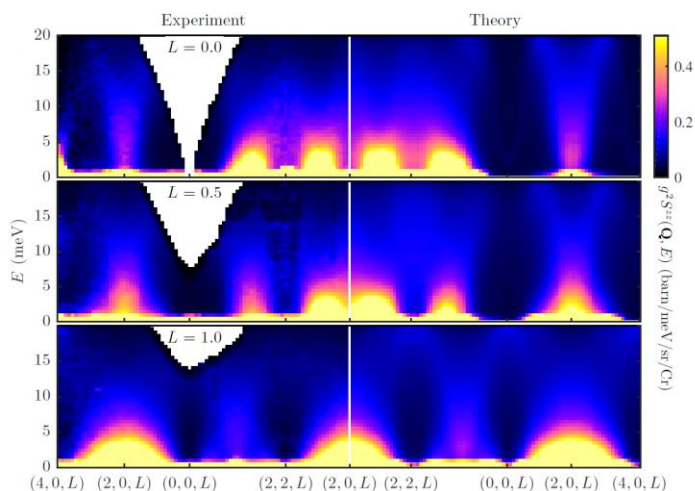


Fig. 1. Comparison between experiment and theory for the spin dynamics of MgCr_2O_4 measured at 20K. Theory is linear spin-wave theory around a disordered spin configuration.

scattering) yields a microscopic Heisenberg model with exchange interactions up to third-nearest neighbors, which quantitatively explains all the details of the dynamic magnetic response. This model is in contrast with the previous “emergent cluster” scenario brought forward to explain the paramagnetic response of both ZnCr_2O_4 [2] and MgCr_2O_4 [3,4,5]. Our further-neighbor exchange model allowed us to demonstrate that the magnetic excitations in paramagnetic MgCr_2O_4 are faithfully represented in the entire Brillouin zone by a theory of magnons propagating in a highly-correlated paramagnetic background [Figure 1]. Thus, in a classical spin-liquid, dynamics is broad because spins ride a disordered background and, at least to first order, this is not because of fractionalization, nor because of magnon decay. Our theoretical approach works because the time-scales of harmonic spin precessions and ground-state reconfigurations vastly differ. Our results also suggest that MgCr_2O_4 is proximate to a spiral spin-liquid phase distinct from the Coulomb phase, which has implications for the magneto-structural phase transition in MgCr_2O_4 below 13K and that we plan to study next.

Highlight II: Quantum versus Classical Spin Fragmentation in Dipolar Kagome Ice

A promising route to realize entangled magnetic states combines geometrical frustration with quantum-tunneling effects [6,7]. Spin-ice materials are canonical examples of frustration, and Ising spins in a transverse magnetic field are the simplest many-body model of quantum tunneling. We have shown that the tripod kagome lattice material $\text{Ho}_3\text{Mg}_2\text{Sb}_3\text{O}_{14}$ unites an ice-like magnetic

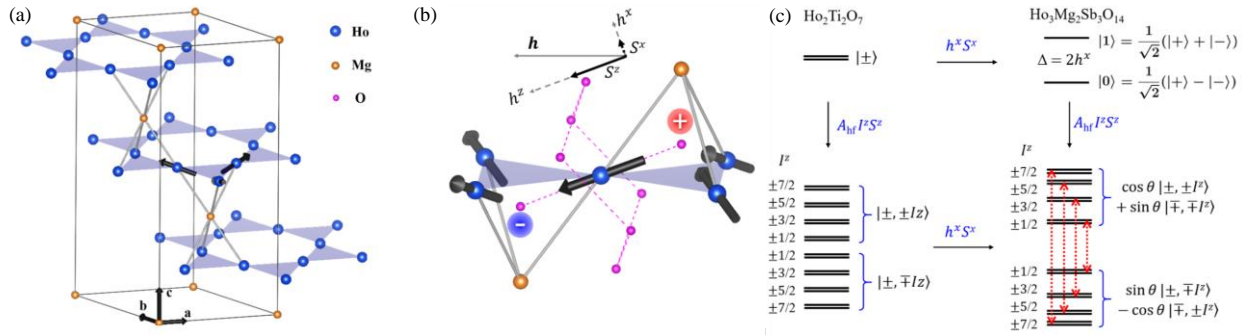


Fig. 2. (a) Crystal structure of $\text{Ho}_3\text{Mg}_2\text{Sb}_3\text{O}_{14}$. (b) Local symmetry of magnetic ions in $\text{Ho}_3\text{Mg}_2\text{Sb}_3\text{O}_{14}$ and transverse-field effects induced by the non-Kramers nature of Ho^{3+} . (c) Combined effects of intrinsic transverse field and hyperfine interactions on the single-ion physics of Ho^{3+} in $\text{Ho}_3\text{Mg}_2\text{Sb}_3\text{O}_{14}$ compared to $\text{Ho}_2\text{Ti}_2\text{O}_7$.

degeneracy with quantum-tunneling terms generated by an intrinsic splitting of the Ho^{3+} ground-state doublet. Using a sol-gel technique, we prepared very high-quality polycrystalline samples of $\text{Ho}_3\text{Mg}_2\text{Sb}_3\text{O}_{14}$, free from magnetic impurity phases. Using neutron scattering and thermodynamic experiments, we observe a symmetry-breaking transition at 320 mK to a remarkable quantum state with three peculiarities: a continuous magnetic excitation spectrum; a macroscopic degeneracy of low energy ice-like states; and a fragmentation of the spin into periodic and aperiodic components strongly affected by quantum fluctuations. We explained these observations with a frustrated transverse Ising model using theoretical approaches, including random phase approximation, mean-field approximation, and exact diagonalization. Our results established the existence a highly entangled quantum spin fragmented state in a region where the transverse field remains a perturbation to the classical spin fragmentation energy. However, we find that hyperfine interactions play a crucial role for suppressing many-body quantum correlations in this frustrated magnet [Figure 2]. Hence, the spin fragmentation in $\text{Ho}_3\text{Mg}_2\text{Sb}_3\text{O}_{14}$ is quantum mostly at the single ion level, and semi-classical at the two-ion level, characterized by magnetic monopole-like excitations. Our work has advanced both the synthesis and modeling arms of our program by providing a complex and versatile material platform to investigate and train students and postdoc.

Highlight III: Synthesis of new frustrated spin-orbit magnets

We ramped-up the material synthesis arm in our laboratory at Georgia Tech. We synthesized several novel frustrated spin-orbit magnets for neutron scattering investigations. In one instance, we benefited from the crystal growth facilities at Johns Hopkins PARADIM facility to grow a large single-crystal of a material with a complex field-induced phase diagram [Figure 3].

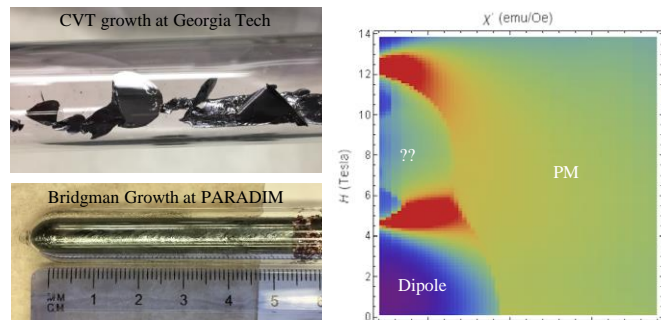


Fig. 3. Synthesis of crystals of a spin-orbit frustrated magnet and phase diagram characterization.

Future Plans

Our future plans will leverage the discoveries and progresses highlighted above. On the front of the simulation of the complex neutron scattering response of classical frustrated magnets, as relevant for MgCr_2O_4 , we will investigate the spin dynamics of this compound at high temperatures, where the separation of time-scales between harmonic fluctuations and ground-state reconfigurations is not valid. To do so, we will use the polarized neutron capability of the HYSPEC spectrometer to get rid of the phonon and incoherent background and continue to collaborate with theorists. We will also investigate the complex magneto-structural ordering below 13 K. To do so, we will use the spin-wave dispersions in the ordered phases to identify a magnetic structure, a problem for which traditional approaches have failed.

We will continue our investigation of tripod kagome systems, with the detailed powder studies of $\text{Er}_3\text{Mg}_2\text{Sb}_3\text{O}_{14}$ and $\text{Yb}_3\text{Mg}_2\text{Sb}_3\text{O}_{14}$ which we have already obtained as high-quality samples using our sol-gel method. We will continue our promising and on-going work to produce single-crystal samples of members of this material family. This would enable detailed diffuse scattering studies using the CORELLI spectrometer at ORNL.

Finally, we will perform inelastic studies on two families of frustrated spin-orbit materials that we recently produced in single-crystal form and that display putative quantum orders at high magnetic fields.

References

- [1] R. Moessner and J. T. Chalker, *Phys. Rev. Lett.* **80**, 2929 (1998)
- [2] S. H. Lee, C. Broholm, W. Ratcliff, G. Gasparovic, Q. Huang, T. H. Kim, and S. W. Cheong, *Nature* **418**, 856 (2002).
- [3] K. Tomiyasu, H. Suzuki, M. Toki, S. Itoh, M. Matsuura, N. Aso, and K. Yamada, *Phys. Rev. Lett.* **101**, 177401 (2008).
- [4] K. Tomiyasu, T. Yokobori, Y. Kousaka, R. I. Bewley, T. Guidi, T. Watanabe, J. Akimitsu, and K. Yamada, *Phys. Rev. Lett.* **110**, 077205 (2013).
- [5] S. Gao, K. Guratinder, U. Stuhr, J. S. White, M. Mansson, B. Roessli, T. Fennell, V. Tsurkan, A. Loidl, M. Ciomaga Hatnean, G. Balakrishnan, S. Raymond, L. Chapon, V. O. Garlea, A. T. Savici, A. Cervellino, A. Bombardi, D. Chernyshov, C. Ruegg, J. T. Haraldsen, and O. Zaharko, *Phys. Rev. B* **97**, 134430 (2018).
- [6] L. Savary and L. Balents, *Phys. Rev. Lett.* **118**, 087203 (2017).
- [7] J.-J. Wen, S. M. Koohpayeh, K. A. Ross, B. A. Trump, T. M. McQueen, K. Kimura, S. Nakatsuji, Y. Qiu, D. M. Pajerowski, J. R. D. Copley, and C. L. Broholm, *Phys. Rev. Lett.* **118**, 107206 (2017).

Publications

1. “Magnetic excitations of the classical spin liquid MgCr_2O_4 ”, X. Bai, J. A. M. Paddison, E. Kapit, S. M. Koohpayeh, J.-J. Wen, S. E. Dutton, A. T. Savici, A. I. Kolesnikov, G. E. Granroth, C. L. Broholm, J. T. Chalker, and M. Mourigal, *Physical Review Letters* **122**, 097201 (2019); <https://doi.org/10.1103/PhysRevLett.122.097201>
2. Quantum Spin Fragmentation in Kagome Ice $\text{Ho}_3\text{Mg}_2\text{Sb}_3\text{O}_{14}$, Z. L. Dun, X. Bai, J. A. M. Paddison, E. Hollingworth, N. P. Butch, C. D. Cruz, M. B. Stone, T. Hong, M. Mourigal, H. D. Zhou, Submitted, arXiv:1806.04081 (2018)

Measurement and Modeling of Organic Semiconductor Structure and Dynamics

Adam J. Moulé

University of California, Davis

Department of Chemical Engineering

Program Scope: The long term goal of this project is to gain a comprehensive understanding of and the ability to predict optoelectronic materials properties of organic semiconductors. Our central hypothesis is that the combined use of electronic (DFT) and molecular dynamics (MD) modeling methods validated by neutron scattering data will yield new understanding of the relationship between structural heterogeneity and charge delocalization, charge transport, exciton transport, dopant site choice, and dopant transport. To fully explore and develop this research area, we proposed three specific hypothesis driven aims:

- (1) **Measure dopant and polymer diffusion between DISC processed layers:** Our hypothesis is that entangled polymers do not mix with adjacent layers upon solvent swelling or dedoping but small molecule dopants diffuse and drift across interfaces.
- (2) **Develop model interpretation for the inelastic neutron scattering (INS) spectrum:** Our hypothesis is that the low energy portion of the INS spectrum, which measures delocalized phonon modes, contains information that governs fundamental aspects of the polymer mechanical stability, charge stabilization, and charge transport.
- (3) **Develop multi-scale models of charged polymers:** Our hypothesis is that an understanding of dopant site choice and the change in molecular structure upon doping can be achieved with combined electronic and molecular dynamics modeling validated by inelastic neutron scattering data.

In addition to these proposed aims, we had a considerable backlog of projects from our 2013-16 DOE-BES award that focused on development of doping gradients using solution methods.

Recent Progress: We have made significant progress on our research goals, resulting in 14 new peer reviewed publications in the last 2 years. The progress and challenges in each sub project are described below.

Experimental work related to doping and polymer patterning: This project was primarily carried out by Ph.D. student Ian Jacobs, who both graduated in early 2017 and is now a Newton Postdoctoral Scholar in Cambridge University. He developed methods to pattern semiconducting polymers called dopant induced solubility control (DISC). The mechanism involves adding and removing molecular dopants from the polymer. Addition of dopants charges the polymer and greatly reduces its solubility. **Pub. 1** demonstrates the use of DISC to pattern the polymer P3HT with sub-diffraction limited resolution and **Pub. 2** explores in detail the light induced reaction between the dopant F4TCNQ and the solvent THF that enables the rapid optical patterning of P3HT. **Pub. 3** explores in detail the chemical reaction between primary amines and the dopant F4TCNQ that enables complete (quantitative) removal of F4TCNQ from any semiconducting

polymer film. This combination of ideas is very powerful and is the basis for two new NSF grants led by my group to fabricate short-channel thin-film transistors and light trapping structures for organic photovoltaic devices, respectively. We wrote an invited review (**Pub. 7**) for *Advanced Materials* describing the doping/patterning work, the dopant diffusion work described below, and the dopant synthesis work (older than 2 years) supported by DOE-BES.

Measure dopant and polymer diffusion between DISC processed layers: This project was started by Ph.D. student Jun Li, who graduated in early 2017 and now works for Applied Materials. The project was taken over by Tucker Murrey, who is now in his 4th year. Our hypothesis was/is that doped polymers will not mix across a bi-layer interface even in the presence of solvent, but dopants will diffuse within and between the layers. Our previous 2016 paper¹ proposed a Langmuir isotherm model to explain the uptake of dopants in polymer films. This model posits a fixed number of doping sites on the polymer that are increasingly difficult to fill with increased doping level. **Pub. 6** used QENS measurements to characterize the local dynamics of a proton labeled dopant (F4MCTCNQ) in a deuterated (D-P3HT) sample. We then used confocal fluorescence microscopy to measure the macroscopic diffusion of both dopant species. These measurements allowed us to expand the interpretation of the isotherm model to include equilibrium between charged and neutral dopants within the P3HT film and to quantify the diffusion rate of both dopant species. This was a very important paper because it links the doping density, dopant diffusion rate, molecular energy landscape, and even dopant structure in a comprehensive picture.

Pub. 12 explores evaporative addition of the dopant F4TCNQ through and shadow mask to P3HT films and subsequent patterning by development in various solvents. The important science in this paper is quantification of the dopant diffusion distance under the shadow mask. We show that the isotherm model predicts a larger diffusion distance in more highly crystalline P3HT films because fewer doping sites are available to the dopant. We also explore how local doping level and solvent quality combine to determine the pattern sharpness. Finally we show that dopants with lower diffusion rate (while neutral) lead to sharper polymer patterning.

In **Pub. 14** we quantify solvent swelling in neutral and doped P3HT films using NR. Then we fabricated a 4-layer alternating stack of P3HT and D-P3HT using our DISC method and used NR to measure the interface roughness. Importantly we show that each layer is pure with a sharp interface even though the polymer structure is identical and the deposition solvent is a good solvent. We then soaked the layer stack in this good solvent for 4 hours, removed the solvent and re-measured the layer stack using NR. Although all four films swelled to >50% of their original thickness and the solvent would instantaneously dissolve an undoped film, there was no change in interface roughness, which proved our hypothesis that doped polymer films will not mix across a bi-layer interface. This last result is interesting polymer physics and crucially shows that DISC patterning techniques can be used in an industrial setting (for example roll-to-roll coating with a slot-die or blade coater) for multi-layer film deposition.

Develop model interpretation for the inelastic neutron scattering (INS) spectrum: This project was carried out primarily by Ph.D. student Thomas Harrelson, who graduated in spring 2019. Ph.D. Our first study was focused on P3HT/F4TCNQ with the goal to understand how the presence of F4TCNQ “stiffened” the P3HT with doping. We quickly learned that it was not possible to model amorphous P3HT using DFT and so we could not even begin to model the low energy (less than 800 cm^{-1}) portion of the INS spectrum. **Pub. 5** is therefore a study of the high energy $>800\text{ cm}^{-1}$ portion of the INS spectrum. We first set out to model crystalline P3HT and found that we could not fit the INS spectrum using a single crystalline polymorph, but instead needed to include a weighted average of 3-4 different crystalline polymorphs to match the data. This result is important because interpretation of x-ray data and structure minimization yielded a single “accepted” crystalline polymorph in published literature. Our work shows that in a single crystal, multiple polymorph co-exist. The P3HT side chain angle instead varies as a function of the polymers position within the crystal as shown in Figure 1. In the same paper we also examined the structure of P3HT/F4TCNQ and concluded that in a highly doped sample, only one crystalline polymorph exists with the F4TCNQ intercalated between the P3HT chains. This was the first time any researcher identified the location of the dopant with respect to the polymer.

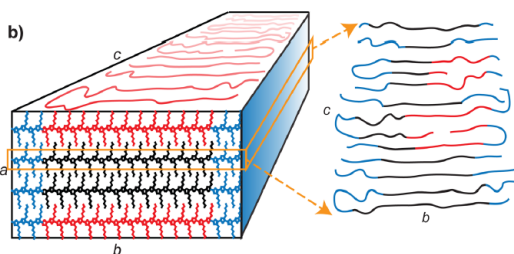


Figure 1. Cartoon depicting how different polymorphs of P3HT can co-exist in different parts of the same crystal.

We realized that the low energy phonon modes we measure using INS should affect the charge transport in organic semiconductors. But as stated above, we are not able to model these modes in polymers. So in **Pub. 11** we measured INS spectra of small molecule organic semiconductors and used plane-wave DFT to model the full phonon spectrum. We had to adjust our functional and sampling of the Brillouin zones until our simulated spectrum matched the measured spectrum. Next we calculated the electron phonon coupling to determine which phonon modes reduce the charge mobility. Because there are 1000’s of modes, we found that the spectral density of modes was a better measure than individual motions. We also considered that only low energy modes ($<200\text{ cm}^{-1}$) are populated at 300K, so only these delocalized modes will affect charge transport. We chose to use a transport model called transient delocalization that considers the reduction in delocalization induced by the molecular motions. This model along with accurate phonon measurements allowed us to predict the single crystal charge mobility with high accuracy, which had not been possible with other models that did not consider dynamic motions of the molecules.

In **Pub. 10** we collaborated with the group of Enrique Gomez (Penn St.) on dynamic measurement of P3HT side chains using QENS and solid state NMR. The study was led by the Gomez group and we provided the NMR measurement and interpretation.

Develop multi-scale models of charged polymers: This aim is still a work in progress as we do not yet have all of the computational tools needed. We made some progress in several areas. **Pub.**

4 is an invited review of multi-scale modeling techniques for organic semiconductors written by Thomas Harrelson.

Pub. 8 models exciton delocalization on the polymer PffBT4T-2DT, which is more crystalline than P3HT. We considered to measure this polymer with INS until we realized that we first need to develop a MD approach to modeling INS data. Our paper showed that this polymer becomes planar quickly when optically excited but relaxes slowly to a coiled configuration.

In **Pub. 9** we discovered a new crystalline structure of P3HT/F4TCNQ that forms in heated samples. Interestingly this polymorph of P3HT/F4TCNQ is blue (not purple/gray like the typical sample). Spectroscopic investigation showed that the blue color comes from a partial charge transfer (local CT state) instead of the quantitative charge transfer that usually forms in P3HT/F4TCNQ. While most of this study was funded from my NSF grant, Thomas Harrelson developed a DFT model of the new structure using funds and expertise developed in INS modeling of P3HT/F4TCNQ. Thus this part of the work was a direct extension of BES funded work.

In **Pub. 13**, we collaborated with the group of Christian Müller from Chalmers University to investigate doping in a thiophene polymer with ethoxy side chains. The Müller group discovered that this polymer could be double doped by F4TCNQ, two holes are created on the polymer backbone for every dopant. They also found that the dopant resides between the side chains, unlike our model of P3HT in which the dopant is between the polymer backbones. We developed a DFT model of the dopant in the side chain to determine the reason for the different placement of the dopant. We found that the ethoxy side chains are attracted to the polar charged dopant and so it is the strong interaction between the side chains and the dopant that determine the dopant position.

Future Plans: Most organic electronic materials are highly heterogeneous in structure and most devices are made with mixtures of materials, such as donor/acceptor or semiconductors with dopants. While we made progress by accurately predicting charge mobility in a perfect crystal for the first time using our INS validated DFT model, it is necessary to develop modeling tools that can incorporate structural and chemical heterogeneity and still predict materials properties. Our future work will involve development of MD and density functional tight binding (DFTB) methods to model phonons and INS spectra. These codes can incorporate much larger samples and more heterogeneity. Our other new research thrust will involve development of a new optical excitation sample environment for the VISION beamline. We will develop this new sample environment so that we can measure the phonon spectrum of optically excited samples. Our hypothesis is that we will see changes in the phonon modes that are important to understand exciton transport.

References

- (1) Jacobs, I. E.; Li, J.; Aasen, E. W.; Lopez, J.; Fonseca, T.; Zhang, G.; Stroeve, P.; Augustine, M. P.; Mascal, M.; Moule, A. J., Comparison of Solution-Mixed and Sequentially Processed P3ht:F4tcnq Films: Effect of Doping-Induced Aggregation on Film Morphology. *Journal of Materials Chemistry C* **2016**, *4*, 3454-3466.

Publications¹⁻¹⁴

- (1) Jacobs, I. E.; Aasen, E. W.; Nowak, D.; Li, J.; Morrison, W.; Roehling, J. D.; Augustine, M. P.; Moule, A. J. Direct-write optical patterning of P3HT films beyond the diffraction limit. *Advanced Materials* **2017**, *29*, 1603221.
- (2) Fuzell, J.; Jacobs, I. E.; Ackling, A.; Harrelson, T. F.; Huang, D. M.; Larsen, D. S.; Moule, A. J. Optical Dedoping Mechanism for P3HT/F4TCNQ Mixtures. *Journal of Physical Chemistry Letters* **2016**, *7*, 4297-4303.
- (3) Jacobs, I. E.; Wang, F.; Hazefi, N.; Medina-Plaze, C.; Harrelson, T. F.; Li, J.; Augustine, M. P.; Mascal, M.; Moule, A. J. Quantitative dedoping of conducting polymers. *Chemistry of Materials* **2017**, *29*, 832-841.
- (4) Harrelson, T. F.; Moulé, A. J.; Faller, R. Modeling organic electronic materials: bridging length and time scales. *Molecular Simulation* **2017**, *43*, 1-13.
- (5) Harrelson, T. F.; Cheng, Y. Q.; Li, J.; Jacobs, I. E.; Ramirez-Cuesta, A. J.; Faller, R.; Moule, A. J. Identifying Atomic Scale Structure in Undoped/Doped Semicrystalline P3HT Using Inelastic Neutron Scattering. *Macromolecules* **2017**, *50*, 2424-2435.
- (6) Li, J.; Koshnick, C.; Diallo, S. O.; Ackling, S.; Huang, D. M.; Jacobs, I. E.; Harrelson, T. F.; Hong, K.; Zhang, G.; Beckett, J.; Mascal, M.; Moule, A. J. Quantitative Measurements of the temperature-dependent microscopic and macroscopic dynamics of a molecular dopant in a conjugated polymer. *Macromolecules* **2017**, *50*, 5476-5489.
- (7) Jacobs, I. E.; Moule, A. J. Controlling Molecular Doping in Organic Semiconductors. *Advanced Materials* **2017**, *29*, 1703063.
- (8) Dantanarayana, V.; Fuzell, J.; Nai, D.; Jacobs, I. E.; He, Y.; Faller, R.; Larsen, D.; Moule, A. J. Put Your Backbone into It: Excited-State Structural Relaxation of PffBT4T-2DT Conducting Polymer in Solution. *Journal of Physical Chemistry C* **2018**, *122*, 7020-7026.
- (9) Jacobs, I. E.; Cendra, C.; Harrelson, T. F.; Bedolla Valdez, Z. I.; Faller, R.; Salleo, A.; Moule, A. J. Polymorphism controls the degree of charge transfer in a molecularly doped semiconducting polymer. *Material Horizons* **2018**, *5*, 655-660.
- (10) Zhan, P.; Zhang, W.; Jacobs, I. E.; Nisson, D.; Moule, A. J.; Milner, S.; Maranas, J.; Gomez, E. D. Side Chain Length Affects Backbone Dynamics in Poly(3-alkylthiophene)s. *Journal of Polymer Science B: Polymer Physics* **2018**, *56*, 1193-1202.
- (11) Harrelson, T. F.; Dantanarayana, V.; Xie, X.; Koshnick, C.; Nai, D.; Fair, R.; Nunez, S. A.; Thomas, A. K.; Murrey, T. L.; Mickner, M. A.; Grey, J. K.; Anthony, J. E.; Gomez, E. D.; Troisi, A.; Faller, R.; Moule, A. J. Direct probe of the nuclear modes limiting charge mobility in molecular semiconductors. *Material Horizons* **2019**, *6*, 182-191.
- (12) Li, J.; Holm, D. M.; Guda, S.; I., B.-V. Z.; G., G.; Jacobs, I. E.; Dettmann, M. A.; Saska, J.; Mascal, M.; Moule, A. J. Effect of processing conditions on additive DISC patterning of P3HT films. *Journal of Materials Chemistry C* **2019**, *7*, 302-313.
- (13) Kiefer, D.; Kroon, R.; Hofmann, A. I.; Sun, H.; Liu, X.; Giovannitti, A.; Stegerer, D.; Cano, A.; Hynynen, J.; Yu, L.; Zhang, Y.; Nai, D.; Harrelson, T. F.; Sommer, M.; Moulé, A. J.; Kemerink, M.; Marder, S. R.; McCulloch, I.; Fahlman, M.; Fabiano, S.; Müller, C. Double Doping of Conjugated Polymers with Monomer Molecular Dopants. *Nature Materials* **2019**, *18*, 149-155.
- (14) Murrey, T. L.; Guo, K.; Mulvey, J. T.; Lee, O. A.; Cendra, C.; Moulin, J.-F.; Hong, K.; Salleo, A.; Moule, A. J. Additive solution deposition of multi-layered semiconducting polymer films for design of sophisticated device architectures. *Journal of Materials Chemistry C* **2019**, *7*, 953-960.

Engineered Protein Nanostructures for Advanced Functional Materials

Bradley D. Olsen

Department of Chemical Engineering, Massachusetts Institute of Technology

Program Scope

Engineering enzymes and optically active proteins into bioelectronic devices for the production of H_2 ,¹⁻² the reduction of CO_2 ,³⁻⁴ or the production of biofuels⁵⁻⁶ allows the evolutionarily optimized performance of the protein to be exploited to produce high-performance biomolecular variants of catalysts. Engineering biocatalytic materials requires achieving a high protein activity and active site density, controlling substrate/product transport through the material, maintaining protein stability, and developing low-cost processes for material fabrication. Analogous to synthetic catalysts⁷⁻⁸ or organic electronics,⁹⁻¹⁰ this requires the arrangement and orientation of the protein at an interface between two phases that provide for the transport of each reagent or charge carrier.

The self-assembly of block copolymers containing an enzyme or optically active protein block provides a bottom-up method to produce nanostructures that simultaneously achieve control over transport through two phases and yield a high density of oriented protein at an interface. This project investigates the fundamental structure and thermodynamics of block copolymer systems containing a globular protein block, enabling the production of functional nanomaterials. Both the folded protein chain shape and the specific interactions between globular proteins differ significantly from the Gaussian coil block copolymers, adding significant complexity to the phase behavior of these systems. The goal of this project is to apply neutron methods and clever biological design of materials to elucidate the fundamental forces that govern self-assembly. Over the past 2.5 years, we have addressed the following questions:

- (1) Why do some globular proteins self-assemble in block copolymers and some do not?

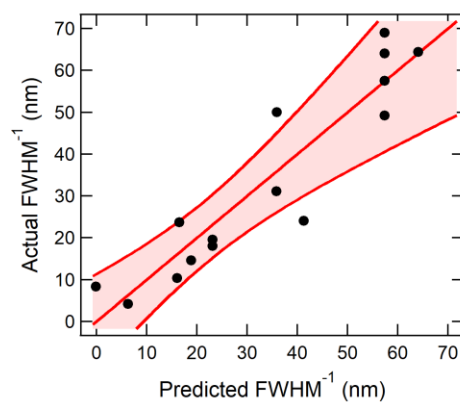
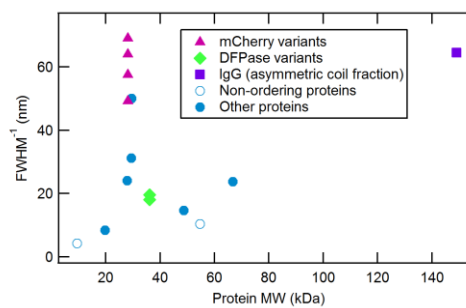
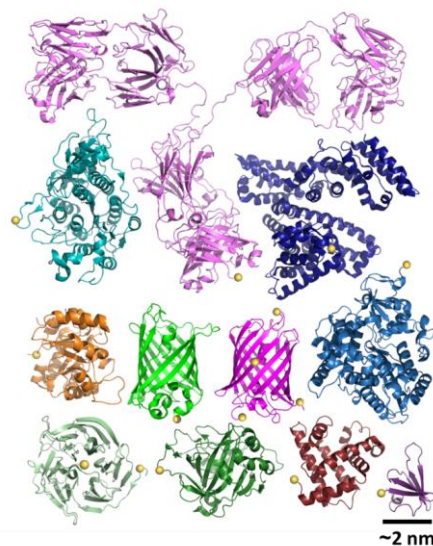


Figure 1. Schematic illustration of proteins in the bioconjugate library (top), correlation of an ordering parameter with molecular weight (middle), and fit of the ordering parameter to a predictive model for protein self-assembly (bottom).

- (2) What is the role that hydration and protein-polymer interactions play in governing self-assembly behavior?
- (3) How can we model protein-polymer block copolymer self-assembly?
- (4) What are the interactions between charged polymers and patchy proteins, and how can they be engineered to promote self-assembly?

Recent Accomplishments

Why Do Some Proteins Self-Assemble and Some Do Not? Early demonstrations of the ability to produce protein-based nanomaterials from proteins such as mCherry were extremely exciting,¹¹⁻¹² but these demonstrations and the studies of phase behavior raised a major question: can these techniques be generalized to other globular proteins, and if so, what are the key properties of the protein that govern self-assembly? Studies indicated that coarse-grained protein properties dominate the self-assembly behavior¹³, but for most properties there is no way to isolate and control a single property at a time. Therefore, we developed an approach of synthesizing a large set of 15 different bioconjugates and used regression methods to identify the most critical coarse-grained parameters for predicting self-assembly (Figure 1). This work indicated that the size of the protein and its β -sheet content are the two most important variables, in addition to its total charge¹⁴, for governing whether or not the protein can be self-assembled. Using cross-validation regression methods, we were able to identify a relatively simple predictive equation for the full width at half maximum (FWHM) of the primary scattering peak, an indicator of the quality of ordering of these nanostructures:

$$\text{Predicted FWHM}^{-1} = -9 + 0.38MW + 42 \left[\frac{0.97^2}{(MW - 28.4)^2 + 0.97^2} \right] + 0.3\beta$$

This equation is extremely powerful because it allows the potential for self-assembly of a protein-polymer conjugate (or by extension fusion protein) to be predicted before costly and challenging synthesis is undertaken. This work has been published in one publication and a second is submitted.

Because some proteins of technological interest are shown not to self-assemble in block copolymers through this work, we have developed two key strategies for improving self-assembly: the first is the use of polymer-protein-polymer triblocks, where polymer-polymer repulsive interactions in aqueous solution may be used to drive self-assembly. The second strategy is the use of a structure-directing protein segment that may be genetically fused to the protein, providing an impetus for self-assembly especially in small protein systems. One of these strategies has been published, and the other has a manuscript in preparation.

What is the Role of Hydration and Protein-Polymer Interactions on Self-Assembly? Contrast variation SANS was used to study the strength and nature of interactions between proteins and polymers that self-assemble when bioconjugated to a globular protein (mCherry). Partial structure factor decomposition and Fourier transformation into real space revealed that PNIPAM and mCherry interact repulsively via a depletion interaction. POEGA formed adsorption layers at the surface of mCherry, leading to a weaker segregation strength. PDMAPS, a zwitterionic polymer, exhibited both repulsive and attractive interactions to the polymer, leading to more complex

behavior that may limit its ability to self-assemble. Therefore, this work shows that PNIPAM has the widest range of self-assembly with proteins because it has the strongest repulsive interactions in water, while POEGA and PDMAPS have weakly attractive interactions that lead to suppressed self-assembly. This method is innovative because it enables studying such interactions at relatively high polymer and protein concentrations, the regime relevant to self-assembly. The results are consistent with previously published work and are under revision for publication.

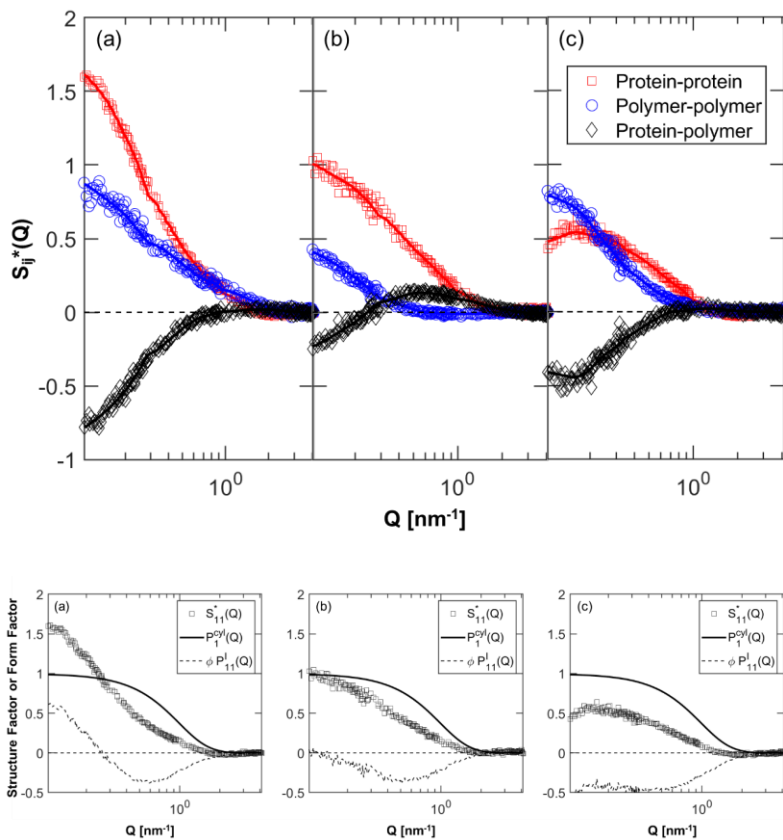


Figure 2. Partial Structure factors (top) and protein form factors and partial structure factors (bottom) for mCherry mixtures with PNIPAM (a), PHPA (b), and PDMAPS (c). In each case the data shows how the presence of polymer affects interactions between the proteins.

bootstrapping method to quantify the uncertainty in the hydration number that can be applied to other scattering experiments where performing replicates is not practical. This will provide both key insight into our self-assembled system as well as useful SANS data analysis contributions for the user community.

Finally, backscattering and disk chopper spectrometry experiments were used to probe the dynamics of different water populations in concentrated solutions of ELP-mCherry fusion proteins that have been shown to self-assemble to understand how water binding and dynamics may be influencing structure and self-assembly. Deuterated proteins were synthesized to allow for the direct measurement of water dynamics. Preliminary data analysis suggests there are differences in solvent interactions for ordered and disordered samples.

To enable design of structured biomaterials, it is necessary to not only determine which polymers are repulsive of proteins but to understand the underlying physics that governs these interactions. We hypothesize that hydration, including the competition for water under high concentration conditions, plays a key role. To better understand how hydration affects protein-polymer interactions, we have developed a new SANS-based analysis method to calculate the hydration number of water-soluble polymers. The method requires no assumptions for either the structure or the form factor. Preliminary results revealed that PNIPAM, which has the strongest propensity for self-assembly, has the highest hydration number. In addition, we are developing a

How Can We Model Protein-Polymer Block Copolymer Self-Assembly? In order to predict the thermodynamics of these complex systems, we have developed a simple coarse-grained model that can allow us to better understand the physical origins of the key properties displayed by these nanomaterials. Our model treats the protein as a single hard sphere and the polymer as a soft sphere or ellipsoid capable of overlapping with neighboring chains and to a lesser extent the hard proteins, capturing the key difference in excluded volume between the different halves of the molecule. This substantial reduction in molecular complexity enables simulation of systems of many molecules, enabling us to produce theoretical phase diagrams as a function of the design of the system, comparing to scattering results. In order to reproduce many of the key qualitative behaviors we observe in bioconjugate self-assembly, explicit solvent must be included into the model. This further reinforces the importance of understanding hydration and solvation effects addressed above.

What are the Interactions Between Charged Polymers and Patchy Proteins, and How Can They Be Engineered to Promote Self-Assembly? To extend the methods considered above to polyelectrolytes such as redox shuttle polymers, the interactions of charged polymers with proteins must be better understood. Typically, proteins aggregate with charged polymers into coacervates, an interaction that contraindicates self-assembly due to strong attractive interactions. We have previously shown that neutralizing protein charge¹⁵ is important to reducing these interactions, but charge patches can still produce negative effects. Here, we have systematically mutated green fluorescent protein (GFP) to produce a series of proteins with varying patch size, and we have explored interactions with various polyelectrolytes. These experiments indicate that redistribution of charge on the protein surface to produce only small patches can prevent coacervation, providing a viable route for synthesis of bioconjugates with even strongly charged polyelectrolytes.

Beyond the key tasks performed under this proposal, several collaborative groups have taken an interest in this work and sought out collaboration, including the groups of Alan Grodzinsky (MIT) and Luis Catalani (University of São Paulo), who have both used our patchy proteins as molecular probes in biological studies, and Hua Lu (Peking University), who is collaborating with us on studying self-assembly of protein-polymer bioconjugates synthesized in his lab.

Future Plans

During the remaining 15 months of our project, we plan to complete our theory and simulation work on the coarse-grained model and also develop a self-consistent field theory approach that is capable of capturing additional molecular details that are beyond the scope of the simpler model. This will provide a solid theoretical basis for understanding key experimental results. In addition, we will complete inelastic scattering experiments described above to characterize water dynamics, and we will continue a nascent collaboration with Wei-Ren Chen on the application of neutron spin echo to understand dynamics in proteins and protein-based materials. Finally, we will complete the synthesis and testing of a protein-polymer conjugate demonstrating electron transport, illustrating that the methods demonstrated herein are also capable of being applied to challenges in bioelectrocatalysis.

References

1. Hambourger, M.; Gervaldo, M.; Svedruzic, D.; King, P. W.; Gust, D.; Ghirardi, M.; Moore, A. L.; Moore, T. A., [FeFe]-Hydrogenase-Catalyzed H₂ production in a photoelectrochemical biofuel cell. *Journal of the American Chemical Society* **2008**, *130* (6), 2015-2022.
2. Krassen, H.; Schwarze, A.; Friedrich, B.; Ataka, K.; Lenz, O.; Heberle, J., Photosynthetic Hydrogen Production by a Hybrid Complex of Photosystem I and [NiFe]-Hydrogenase. *Acs Nano* **2009**, *3* (12), 4055-4061.
3. Reda, T.; Plugge, C. M.; Abram, N. J.; Hirst, J., Reversible interconversion of carbon dioxide and formate by an electroactive enzyme. *Proceedings of the National Academy of Sciences of the United States of America* **2008**, *105* (31), 10654-10658.
4. Parkinson, B. A.; Weaver, P. F., PHOTOELECTROCHEMICAL PUMPING OF ENZYMATIC CO₂ REDUCTION. *Nature* **1984**, *309* (5964), 148-149.
5. Iso, M.; Chen, B. X.; Eguchi, M.; Kudo, T.; Shrestha, S., Production of biodiesel fuel from triglycerides and alcohol using immobilized lipase. *Journal of Molecular Catalysis B-Enzymatic* **2001**, *16* (1), 53-58.
6. Velonia, K.; Rowan, A. E.; Nolte, R. J. M., Lipase polystyrene giant amphiphiles. *Journal of the American Chemical Society* **2002**, *124* (16), 4224-4225.
7. Benson, E. E.; Kubiak, C. P.; Sathrum, A. J.; Smieja, J. M., Electrocatalytic and homogeneous approaches to conversion of CO₂ to liquid fuels. *Chemical Society Reviews* **2009**, *38* (1), 89-99.
8. Mikkelsen, M.; Jorgensen, M.; Krebs, F. C., The teraton challenge. A review of fixation and transformation of carbon dioxide. *Energy & Environmental Science* **3** (1), 43-81.
9. Yang, X.; Loos, J., Toward high-performance polymer solar cells: The importance of morphology control. *Macromolecules* **2007**, *40* (5), 1353-1362.
10. Boudouris, B. W.; Frisbie, C. D.; Hillmyer, M. A., Nanoporous poly(3-alkylthiophene) thin films generated from block copolymer templates. *Macromolecules* **2008**, *41* (1), 67-75.
11. Thomas, C. S.; Glassman, M. J.; Olsen, B. D., Solid-State Nanostructured Materials from Self-Assembly of a Globular Protein-Polymer Diblock Copolymer. *Acs Nano* **2011**, *5* (7), 5697-5707.
12. Lam, C. N.; Olsen, B. D., Phase transitions in concentrated solution self-assembly of globular protein-polymer block copolymers. *Soft Matter* **2013**, *9* (8), 2393-2402.
13. Lam, C. N.; Kim, M.; Thomas, C. S.; Chang, D.; Sanoja, G. E.; Okwara, C. U.; Olsen, B. D., The Nature of Protein Interactions Governing Globular Protein-Polymer Block Copolymer Self-Assembly. *Biomacromolecules* **2014**, *15* (4), 1248-1258.
14. Lam, C. N.; Yao, H.; Olsen, B. D., The Effect of Protein Electrostatic Interactions on Globular Protein-Polymer Block Copolymer Self-Assembly. *Biomacromolecules* **2016**, *17* (9), 2820-2829.
15. Obermeyer, A. C.; Mills, C. E.; Dong, X. H.; Flores, R. J.; Olsen, B. D., Complex coacervation of supercharged proteins with polyelectrolytes. *Soft Matter* **2016**, *12* (15), 3570-3581.

Publications Resulting from Work Supported by DOE-BES Neutron Program Since 2016 Review

1. “Self-Assembly of Differently Shaped Protein-Polymer Conjugates Through Modification of the Bioconjugation Site.” A. Huang and B.D. Olsen. *Macromolecular Rapid Communications* **2016**, *15*, 1268-1274.
2. “The Effect of Protein Electrostatic Interactions on Globular Protein-Polymer Block Copolymer Self-Assembly.” C.N. Lam, H. Yao, and B.D. Olsen. *Biomacromolecules* **2016**, *17*, 2820-2829.
3. “Design of Globular-Coil Protein Fusions for Block Copolymer Self-Assembly.” G. Qin, P. Perez, C.E. Mills, and B.D. Olsen. *Biomacromolecules* **2016**, *17*, 928-934.
4. “Elastin-like polypeptide (ELP) charge influences self-assembly of ELP-mCherry fusion proteins.” C.E. Mills, Z. Michaud, and B.D. Olsen. *Biomacromolecules* **2018**, *19*, 2517-2525.
5. “Green Fluorescent Proteins Engineered for Cartilage-Targeted Drug Delivery: Insights for Transport Into Highly Charged Avascular Tissues.” Y. Krishnan, H.A. Rees, C.P. Rossitto, S. Kim, H.K. Hung, E.H. Frank, B.D. Olsen, D.R. Liu, P.T. Hammond, and A.J. Grodzinsky. *Biomaterials* **2018**, *183*, 218-233.
6. “Topology Effects on Protein-Polymer Block Copolymer Self-Assembly.” T. Suguri and B.D. Olsen. *Polymer Chemistry* **2019**, *10*, 1751-1761.
7. Huang, Aaron; Yao, Helen; Olsen, Bradley D. SANS Partial Structure Factor Analysis for Determining Protein-Polymer Interactions in Semidilute Solution. *In revision* 2019.
8. A. Huang, J.M. Paloni, A. Wang, A.C. Obermeyer, H.V. Sureka, H. Yao, and B.D. Olsen. Predicting Protein-Polymer Block Copolymer Self-Assembly from Protein Properties. *Submitted*.
9. “Predicting Self-Assembly of Globular Protein-Polymer Bioconjugates.” A. Huang. Doctoral Thesis, **2018**.

Discovering Toroidal Materials with Spherical Neutron Polarimetry

Efrain E. Rodriguez, Associate Professor

Department of Chemistry and Biochemistry, University of Maryland, College Park 20742

Program Scope

We describe our work to elucidate the nature of the toroidal moment in crystalline solids through neutron scattering studies. Much less understood than the magnetic and electric dipole moments, the toroidal moment has unique characteristics with respect to its symmetry^{1–4} and physical properties (Fig 1). We define a toroidal moment in a crystalline solid as a moment that develops from the arrangement of spin moments on a vortex ring. We use the term toroidal materials to encompass any system where the toroidal moments may be found in an ordered state below a transition temperature. Space inversion and time reversal symmetries can flip the direction of the toroidal moment, which gives toroidal materials their unique response to external electric (**E**) and magnetic (**M**) fields. Our research focuses on the synthesis and solid state chemistry of materials with long-range ordering of these toroidal moments.

We seek to establish the relationship between crystallography and magnetism in toroidal moments using neutron scattering. Due to the neutron's spin, neutron scattering readily probes the internal magnetic order in a material. While neutron diffraction, both powder and single crystal, are highly important in uncovering toroidal order, more advanced neutron techniques are required to carry out this work. In short, we use spherical neutron polarimetry (SNP) to understand the toroidization in a material. SNP is a tool by which the polarization of the neutron beam can be prepared in any direction and the full polarization of the scattered beam recovered.^{5–6} As such, it is a powerful tool that unambiguously describes complex magnetic ordering such helical, conical, or cycloidal order, chiral systems, and spin density waves. Since it can also detect antiferromagnetic domains, it is particularly suitable for exploring toroidal materials.

A related goal in this program is to develop SNP techniques and instrumentation in North American neutron sources. While the U.S. has several efforts in polarized neutron scattering, SNP has been less pursued than our peer institutions in Europe such as the Institut Laue-Langevin (ILL). Our goal has been to develop SNP apparatus for both small-angle and wide-angle scattering geometries.

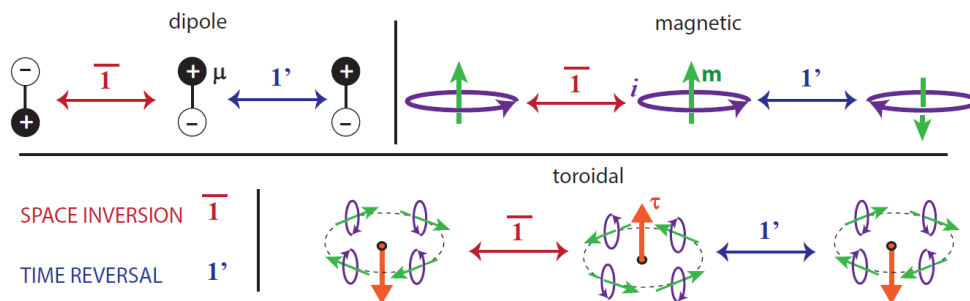


Figure 1. The behavior of an electric dipole moment, magnetic moment, and toroidal moment with respect to certain symmetry elements. While space inversion symmetry ($\vec{1}$) flips the sign of an electric dipole, it does not have the same effect for a magnetic moment. Conversely, the time reversal symmetry operation $1'$ flips a magnetic moment but has no effect on the dipole moment. The toroidal moment is unique in that it is not invariant under both operations.

Recent Progress

We present our results on the metal orthophosphates known as triphylites with the formula LiMPO_4 for $M = \text{Mn, Fe, Co, and Ni}$. These triphylites crystallize in the olivine-type structure (Fig. 2) and are some of the leading candidates for ferrotoroidicity, whereby the toroidal moments order in a ferroic manner. We have prepared both powders and single crystals of these triphylites and their solid solutions through hydrothermal synthesis and salt flux crystal growth. We find through powder neutron diffraction (POWGEN, SNS and

BT-1, NIST) the effects on magnetic order and moment size from preparing the mixed-metal solutions $\text{LiM}_{1-x}\text{M}'_x\text{PO}_4$. Through SNP measurements using the CRYOPAD apparatus at the ILL, we find that the toroidal moment direction of LiFePO_4 can be controlled through the application of a crossed $\mathbf{E} \times \mathbf{H}$ field (Fig. 2). Our research plan includes the continuation of our studies of LiMPO_4 and its de-lithiated MPO_4 phases, which can increase the transition temperature by as much as 75 K.

We describe the design, construction, and testing of our first prototype of an SNP apparatus at the NIST Center for Neutron Research (NCNR). We call this new apparatus the Small Angle Neutron Polarimetry Apparatus or SANPA. SANPA does not include moving parts or require cryogenics and is optimized for small angle scattering geometries. Its simple design establishes a zero-field chamber around the sample from superconducting niobium. The precession coils that control the beam's polarization are also housed in the Meissner shield. We describe the software and hardware associated with SANPA and the preliminary testing on the PHADES beamline at the NCNR.

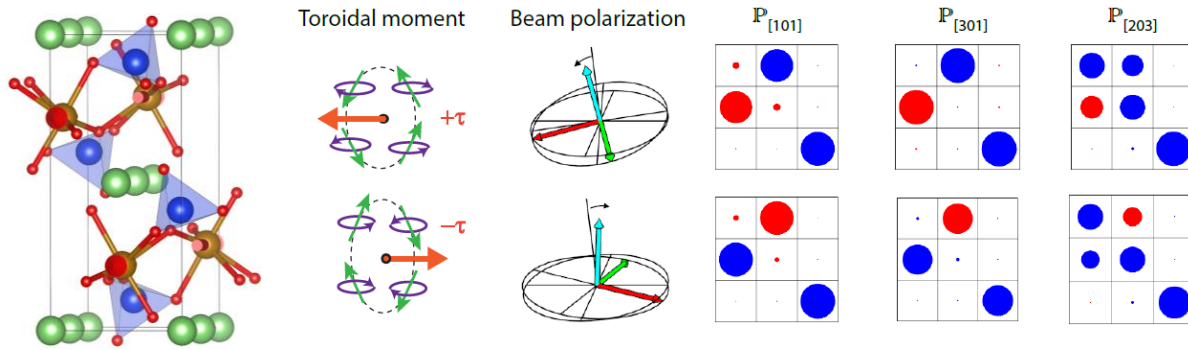


Figure 2. Crystal structure of LiFePO_4 and its magnetic moments leading to a toroidal moment which can rotate the neutron beam polarization. Depending on whether the toroidal moment points one of two directions, the off-diagonal terms of the polarization matrix changes sign for three Bragg reflections, (101), (301), and (203). The polarization measurements were carried out at ILL with CRYOPAD. The red and blue circles indicate opposite polarization, and the size of the circle scales with amount of polarization from 0 to 100 %. The 9 entries represent the 3×3 entries in the polarization matrix.

Future Work

Our proposed plan is to continue to understand the mixed-metal triphylites $\text{LiM}_{1-x}\text{M}'_x\text{PO}_4$ and their de-lithiated analogues also includes the synthesis of new systems that have similar chemistry and symmetry to the triphylites. These include the thiophosphates and silicates such as $\text{Li}_2\text{FeP}_2\text{S}_6$, KNiPS_4 , and LiFeSiO_4 . As in the triphylites, we can also manipulate the magnetic order and transition temperature through de-lithiation.

We propose to keep testing SANPA on the PHADES beamline and then utilize it to carry out small angle neutron scattering studies on appropriate materials systems. This new SANPA could be highly useful in measuring non-collinear antiferromagnets with long-range structures such as skyrmion lattices. Furthermore, some of these skyrmion systems support either helical or cycloidal antiferromagnetism with long pitches for the modulated structures, which are ideal for SANS measurements. SANPA could reveal with unprecedented detail the helicity and spin texture of these materials. Due to its compactness and small footprint, SANPA could be transported between NIST and HFIR for testing at both reactor sources.

Building on our previous development of SANPA, we plan to design and construct a new wide angle SNP apparatus. We call this new device the Wide Angle Apparatus for Spherical Polarimetry or WAASP (Fig. 3). The design of WAASP is similar to that of CRYOPAD but with one key difference: WAASP will use a

cooling system that avoids the use of an expensive and non-renewable resource—liquid helium. In WAASP, the superconducting Meissner shield is much like that in SANPA; it is cooled by a closed cycle refrigerator. For the incident beam, WAASP will use a square precession coil much like that in SANPA. For the scattered beam, a toroidal-shaped precession coil is used that covers 120° in scattering angle. We provide details of the team and timeline for the completion of WAASP and other research activities.

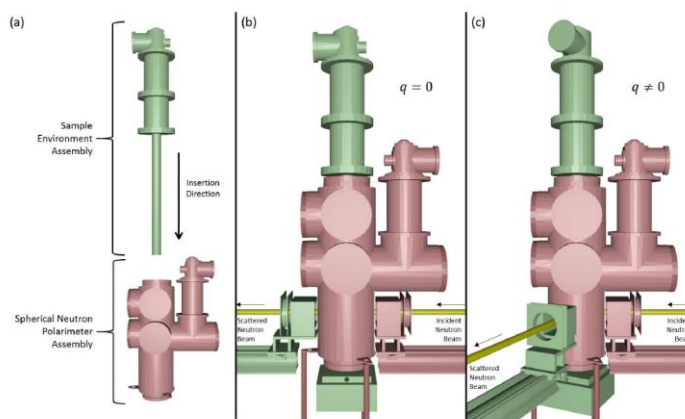


Figure 3. Technical drawings of WAASP. This apparatus will be a cryogen-free way to perform spherical neutron polarimetry on wide angle instruments.

References

1. A. A. Gorbatsevich and Y. V. Kopaev, "Toroidal order in crystals," *Ferroelectrics*, vol. 161, pp. 321–334, 1994.
2. N. A. Spaldin, M. Fiebig, and M. Mostovoy, "The toroidal moment in condensed-matter physics and its relation to the magnetoelectric effect," *Journal of Physics: Condensed Matter*, vol. 20, p. 434203, 2008.
3. B. B. Van Aken, J.-P. Rivera, H. Schmid, and M. Fiebig, "Observation of ferrotoroidic domains," *Nature*, vol. 449, no. 7163, pp. 702–705, 2007.
4. M. Fiebig, "Crystallography: Let's do the twist," *Nature of Materials*, vol. 10, pp. 339–340, 2011.
5. F. Tasset, P. Brown, E. Lelievre-Berna, T. Roberts, S. Pujol, J. Allibon, and E. Bourgeat-Lami, "Spherical neutron polarimetry with Cryopad-II," *Physica B: Condensed Matter*, vol. 267–268, pp. 69–74, 1999.
6. L. Regnault, B. Geray, P. Fouilloux, B. Longuet, F. Mantegazza, F. Tasset, E. Lelievre-Berna, S. Pujol, E. Bourgeat-Lami, N. Kernavanois, M. Thomas, and Y. Gibert, "Spherical neutron polarization analysis on the three-axis spectrometer IN22," *Physica B: Condensed Matter*, vol. 350, no. 1–3, Supplement, pp. E811–E814, 2004. Proceedings of the Third European Conference on Neutron Scattering.

Publications

1. S. Gnewuch and E. E. Rodriguez, "The fourth ferroic order: Current status on ferrotoroidic materials," *Journal of Solid State Chemistry*, vol. 271, pp. 175–190, 2019.
2. J. Tosado, W. C. Chen, S. Gnewuch, T. Hasaan, T. Dax, and E. E. Rodriguez, "Small-Angle Neutron Polarimetry Apparatus (SANPA): Development at the NIST Center for Neutron Research," *Review of Scientific Instruments*, 2019, in press.
3. J. Tosado, W. C. Chen, and E. E. Rodriguez, "A strategy for handling aberration in Spherical Neutron Polarimetry," *IOP Conference Series, Proceedings of the 2018 Polarised Neutrons in Condensed Matter Investigations*, 2019, in press.

Neutron and x-ray scattering studies of complex phenomena in bulk materials and heterostructures of strongly correlated systems

S. Rosenkranz, O. Chmaissem*, R. Osborn, D. Phelan, S.G.E. te Velthuis
Argonne National Laboratory; *and Northern Illinois University

Program Scope

The assumption of a long-range-ordered crystalline lattice has provided a very successful foundation for describing a diverse range of properties of condensed matter for over a century. Many phenomena of recent interest are, however, associated with the presence of complex disorder and short-range correlations that emerge as a consequence of competing, coexisting, or intertwined order, and are poorly described within the old paradigm. Such heterogeneities on the nano- to mesoscale are now recognized as key drivers for advanced functionality, with materials that possess short-range correlations and disorder generally exhibiting strongly enhanced responses to external stimuli such as magnetic or electric fields. This program utilizes, and develops when necessary to advance the scientific program, the latest advances in neutron and synchrotron x-ray instrumentation to study complex disorder and short-range correlations in bulk and heterostructures of strongly correlated systems on a range of length and time scales. Our goal is to utilize efficient techniques that we have been developing to characterize nanoscale fluctuations in the competing order, both static and dynamic, in order to make a major impact on our progress towards understanding how complex disorder affects material functionality of interest including superconductivity, magnetism, thermoelectricity, ionic conduction, *etc.* This program is focused on studies of electronic and ionic disorder to address the following topics: i) determine the nature, origin, and influence of spin and charge correlations in bulk compounds ii) study the effects of short-range modifications to spin and charge order induced at interfaces in heterostructures of complex oxides iii) explore the consequences of atomic disorder and ionic correlations on materials properties. These investigations are enhanced by our developments of novel methods to study short-range correlations and disorder utilizing neutron and synchrotron x-ray scattering.

Recent Progress

By combining inelastic neutron scattering data from CePd₃ over large volumes of four-dimensional energy and momentum transfers with DMFT calculations, we obtain very good agreement on an *absolute* intensity scale without any adjustable parameters (Fig. 1),

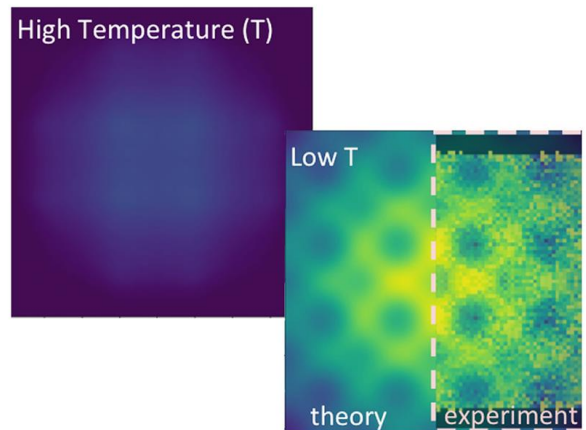


Fig. 1: Experimentally observed neutron scattering and ab-initio calculation of the generalized susceptibility in the coherent state of CePd₃ (bottom right) The quantitative excellent agreement validates a decades old prediction of the crossover to random electronic excitations observed at high temperature (left).

thereby providing a quantitative comparison of intra-band scattering in a system without collective excitations. These results provide the validation of the long-postulated crossover from coherent to incoherent electronic excitations with increasing temperature, and show that inelastic neutron scattering can be utilized as an alternative bulk spectroscopic probe of quasiparticle coherence. Such crossovers are fundamental to many physical phenomena in strongly correlated systems and are now comprehensively understood by combining the latest advances in experiment and theory.

In the hole-doped iron arsenide superconductors, we have determined the prevalence and relation to superconductivity of the new tetragonal, magnetic C_4 phase, which we discovered and showed to be a rare double Q -magnetic structure with non-uniform magnetization. Using neutron and synchrotron x-ray pair distribution (PDF) measurements, we showed that strong local nematic correlations persist even within this long-range ordered, tetragonal magnetic C_4 phase, and indeed over a wide range of the phase diagram of hole-doped iron arsenide superconductors.

In order to investigate the origin of superconductivity and its relation to charge density wave (CDW) correlations, we studied the evolution of the soft mode with inelastic x-ray scattering in Cu_xTiSe_2 upon suppressing CDW order with pressure and doping and found evidence for the presence and hybridization of phonon and exciton modes. These observations indicate that under pressure, TiSe_2 is proximal to the elusive excitonic superconducting state. We further found that superconductivity only sets in when the CDW order becomes incommensurate, providing evidence that although perfect, commensurate CDW order is detrimental to superconductivity, CDW incommensuration and domain wall formation may facilitate it.

We further investigated the origin of charge and spin correlations in trilayer nickelates. Previous synchrotron x-ray diffraction measurements provided evidence for the presence of charge stripes, providing a novel, Cu-free route to investigate the stripe physics surrounding the closely related cuprate superconductors. By utilizing single crystal neutron diffraction, both polarized and unpolarized, we establish that the ground-state is indeed magnetic, in the form of antiferromagnetic spin stripes that are commensurate with the charge stripes. However, in contrast to other oxides, including cuprates, the charge and spin stripe order appear simultaneously, suggesting a stronger coupling between the spin and charge correlations in the trilayer nickelates than in the more two-dimensional cuprates.

Utilizing the single crystal diffuse scattering instrument *Corelli*, we investigated the spin correlations in Fe_2TiO_5 , a poorly understood spin glass whose bulk properties shows purely Ising-type freezing despite being solely comprised of isotropic Heisenberg spins. Our detailed analysis of the magnetic diffuse scattering reveals the emergence of surfboard-shaped regions of spins that are aligned antiferromagnetically perpendicular to the Ising axis, indicating that the transverse fluctuations of the surfboard-regions are the quasi-spin degrees of freedom that freeze. This represents a new mechanism for generating spin anisotropy and thus, the Ising anisotropy in this compound is an interaction-driven, emergent property.

We started to investigate how competing and coexisting magnetic and ferroelectric order affect physical properties in bulk compounds and heterostructures. We have synthesized bulk,

polycrystalline $\text{Sr}_{1-x}\text{Ba}_x\text{Mn}_{1-y}\text{Ti}_y\text{O}_3$ compounds that exhibit a large coupling between the magnetic and ferroelectric order parameters with a wide tunability of this coupling with compositional changes. In heterostructures of the corresponding parent materials, composed as trilayers of ferromagnetic $\text{La}_{0.7}\text{Sr}_{0.3}\text{MnO}_3$ (LSMO)/ferroelectric BaTiO_3 /LSMO grown on SrTiO_3 substrates, we show that spin reconstruction at the interfaces of this multiferroic tunnel junction results in a spin filtering functionality, which significantly modulates the tunneling magnetoresistance by two orders of magnitude by reversing the ferroelectric polarization. Our identification of a net Ti moment with XMCD and magnetic depth profile determination with polarized neutron reflectivity measurements contributed to explaining the transport behavior. In superlattices of the ferromagnetic LSMO and the correlated metal LaNiO_3 , we discovered an unusual noncollinear magnetic structure that results from the coupling of the LSMO layers to a helical spin state within LaNiO_3 , which results from the interaction between a spatially varying spin susceptibility within the LaNiO_3 layer and an interfacial charge transfer that creates localized Ni^{2+} states. These observations suggest a new approach to engineering noncollinear spin textures in metallic oxide heterostructures.

In order to explore phenomena, such as skyrmions, expected to emerge at interfaces between complex oxide ferromagnets and materials with strong spin-orbit coupling, we investigated bilayers of LSMO/ SrIrO_3 (SIO) with polarized neutron reflectivity and soft and hard x-ray XMCD measurements. These investigations revealed significant changes in the magnetic anisotropy depending on the stacking sequence: in bilayers with LSMO grown on the substrate, the LSMO magnetization is very similar to that of a single LSMO layer with a low coercivity. However, if SIO is deposited first, LSMO exhibits a significantly higher anisotropy and SIO exhibits a magnetic Ir moment that is oriented antiparallel to the Mn moment and follows a linear decrease with temperature. Our analysis of the polarized neutron reflectivity data further revealed an LSMO-like interfacial layer with a magnetization parallel to the main LSMO layer, but which also exhibits a linear temperature dependence.

In order to explore the consequences of atomic disorder, we have developed advanced techniques for measuring and analyzing single crystal diffuse scattering and applied it to study the origin of relaxor behavior, as discussed in a separate abstract. These developments also enabled us to determine the presence of an antiferromagnetic defect structure embedded in single crystals of $\text{LaNiO}_{3-\delta}$ and conclude that pure LaNiO_3 is indeed non-magnetic, and lead to the discovery of an unusual charge density wave in novel polymorphs of $\text{Sm}_2\text{Ru}_3\text{Ge}_5$. These developments will also be utilized in our future plans to study short-range spin and charge correlations (as well as ionic correlations, discussed elsewhere), and to provide novel, unique insight into many phenomena driven by competing and coexisting order.

Future Plans

Following our finding that the magnetic C_4 phase is universally observed in hole doped 122 systems, we plan detailed high-resolution powder diffraction investigations of the series of compounds $(\text{Ba}_{1-x-y}\text{Sr}_x\text{Na}_y)\text{Fe}_2\text{As}_2$ and $(\text{Ca}_{1-x-y}\text{Sr}_x\text{Na}_y)\text{Fe}_2\text{As}_2$, in order to determine the structural

parameters that stabilize the C_4 phase. We further plan to determine whether the C_4 state occurs in other families of iron-based superconductors, in particular the ‘1111’ compounds, whose structural and magnetic phase diagrams have not yet been investigated in detail. We are also planning single crystal diffuse scattering measurements to investigate in detail the morphology of the nematic correlations previously observed with Powder PDF, and to search for charge ordering signatures associated with the C_4 phase.

In order to obtain a better understanding of the influence of stripe phases on physical properties, we will continue our investigations using various neutron and synchrotron x-ray scattering techniques to investigate the novel trilayer nickelates $R_4\text{Ni}_3\text{O}_8$ and $R_4\text{Ni}_3\text{O}_{10}$ ($R=\text{La,Pr}$). The influence of disorder and short-range CDW correlations will be further investigated by detailed single crystal diffuse as well as inelastic measurements of the CDW correlations in Pd_xErTe_3 , which is a promising pseudo-tetragonal model system to study the interrelation of charge order, superconductivity, and other ground states, in the presence of quenched disorder. Another CDW system of interest is TaSe_2 , which first exhibits incommensurate order upon cooling but locks into a commensurate CDW at low temperature. While previous neutron scattering investigations reported unusual behavior with incomplete softening and possibly a central peak, the behavior of this system and how it compares to other strong-coupling compounds remains unclear.

We plan to further investigate the novel interfacial phenomena and modified magnetic properties that are expected to emerge in heterostructures in which ferromagnetic manganites or ruthenates are exposed to oxides with strong spin orbit coupling, such as SrIrO_3 . New ground states are expected to arise as a result of the interplay between the double or super exchange interaction in the manganite and symmetry breaking and/or spin orbit interactions in the iridate. We will probe changes in anisotropy and interfacial magnetism and look for chiral magnetic states.

We are in the process of synthesizing single crystals of multiferroic $\text{Sr}_{1-x}\text{Ba}_x\text{Mn}_{1-y}\text{Ti}_y\text{O}_3$ and will investigate the structural and magnetic order, correlations, and excitations using a variety of neutron scattering techniques. We will utilize our most recent developments in single crystal diffuse scattering methods to investigate the influence of short-range correlations that may be induced by the presence of the competing magnetic and ferroic states in these compounds. We will also investigate the role of oxygen vacancies in the multiferroic tunnel junctions. Transport experiments indicate resistance changes that could be tied to voltage-induced motion of oxygen vacancies. We will study the role of these oxygen vacancies in a controlled manner following an interface engineering approach, by inserting an ultrathin layer of $\text{La}_{0.84}\text{Sr}_{0.16}\text{CuO}_{3-\delta}$ as oxygen vacancy source at one of the $\text{BaTiO}_3/\text{LSMO}$ interfaces.

Publications

1. P.G. LaBarre, D. Phelan, Y. Xin, F. Ye, T. Besara, T. Siegrist, S. Rosenkranz, A.P. Ramirez, Emergent Quasi-Spin Anisotropy in Highly Frustrated Pseudobrookite Fe_2TiO_5 , *Phys. Rev. Lett.* submitted (2019).
2. M.J. Krogstad, S. Rosenkranz, J.M. Wozniak, G. Jennings, J.P.C. Ruff, J.T. Vaughey, R. Osborn, Reciprocal Space Imaging of Ionic Correlations in Intercalation Compounds, *Nature Materials* under review (2019).
3. K. Chapagain, D.E. Brown, S. Kolesnki, S. Lapidus, B. Haberl, J. Molaison, C. Lin, C. Kenney-Benson, C. Park, W. Markiewicz, B. Andrezejewski, J.W. Lynn, S. Rosenkranz, B. Dabrowski, O. Chmaissem, Tunable Multiferroic Order Parameters in $\text{Sr}_{1-x}\text{Ba}_x\text{Mn}_{1-y}\text{Ti}_y\text{O}_3$, *Phys. Rev. Materials* submitted (2019)
4. J.A.W. Straquadine, F. Weber, S. Rosenkranz, A.H. Said, I.R. Fisher, Suppression of charge density wave order by disorder in Pd-intercalated ErTe_3 , *Phys. Rev. B*, in press (2019).
5. J. Zhang, D.M. Pajerowski, A.S. Botana, L. Harriger, J. Rodriguez-Rivera, J.P.C. Ruff, N.J. Schreiber, B. Wang, Yu-Sheng Chen, M.R. Norman, S. Rosenkranz, J.F. Mitchell, D. Phelan, Spin-stripe order in a square planar trilayer nickelate, *Phys. Rev. Lett.* in press (2019).
6. Wanjun Jiang, Sheng Zhang, Xiao Wang, Chardutta Phatak, Qiang Wang, Wei Zhang, M.B. Jungfleisch, J.E. Pearson, Yizhou Liu, Jiadong Zang, Xuemei Cheng, Amanda Petford-Long, A. Hoffmann, S.G.E te Velthuis, Quantifying chiral exchange interaction for Néel-type skyrmions via Lorentz transmission electron microscopy, *Phys. Rev. B* **99**, 104402 (2019).
7. J. Tornos, F. Gallego, S. Valencia, Y. H. Liu, V. Rouco, V. Lauter, R. Abrudan, C. Luo, H. Ryll, Q. Wang, D. Hernandez-Martin, G. Orfila, M. Cabero, F. Cuellar, D. Arias, F. J. Mompean, M. Garcia-Hernandez, F. Radu, T. R. Charlton, A. Rivera-Calzada, Z. Sefrioui, S. G. E. te Velthuis, C. Leon, and J. Santamaria, Ferroelectric control of interface spin filtering in multiferroic tunnel junctions, *Phys. Rev. Lett.* **122**, 037601 (2019).
8. B.A. Frandsen, K.M. Taddei, D.E. Bugaris, R. Stadel, M. Yi, A. Acharya, R. Osborn, S. Rosenkranz, O. Chmaissem, R.J. Birgeneau, Widespread orthorhombic fluctuations in the $(\text{Sr},\text{Na})\text{Fe}_2\text{As}_2$ family of superconductors, *Phys. Rev. B* **98**, 180505 (R) (2018).
9. M. Maschek, D.A. Zocco, S. Rosenkranz, R. Heid, A.H. Said, A. Alatas, P. Walmsley, I.R. Fisher, F. Weber, Competing soft phonon modes at charge-density-wave transition in DyTe_3 , *Phys. Rev. B* **98**, 094304 (2018).
10. E. McCalla, D. Phelan, M.J. Krogstad, B. Dabrowski, C. Leighton, Electrical transport, magnetic, and thermodynamic properties of La-, Pr-, and Nd-doped $\text{BaSnO}_{3-\delta}$ single crystals, *Phys. Rev. Materials* **2**, 084601 (2018).
11. M.J. Krogstad, P.M. Gehring, S. Rosenkranz, R. Osborn, Feng Ye, Yaohua Liu, J.P.C. Ruff, W. Chen, J.M. Wozniak, H. Luo, O. Chmaissem, Z.-G. Ye, and Daniel Phelan, The Relation of Local Order to Material Properties in Relaxor Ferroelectrics, *Nature Materials* **17**, 718 – 724 (2018).
12. V. Soldatov, W. Jiang, S.G.E. te Velthuis, A. Hoffmann, R. Schäfer, Size analysis of sub-resolution objects in Kerr microscopy, *Appl. Phys. Lett.* **112**, 262404 (2018).
13. B. Wang, S. Rosenkranz, X. Rui, J. Zhang, F. Ye, R.F. Klie, J.F. Mitchell, D. Phelan, Antiferromagnetic defect structure in $\text{LaNiO}_{3-\delta}$ single crystals, *Phys. Rev. Materials* **2**, 064404 (2018).
14. D. Phelan, F. Han, A. Lopez-Bezanilla, M.J. Krogstad, Y. Gim, Y. Rong, J. Zhang, D. Parshall, H. Zheng, S. L. Cooper, M. Feygenson, Wenge Yang, Yu-Sheng Chen, Structural Properties of Barium Stannate, *J. Solid State Chem.* **262**, 142-148 (2018).

15. H. Somaily, S. Kolesnik, J. Mais, D. Brown, K. Chapagain, B. Dabrowski, O. Chmaissem, Strain-induced tetragonal distortions and multiferroic properties in polycrystalline $\text{Sr}_{1-x}\text{Ba}_x\text{MnO}_3$ ($x = 0.43 - 0.45$) perovskites, *Phys. Rev. Materials* **2**, 054408 (2018).
16. Feng Ye, Yaohua Liu, Ross Whitfield Ray Osborn, Stephan Rosenkranz, Implementation of cross correlation for energy discrimination on the time-of-flight spectrometer CORELLI, *J. Appl. Cryst.* **51**, 315-322 (2018).
17. E.A. Goremychkin, Hyowon Park, R. Osborn, S. Rosenkranz, J.-P. Castellan, V.R. Fanelli, A.D. Christianson, M.B. Stone, E.D. Bauer, K.J. McClellan, D.D. Byler, J.M. Lawrence, Coherent band excitations in CePd_3 : A comparison of neutron scattering and ab-initio theory, *Science* **359**, 186 - 191 (2018).
18. Y. Rong, H. Zheng, M.J. Krogstad, J.F. Mitchell, D. Phelan, Single Crystal growth of 67% BiFeO_3 -33% BaTiO_3 solution by the floating zone method, *J. Crystal Growth* **481**, 23-28 (2018).
19. B.A. Frandsen, K.M. Taddei, M. Yi, A. Frano, Zurab Guguchia, Rong Yu, Qimiao Si, D.E. Bugaris, R. Stadel, R. Osborn, S. Rosenkranz, O. Chmaissem, R.J. Birgeneau, Local orthorhombicity in the magnetic C_4 phase of the hole-doped iron-arsenide superconductor $\text{Sr}_{1-x}\text{Na}_x\text{Fe}_2\text{As}_2$, *Phys. Rev. Lett.* **119**, 187001 (2017).
20. Wanjun Jiang, Gong Chen, Kai Liu Jiadong Zang, Suzanne G. E. te Velthuis, Axel Hoffmann, Skymions in Magnetic Multilayers, *Physics Reports* **704**, 1-49, (2017)
21. J. Zhao, C.D. Malliakas, K. Wijayarathne, V. Karlapati, N. Appathurai, D.Y. Chung, S. Rosenkranz, M.G. Kanatzidis, U. Chatterjee, Spectroscopic evidence for temperature-dependent convergence of light- and heavy-hole valence bands of PbQ ($\text{Q}=\text{Te, Se, S}$), *Europhys. Lett.* **117**, 27006 (2017).
22. D.E. Bugaris, C.D. Malliakas, Fei Han, N.P. Calta, M. Sturza, M.J. Krogstad, R. Osborn, S. Rosenkranz, J.P.C. Ruff, G. Trimarchi, S.L. Bud'ko, M. Balasubramanian, D.Y. Chung, M.G. Kanatzidis, Charge Density Wave in the Novel Polymorphs of $\text{RE}_2\text{Ru}_3\text{Ge}_5$ ($\text{RE} = \text{Pr, Sm, Dy}$), *J. Am. Chem. Soc.* **139**, 4130 (2017).
23. K.M. Taddei, J.M. Allred, D.E. Bugaris, S.H. Lapidus, M.J. Krogstad, H. Claus, D.Y. Chung, M.G. Kanatzidis, R. Osborn, S. Rosenkranz, O. Chmaissem, Observation of the magnetic C_4 phase in $\text{Ca}_{1-x}\text{Na}_x\text{Fe}_2\text{As}_2$ and its universality in the hole-doped 122 superconductors, *Phys. Rev. B* **95**, 064508 (2017).
24. Wanjun Jiang, Xichao Zhang, Guoqiang Yu, Wei Zhang, Xiao Wang, M. Benjamin Jungfleisch, John E. Pearson, Xuemei Cheng, Olle Heinonen, Kang L. Wang, Yan Zhou, Axel Hoffmann, Suzanne G. E. te Velthuis, Direct Observation of the Skymion Hall Effect, *Nat. Phys.* **13**, 162 (2017).
25. A. Kogar, G.A de la Pena, Sangjun Lee, Y. Fang, S.X.-L. Sun, D.B. Lioi, G. Karapetrov, K.D. Finkelstein, J.P.C. Ruff, P. Abbamonte, S. Rosenkranz, Observation of a Charge Density Wave Incommensuration Near the Superconducting Dome in Cu_xTiSe_2 , *Phys. Rev. Lett.* **118**, 027002 (2017).
26. M. Maschek, S. Rosenkranz, R. Hott, R. Heid, Michael Merz, D.A. Zocco, A.H. Said, A. Alatas, G. Karapetrov, Shan Zhu, J. van Wezel, F. Weber, Superconductivity and hybrid soft modes in TiSe_2 , *Phys. Rev. B* **94**, 214507 (2016).
27. J.D. Hoffman, B.J. Kirby, J. Kwon, G. Fabbris, D. Meyers, J.W. Freeland, I. Martin, O.G. Heinonen, P. Steadman, H. Zhou, C.M. Schlepuetz, M.P.M. Dean, S.G.E te Velthuis, J.-M. Zuo, A. Bhattacharya, Oscillatory non-collinear magnetism induced by interfacial charge transfer in superlattices composed of metallic oxides, *Phys. Rev. X* **6**, 041038 (2016).

DOE BES Grant # DE-SC0014461

Study of Two-Dimensional Magnetic and Antiferromagnetic Lattice: From Fundamental understanding to Novel platform for Spintronics Research

PI- Deepak Kumar Singh; University of Missouri, Columbia

Program Scope

Two-dimensional magnetic nanostructured geometry, such as an artificial magnetic honeycomb lattice, provides facile platform to explore many novel properties of magnetic materials in one system. Originally envisaged to explore the physics of effective magnetic monopoles and magnetic field-induced avalanche of Dirac string, artificial magnetic honeycomb lattice has emerged as a key playground to discover new and exotic magnetic phases, such as the magnetic charge ordered state and the spin solid state, in disorder free environment.[1-3] We have created a new artificial magnetic honeycomb lattice of ultra-small connected element, with the typical length of ~ 12 nm, in this pursuit. Using neutron scattering and complementary measurements on the newly created honeycomb lattice, we have investigated emergent phenomena of short-range quasi-spin ice and long range spin solid order. The main objectives of the current research are (a) to understand the role of magnetic charge correlation in the evolution of emergent magnetic phases, (b) develop qualitative understanding behind the competing energetics between dipolar magnetic interaction and next nearest neighbor exchange interaction in the phase transition to the spin solid ground state, (c) explain the underlying mechanism behind the observation of magnetic diode type rectification in permalloy honeycomb, (d) explore new neutron measurement technique(s), such as neutron spin echo, to elucidate the dynamic properties of magnetic charges. Study of complementary bulk materials, such as the honeycomb lattice structured Na_2RuO_3 or disorder induced novel magnetic phenomena, can act as guide in this pursuit. Complementary study of bulk materials not only add impetus to the ongoing research, but also provides new ideas in understanding an intriguing phenomenon in two dimensional artificial magnetic honeycomb lattice.

Recent Progress

Using detailed experimental investigations on the newly created artificial magnetic honeycomb lattice of 'connected' elements, we have demonstrated two important properties that were not possible before: (1) temperature dependent evolution of novel magnetism, and (2) the dominance of novel spin solid state over the closely followed magnetic charge ordered state as $T \rightarrow 0$ K. It was the first time, the existence of spin solid state was experimentally demonstrated in a 'connected' magnetic honeycomb lattice. [publications 1, 4, 5, 7, 9] The second term in the Hamiltonian (first term is nearest neighbor exchange energy) is key to the fundamental understanding of temperature dependent evolution of this novel phase. Decoding the nature of intermediate magnetic phases is crucial to understand the second term in the Hamiltonian, which is the deciding factor behind the phase transition mechanism to the spin solid order at low

temperature. We have actively pursued this project in the last one year. Analysis of PNR and VSANS data suggests the competing role of next nearest neighbor exchange energy in the system. We have also performed temperature dependent micromagnetic simulations on a similar size artificial honeycomb lattice that strongly complements the experimental results of temperature dependent evolution of magnetic phenomena in this two-dimensional structure. Additionally, two new properties of Wigner crystal type state of magnetic charges and magnetic diode-type rectification are discovered in the newly created artificial honeycomb lattice systems. [publications 6, 11] Synergistic study of neutron-based experimental investigation and the model calculations suggest the dynamic role of magnetic charges on the vertices of the honeycomb lattice via the emission and absorption of net charge defect between the nearest neighbors. While the low integer charges provide conducive pathway for electrical conduction, lattice vertices occupied with high integer charges act as the high energy scattering center for electric charge carriers and impede conduction. Concurrent measurements of the polarized neutron reflectivity and electrical conductivity further reveal the current induced near surface tuning of magnetization in honeycomb lattice, thereby making it a topological effect with fractional change in the magnetic charge density. To fully understand the dynamic properties of magnetic charges, neutron spin echo measurements on a large stack of 2D honeycomb lattice is underway. The preliminary results, from the NSE measurements on a stack of 40 samples at SNS-ORNL, suggest sub-nano seconds relaxation time of magnetic charges, which is comparable to the relaxation time of electric charge carriers and the diffusion length in a metallic system. The new study is expected to elucidate the intrinsic nature of static and dynamic properties of magnetic charges in two-dimensional geometrically frustrated magnetic system in general, with strong implication to the design of the next generation spintronics devices.

Future Plans

In the near future, we plan to perform several new experiments and develop new analysis methods to achieve the stated objectives. One of the objectives is to understand the dynamic properties of magnetic charges in artificial two-dimensional frustrated magnetic lattice. Neutron spin echo is a powerful probe to reveal the relaxation time of magnetic charge dynamics. For this purpose, we are creating a stack of 120 samples to perform detailed neutron spin echo measurements at SNS, ORNL (a preliminary measurement was previously performed on a stack of 40 samples). We plan to perform NSE measurements at different temperatures and different q values to obtain the temperature dependence of magnetic charge's relaxation time. Analysis of experimental results is expected to provide first evidence of magnetic charge dynamics, which can be compared with the relaxation mechanism of electric charge carriers. We are also performing detailed Hall's measurements to determine the density of magnetic charge carriers. Together, these results will help us consolidate the argument that magnetic charges play "equally" important role in electrical conduction in magnetic materials.

In addition to understanding the dynamic properties of magnetic charges, we plan to perform several experiments to understand the temperature dependent evolution of intermediate phases of

magnetic charges in artificial magnetic honeycomb lattice. More recently, we obtained evidences to the role of magnetism in magnetic diode behavior using concurrent measurements of electrical conductivity and polarized neutron reflectometry. Further research works will elucidate the implication of fractional correction to magnetic charge correlation on the vertices of honeycomb lattice to asymmetric electrical conduction in this system. Full spin polarization analysis of PNR patterns for both forward and backward current biases are important in this regard.

Study of bulk materials complement the main research theme. We have synthesized high quality sample of honeycomb structured Na_2RuO_3 , which is known to manifest strong spin-orbital coupling. We plan to investigate the possible quantum magnetic phenomena at low temperature in this system. We will also explore the resemblances in the local magnetic configurations between the artificial spin ice and Na_2RuO_3 compound in the coming months.

References

- [1] C. Nisoli, R. Moessner and P. Schiffer, Colloquium: Artificial spin ice: Designing and imaging magnetic frustration, *Rev. Mod. Phys.* **85**, 1473 (2013)
- [2] E. Mengotti, L. J. Heyderman, A. F. Rodriguez, F. Nolting, R.V. Hugli, and H.-B. Braun, Real space observation of emergent magnetic monopoles and associated Dirac strings in artificial Kagome spin ice, *Nature Phys.* **7**, 68 (2011)
- [3] O. Sendetskyi, L. Anghinolfi, V. Scagnolli, G. Moller, N. Leo, A. Alberca, J. Kohlbrecher, J. Lüning, U. Staub, and L. Heyderman, Magnetic diffuse scattering in artificial Kagome spin ice, *Phys. Rev. B* **93**, 224413 (2016)

Publications resulting from work supported by DOE-BES grant in last two years

- [1] B. Summers, Y. Chen, A. Dahal and D. K. Singh, New description of magnetic phase transition in artificial honeycomb lattice of connected elements, *Sci. Rep.* **7**, 16080 (2017).
- [2] A. Dahal, J. Gunasekera and D. K. Singh, Possible superconductivity in chemically doped $\text{CrSb}_{1\pm\delta}$, *Rapid Research Letter (PSS)* **11**, 1700211 (2017).
- [3] L. Harriger, S. Disseler, J. Gunasekera, J. Rodriguez-Rivera, J. Pixley, P. Manfrinetti, S. K. Dhar and D. K. Singh, Gapped excitation in dense Kondo lattice CePtZn , *Phys. Rev. B (Rapid Communication)* **95**, 041102(R) (2017).
- [4] B. Summers, L. Debeer-Schmitt, A. Dahal, A. Glavic, P. Kampshroeder, J. Gunasekera and D. K. Singh, Temperature Dependent Magnetism in Artificial Honeycomb Lattice of Connected Elements, *Phys. Rev. B* **97**, 014401 (2018)
- [5] A. Glavic, B. Summers, A. Dahal, R. J. Kline, W. Van Herck, A. Sukhov, A. Ernst and D. K. Singh, Spin Solid versus Magnetic Charge Ordered State in Artificial Honeycomb Lattice of Connected Elements, *Advanced Science* **1700856**, 2018; DOI: 10.1002/advs.201700856.
- [6] B. Summers, A. Dahal and D. K. Singh, Magnetic diode behavior at room temperature in two-dimensional honeycomb, *Advanced Electronic Materials* **2018**, 1700500 (DOI:10.1002/aelm.201700500).
- [7] A. Dahal, B. Summers and D. K. Singh, Fractional electrical dimensionality in the spin solid phase of artificial honeycomb lattice, *Appl. Phys. Lett.* **112**, 062407 (2018)

- [8] J. Gunasekera, A. Dahal, J. Rodriguez, L. Harriger, S. Thomas, T. Heitmann, V. Dugaev, A. Ernst and D. K. Singh, Quantum magnetic properties in perovskite with Anderson localized artificial spin-1/2, *Advanced Science* **2018**, 1700978 (DOI: 10.1002/advs.201700978).
- [9] A. Dahal, Y. Chen, B. Summers and D. K. Singh, Scaling of non-linear susceptibilities in artificial permalloy honeycomb lattice, *Phys. Rev. B* **97**, 214420 (2018).
- [10] Y. Chen, A. Dahal, J. Rodriguez, G. Xu, L. Harriger, T. Heitmann, V. Dugaev, A. Ernst, D. J. Singh and D. K. Singh, Quantum continuum fluctuation in glassy perovskite $\text{Ca}(\text{Co}_{0.15}\text{Ru}_{0.85})\text{O}_3$, Under review 2018; Preprint available on cond-mat arXiv-arXiv:1807.05404.
- [11] Y. Chen, B. Summers, A. Dahal, V. Lauter, G. Vignale and D. K. Singh, Field and current control of the electrical conductivity of an artificial two-dimensional honeycomb lattice, *Advanced Materials* **2019**, 201808298 (DOI: 10.1002/adma.201808298)
- [12] A. Dahal, Y. Chen, T. Heitmann, A. Thamizhavel, S. K. Dhar and D. K. Singh, Spin correlation in trigonal EuMn_2As_2 , *Physical Review B* **99**, 085135 (2019).
- [13] G. Yumnam, Y. Zhao, Y. Chen, A. Thamizhavel, S. K. Dhar and D. K. Singh, Microscopic nature of magnetic ground state in CeAuSb_2 , (Under review 2019).

Neutron and X-Ray Studies of Spin and Charge Manipulation in Magnetic Nanostructures

Sunil K Sinha, Dept. of Physics, University of California San Diego and Eric Fullerton, Center for Magnetic Recording Research, University of California San Diego

Program Scope: Our program is focused on the study of competing, frustrated and disordered magnetic systems. In particular, we are interested in (i) the static and dynamic properties of chiral magnetic systems, (ii) spin fluctuations in jammed and frustrated magnetic systems, such as spin glasses, domain walls in antiferromagnets, and slow fluctuations in spin liquids and spin glasses, which can be probed with neutron spin echo techniques and XPCS and (iii) magnetic/superconducting heterostructures. We believe this research could lead us to new understandings of basic physics processes in magnetic and electronic systems using a combination of neutron and x-ray techniques.

Recent Progress:

(a) Critical behavior at the spin-glass phase transition.

We have completed our first studies of the dynamics of the freezing transition of the classical spin glass $\text{Cu}_{0.88}\text{Mn}_{0.12}$ and a MS is about to be submitted for publication. We have used coherent resonant magnetic X-ray scattering to carry out X-ray Photon Correlation Spectroscopy (XPCS) experiments [1] to elucidate the dynamical critical behavior and observed true critical behavior for the first time in a scattering experiment, something which has not been possible with neutron scattering, although researchers have tried for over 40 years [2,3]. This is (i) because of the unprecedented long time scales available for studying slow fluctuations with XPCS (thousands of seconds), which cannot be matched by neutron spin echo or by carrying out equivalent high-resolution quasi-elastic scattering experiments, and (ii) because XPCS, which measures the intensity-intensity autocorrelation functions in real time, measures the true 4-spin correlation functions corresponding to fluctuations of the actual spin glass order parameter, while neutron scattering measures the 2-spin correlation function. Figure 1 shows the XPCS autocorrelation function $g_2(\mathbf{q},t)$ for the resonant magnetic scattering for $\text{Cu}_{0.88}\text{Mn}_{0.12}$ for various temperatures, illustrating how the relaxation becomes slower and slower as the temperature approaches the spin glass transition temperature (44 K). The curves can be fitted with pure exponential functions, as expected from true critical behavior.

Thus, it appears that the answer to the long-standing question as to whether there is a true dynamical 2nd-order phase transition for a spin glass can be answered in the affirmative, reinforcing earlier, more indirect, measurements of the non-linear magnetic susceptibility [4]. By contrast, the off-resonant x-ray scattering (which corresponds to static charge scattering) showed no relaxation of the g_2 autocorrelation function, as expected.

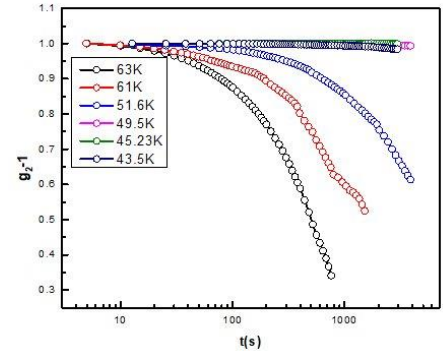


Figure 1: The functions $[g_2(\mathbf{q},t)-1]$ at $q=6.4 \times 10^{-3} \text{ \AA}^{-1}$ for several different temperatures.

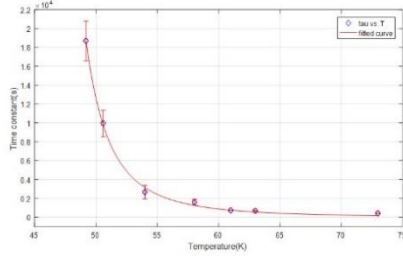


Figure 2: Temperature dependence of relaxation time vs. temperature with power law fit.

Figure 2 shows the measured relaxation times as a function of temperature, with a fit representing a power law divergence at T_g . The obtained dynamical critical exponent was not very different from simple mean-field theory predictions.

This technique can be applied to study other magnetic systems of great interest currently, such as spin liquids and spin ices and their quantum analogs. We have also recently made preliminary measurements of the reproducibility of the magnetic speckle pattern (which is a “fingerprint” of the spin configuration) in the frozen spin glass state on heating and cooling through the spin glass transition in order to try to

answer the long-standing theoretical question regarding whether there is a unique state or an infinite number of ground states for a spin glass. The results are currently being analyzed.

(b) Magnetic Skyrmions.

We have continued to use Fe/Gd multilayers as a model system to study chiral magnetic structures and we have probed them by neutron reflectivity, small-angle neutron scattering (SANS) (see Fig. 3), resonant soft x-ray scattering, resonant soft x-ray imaging, XPCS, Lorentz TEM, ferromagnetic resonance, magneto-transport and modeling. This has resulted in a number of publications and invited talks that addressed the skyrmions field-temperature phase diagram, the chirality of domain structures, and the dynamics of the skyrmion phase. The PRL **119**, 067403 (2017) highlighted the potential at free electron x-ray lasers for XPCS to study the spin fluctuation dynamics of magnetic skyrmions in the sub nanosecond time scale. We used the Fe/Gd system for the extension of the XPCS method that exploits the recent development of the two-pulse mode at the Linac Coherent Light Source, as shown schematically

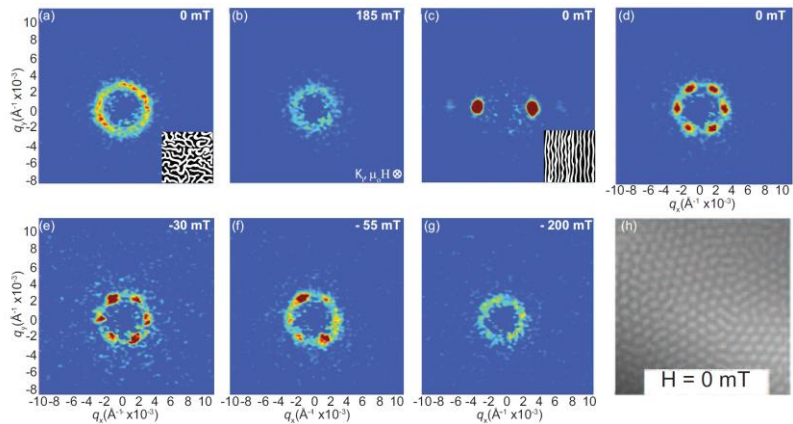


Figure 3: Measured SANS pattern at sequential fields for an Fe/Gd multilayer: (a) $\mu_0 H = 0$ T after out-of-plane saturation and (b) $\mu_0 H = 185$ mT. The sample was then saturated in an angled field and (c) the SANS pattern shows two peaks corresponding to a well-ordered stripe domain. The out-of-plane magnetic field was increased to $\mu_0 H = 185$ mT. SANS patterns were measured as the magnetic field was reduced towards negative saturation, with measurements shown in (d) – (g). (h) soft X-ray microscopy images taken at $\mu_0 H = 0$ T.

in Fig. 4. By using coherent resonant x-ray magnetic scattering, we studied spontaneous fluctuations on nanosecond time scales in thin films of multilayered Fe/Gd that exhibit ordered stripe and skyrmion lattice phases. The correlation time of the fluctuations was found to differ between the skyrmion phase and near the stripe-skyrmion boundary. This technique will enable a significant new area of research on the study of equilibrium fluctuations in condensed matter with free electron lasers at timescales that previously were not accessible to XPCS.

In a related study we explored the stochastic domain cascades avalanches and abrupt motion of magnetic domains in both the stripe and skyrmion phases. We show that the stochastic domain cascades follow different scaling laws in stripe and skyrmion phases. In the skyrmion

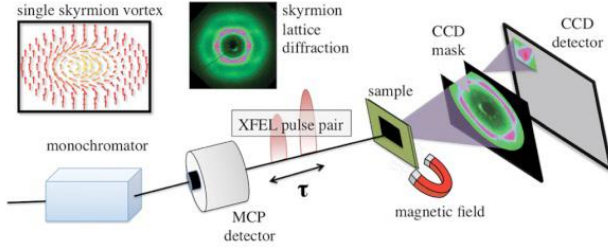


Figure 4: Schematic of the geometry of the experiment at the LCLS. Inset: a cartoon of the spin configuration of a chiral magnetic skyrmion, a single unit of the skyrmion lattice, and the resonant x-ray scattering from the skyrmion lattice, as measured at the ALS.

we have extended the study of Fe/Gd thin films to include thin Ir/Pt bilayers to provide symmetry breaking leading to chirality control (presumably through the introduction of DMI). We observe fixed chirality of domain wall and evidence of the topological Hall effect from a chiral magnetic order.

(c) Interface Structure of Ho films with a canted magnetic spiral structure.

We have initiated research of epitaxial rare-earth films onto ultrathin seed layers. This will allow the incorporation of rare-earth materials with their unusual spin-spiral structures, high spin-orbit interactions and strong magneto-striction effects in geometries compatible with spin-transport and ultrafast optical excitations. We have successfully grown Tb, Dy and Ho films with bulk-like phase diagrams down to thicknesses of 10 nm. We have carried out neutron reflectivity measurements at the NIST Center for Neutron Research (NCNR) on thin films of Holmium grown on MgO(110) substrates so that the orientation of the Ho crystalline c-axis (and thus the axis of the antiferromagnetic spiral in Ho) was tilted 40 degrees from the normal to the Ho-substrate interface, which could lead to boundary effects and distortion of the magnetic structure of the spiral. The analysis of the results show subtle non-spiral ferromagnetic effects at the interface.

Future Plans:

We plan to carry out further studies of jammed and frustrated magnetic systems. We have been allocated beam time at SNS to carry out Neutron Spin Echo studies of the dynamics of the domain wall fluctuations in simple cubic antiferromagnets, such as the model conventional antiferromagnet MnAl_2O_4 in the vicinity of the antiferromagnetic transition to see if they can be described by a relaxation of the Kohlrausch-Williams-Watts (KWW) compressed exponential form typical of jammed systems, as seen previously in the spiral antiferromagnet Dy metal [1]. This will enable us to decide if that behavior was in fact universal for antiferromagnets, as we have conjectured.

We will continue to use the Fe/Gd system (shown above) as a model system to study the behavior of skyrmions. First will continue SANS studies by applying RF magnetic fields to measure gigahertz breathing modes in magnetic skyrmions and to measure the results of AC currents on the lattice dynamics. We will also continue work on proximity based interactions between skyrmions and superconducting vortices where the magnetic layer is either in direct

phase the size distribution of the cascades follows a power law suggesting that it is in a critical state. Distinctly separate critical exponents along with temperature independent scaling-collapse within each phases indicates that the scaling behavior belongs to a different universality class as the topology of the magnetic system changes from stripe to skyrmion.

We have ongoing studies of current-induced skyrmion motion by imaging while applying current pulsed to a patterned wires. This is the first demonstration of current control of skyrmions without a DMI interaction to control the chirality. Finally,

contact or interacts indirectly through dipolar fields. We will also study full films of Ni/NiO/Nb and Ni/Au/Nb to study the difference of the depth dependent magnetic profile above and below the superconducting transition and in various applied in-plane magnetic field. We will, in parallel, study S/F'/N/F/N'/S type structures where we will probe F/N/F'/S structures by neutron reflectivity and transport measurements. The initial structures to study will be Ni/Au/FeNi(t)/Nb where the magnetically soft NiFe layer can be rotated relative to the Ni layer (the anisotropy of Ni increases at low temperature making it much harder than FeNi).

The binary Rare earth dialuminides reveal interesting physics, such as strong crystal field (CF) effects due to anisotropic $4f$ charge density as well as the competition between different magnetic and crystal structures. PrAl_2 and ErAl_2 exhibit ferromagnetic to paramagnetic transitions at 32.5 K and 14 K, respectively. On the other hand, $(\text{Pr,Er})\text{Al}_2$ undergoes a paramagnetic to ferrimagnetic (FIM) transition at $T_C = 24$ K. In the FIM phase, the Pr and Er moments are aligned antiparallel, and this material shows several further magnetic transitions at high applied magnetic fields. In particular, at low fields and below a temperature of 26 K, it shows what is believed to be a Griffiths phase [5]. We wish to use a combination of SANS and magnetic neutron diffraction to understand several of the novel magnetic phases observed in $(\text{Pr}_{0.6}\text{Er}_{0.4})\text{Al}_2$, including the detailed nature of the ferrimagnetic phase, and the nature of the ferromagnetic transitions in applied fields of 20 KOe and greater. Initially, however, we wish to start by studying the nature of the Griffiths phase using SANS at the NIST NCNR facility. The Griffiths phase [6] in a system with quenched-in disorder, is a phase which exists at temperatures above the true long-range ordering temperature where quantities such as the magnetization, free energy, etc. are non-analytic functions of magnetic field and temperature. It is characterized by local clusters of ordered spins, presumably ferrimagnetic clusters in this case.

References:

- [1] S.-W. Chen et al., *Phys. Rev. Lett.* **110**, 217201 (2013)
- [2] A.P. Murani and A. Heidemann, *Phys. Rev. Lett.* **41**, 1402 (1978)
- [3] F. Mezei and A.P. Murani, *Phys. Rev. Lett.* **14**, 211 (1979)
- [4] L.P. Levy, *Phys. Rev. B* **38**, 4963 (1988)
- [5] A. K. Pathak et al., *Phys. Rev. B* **89**, 224411 (2014).
- [6] R.B. Griffiths, *Phys. Rev. Lett.* **23**, 17 (1969)

Publications:

L. M. DeBeer-Schmitt, R. D. Desautels, S. Montoya, J. A. Borchers, S.-G. Je, M.-Y. Im, M. R. Fitzsimmons, E. E. Fullerton, D. A. Gilbert, "Realization of magnetic skyrmions in thin films at ambient conditions", *Physical Review Materials*, under review (2019).

A. Singh, J. C. T Lee, K. E. Avila, Y. Chen, S. Montoya, E. E. Fullerton, P. Fischer, K. A. Dahmen, S. D. Kevan, M. K. Sanyal, S. Roy, "Scaling of domain cascades in stripe and skyrmion phases", *Nature Communications* **10**, 1988 (2019).

S. A. Montoya, R. Tolley, I. Gilbert, S.-G. Je, M.-Y. Im, and E. E. Fullerton, "Spin-orbit torque induced dipole skyrmion motion at room temperature", *Physical Review B* **98**, 104432 (2018).

- A. Singh, M.K. Sanyal, J.C.T. Lee, Y. Chen, S. Montoya, E.E. Fullerton, S. Roy, “Resonant X-ray Magnetic Scattering Study Of Domain Morphology In FeGd Thin Film”, in 62nd DAE Solid State Physics Symposium (2018).
- F. Pressacco, V. Uhlíř, M. Gatti, A. Nicolaou, A. Bendounan, J. A. Arregi, S. K. K. Patel, E. E. Fullerton, D. Krizmancic, F. Sirotti, “Laser induced phase transition in epitaxial FeRh layers studied by pump-probe valence band photoemission”, *Structural Dynamics* **5**, 034501 (2018).
- J. A. Arregi, M. Horký, K. Fabianová, R. Tolley, E. E. Fullerton, and V. Uhlíř, “Magnetization reversal and confinement effects across the metamagnetic phase transition in mesoscale FeRh structures”, *Journal of Physics D: Applied Physics* **51**, 105001 (2018).
- D. J. Keavney, Y. Choi, M. V. Holt, V. Uhlíř, D. Arena, E.E. Fullerton, P.J. Ryan, J.-W. Kim, “Phase coexistence and kinetic arrest in the magnetostructural transition of the ordered alloy FeRh”, *Scientific Reports* **8**, 1778 (2018).
- A. H. Reid, X. Shen, P. Maldonado, T. Chase, E. Jal, P. Granitzka, K. Carva, R. K. Li, J. Li, L. Wu, T. Vecchione, T. Liu, Z. Chen, D. Higley, N. Hartmann, R. Coffe, J. Wu, G. L. Dakowski, W. Schlotter, H. Ohldag, Y.K. Takahashi, V. Mehta, O. Hellwig, A. Fry, Y. Zhu, J. Cao, E. E. Fullerton, J. Stöhr, P. M. Oppeneer, X. J. Wang & H.A. Dürr, “Beyond a phenomenological description of magnetostriction” *Nature Communications* **9**, 388 (2018).
- J.Q. Lin, X. Liu, E. Blackburn, S. Wakimoto, H. Ding, Z. Islam, and S.K. Sinha, "Quantitative Characterization of the Nanoscale Local Lattice Strain Induced by Sr Dopants in La_{1.92}Sr_{0.08}CuO₄", *Physical Review Letters* **120**, 197001 (2018).
- D. Sander, S. Valenzuela, D. Makarov, C. Marrows, E. E. Fullerton, P. Fischer, J. McCord, P. Vavassori, S. Mangin, P. Pirro, B. Hillebrands, A. Kent, T. Jungwirth, O. Gutfleisch, C.-G. Kim, and A Berger, “The 2017 Magnetism Roadmap”, *Journal of Physics D: Applied Physics* **50**, 363001 (2017).
- M. H. Seaberg, B. Holladay, J. C. T. Lee, M. Sikorski, A. H. Reid, S. A. Montoya, G. L. Dakovski, J. D. Koralek, G. Coslovich, S. Moeller, W. F. Schlotter, R. Streubel, S. D. Kevan, P. Fischer, E. E. Fullerton, J. L. Turner, F.-J. Decker, S. K. Sinha, S. Roy, and J. J. Turner, “Nanosecond X-ray Photon Correlation Spectroscopy on Magnetic Skyrmions”, *Physical Review Letters* **119**, 067403 (2017).
- F. Hellman, A. Hoffmann, Y. Tserkovnyak, G. S. D. Beach, E. E. Fullerton, C. Leighton, A. H. MacDonald, D. C. Ralph, D. A. Arena, H. A. Dürr, P. Fischer, J. Grollier, J. P. Heremans, T. Jungwirth, A. V. Kimel, B. Koopmans, I. N. Krivorotov, S. J. May, A. K. Petford-Long, J. M. Rondinelli, N. Samarth, I. K. Schuller, A. N. Slavin, M. D. Stiles, O. Tchernyshyov, A. Thiaville and B. L. Zink, “Interface-induced phenomena in magnetism”, *Review of Modern Physics* **89**, 025006 (2017)
- S. A. Montoya, S. Couture, J. J. Chess, J. C. T Lee, N. Kent, M.-Y. Im, S.D. Kevan, P. Fischer, B. J. McMorrnan, S. Roy, V. Lomakin, and E.E. Fullerton, Resonant properties of dipole skyrmions in amorphous Fe/Gd multilayers, *Physical Review B* **95**, 224405 (2017).

Neutron Scattering Studies of Unconventional Superconductors

John M. Tranquada, Genda Gu, Cedomir Petrovic, and Igor A. Zaliznyak

Condensed Matter and Materials Science Division

Brookhaven National Laboratory, Upton, NY 11973-5000

Program Scope

We combine exploratory synthesis, crystal growth, and neutron scattering techniques to address key questions associated with strong interactions in quantum materials, from high-temperature superconductors to magnetic semi-metals. In particular, how can we properly understand itinerant antiferromagnetism, and what is the role of intertwined orders in cuprate and iron-based superconductors? What is the role of electron-phonon coupling in strongly anharmonic topological crystalline insulators that become superconductors on doping? Can one exploit the interaction of spin-polarized itinerant states with local magnetic moments to obtain unprecedented responses to external stimuli? Advanced synthesis techniques are used to discover new model compounds, and high-quality crystals are grown of the most interesting materials. We exploit the latest neutron-scattering technologies available at national neutron user facilities, such as the Spallation Neutron Source and the High Flux Isotope Reactor, to obtain direct information on spin correlations and atomic displacements necessary to provide transformative answers to these questions. One such technology, in whose development we have actively participated, is time-of-flight, polarized, inelastic neutron spectroscopy. Complementary characterizations and theoretical analysis are performed in collaboration with other groups in the Condensed Matter Physics and Materials Science Division, especially using the National Synchrotron Light Source II and the Center for Functional Nanomaterials.

Recent Progress

Spin correlations and superconductivity in cuprates: We have continued our efforts to understand the connection between antiferromagnetism and superconductivity in the cuprates. In particular, from neutron scattering measurements on crystals of $\text{La}_{2-x}\text{Sr}_x\text{CuO}_4$ with $x = 0.17$ and 0.21 performed on SEQUOIA, we found evidence that the spin gap that develops below the superconducting transition, T_c , limits the coherent superconducting gap. From a search of the literature, we found that this is a general result for cuprates that exhibit spatially-uniform superconductivity [80]. If one takes electronic inhomogeneity into account, it suggests that regions with low-energy antiferromagnetic fluctuations limit the development of long-range superconducting order.

We have successfully grown crystals of $\text{La}_{1.9}\text{Ca}_{1.1}\text{Cu}_2\text{O}_6$ and annealed them in high-pressure oxygen to achieve superconductivity with T_c as high as 55 K. Neutron diffraction measurements demonstrated that intergrowths of La_2CuO_4 and $\text{La}_8\text{Cu}_8\text{O}_{20}$ were formed in the high-pressure treatment, so that the doping of the main $\text{La}_{2-x}\text{Ca}_{1+x}\text{Cu}_2\text{O}_6$ is likely achieved by enhancing the Ca concentration [33]. Measurements of anisotropic resistivity in the superconducting samples demonstrated that a c-axis magnetic field can decouple the superconducting bilayers [37]. Measurements of the spin excitations on SEQUOIA revealed rather steep dispersion of the spin excitations and the absence of a spin gap in the superconducting state [81]. The lack of a spin gap and the field-induced decoupling of superconducting layers are similar to the behaviors we have previously observed in underdoped $\text{La}_{2-x}(\text{Ba},\text{Sr})_x\text{CuO}_4$, suggesting that intertwining of the superconducting and spin correlations is likely to be present.

As another test of a possible pair-density-wave state, we measured the in-plane resistivity at low temperature and for c-axis magnetic fields up to 35 T in $\text{La}_{2-x}\text{Ba}_x\text{CuO}_4$ with $x = 0.125$ at the NHMFL in Tallahassee. We found evidence for transitions from 3D superconductivity to re-entrant 2D superconductivity to a metallic phase with an exceptionally high resistance (but not insulating). The charge carriers in the latter metallic phase appear to have particle-hole symmetry, suggesting that they could involve residual pairs that move incoherently between charge stripes [81]. In a separate experiment on the same material, it was discovered that the introduction of disorder through proton irradiation can actually decrease the stripe order and raise the superconducting transition temperature [79].

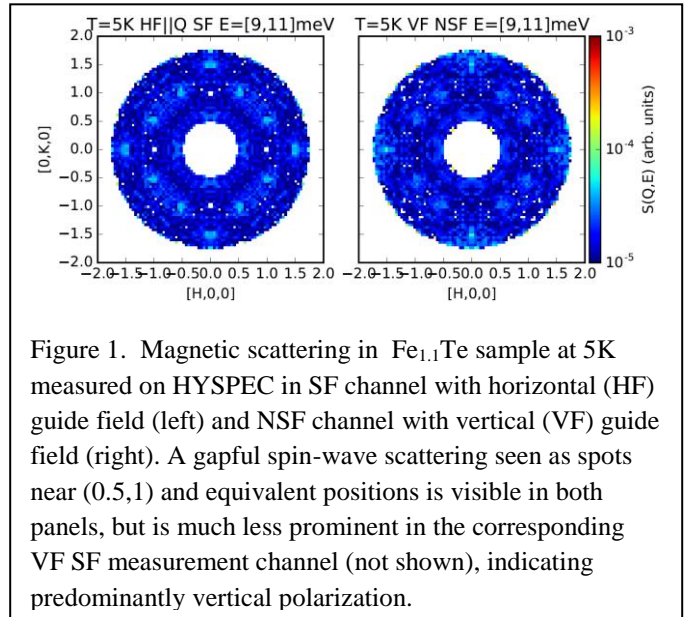
Unusual temperature dependence of magnetic correlations in $\text{Fe}_{1+y}\text{Te}_{1-x}\text{Se}_x$. Our inelastic neutron scattering measurements of low energy (< 10 meV) magnetic excitations in $\text{Fe}_{1+y}\text{Te}_{1-x}\text{Se}_x$ established that the spin correlations that are two-dimensional (2D) in the superconducting samples at low temperature appear much more three-dimensional when the temperature is increased well above $T_c \sim 15$ K, with a clear increase of the (dynamic) spin correlation length perpendicular to the Fe planes [35]. The spontaneous change of dynamical spin correlations from 2D to 3D on warming is unexpected and cannot be explained when only the spin degree of freedom is considered, since thermal fluctuations would tend to work against such a trend. Our results suggest that the low temperature physics in the “11” system, in particular the evolution of low-energy spin excitations towards superconducting pairing, is driven by changes in orbital correlations. In related work, neutron measurements on samples with small Se concentration, rendered superconducting by annealing in Te vapor, revealed a spin gap and spin resonance with stripe character, even in the presence of a strong background of double-stripe-like spin correlations [36].

X-ray and neutron scattering measurements on our samples of $\text{KFe}_{0.8}\text{Ag}_{1.2}\text{Te}_2$ have determined that the Fe atoms form isolated 2×2 clusters, surrounded by non-magnetic Ag atoms. Nevertheless, the system orders antiferromagnetically below 35 K [87].

Polarized neutron measurements on HYSPEC: magnetism and lattice dynamics in $Fe_{1+y}Te_{1-x}Se_x$.

The magnetism and the lattice in iron chalcogenides are closely coupled. The magnetic and lattice excitations can be disentangled by using the neutron polarization analysis.

We performed the first polarized neutron scattering measurements at HYSPEC spectrometer at the Spallation Neutron Source, Oak Ridge National Laboratory, where magnetic and structural scattering were uniquely identified through polarization analysis and their temperature dependence was studied [4]. We worked out the details of the instrument setup and developed the experimental and analysis procedures for polarization analysis [4,61]. An example of polarized inelastic neutron data obtained on a single-crystal sample is presented in Fig. 1.



Emergent quantum spins and non-Fermi-liquid behavior in an antiferromagnetic metal. We have collaborated on studies of Yb_2Pt_2Pb , a metallic system in which local magnetism is rooted in orbital moments of localized 4f electrons of Yb in the presence of strong spin-orbit coupling. Neutron scattering measurements of magnetic excitations in Yb_2Pt_2Pb revealed a broad magnetic continuum, dispersing in only one direction, that is quantitatively described by spinons in the model of a spin- $1/2$ chain. The system exhibits emergence of effective quantum spin- $1/2$ degrees of freedom in a system of Yb ($J = 7/2$) magnetic moments that are immersed in a Fermi sea of conduction electrons, with which they interact. The effective spin- $1/2$ subsystem can be driven to criticality in a relatively weak magnetic field, where it behaves like a Luttinger liquid. In a theoretical study inspired by these results, calculation of the electronic relaxation rate and the DC resistivity established the quasilinear temperature dependence of the latter [40]. We thus uncovered a non-Fermi liquid behavior of conduction electrons, similar to behavior observed in cuprates, which in the case of Yb_2Pt_2Pb arises from the spin criticality in a system with different effective spatial dimensionalities of the two interacting subsystems. With increasing magnetic field, we have experimentally observed that the inter-chain interaction becomes important, leading to a spinon confinement phenomenon [74]. This effectively decouples fractional spinon excitations in antiferromagnetic chains from conduction electrons, which regain Fermi-liquid behavior.

Future Plans

Anomalous phonons in (Pb,Sn,In)Te: We have shown that with In doping, $\text{Pb}_{0.5}\text{Sn}_{0.5}\text{Te}$ can be driven initially into a crystalline-topological-insulator phase and then into a superconducting state [2]. Neutron-scattering measurements of the phonon density of states in the superconducting phase of a polycrystalline sample revealed unexpected low-energy features, inconsistent with the average phonon behavior [60]. We will perform measurements on appropriate single-crystals samples to determine the character of these anomalous phonons.

Testing for spin-lattice coupling in $\text{La}_{2-x}\text{Sr}_x\text{CuO}_4$ with polarization analysis: Bruce Gaulin's group has presented evidence for coupling between magnetic excitations and a phonon mode at an energy of ~ 18 meV. To further test this picture, we will use polarized neutrons to characterize the relevant excitation and test that the enhanced spectral weight at the antiferromagnetic wave vector is truly magnetic.

Resolving curious temperature-dependent behaviors in stripe-ordered $\text{La}_{1.67}\text{Sr}_{0.33}\text{NiO}_4$: There are a number of independent observations of temperature dependent behavior of charge and spin-related phenomena that are puzzling. We will test for a common underlying cause through a re-examination of the thermal evolution of the spin order.

Polarized Neutron Scattering Study of Orbital Selective Magnetic Excitations on HYSPEC: While distinguishing SF and NSF scattering at HYSPEC is now a straightforward procedure, the full XYZ neutron polarization analysis (NPA) is not. It requires a complex procedure accounting for the time of flight and detector position, which we will continue to develop. Another challenge is in devising a resolution correction procedure for the XYZ NPA, which is particularly important at small angles. We will further develop the polarization analysis on HYSPEC aiming to fully commission the XYZ NPA capability. We will use these new capabilities to investigate the evolution of dynamical magnetism in $\text{Fe}_{1+y}\text{Te}_{1-x}\text{Se}_x$ superconductors with temperature and doping.

Publications

1. E. G. Sergeicheva, S. S. Sosin, L. A. Prozorova, G. D. Gu, and I. A. Zaliznyak, "Unusual magnetic excitations in the weakly ordered spin-1 chain antiferromagnet Sr_2CuO_3 : Possible evidence for Goldstone magnon coupled with the amplitude mode," *Phys. Rev. B* **95**, 020411 (2017).
2. R. Zhong, J. Schneeloch, Q. Li, W. Ku, J. Tranquada, and G. Gu, "Indium Substitution Effect on the Topological Crystalline Insulator Family $(\text{Pb}_{1-x}\text{Sn}_x)_1\text{yInyTe}$: Topological and Superconducting Properties," *Crystals* **7**, 55 (2017).
3. T. Liu, C. He, F. Wang, Y. Liu, X. Xi, R. Zhong, and Genda Gu, "Shockwave-Loading-Induced Enhancement of T_c in Superconducting $\text{Bi}_2\text{Sr}_2\text{CaCu}_2\text{O}_{8+\delta}$," *Sci. Rep.* **7**, 6710 (2017).

4. Igor A. Zaliznyak, A. T. Savici, V. O. Garlea, B. Winn, U. Filges, J. Schneeloch, John M. Tranquada, Genda Gu, A. Wang, and Cedomir Petrovic, “Polarized neutron scattering on HYSPEC: the HYbrid SPECTrometer at SNS,” *J. Physics: Conf. Series* **862**, 012030 (2017).
5. R. Zhong, B. L. Winn, Genda Gu, D. Reznik, and J. M. Tranquada, “Evidence for a Nematic Phase in $\text{La}_{1.75}\text{Sr}_{0.25}\text{NiO}_4$,” *Phys. Rev. Lett.* **118**, 177601 (2017).
6. X. M. Chen, V. Thampy, C. Mazzoli, A. M. Barbour, H. Miao, G. D. Gu, Y. Cao, J. M. Tranquada, M. P. M. Dean, and S. B. Wilkins, “Remarkable Stability of Charge Density Wave Order in $\text{La}_{1.875}\text{Ba}_{0.125}\text{CuO}_4$,” *Phys. Rev. Lett.* **117**, 167001 (2016).
7. U. Erdenemunkh, B. Koopman, L. Fu, K. Chatterjee, W. D. Wise, G. D. Gu, E. W. Hudson, and M. C. Boyer, “Suppression of Superfluid Density and the Pseudogap State in the Cuprates by Impurities,” *Phys. Rev. Lett.* **117**, 257003 (2016).
8. S. Rajasekaran, E. Casandruc, Y. Laplace, D. Nicoletti, G. D. Gu, S. R. Clark, D. Jaksch, and A. Cavalleri, “Parametric amplification of a superconducting plasma wave,” *Nat. Phys.* **12**, 1012 (2016).
9. W. Schottenhamel, M. Abdel-Hafiez, R. Fittipaldi, V. Granata, A. Vecchione, M. Hücker, A. U. B. Wolter, and B. Büchner, “Dilatometric study of the metamagnetic and ferromagnetic phases in the triple-layered $\text{Sr}_4\text{Ru}_3\text{O}_{10}$ system,” *Phys. Rev. B* **94**, 155154 (2016).
10. J. Tao, K. Sun, W.-G. Yin, L. Wu, H. Xin, J. G. Wen, W. Luo, S. J. Pennycook, J. M. Tranquada, and Y. Zhu, “Direct observation of electronic-liquid-crystal phase transitions and their microscopic origin in $\text{La}_{1/3}\text{Ca}_{2/3}\text{MnO}_3$,” *Sci. Rep.* **6**, 37624 (2016).
11. A. Wang, I. Zaliznyak, W. Ren, L. Wu, D. Graf, V. O. Garlea, J. B. Warren, E. Bozin, Y. Zhu, and C. Petrovic, “Magnetotransport study of Dirac fermions in YbMnBi_2 antiferromagnet,” *Phys. Rev. B* **94**, 165161 (2016).
12. Z.-G. Chen, R. Y. Chen, R. D. Zhong, J. Schneeloch, C. Zhang, Y. Huang, F. Qu, R. Yu, Q. Li, G. D. Gu, and N. L. Wang, “Spectroscopic evidence for bulk-band inversion and three-dimensional massive Dirac fermions in ZrTe_5 ,” *Proc. Natl. Acad. Sci. USA* **114**, 816 (2017).
13. H. Chi, C. Zhang, G. Gu, D. E. Kharzeev, X. Dai, and Q. Li, “Lifshitz transition mediated electronic transport anomaly in bulk ZrTe_5 ,” *New J. Phys.* **19**, 015005 (2017).
14. G. Du, Y. Li, J. Schneeloch, R. D. Zhong, G. Gu, H. Yang, H. Lin, and H.-H. Wen, “Superconductivity with two-fold symmetry in topological superconductor $\text{Sr}_x\text{Bi}_2\text{Se}_3$,” *Science China Physics, Mechanics & Astronomy* **60**, 037411 (2017).
15. D. Pelc, H.-J. Grafe, G. D. Gu, and M. Pozek, “Cu nuclear magnetic resonance study of charge and spin stripe order in $\text{La}_{1.875}\text{Ba}_{0.125}\text{CuO}_4$,” *Phys. Rev. B* **95**, 054508 (2017).
16. Y. Tian, S. Jia, R. J. Cava, R. Zhong, J. Schneeloch, G. Gu, and K. S. Burch, “Understanding the evolution of anomalous anharmonicity in $\text{Bi}_2\text{Te}_{3-x}\text{Se}_x$,” *Phys. Rev. B* **95**, 094104 (2017).
17. J. Zhao, Z. Yu, Q. Hu, Y. Wang, J. Schneeloch, C. Li, R. Zhong, Y. Wang, Z. Liu, and G. Gu, “Structural phase transitions of $(\text{Bi}_{1-x}\text{Sb}_x)_2(\text{Te}_{1-y}\text{Se}_y)_3$ compounds under high pressure and the influence of the atomic radius on the compression processes of tetradymites,” *Phys. Chem. Chem. Phys.* **19**, 2207 (2017).

18. G. Fabbris, D. Meyers, L. Xu, V. M. Katukuri, L. Hozoi, X. Liu, Z.-Y. Chen, J. Okamoto, T. Schmitt, A. Uldry, B. Delley, G. D. Gu, D. Prabhakaran, A. T. Boothroyd, J. van den Brink, D. J. Huang, and M. P. M. Dean, “Doping Dependence of Collective Spin and Orbital Excitations in the Spin-1 Quantum Antiferromagnet $\text{La}_{2-x}\text{Sr}_x\text{NiO}_4$ Observed by X Rays,” *Phys. Rev. Lett.* **118**, 156402 (2017).
19. Z. Guguchia, B. Roessli, R. Khasanov, A. Amato, E. Pomjakushina, K. Conder, Y. J. Uemura, J. M. Tranquada, H. Keller, and A. Shengelaya, “Complementary Response of Static Spin-Stripe Order and Superconductivity to Nonmagnetic Impurities in Cuprates,” *Phys. Rev. Lett.* **119**, 087002 (2017).
20. S. Li, Y. Gan, J. Wang, R. Zhong, J. A. Schneeloch, Z. Xu, W. Tian, M. B. Stone, S. Chi, M. Matsuda, Y. Sidis, P. Bourges, Qiang Li, Genda Gu, J. M. Tranquada, Guangyong Xu, R. J. Birgeneau, and J. Wen, “Suppression of the antiferromagnetic order when approaching the superconducting state in a phase-separated crystal of $\text{K}_x\text{Fe}_{2-y}\text{Se}_2$,” *Phys. Rev. B* **96**, 094503 (2017).
21. B. Loret, S. Sakai, S. Benhabib, Y. Gallais, M. Cazayous, M. A. Méasson, R. D. Zhong, J. Schneeloch, G. D. Gu, A. Forget, D. Colson, I. Paul, M. Civelli, and A. Sacuto, “Vertical temperature boundary of the pseudogap under the superconducting dome in the phase diagram of $\text{Bi}_2\text{Sr}_2\text{CaCu}_2\text{O}_{8+\delta}$,” *Phys. Rev. B* **96**, 094525 (2017).
22. D. Mou, A. Kaminski, and G. Gu, “Direct observation of self-energy signatures of the resonant collective mode in $\text{Bi}_2\text{Sr}_2\text{CaCu}_2\text{O}_{8+\delta}$,” *Phys. Rev. B* **95**, 174501 (2017). [\[1\]](#) [\[5EP\]](#)
23. J. Tao, K. Sun, J. M. Tranquada, and Y. Zhu, “Anomalous nanoclusters, anisotropy, and electronic nematicity in the doped manganite $\text{La}_{1/3}\text{Ca}_{2/3}\text{MnO}_3$,” *Phys. Rev. B* **95**, 235113 (2017).
24. V. Thampy, X. M. Chen, Y. Cao, C. Mazzoli, A. M. Barbour, W. Hu, H. Miao, G. Fabbris, R. D. Zhong, G. D. Gu, J. M. Tranquada, I. K. Robinson, S. B. Wilkins, and M. P. M. Dean, “Static charge-density-wave order in the superconducting state of $\text{La}_{2-x}\text{Ba}_x\text{CuO}_4$,” *Phys. Rev. B* **95**, 241111 (2017).
25. P. Zarepour, J. Xu, S. Y. F. Zhao, A. Jain, Z. Xu, T. S. Liu, G. D. Gu, and K. S. Burch, “Modeling tunneling for the unconventional superconducting proximity effect,” *Supercond. Sci. Technol.* **29**, 125006 (2016).
26. J. He, T. R. Mion, S. Gao, G. T. Myers, M. Arita, K. Shimada, G. D. Gu, and R.-H. He, “Angle-resolved photoemission with circularly polarized light in the nodal mirror plane of underdoped $\text{Bi}_2\text{Sr}_2\text{CaCu}_2\text{O}_{8+\delta}$ superconductor,” *Appl. Phys. Lett.* **109**, 182601 (2016).
27. D. Ahmad, W. J. Choi, Y. I. Seo, S. Seo, S. Lee, T. Park, J. Mosqueira, Genda Gu, and Y. S. Kwon, “Effect of proton irradiation on the fluctuation-induced magnetoconductivity of $\text{FeSe}_{1-x}\text{Te}_x$ thin films,” *New J. Phys.* **19**, 093004 (2017).
28. M. K. Frampton, J. Crocker, D. A. Gilbert, N. Curro, K. Liu, J. A. Schneeloch, G. D. Gu, and R. J. Zieve, “First-order reversal curve of the magnetostructural phase transition in FeTe ,” *Phys. Rev. B* **95**, 214402 (2017).

29. S. Seo, J.-H. Kang, M. J. Oh, I.-S. Jeong, J. Jiang, Genda Gu, J.-W. Lee, J. Lee, H. Noh, M. Liu, P. Gao, E. E. Hellstrom, J.-H. Lee, Y. J. Jo, C.-B. Eom, and S. Lee, “Origin of the emergence of higher T_c than bulk in iron chalcogenide thin films,” *Sci. Rep.* **7**, 9994 (2017).
30. P. Zareapour, A. Hayat, S. Y. F. Zhao, M. Kreshchuk, Z. Xu, T. S. Liu, G. D. Gu, S. Jia, R. J. Cava, H.-Y. Yang, Y. Ran, and K. S. Burch, “Andreev reflection without Fermi surface alignment in high- T_c van der Waals heterostructures,” *New J. Phys.* **19**, 043026 (2017).
31. Y. Ma, Y. Hou, C. Lu, L. Li, and C. Petrovic, “Possible origin of nonlinear conductivity and large dielectric constant in the commensurate charge-density-wave phase of 1T-TaS₂,” *Phys. Rev. B* **97**, 195117 (2018).
32. W. Ren, A. Wang, D. Graf, Y. Liu, Z. Zhang, W.-G. Yin, and C. Petrovic, “Absence of Dirac states in BaZnBi₂ induced by spin-orbit coupling,” *Phys. Rev. B* **97**, 035147 (2018).
33. J. A. Schneeloch, Z. Guguchia, M. B. Stone, W. Tian, R. Zhong, K. M. Mohanty, G. Xu, G. D. Gu, and J. M. Tranquada, “Growth and structural characterization of large superconducting crystals of La_{2-x}Ca_{1+x}Cu₂O₆,” *Phys. Rev. Materials* **1**, 074801 (2017).
34. A. Wang, D. Graf, A. Stein, Y. Liu, W. Yin, and C. Petrovic, “Magnetotransport properties of MoP₂,” *Phys. Rev. B* **96**, 195107 (2017).
35. Z. Xu, J. A. Schneeloch, J. Wen, B. L. Winn, G. E. Granroth, Y. Zhao, G. Gu, I. Zaliznyak, J. M. Tranquada, R. J. Birgeneau, and G. Xu, “Surprising loss of three-dimensionality in low-energy spin correlations on approaching superconductivity in Fe_{1+y}Te_{1-x}Sex,” *Phys. Rev. B* **96**, 134505 (2017).
36. Z. Xu, J. A. Schneeloch, M. Yi, Y. Zhao, M. Matsuda, D. M. Pajerowski, S. Chi, R. J. Birgeneau, G. Gu, J. M. Tranquada, and G. Xu, “Coexistence of superconductivity and short-range double-stripe spin correlations in Te-vapor annealed FeTe_{1-x}Sex ($x \leq 0.2$),” *Phys. Rev. B* **97**, 214511 (2018).
37. R. Zhong, J. A. Schneeloch, H. Chi, Q. Li, G. Gu, and J. M. Tranquada, “Evidence for magnetic-field-induced decoupling of superconducting bilayers in La_{2-x}Ca_{1+x}Cu₂O₆,” *Phys. Rev. B* **97**, 134520 (2018).
38. F. Boschini, E. H. da Silva Neto, E. Razzoli, M. Zonno, S. Peli, R. P. Day, M. Michiardi, M. Schneider, B. Zwartsenberg, P. Nigge, R. D. Zhong, J. Schneeloch, G. D. Gu, S. Zhdanovich, A. K. Mills, G. Levy, D. J. Jones, C. Giannetti, and A. Damascelli, “Collapse of superconductivity in cuprates via ultrafast quenching of phase coherence,” *Nat. Mater.* **17**, 416 (2018).
39. M. Chinotti, J. Ethiraj, C. Mirri, X. Zhu, L. Li, C. Petrovic, and L. Degiorgi, “Impact of the charge density wave state in the electrodynamic response of ZrTe_{3-x}Sex: Optical evidence for a pseudogap phase,” *Phys. Rev. B* **97**, 045117 (2018).
40. L. Classen, I. Zaliznyak, and A. M. Tsvelik, “Three-Dimensional Non-Fermi-Liquid Behavior from One-Dimensional Quantum Critical Local Moments,” *Phys. Rev. Lett.* **120**, 156404 (2018).

41. S. V. Dordevic, H. Lei, C. Petrovic, J. Ludwig, Z. Q. Li, and D. Smirnov, “Observation of cyclotron antiresonance in the topological insulator Bi₂Te₃,” *Phys. Rev. B* **98**, 115138 (2018).
42. W. J. Gannon, L. S. Wu, I. A. Zaliznyak, W. H. Xu, A. M. Tsvelik, Y. Qiu, J. A. Rodriguez-Rivera, and M. C. Aronson, “Local quantum phase transition in YFe₂Al₁₀,” *Proc. Natl. Acad. Sci. U.S.A.* **115**, 6995 (2018).
43. A. M. Ganose, L. Gannon, F. Fabrizi, H. Nowell, S. A. Barnett, H. Lei, X. Zhu, C. Petrovic, D. O. Scanlon, and M. Hoesch, “Local corrugation and persistent charge density wave in ZrTe₃ with Ni intercalation,” *Phys. Rev. B* **97**, 155103 (2018).
44. P. M. Gehring, D. Parshall, L. Harriger, C. Stock, G. Xu, X. Li, and H. Luo, “Correspondence: Phantom phonon localization in relaxors,” *Nat. Commun.* **8**, 1935 (2017).
45. A. A. Gippius, S. V. Zhurenko, R. Hu, C. Petrovic, and M. Baenitz, “121,123Sb nuclear quadrupole resonance as a microscopic probe in the Te-doped correlated semimetal FeSb₂: Emergence of electronic Griffith phase, magnetism, and metallic behavior,” *Phys. Rev. B* **97**, 075118 (2018).
46. K. Katsumi, N. Tsuji, Y. I. Hamada, R. Matsunaga, J. Schneeloch, R. D. Zhong, G. D. Gu, H. Aoki, Y. Gallais, and R. Shimano, “Higgs Mode in the d-Wave Superconductor Bi₂Sr₂CaCu₂O_{8+x} Driven by an Intense Terahertz Pulse,” *Phys. Rev. Lett.* **120**, 117001 (2018).
47. J. Klotz, K. Gotze, I. Sheikin, T. Forster, D. Graf, J.-H. Park, E. S. Choi, R. Hu, C. Petrovic, J. Wosnitza, and E. L. Green, “Fermi surface reconstruction and dimensional topology change in Nd-doped CeCoIn₅,” *Phys. Rev. B* **98**, 081105 (2018).
48. T. Konstantinova, J. D. Rameau, A. H. Reid, O. Abdurazakov, L. Wu, R. Li, X. Shen, G. Gu, Y. Huang, L. Rettig, I. Avigo, M. Ligges, J. K. Freericks, A. F. Kemper, H. A. Durr, U. Bovensiepen, P. D. Johnson, X. Wang, and Y. Zhu, “Nonequilibrium electron and lattice dynamics of strongly correlated Bi₂Sr₂CaCu₂O_{8+δ} single crystals,” *Sci. Adv.* **4** (2018), 10.1126/sciadv.aap7427.
49. J. Lee, M. Matsuda, J. A. Mydosh, I. Zaliznyak, A. I. Kolesnikov, S. Sullow, J. P. C. Ruff, and G. E. Granroth, “Dual Nature of Magnetism in a Uranium Heavy-Fermion System,” *Phys. Rev. Lett.* **121**, 057201 (2018).
50. M. Liao, Y. Zhu, J. Zhang, R. Zhong, J. Schneeloch, G. Gu, K. Jiang, D. Zhang, X. Ma, and Q.-K. Xue, “Superconductor–Insulator Transitions in Exfoliated Bi₂Sr₂CaCu₂O_{8+δ} Flakes,” *Nano Letters* **18**, 5660 (2018).
51. B. Loret, Y. Gallais, M. Cazayous, R. D. Zhong, J. Schneeloch, G. D. Gu, A. Fedorov, T. K. Kim, S. V. Borisenko, and A. Sacuto, “Raman and ARPES combined study on the connection between the existence of the pseudogap and the topology of the Fermi surface in Bi₂Sr₂CaCu₂O_{8+δ},” *Phys. Rev. B* **97**, 174521 (2018).
52. H. Miao, J. Lorenzana, G. Seibold, Y. Y. Peng, A. Amorese, F. Yakhov-Harris, K. Kummer, N. B. Brookes, R. M. Konik, V. Thampy, G. D. Gu, G. Ghiringhelli, L. Braicovich, and M. P.

- M. Dean, “High-temperature charge density wave correlations in $\text{La}_{1.875}\text{Ba}_{0.125}\text{CuO}_4$ without spin–charge locking,” *Proc. Natl. Acad. Sci. U.S.A.* **114**, 12430 (2017).
53. H. Miao, D. Ishikawa, R. Heid, M. Le Tacon, G. Fabbris, D. Meyers, G. D. Gu, A. Q. R. Baron, and M. P. M. Dean, “Incommensurate Phonon Anomaly and the Nature of Charge Density Waves in Cuprates,” *Phys. Rev. X* **8**, 011008 (2018).
 54. H. Miao, W. H. Brito, Z. P. Yin, R. D. Zhong, G. D. Gu, P. D. Johnson, M. P. M. Dean, S. Choi, G. Kotliar, W. Ku, X. C. Wang, C. Q. Jin, S.-F. Wu, T. Qian, and H. Ding, “Universal $2\Delta_{\text{max}}/k_B T_c$ scaling decoupled from the electronic coherence in iron-based superconductors,” *Phys. Rev. B* **98**, 020502 (2018).
 55. A. Milosavljevic, A. Solajic, J. Pesic, Y. Liu, C. Petrovic, N. Lazarevic, and Z. V. Popovic, “Evidence of spin-phonon coupling in CrSiTe_3 ,” *Phys. Rev. B* **98**, 104306 (2018).
 56. M. Mitrano, A. A. Husain, S. Vig, A. Kogar, M. S. Rak, S. I. Rubeck, J. Schmalian, B. Uchoa, J. Schneeloch, R. Zhong, G. D. Gu, and P. Abbamonte, “Anomalous density fluctuations in a strange metal,” *Proc. Natl. Acad. Sci. U.S.A.* **115**, 5392 (2018).
 57. A. Pal, M. Chinotti, L. Degiorgi, W. Ren, and C. Petrovic, “Optical properties of YbMnBi_2 : A type II Weyl semimetal candidate,” *Physica B Condens. Matter* **536**, 64 (2018).
 58. S. Parham, H. Li, T. J. Nummy, J. A. Waugh, X. Q. Zhou, J. Griffith, J. Schneeloch, R. D. Zhong, G. D. Gu, and D. S. Dessau, “Ultrafast Gap Dynamics and Electronic Interactions in a Photoexcited Cuprate Superconductor,” *Phys. Rev. X* **7**, 041013 (2017).
 59. S. Rajasekaran, J. Okamoto, L. Mathey, M. Fechner, V. Thampy, G. D. Gu, and A. Cavalleri, “Probing optically silent superfluid stripes in cuprates,” *Science* **359**, 575 (2018).
 60. K. Ran, R. Zhong, T. Chen, Y. Gan, J. Wang, B. L. Winn, A. D. Christianson, S. Li, Z. Ma, S. Bao, Z. Cai, G. Xu, J. M. Tranquada, G. Gu, J. Sun, and J. Wen, “Unusual phonon density of states and response to the superconducting transition in the In-doped topological crystalline insulator $\text{Pb}_{0.5}\text{Sn}_{0.5}\text{Te}$,” *Phys. Rev. B* **97**, 220502 (2018).
 61. A. T. Savici, I. A. Zaliznyak, V. O. Garlea, and B. Winn, “Data processing workflow for time of flight polarized neutrons inelastic measurements,” *J. Phys. Conf. Series* **862**, 012023 (2017).
 62. X. Shi, I. K. Dimitrov, T. Ozaki, G. Gu, and Q. Li, “Quasi-two-dimensional fluctuations in the magnetization of $\text{La}_{1.9}\text{Ca}_{1.1}\text{Cu}_2\text{O}_{6+\delta}$ superconductors,” *Phys. Rev. B* **96**, 184519 (2017).
 63. D. Wang, L. Kong, P. Fan, H. Chen, S. Zhu, W. Liu, L. Cao, Y. Sun, S. Du, J. Schneeloch, R. Zhong, G. Gu, L. Fu, H. Ding, and H.-J. Gao, “Evidence for Majorana bound states in an iron-based superconductor,” *Science* **362**, 333-335 (2018).
 64. R. Yu, S. Banerjee, H. C. Lei, R. Sinclair, M. Abeykoon, H. D. Zhou, C. Petrovic, Z. Guguchia, and E. S. Bozin, “Absence of local fluctuating dimers in superconducting $\text{Ir}_{1-x}(\text{Pt,Rh})_x\text{Te}_2$,” *Phys. Rev. B* **97**, 174515 (2018).
 65. P. Zhang, K. Yaji, T. Hashimoto, Y. Ota, T. Kondo, K. Okazaki, Z. Wang, J. Wen, G. D. Gu, H. Ding, and S. Shin, “Observation of topological superconductivity on the surface of an iron-based superconductor,” *Science* **360**, 182 (2018).

66. S. J. Zhang, Z. X. Wang, L. Y. Shi, T. Lin, M. Y. Zhang, G. D. Gu, T. Dong, and N. L. Wang, “Light-induced new collective modes in the superconductor $\text{La}_{1.905}\text{Ba}_{0.095}\text{CuO}_4$,” *Phys. Rev. B* **98**, 020506 (2018).
67. J. Zhang, Y. Ding, C.-C. Chen, Z. Cai, J. Chang, B. Chen, X. Hong, A. Fluerasu, Y. Zhang, C.-S. Ku, D. Brewe, S. Heald, H. Ishii, N. Hiraoka, K.-D. Tsuei, W. Liu, Z. Zhang, Y. Q. Cai, G. Gu, T. Irifune, and H.-k. Mao, “Evolution of a Novel Ribbon Phase in Optimally Doped $\text{Bi}_2\text{Sr}_2\text{CaCu}_2\text{O}_{8+\delta}$ at High Pressure and Its Implication to High-Tc Superconductivity,” *J. Phys. Chem. Lett.* **9**, 4182 (2018).
68. H. Zhao, B. Rachmilowitz, Z. Ren, R. Han, J. Schneeloch, R. Zhong, G. Gu, Z. Wang, and I. Zeljkovic, “Superconducting proximity effect in a topological insulator using $\text{Fe}(\text{Te}, \text{Se})$,” *Phys. Rev. B* **97**, 224504 (2018).
69. X. Sun, W.-T. Zhang, L. Zhao, G.-D. Liu, G.-D. Gu, Q.-J. Peng, Z.-M. Wang, S.-J. Zhang, F. Yang, C.-T. Chen, Z.-Y. Xu, and X.-J. Zhou, “Temperature Evolution of Energy Gap and Band Structure in the Superconducting and Pseudogap States of $\text{Bi}_2\text{Sr}_2\text{CaCu}_2\text{O}_{8+\delta}$ Superconductor Revealed by Laser-Based Angle-Resolved Photoemission Spectroscopy,” *Chin. Phys. Lett.* **35**, 017401 (2018).
70. Ping Ai, Qiang Gao, Jing Liu, Yuxiao Zhang, Cong Li, Jianwei Huang, Chunyao Song, Hongtao Yan, Lin Zhao, Guo-Dong Liu, Gen-Da Gu, Feng-Feng Zhang, Feng Yang, Qin-Jun Peng, Zu-Yan Xu, and Xing-Jiang Zhou, “Distinct Superconducting Gap on Two Bilayer-Split Fermi Surface Sheets in $\text{Bi}_2\text{Sr}_2\text{CaCu}_2\text{O}_{8+\delta}$ Superconductor,” *Chin. Phys. Lett.* **36**, 067402 (2019).
71. X. M. Chen, C. Mazzoli, Y. Cao, V. Thampy, A. M. Barbour, W. Hu, M. Lu, T. A. Assefa, H. Miao, G. Fabbris, G. D. Gu, J. M. Tranquada, M. P. M. Dean, S. B. Wilkins, and I. K. Robinson, “Charge density wave memory in a cuprate superconductor,” *Nat. Commun.* **10**, 1435 (2019).
72. I.K. Drozdov, I. Pletikovic, C. K. Kim, K. Fujita, G. D. Gu, J. C. Seamus Davis, P. D. Johnson, I. Bozovic, and T. Valla, “Phase diagram of $\text{Bi}_2\text{Sr}_2\text{CaCu}_2\text{O}_{8+\delta}$ revisited,” *Nat. Commun.* **9**, 5210 (2018).
73. S. Freutel, J. D. Rameau, L. Rettig, I. Avigo, M. Ligges, Y. Yoshida, H. Eisaki, J. Schneeloch, R. D. Zhong, Z. J. Xu, G. D. Gu, U. Bovensiepen, and P. D. Johnson, “Optical perturbation of the hole pockets in the underdoped high-Tc superconducting cuprates,” *Phys. Rev. B* **99**, 081116(R) (2019).
74. W. J. Gannon, I. A. Zaliznyak, L. S. Wu, A. E. Feiguin, A. M. Tsvelik, F. Demmel, Y. Qiu, J. R. D. Copley, M. S. Kim, and M. C. Aronson, “Spinon confinement and a sharp longitudinal mode in $\text{Yb}_2\text{Pt}_2\text{Pb}$ in magnetic fields,” *Nat. Commun.* **10**, 1123 (2019).
75. Qiangqiang Gu, Siyuan Wan, Qingkun Tang, Zengyi Du, Huan Yang, Qiang-Hua Wang, Ruidan Zhong, Jinsheng Wen, G. D. Gu, and Hai-Hu Wen, “Directly visualizing the sign change of d-wave superconducting gap in $\text{Bi}_2\text{Sr}_2\text{CaCu}_2\text{O}_{8+\delta}$ by phase-referenced quasi-particle interference,” *Nat. Commun.* **10**, 1603 (2019).

76. Moritz Hoesch, Liam Gannon, Kenya Shimada, Benjamin J. Parrett, Matthew D. Watson, Timur K. Kim, Xiangde Zhu, and Cedomir Petrovic, “Disorder Quenching of the Charge Density Wave in ZrTe₃,” *Phys. Rev. Lett.* **122**, 017601 (2019).
77. Feng Jin, Nenad Lazarevic, Changle Liu, Jianting Ji, Yimeng Wang, Shuna He, Hechang Lei, Cedomir Petrovic, Rong Yu, Zoran V. Popović, and Qingming Zhang, “Phonon anomalies and magnetic excitations in BaFe₂Se₂O,” *Phys. Rev. B* **99**, 144419 (2019).
78. S. H. Joo, J.-J. Kim, J. H. Yoo, M. S. Park, K. S. Lee, G. Gu, and Jinho Lee, “Cooper Pair Density of Bi₂Sr₂CaCu₂O_{8+x} in Atomic scale at 4.2 K,” *Nano Lett.* **19**, 1112–1117 (2019).
79. Maxime Leroux, Vivek Mishra, Jacob P. C. Ruff, Helmut Claus, Matthew P. Smylie, Christine Opagiste, Pierre Rodiere, Asghar Kayani, G. D. Gu, John M. Tranquada, Wai-Kwong Kwok, Zahirul Islam, and Ulrich Welp, “Disorder raises the critical temperature of a cuprate superconductor,” *Proc. Natl. Acad. Sci. USA* **116**, 10691-10697 (2019).
80. Yangmu Li, Ruidan Zhong, M. B. Stone, A. I. Kolesnikov, G. D. Gu, I. A. Zaliznyak, and J. M. Tranquada, “Low-energy antiferromagnetic spin fluctuations limit the coherent superconducting gap in cuprates,” *Phys. Rev. B* **98**, 224508 (2018).
81. Yangmu Li, J. Terzic, P. G. Baity, Dragana Popovic, G. D. Gu, Qiang Li, A. M. Tsvelik, and J. M. Tranquada, “Tuning from failed superconductor to failed insulator with magnetic field,” *Sci. Adv.* **5**, eaav7686 (2019).
82. Yongchang Ma, Zequn Wang, Yanhui Hou, Dong Wu, Cuimin Lu, and Cedomir Petrovic, “Observation of multiple metastable states induced by electric pulses in the hysteresis temperature range of 1T-TaS₂,” *Phys. Rev. B* **99**, 045102 (2019).
83. D. Nicoletti, D. Fu, O. Mehio, S. Moore, A. S. Disa, G. D. Gu, and A. Cavalleri, “Magnetic-Field Tuning of Light-Induced Superconductivity in Striped La_{2-x}Ba_xCuO₄,” *Phys. Rev. Lett.* **121**, 267003 (2018).
84. J. Pasztorova, A. Howell, M. Songvilay, P. M. Sarte, J. A. Rodriguez-Rivera, A. M. Arevalo-Lopez, K. Schmalzl, A. Schneidewind, S. R. Dunsiger, D. K. Singh, C. Petrovic, R. Hu, and C. Stock, “Relaxing Kondo-screened Kramers doublets in CeRhSi₃,” *Phys. Rev. B* **99**, 125144 (2019).
85. J. D. Rameau, N. Zaki, G. D. Gu, P. D. Johnson, and M. Weinert, “Interplay of paramagnetism and topology in the Fe-chalcogenide high-T_c superconductors,” *Phys. Rev. B* **99**, 205117 (2019).
86. John A. Schneeloch, Ruidan Zhong, M. B. Stone, I. A. Zaliznyak, G. D. Gu, Guangyong Xu, and J. M. Tranquada, “Gapless spin excitations in superconducting La_{2-x}Ca_{1+x}Cu₂O₆ with T_c up to 55 K,” *Phys. Rev. B* **99**, 174515 (2019).
87. Yu Song, Huibo Cao, B. C. Chakoumakos, Yang Zhao, Aifeng Wang, Hechang Lei, C. Petrovic, and Robert J. Birgeneau, “Intertwined Magnetic and Nematic Orders in Semiconducting KFe_{0.8}Ag_{1.2}Te₂,” *Phys. Rev. Lett.* **122**, 087201 (2019).
88. Fangdong Tang, Yafei Ren, Peipei Wang, Ruidan Zhong, John Schneeloch, Shengyuan A. Yang, Kun Yang, Patrick A. Lee, Genda Gu, Zhenhua Qiao, and Liyuan Zhang, “Three-

- dimensional quantum Hall effect and metal–insulator transition in ZrTe₅,” *Nature* **569**, 537–541 (2019).
89. Fangdong Tang, Peipei Wang, Peng Wang, Yuan Gan, G D Gu, Wei Zhang, Mingquan He, and Liyuan Zhang, “Quasi-2D superconductivity in FeTe_{0.55}Se_{0.45} ultrathin film,” *J. Phys. Condens. Matter* **31**, 265702 (2019).
 90. Jianjun Tian, Valentin N. Ivanovski, David Szalda, Hechang Lei, Aifeng Wang, Yu Liu, Weifeng Zhang, Vasil Koteski, and Cedomir Petrovic, “Fe_{0.36(4)}Pd_{0.64(4)}Se₂: Magnetic Spin-Glass Polymorph of FeSe₂ and PdSe₂ Stable at Ambient Pressure,” *Inorg. Chem.* **58**, 3107–3114 (2019).
 91. Dongfei Wang, Lingyuan Kong, Peng Fan, Hui Chen, Shiyu Zhu, Wenyao Liu, Lu Cao, Yujie Sun, Shixuan Du, John Schneeloch, Ruidan Zhong, Genda Gu, Liang Fu, Hong Ding, and Hong-Jun Gao, “Evidence for Majorana bound states in an iron-based superconductor,” *Science* **362**, 333–335 (2018).
 92. Kristin Willa, Roland Willa, Kok Wee Song, G. D. Gu, John A. Schneeloch, Ruidan Zhong, Alexei E. Koshelev, Wai-Kwong Kwok, and Ulrich Welp, “Nanocalorimetric evidence for nematic superconductivity in the doped topological insulator Sr_{0.1}Bi₂Se₃,” *Phys. Rev. B* **98**, 184509 (2018).
 93. R. Yu, S. Banerjee, H. Lei, M. Abeykoon, C. Petrovic, Z. Guguchia, and E. S. Bozin, “Phase separation at the dimer-superconductor transition in Ir_{1-x}Rh_xTe₂,” *Phys. Rev. B* **98**, 134506 (2018).
 94. Peng Zhang, Zhijun Wang, Xianxin Wu, Koichiro Yaji, Yukiaki Ishida, Yoshimitsu Kohama, Guangyang Dai, Yue Sun, Cedric Bareille, Kenta Kuroda, Takeshi Kondo, Kozo Okazaki, Koichi Kindo, Xiancheng Wang, Changqing Jin, Jiangping Hu, Ronny Thomale, Kazuki Sumida, Shilong Wu, Koji Miyamoto, Taichi Okuda, Hong Ding, G. D. Gu, Tsuyoshi Tamegai, Takuto Kawakami, Masatoshi Sato, and Shik Shin, “Multiple topological states in iron-based superconductors,” *Nat. Phys.* **15**, 41–47 (2019).
 95. He Zhao, Zheng Ren, Bryan Rachmilowitz, John Schneeloch, Ruidan Zhong, Genda Gu, Ziqiang Wang, and Ilija Zeljkovic, “Charge-stripe crystal phase in an insulating cuprate,” *Nat. Mater.* **18**, 103–107 (2019).
 96. Y.-G. Zhong, J.-Y. Guan, X. Shi, J. Zhao, Z.-C. Rao, C.-Y. Tang, H.-J. Liu, Z. Y. Weng, Z. Q. Wang, G. D. Gu, T. Qian, Y.-J. Sun, and H. Ding, “Continuous doping of a cuprate surface: Insights from in situ angle-resolved photoemission,” *Phys. Rev. B* **98**, 140507 (2018).
 97. Hyejin Ryu, Se Young Park, Lijun Li, Weijun Ren, Jeffrey B. Neaton, Cedomir Petrovic, Choongyu Hwang and Sung-Kwan Mo, “Anisotropic Dirac Fermions in BaMnBi₂ and BaZnBi₂” *Scientific Reports* **8**, 15322 (2018).
 98. T. Konstantinova, L. Wu, M. Abeykoon, R. J. Koch, A. F. Wang, R. K. Li, X. Shen, J. Li, J. Tao, I. A. Zaliznyak, C. Petrovic, S. J. L. Billinge, X. J. Wang, E. S. Bozin, and Y. Zhu, “Photoinduced dynamics of nematic order parameter in FeSe,” *Phys. Rev. B* **99**, 180102(R) (2019).

Orbitally Active NaMO₂ as a Platform for Novel Magnetism and Entangled Electronic States

Stephen D. Wilson, Materials Department, University of California, Santa Barbara

Program Scope

This program supports a combined neutron scattering and crystal growth study of novel forms of spin behavior and entangled electronic states in lamellar compounds comprised of layered triangular lattices and orbitally active M-sites. Orbitally-active denotes an orbital moment on the metal site—one that may be later quenched via coupling to the lattice or via relativistic spin-orbit interactions. New forms of magnetism ranging from emergent longitudinal modes, to manifestations of Kitaev exchange [1], to new settings for quantum spin liquids [2] are predicted to emerge in this class of materials, and, more broadly, their spin degrees of freedom are also often intertwined with orbital and structural symmetry breaking [3]. The goal is to develop a microscopic understanding of the unconventional spin and orbital phase behaviors that emerge in these systems and, ultimately, to advance the frontier of new quantum materials and manifestations of spin-orbit entangled states.

The α -phase of the NaMO₂ structure, which is comprised of a triangular lattice of edge-sharing MO₆ octahedra, provides a versatile model platform for exploring distinct regimes of spin and orbital phase behaviors, each carrying predictions for the appearance of novel states (see Fig. 1 for examples). This program seeks to synthesize high purity crystals of these materials via novel floating zone methods and to investigate their magnetic properties via neutron scattering-based studied and complementary techniques.

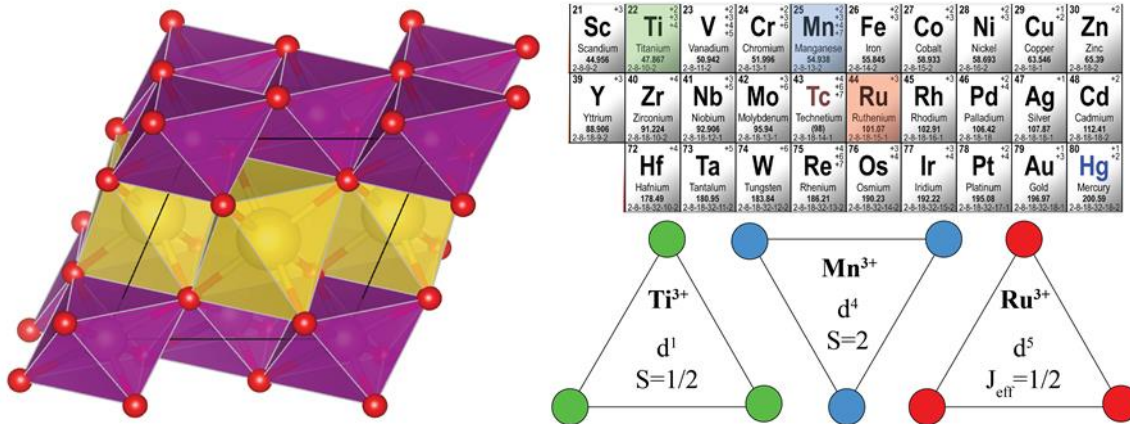


Fig. 1: (left) Example structure of the α -phase of the NaMO₂. Purple spheres are the Mn metal sites surrounded by eight oxygen atoms (red spheres). Between Mn layers are octahedrally coordinated Na-sites (yellow spheres). (right) Periodic table highlighting a few orbitally active M-variants that form the NaMO₂ structure.

Recent Progress

Our recent work focuses on the exploration of two triangular lattice NaMnO₂ systems; M=Mn where a strong coherent Jahn-Teller distortion driven by the 3d⁴ electrons orbital degeneracy generates a highly one-dimensional spin system, and M=Yb where 4f¹³ electrons freeze into anisotropic $J_{\text{eff}}=1/2$ moments at low temperature and render a field-tunable quantum disordered ground state. Both of these materials render unconventional magnetic states with a large degree of underlying frustration.

As one highlight of our recent work, in our studies of NaMnO₂, we reveal that the triangular lattice of Mn-moments (whose geometric frustration is strongly lifted via a coherent Jahn-Teller distortion) realizes a highly one-dimensional magnetic ground state [a]. The result is a dense network of S=2 chains where interchain frustration generates an effective interchain coupling nearly 10 times smaller than the intrachain coupling. The strong uniaxial single-ion anisotropy of this one-dimensional network of spin chains was found to generate a substantial binding energy between magnons and engenders the formation of a coherent, longitudinal branch of two-magnon excitations (Fig. 2). Furthermore, the ordered phase of the system is

found to follow predictions for a mean field model of weakly coupled Ising spin chains [b]. This work establishes NaMnO₂ as a promising template for exploring the predictions of interacting magnons in a dense, classical network of one-dimensional spin chains.

As a second highlight, in our studies of NaYbO₂ we have shown that this material system realizes an ideal triangular lattice of $J_{\text{eff}}=1/2$ moments with minimal exchange disorder due to lattice defects. The spin system fails to order at temperatures as low as 20 mK, despite a strong exchange field of 10 K resolved in susceptibility measurements. The highly frustrated lattice of Yb-moments instead forms a quantum disordered ground state with properties suggestive of a Dirac quantum spin liquid, and equally intriguingly, the spin system can be driven into a fluctuation-stabilized, collinear ordered antiferromagnetic state under modest magnetic field strengths (see. Fig. 3) [c]. We propose that the interlayer frustration inherent to this lattice type prevents long-range 120° order at zero field and is quickly lifted under the application of a magnetic field, resulting in the formation of the canonical *up-up-down* state for a triangular lattice. Our results establish this material and related compounds as model systems for exploring the critical phase boundaries between quantum disordered (potentially spin liquid) states and long-range ordered states at experimentally accessible fields.

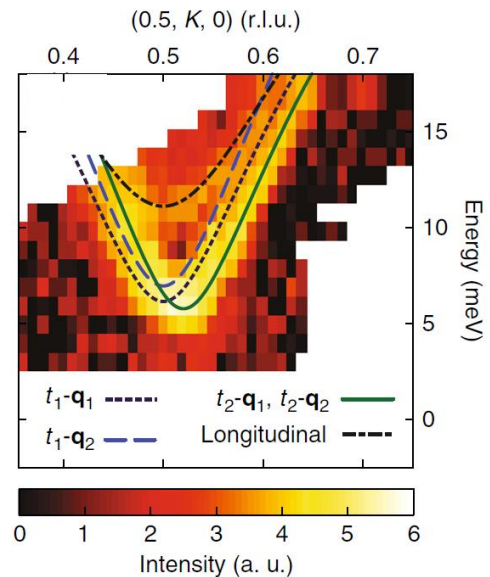


Fig. 2: Spin wave spectrum of NaMnO₂. Four 1D transverse magnon modes from twin domains are apparent with a 6 meV zone center gap at (0.5, 0.5, 0); however above this energy, at 11 meV, a longitudinally polarized mode appears consisting of a two-magnon bound state.

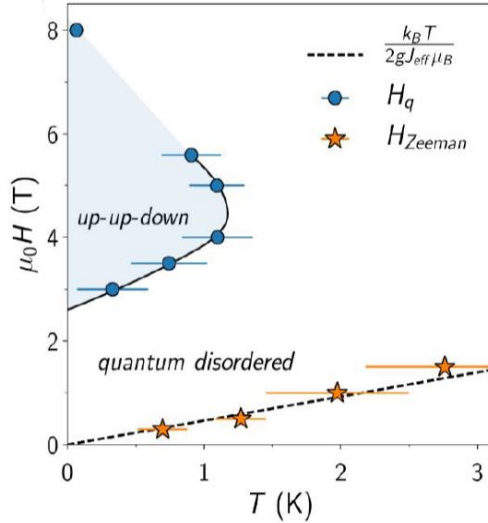


Fig. 3: Temperature and magnetic field phase diagram of NaYbO₂. The zero field quantum disordered state's underlying frustration is lifted under applied field to form an up-up-down collinear state. H_q points denote the boundary between disordered and the up-up-down state and H_{Zeeman} marks the fields above which free Yb moments are quenched.

Future Plans

The project is continuing to develop new materials platforms for exploring the unusual magnetic ground state manifest on the triangular lattice of magnetic ions with active orbital degrees of freedom. In the coming year, we are developing crystals of $4d$ transition metal variants of these compounds such as NaRuO₂ as well as other variants with rare-earth metal sites. Single crystal growth of these systems will be the focus of our materials efforts using high pressure floating zone techniques.

Neutron scattering efforts will focus on further exploring the unusual magnon-magnon interactions inherent to NaMnO₂ as well as more deeply exploring the phase diagram and critical phase boundaries of NaYbO₂ in Fig. 3. As new single crystals become available, we will begin exploring both the static spin structures and spin dynamics in NaMO₂ variants with $M=\text{Ru}$ and $M=\text{Yb}$ in order to experimentally assess the presence of quantum spin liquid ground states predicted in both of these systems. Preliminary powder studies of many of these variants are already underway and will direct the single crystal-based efforts.

References

- [1] Itamar Kimchi and Ashvin Vishwanath. "Kitaev-Heisenberg models for iridates on the triangular, hyperkagome, kagome, fcc, and pyrochlore lattices." *Physical Review B* 89, 014414 (2014).
- [2] Yao-Dong Li, Xiaoqun Wang, and Gang Chen. "Anisotropic spin model of strong spin-orbit-coupled triangular antiferromagnets." *Physical Review B* 94, 035107, (2016).
- [3] G. Jackeli, and D. A. Ivanov. "Dimer phases in quantum antiferromagnets with orbital degeneracy." *Physical Review B* 76, 132407 (2007).

Publications

- [a] Rebecca L. Dally, Robin Chisnell, Leland Harriger, Yaohua Liu, Jeffrey W. Lynn, and Stephen D. Wilson, "Thermal evolution of quasi-one-dimensional spin correlations within the

anisotropic triangular lattice of α - NaMnO_2 " *Physical Review B* 98, 144444 (2018). [DOI: 10.1103/PhysRevB.98.144444]

[b] R. L. Dally, Y. Zhao, Z. Xu, R. Chisnell, M. B. Stone, J. W. Lynn, L. Balents, and Stephen D. Wilson, "Amplitude mode in the planar triangular antiferromagnet $\text{Na}_{0.9}\text{MnO}_2$ ", *Nature Communications*, 9, 2188 (2018). [DOI: 10.1038/s41467-018-04601-1]

[c] Mitchell Bordelon, Chunxiao Liu, Eric Kenney, Tom Hogan, Lorenzo Posthuma, Marzieh Kavand, Yuanqi Lyu, Mark Sherwin, N. P. Butch, Craig Brown, M. J. Graf, Leon Balents, Stephen D. Wilson, "Field-tunable quantum disordered ground state in the triangular lattice antiferromagnet NaYbO_2 " arXiv:1901.09408

Searching for the Universality of Collective Excitations in Liquids at and away from Equilibrium

Yang Zhang, Department of Nuclear, Plasma, and Radiological Engineering, Department of Materials Science and Engineering, Department of Electrical and Computer Engineering, Beckman Institute for Advanced Science and Technology, University of Illinois at Urbana-Champaign

Program Scope

Liquids, ubiquitous on earth, are prototypical disordered condensed matter. However, the physics of liquids is far from being completely understood. As the intermediate phase between non-structured gases and ordered solids, liquids and liquid-like matter possess the complexities absent on either extreme counter phase, especially when driven out of equilibrium. Many anomalous properties of liquids present fundamental challenges to our current understanding of condensed matter. Furthermore, numerous soft and biological materials of amazing far-from-equilibrium complexity seem to share many intriguing features of liquids. Therefore, quantitative descriptions of the structure and dynamics of liquids at and away from equilibrium will likely impact a wide range of disciplines in physics, chemistry, and materials science and engineering. Our research activities center around the searching for the universality of liquid dynamics (including metallic, molecular, and network liquids), both at and away from equilibrium, using integrated quasi-elastic and inelastic neutron scattering experimental probes and atomistic theory, computation, and simulation. The focus of the last two years was on studying the collective excitations in liquids and glasses.

Recent Progress

1. We developed a ViscoElastic Hydrodynamic (VEH) theory to describe the collective excitations of liquids characterized by the coherent dynamic structure factor. [1]

Recent experimental and computational studies of the collective modes in liquids suggested that transverse acoustic excitations not only exist in liquids but also contribute to the density fluctuations characterized by the dynamic structure factor. However, the classical hydrodynamic theory, which is only valid in long wavelengths and low frequencies, fails to explain these observations. Herein, we extend the hydrodynamic theory by incorporating viscoelasticity and anisotropy, as a result of breaking continuous symmetry at short distances. Consequently, transverse acoustic excitations emerge from the viscoelasticity of liquids, and deviation from isotropic symmetry causes a coupling mechanism between the longitudinal and transverse modes, which altogether contribute to the density fluctuations. This approach not only provides an inverse method to examine the density and current correlation functions in liquids beyond the hydrodynamic regime but also serves as a generalized hydrodynamic theory for viscoelastic materials.

2. We detected and confirmed the microheterogeneity in highly concentrated nonaqueous electrolyte solutions using QENS as the microscopic mechanism of enhanced viscosity. [3] We also parametrized a new MD force field for the complex electrolyte solutions by benchmarking both NPDF and diffusion coefficient. [2]

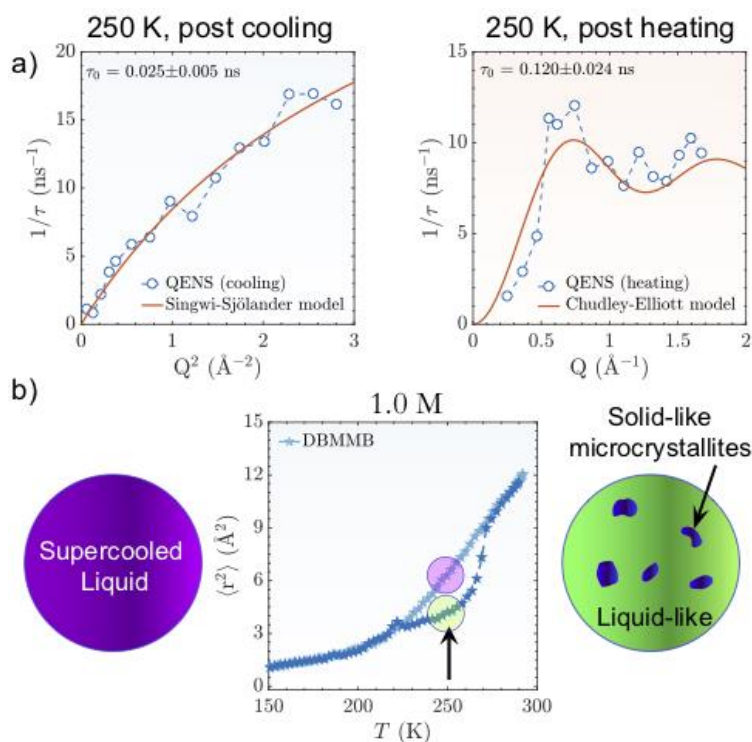


Figure 1. (a) 1.0 M DBMMB at 250 K follows the Singwi–Sjölander jump diffusion model after cooling, suggesting a more homogeneous phase, and (b) the Chudley–Elliott jump diffusion model after heating, suggesting mixed solid-like microcrystalline and liquid-like domains; (c) cartoon denoting these regimes. [3]

fluid phases. Our findings indicate molecular clustering and point to solvation inhomogeneities and molecular crowding in these concentrated fluids.

3. We systematically studied the spatial and thermal signatures of α and β relaxations in glassy and glacial aliphatic ionic liquids using QENS. [4]

The competition between Coulomb and van der Waals interactions brings forth unique dynamic features and broad applications to ionic liquids. Herein, we present a combined calorimetric, X-ray diffraction, incoherent elastic and quasi-elastic neutron scattering study, over a wide temperature range (180 – 340 K), of the relaxational dynamics of the liquid, supercooled liquid, crystalline, glassy, and glacial states of two model ionic liquids: tributylmethylammonium (a good glass-former) and butyltrimethylammonium (a good crystal-former) cations and the bis(trifluoromethanesulfonyl)imide anion. In both systems, we observed two distinct relaxation processes. The Q-dependence of the respective relaxation time shows that the α -process is diffusive, while the β -process is modulated by the structure of the liquids.

4. We developed a parallel and extendable C++ numerical library – *LiquidLib* <http://z-laboratory.github.io/LiquidLib/> for computing the statistical quantities of liquids and liquid-like systems from classical and *ab initio* molecular dynamics trajectories, which can be directly compared with neutron scattering experiments. [8]

The development of models to describe structure and dynamics of nonaqueous electrolyte solutions is challenging, and experimental observations are needed to form a foundation. Here, neutron scattering is used to probe molecular dynamics in nonaqueous organic electrolytes. Two solutions were compared: one contained symmetrical electrolyte molecules prone to crystallize, and one contained desymmetrized electrolyte molecules preferring disordered states. For the latter, calorimetry and neutron data show that a disordered fluid persists to very low temperatures at high concentrations. Upon heating, localized cold crystallization occurs, leading to burst nucleation of microcrystalline solids within

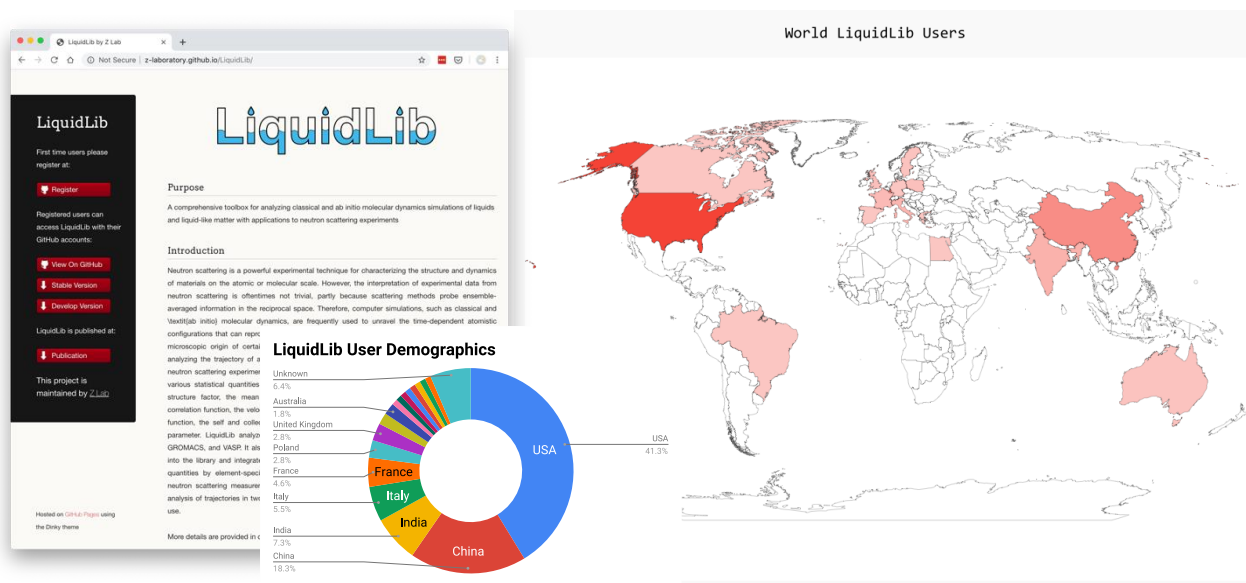


Figure 2. A snapshot of the website of *LiquidLib*, and the user demographics.

Often to understand the results of neutron scattering experiments, computer simulations, including classical and *ab initio* molecular dynamics (MD), are used to compare to the experiments. *LiquidLib* is a post-processing package for computing the statistical quantities of liquids and liquid-like systems from classical and *ab initio* MD trajectories. *LiquidLib* allows computation of various statistical quantities relevant to neutron scattering measurements. New quantities can easily be integrated into the library. *LiquidLib* can read MD trajectories of LAMMPS, GROMACS, and VASP. *LiquidLib* also offers an easy platform to extend the program to be able to read simulation trajectories organized in other file formats not included or from other packages. Incorporation of materials' neutron scattering lengths to weight the quantities' computations provides results comparable to neutron scattering measurements. Lastly, *LiquidLib* is dimensionally independent, which allows for trajectories in higher dimensions to be analyzed. Up to date, *LiquidLib* has ~170 users worldwide.

Future Plans

We will perform systematic studies of the collective dynamics (phonon-like excitations and collective diffusions) of three types of liquids with representative interactions (metallic, van der Waals, and ionic) and with different fragilities (fragile vs strong), using synergistically integrated coherent Inelastic Neutron Scattering (INS) experiments, a ViscoElastic Hydrodynamics theory we have been developing, and Molecular Dynamics (MD) simulations and analysis using our statistical analysis package *LiquidLib*®. We will combine several high-resolution time-of-flight spectrometers recently built at the new generation of high-flux neutron sources (as well as advanced X-ray spectrometers) to cover a wide dynamic range and wave vector transfer range. We will use newly-built containerless levitators (along with traditional sample holders) to reduce surface effect and undesired background signals. For hydrogen-containing liquids, we will use deuterated samples and further use neutron polarization analysis to suppress/separate the incoherent scattering. We will use MD simulations to achieve robust interpretations of the experimental results and gain deeper insights from computed physical quantities otherwise inaccessible by experiments. Inspired by the experimental data and simulations, we will continue developing the ViscoElastic Hydrodynamic theory to provide a universal framework to analyze

the inelastic scattering data and understand the fundamental excitations and collective dynamics in liquids. We will maintain and further develop the functions and usability of *LiquidLib*.

Publications (2017.01 – 2019.05)

- [1] Z. Cai, **Y Z***, “A viscoelastic hydrodynamic theory of the transverse acoustic excitations in liquids”, *Phys. Rev. Lett.* (submitted)
- [2] Z. Li, L. A. Robertson, I. A. Shkrob, J. C. Neufeind, K. C. Smith, L. Zhang, J. S. Moore, and **Y Z***, “When dynamics matters: insufficiency of structure matching for development of realistic force fields for nonaqueous electrolytes”, *J. Phys. Chem. Lett.* (submitted)
- [3] L. A. Robertson, Z. Li, Y. Cao, I. A. Shkrob, M. Tyagi, K. C. Smith, L. Zhang, J. S. Moore, and **Y Z***, “Observation of Microheterogeneity in Highly Concentrated Nonaqueous Electrolyte Solutions”, *J. Am. Chem. Soc.* 141(20), 8041 (2019)
- [4] T. A. Lima, Z. Li, M. Tyagi, M. C.C. Ribeiro, **Y Z***, “Spatial and thermal signatures of α and β relaxations in glassy and glacial aliphatic ionic liquids”, *J. Chem. Phys.* 150, 144506 (2019)
- [5] R. Ashkar, ..., **Y. Zhang**, J. C. Smith, “Neutron scattering in the biological sciences: progress and prospects”, *Acta Cryst.* D74, 1129 (2018).
- [6] T. P. Moneypenny II, A. Yang, N. P. Walter, T. J. Woods, D. L. Gray, **Y. Zhang**, J. S. Moore, “Product distribution from precursor bite angle variation in multitopic alkyne metathesis: evidence for a putative kinetic bottleneck”, *J. Am. Chem. Soc.* 140(17), 5825 (2018)
- [7] Z. Cai, **Y. Zhang***, “Hydrophobicity-driven thermal unfolding of Trp-cage encapsulated between graphene sheets”, *Colloids Surf. B* 168, 103 (2018)
- [8] N. P. Walter, A. Jaiswal, Z. Cai, **Y. Zhang***, “*LiquidLib*: A comprehensive toolbox for analyzing classical and *ab initio* molecular dynamics simulations of liquids and liquid-like matter with applications to neutron scattering experiments”, *Comput. Phys. Commun.* 228, 209 (2018)
- [9] T. P. Moneypenny II, N. P. Walter, Z. Cai, Y.-R. Miao, D. L. Gray, J. J. Hinman, S. Lee, **Y. Zhang***, J. S. Moore, “Impact of shape persistence on the porosity of molecular cages”, *J. Am. Chem. Soc.* 139(8), 3259 (2017)
- [10] Z. Cai, “A Viscoelastic Hydrodynamic Approach to The Density Fluctuations in Simple Liquids”, Ph.D. thesis, August 2019.
- [11] N. P. Walter, “Studies of Long Timescale Phenomena with Energy Landscape Sampling Methods”, M.S. thesis, August 2019.
- [12] Y. Zhai, “Molecular Dynamics and Neutron Scattering Studies of Surface Dynamics and Dynamic Heterogeneity of Supercooled Metallic Liquid”, M.S. thesis, August 2019
- [13] Z. Li, “Molecular Dynamics Simulation and Neutron Scattering Studies of Nonaqueous Electrolyte Solutions”, M.S. thesis, August 2018

***Poster
Abstracts***

Investigation of Short-Range Ordering in Transition Metal Compounds by Diffuse Scattering

Jared M. Allred, The Department of Chemistry and Biochemistry, The University of Alabama

Program Scope

For one half of the program, we are studying the structural instability component of the metal to insulator transition (MIT) in rutile VO_2 , especially focusing on effects that doping can cause on the local structure. X-ray and neutron total scattering experiments are used to measure both Bragg and diffuse scattering, and the resulting scattering data is analyzed through various methods, including 3D- Δ PDF. Further, we use isotropic group-subgroup relations to interpret the data, and to develop methods for modelling the distortions. We are also extending the same methods to study other systems that are known to or may exhibit structural distortions. This includes materials discovery related to the ZrMnSi_2 phase diagram, and the relationship between superconductivity and the structural distortion in condensed Chevrel phases $A_nM_6X_6$ ($n=2,4$; $M=\text{Cr,Mo}$, $X=\text{As, S, Se, Te}$).

Recent Progress

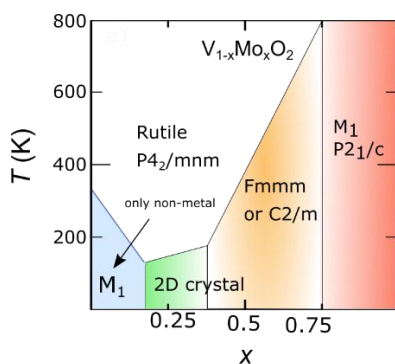


Figure 1: New $\text{V}_{1-x}\text{Mo}_x\text{O}_2$ phase diagram determined from this program

At the beginning of this program, we already had found a way to synthesize single crystals of $\text{V}_{1-x}\text{Mo}_x\text{O}_2$ with $x < 0.4$ using chemical vapor transport (CVT) and TeCl_4 as a transport agent, but were unable to go higher due to the formation of by-products such as $\text{Mo}_{12}\text{O}_{29}$ and $\text{TeMo}_5\text{O}_{16}$. During this period we found a way to grow crystals with $x > 0.4$ using a two-step synthesis. Very small crystals are grown first grown using MoCl_3 first, and then TeCl_4 is used to grow large, rod-like crystals in the second step. This process helps suppress the extra volatility of Mo, and allows the synthesis of crystals at any x .

X-ray total scattering experiments on $\text{V}_{1-x}\text{Mo}_x\text{O}_2$ ($0 < x < 0.65$) showed a complex structural landscape. Four phase regions, shown in Figure 1 were determined. From left to right, they are I) From $0 < x < 0.19$ the standard MIT and structural transition from rutile (R) to the monoclinic MoO_2 -type structure (M_1) is observed. II) From $0.19 < x < \sim 0.40$ a very unusual rutile-derived phase shows long-ranged structural distortions in 2D, with extremely short correlations in the third axis. III) Between $x = 0.4$ and ~ 0.8 , a new phase is formed that seems to have a monoclinic structure that is a compromise

between the 2D phase and another monoclinic phase (M_2). IV) Above $x = \sim 0.8$, the standard MoO_2 (M_1) structure is formed again.

The special ordering observed in region II is shown in Figure 2. We have modelled both the diffuse scattering and the 3D- Δ PDF, and determined that the structure exactly follows a recent theoretical model¹, which is a two component Ising-type model based on long-range electron-lattice coupling that is also geometrically frustrated. This model is generalized to all rutile phases. Thus, the findings make a significant contribution to our understanding of the structural instability of VO_2 , which is at the heart of the MIT. This will be among the first structure solutions using 3D- Δ PDF and x-ray total scattering ever reported.

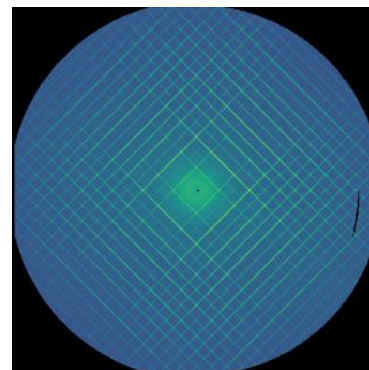


Figure 2: Total x-ray scattering of the $l = 1/2$ plane in $\text{V}_{0.81}\text{Mo}_{0.19}\text{O}_2$.

The phase found in region III appears superficially to be some kind of unknown tetragonal phase, but using advanced single crystal structure solution methods, we have been able to show that it is likely monoclinic that is mimicking higher symmetry. We were then able to solve its crystal structure.

We have extended our developed new CVT methods for synthesizing VO_2 doped with Cr, Nb, and W. Nb is particularly challenging, chemically, though it seems to form new rutile distortions that have not been reported. Also, the process we also serendipitously synthesized single crystals of a new mixed Nb,V oxide, $\text{V}_7\text{Nb}_6\text{O}_{29}$. It exhibits partial site ordering (it is actually $\text{V}_5(\text{V}_{0.15}\text{Nb}_{0.85})_4(\text{V}_{0.35}\text{Nb}_{0.65})_4\text{O}_{29}$) with site occupancy seeming to match a full $\text{V}^{4+}, \text{Nb}^{5+}$ stoichiometry. Moreover, our best model is in the $P4$ spacegroup, and appears to be ferroelectric in structure. No bulk property measurements have verified this.

We have synthesized many phases in the 3 subtypes of the TiMnSi_2 family. We have uncovered evidence of magnetic ordering in ZrMnSi_2 , while ZrMnGe_2 , ZrCrGe_2 , and ZrFeGe_2 , ZrRuGe_2 all seems to only exhibit weak Curie-Weiß-like interactions without any ordering. We have also managed to synthesize a few new phases with this crystal symmetry that have not been reported yet, although they have not been synthesized in phase pure form: TiCrSi_2 , $\text{ZrCr}_{0.67}\text{Mn}_{0.33}\text{Ge}_2$, $\text{ZrCr}_{0.5}\text{Mn}_{0.5}\text{Ge}_2$, and $\text{ZrMnGe}_{1.6}\text{Al}_{0.4}$. These include the first quaternary phases reported with this structure, and the latter is the first compound with this structure type containing a group 13 element.

We accidentally learned how to grow crystals of β - ZrSi from a Zr-Mn-Si melt, and in the process found that the reported structure is incorrect. We now have an improved crystal structure for this compound.

Future Plans

X-ray total scattering experiments are planned on Cr, W, and Nb doped VO₂, in order to extend our model for the structural instability to these phases. While more literature exists on these materials than the Mo-doped phase, we now have reason to believe some findings are incorrect.

Neutron total scattering experiments are planned on Corelli at the SNS to determine which correlations in V_{0.81}Mo_{0.19}O₂ are dynamic, and which are static. This will also give information on any special Mo site ordering or size effects, as neutrons are not sensitive to V.

Inelastic Neutron scattering experiments were already proposed and accepted on HFIR HB-3 to search for evidence of incipient magnetism in Rb₂Mo₆Se₆ and In₂Mo₆Se₆, and then specifically compare them to the superconductors K₄Mo₆As₆ and K₄Cr₆As₆.

Standard powder neutron diffraction is planned at HB-2A or POWGEN on ZrMnSi₂ and related phases in order to determine their magnetic structure at low-T.

References

- 1) T. Lovorn and S. Sarker, Phys. Rev. Lett, **119**, 045501 (2017)

Publications

N/A

Characterizing magnetic quantum materials by neutron scattering

Huibo Cao

Neutron Scattering Division, Oak Ridge National Laboratory

Program Scope

Understanding the interactions leading to magnetic quantum phenomena in a wide range of quantum materials is extremely important for development of new quantum materials and future technologies. Quantifying these interactions in materials that potentially exhibit exotic states such as quantum spin liquids, topological insulators, and Weyl semimetals, are currently being limited by a range of challenges including the lack of sizable crystals, limited sample environment conditions, and the ability to disentangle the intrinsic quantum phenomena versus effects from defects and site-disorder. This project is to use and develop neutron scattering techniques, especially polarized neutron scattering, for characterizing magnetic quantum materials. In this presentation, I will introduce our neutron scattering studies on the multifunctional and quantum candidate materials and recent development of neutron scattering techniques in the first year of the project.

Recent Progress

In the first year of the award project, we have made progress on searching/characterizing quantum materials and developing neutron scattering techniques including polarizing neutrons and data analysis software, high pressure, ultra-low temperature, cryomagnetic field. Two initial polarized neutron diffraction experiments have been performed with the available and newly developed polarizers. The one was on a single-molecular magnet and the other one was on a “quantum” paraelectric system EuTiO_3 . The strategy of the data collection was established, the data reduction was optimized with a smart peak integration program, the analysis software was tested with the measured data, further development is under way. High pressure studies on field-sensitive and strain-sensitive magnetoelectric systems introduce two new areas in the field of multifunctional materials. We are also working on exploring magnetic topological and quantum materials by neutron scattering to achieve the goal of the project. Besides the science progress, we get ready for commissioning the upgraded instrument, DEMAND (Dimensional Extreme Magnetic Neutron Diffractometer) at the High Flux Isotope Reactor (HFIR) at ORNL, which was called as Four-circle diffractometer before the upgrade. New capabilities of extreme sample environment conditions (ultra-low temperature, high magnetic field, high pressure) and polarized neutron diffraction are designed for exploring and charactering quantum materials. The details of the project progress are introduced as follows.

Multifunctional systems: Magnetism driven ferroelectricity, called as type-ii multiferroic, has been one of central topics for decades due to fundamental science interests and technology application potentials. Although many magnetoelectric materials have been discovered and studied, some mechanisms of strong spin-lattice coupling are still under debate, such as magnetic “quantum” paraelectric EuTiO_3 , also the quest for multiferroics toward application is not satisfying due to lacking high magnetoelectric coupling materials. We selected three types of systems and have made some progress on each direction. One is that we discovered a ferroelectric reentrance behavior in a strain sensitive multiferroic $(\text{NH}_4)_2[\text{FeCl}_5 \cdot \text{H}_2\text{O}]$, which is likely caused by quantum fluctuation and leads to a ferroelectric criticality (Figure 1). The other one is on a hexaferrite, a field sensitive multiferroic system. In this system we have achieved a record high magnetoelectric coupling in single phase materials and a possible near-room-temperature ferrimagnetic ferroelectric phase that can be mutually controlled by electric or magnetic field (Figure 2). The last one is on EuTiO_3 , besides the detailed inelastic neutron scattering measurements we have carried out for understanding phonon and spin wave excitations, we employed polarized neutron diffraction to visualize spin density distribution in 3-dimensional space for fully understanding how spin-spin and spin-lattice interactions lead to strong magnetoelectric effect and abnormal phonon instability (Figure 3).

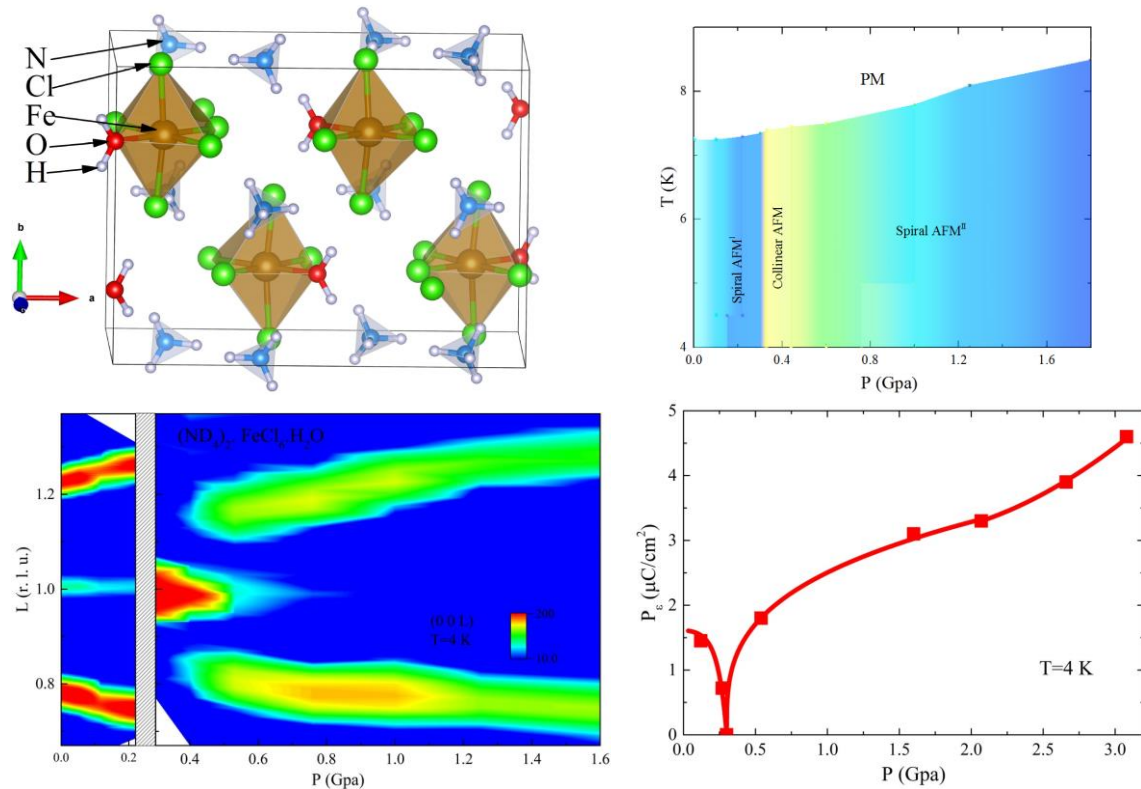


Figure 1 Strain sensitive multiferroic $(\text{NH}_4)_2[\text{FeCl}_5 \cdot \text{H}_2\text{O}]$. Top: crystal structure and temperature-pressure phase diagram. The collinear non-ferroelectric antiferromagnetic (AFM) phase occurs between two spiral-AFM ferroelectric phase, i.e. the pressure driven ferroelectric reentrance, which is observed for the first time in multiferroic systems. Bottom: neutron diffraction scan along the reciprocal L-direction and spontaneous polarization versus pressure. A critical region without ferroelectric order is induced by pressure, likely caused by enhanced fluctuation when there appears a strength crossover of neighbor magnetic interactions.

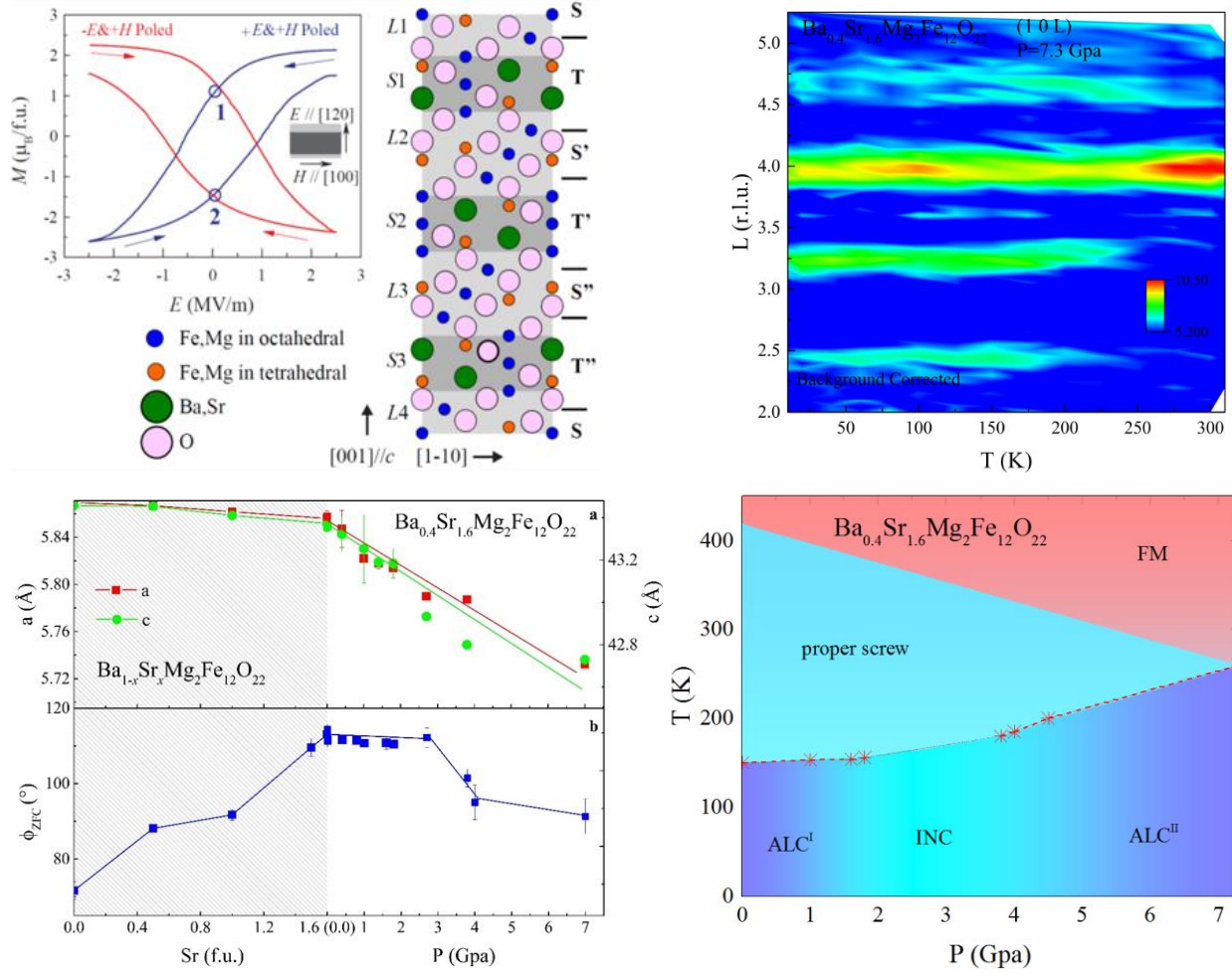


Figure 2 Field sensitive magnetoelectric hexaferrite $Ba_{0.4}Sr_{1.6}Mg_2Fe_{12}O_{22}$. Top left: crystal Structure and electric field-controlled magnetism [1]. Top right: contour plot of temperature dependent neutron diffraction scan along the reciprocal L -direction at 7.3 GPa with the diamond anvil cell. Bottom left: pressure dependence of lattice parameters and spin turning angle of spiral magnetic structure. Bottom right: temperature-pressure phase diagram.

Magnetic quantum matter: quantum matter has become a rapidly developing field for high importance in both fundamental science and future quantum technologies. searching/designing quantum materials by neutron scattering is one of major driving forces of this award project. Due to unexpected extension of the reactor outage at the HFIR, we spent extra efforts for searching high potential quantum material candidates using other available techniques including bulk measurements (especially bulk magnetic susceptibility), x-ray, neutron diffuse scattering and inelastic neutron scattering at the Spallation Neutron Source (SNS) at the ORNL. Published and submitted papers include quantum spin liquid candidates $YbCl_3$ and $Ce_2Zr_2O_7$, topological magnets $EuSn_2P_2$ and $MnBi_4Te_7$. These materials were selected for further studies by polarized neutron diffraction and the Local Site Magnetic Susceptibility method in the following years.

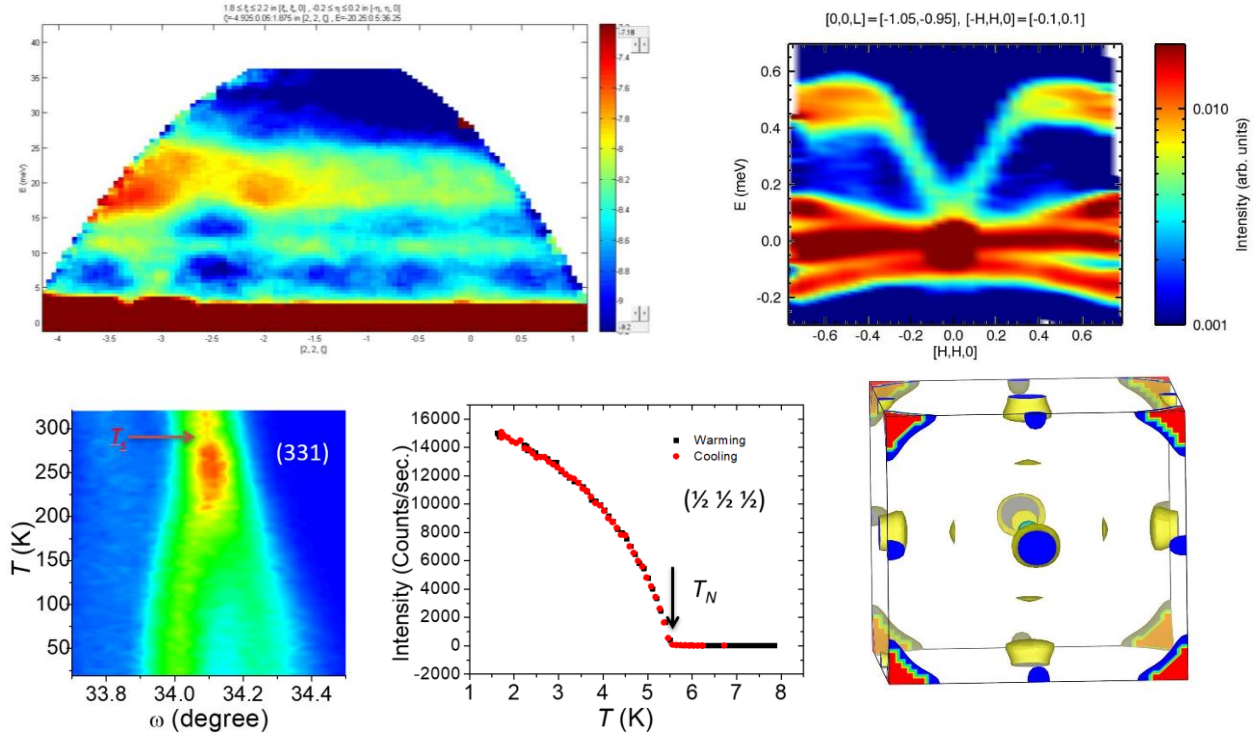


Figure 3 Magnetic “quantum” paraelectric EuTiO_3 . Top: phonon dispersion and spin wave excitation in the $[HHL]$ scattering plane. Bottom left: structural transition shown by temperature dependence of rocking curve scan at $(3\ 3\ 1)$ Bragg peak. Bottom middle: antiferromagnetic transition shown by temperature dependent peak intensity at $(\frac{1}{2}\ \frac{1}{2}\ \frac{1}{2})$. Bottom right: 3-dimensional spin density map analyzed from the preliminary polarized neutron diffraction data with the drop-in He-3 cell at the DEMAND at the HFIR.

Future Plans

Besides publishing the current results, we will continue developing polarized neutron diffraction and the Local Site Magnetic Susceptibility method mainly on the DEMAND and apply them on the proposed and new quantum matter candidates (EuTiO_3 , $(\text{ND}_4)_2\text{FeCl}_5(\text{D}_2\text{O})$, RuCl_3 , YbCl_3 , $\text{Yb}_2\text{Si}_2\text{O}_7$, $\text{Yb}_2\text{Ti}_2\text{O}_7$, $\text{Ce}_2\text{Zr}_2\text{O}_7$, $\text{Nd}_2\text{Ir}_2\text{O}_7$) and selected magnetic topological insulators. Magnetic interaction and crystal field parameters extracted from local magnetic susceptibilities will be used to characterize magnetic quantum matter together with inelastic neutron scattering and other spectroscopy techniques. Molecular magnetism is another science area requires polarized neutron diffraction and will be explored.

References

[1] Kun Zhai, Yan Wu, Shipeng Shen, Wei Tian, Huibo Cao, Yisheng Chai, Bryan C. Chakoumakos, Dashan Shang, Liqin Yan, Fangwei Wang, Young Sun, Giant magnetoelectric effects achieved by tuning spin cone symmetry in Y-type hexaferrites, *Nature Communications* **8** 519 (2017)

Publications

Huibo Cao, Bryan C. Chakoumakos, Katie M. Andrews, Yan Wu, Richard A. Riedel, Jason Hodges, Wenduo Zhou, Ray Gregory, Bianca Haberl, Jamie Molaison, Gary W. Lynn, DEMAND, a Dimensional Extreme Magnetic Neutron Diffractometer at the High Flux Isotope Reactor, *Crystals*, **9**(1), 5 (2019). <https://doi.org/10.3390/cryst9010005>

Acknowledgments. — *The research using polarized neutron diffraction and high pressure is supported by the U.S. Department of Energy (DOE), Office of Science, Office of Basic Energy Sciences, Early Career Research Program Award KC0402010, under Contract DE-AC05-00OR22725. This research used resources at the High Flux Isotope Reactor, a DOE Office of Science User Facility operated by the Oak Ridge National Laboratory*

Xin Gui, Ivo Pletikosic, **Huibo Cao**, Hung-Ju Tien, Xitong Xu, Ruidan Zhong, Guangqiang Wang, Tay-Rong Chang, Shuang Jia, Tonica Valla, Weiwei Xie, Robert Cava, A new magnetic topological quantum material candidate by design, *ACS Central Science* **5**, 5, 900-910 (2019).

<https://doi.org/10.1021/acscentsci.9b00202>

Acknowledgments. — *The work at Princeton was supported by the ARO MURI on Topological Insulators, grant W911NF1210461. W.X. at LSU was supported by a Beckman Young Investigator award. X.G. at LSU is supported by the National Science Foundation under NSF-OIA-1832967. H.B.C. acknowledges support of US DOE BES Early Career Award KC0402010 under Contract DE-AC05-00OR22725. This research used resources at the High Flux Isotope Reactor, a DOE Office of Science User Facility operated by the Oak Ridge National Laboratory. This research also used resources of the National Synchrotron Light Source II, a U.S. Department of Energy (DOE) Office of Science User Facility operated for the DOE Office of Science by Brookhaven National Laboratory under Contract No. DE-SC0012704. IP thanks J. Jiang, E. Vescovo, and K. Kaznatcheev for their help with setting up the experiment at the 21-ID-1 (ESM-ARPES) beamline. T.-R.C. was supported from Young Scholar Fellowship Program by Ministry of Science and Technology (MOST) in Taiwan, under MOST Grant for the Columbus Program MOST107-2636-M-006-004, National Cheng Kung University, Taiwan, and National Center for Theoretical Sciences (NCTS), Taiwan. W.X. and X.G. thank D. Vineyard for helping with electron paramagnetic resonance measurement.*

Y. Song, **H.B. Cao**, B.C. Chakoumakos, Y. Zhao, A. Wang, H. Lei, C. Petrovic, R.J. Birgeneau, Intertwined magnetic and nematic orders in semiconducting $\text{KFe}_{0.8}\text{Ag}_{1.2}\text{Te}_2$, *Physical Review Letters*, **122**, 8, 087201 (2019). <https://doi.org/10.1103/PhysRevLett.122.087201>

Acknowledgments. — *The work at ORNL's HFIR was sponsored by the Scientific User Facilities Division, Office of Science, Basic Energy Sciences (BES), U.S. Department of*

Energy (DOE). H. B. C. acknowledges support of U.S. DOE BES Early Career Award No. KC0402010 under Contract No. DE-AC05-00OR22725. The work at Lawrence Berkeley National Laboratory was supported by the Office of Science, Office of BES, Materials Sciences and Engineering Division, of the U.S. DOE under Contract No. DE-AC02-05-CH11231 within the Quantum Materials Program (KC2202). The work at Brookhaven National Laboratory was supported by the U.S. DOE under Contract No. DE-SC0012704

Submitted

Jie Xing, **Huibo Cao**, Eve Emmanouilidou, Chaowei Hu, Jinyu Liu, David Graf, Arthur P. Ramirez, Gang Chen, and Ni Ni, Rare-earth Kitaev material candidate YbCl_3 , submitted to *Physical Review Letters* (2019) [arXiv:1903.03615](https://arxiv.org/abs/1903.03615)

***Acknowledgments.** — Work at UCLA was supported by NSF DMREF program under the award NSF DMREF project DMREF-1629457. Work at UCSC was supported by DOE grant DE-SC0017862. This research used resources at the High Flux Isotope Reactor, a DOE Office of Science User Facility operated by the Oak Ridge National Laboratory. Work at NHMFL, Tallahassee is supported by NSF through NSF/DMR-1644779 and the State of Florida. GC acknowledges the support by the ministry of science and technology of China with Grant from No. 2016YFA0301001 and 2016YFA0300500. HC acknowledges the support from US DOE BES Early Career Award KC0402010 under Contract DE-AC05-00OR22725.*

Bin Gao, Tong Chen, David W. Tam, Chien-Lung Huang, Kalyan Sasmal, Devashibhai T. Adroja, Feng Ye, **Huibo Cao**, Gabriele Sala, Matthew B. Stone, Christopher Baines, Joel A. T. Barker, Haoyu Hu, Jae-Ho Chung, Xianghan Xu, Sang-Wook Cheong, Manivannan Nallaiyan, Stefano Spagna, M. Brian Maple, Andriy H. Nevidomskyy, Emilia Morosan, Gang Chen, and Pengcheng Dai, Experimental signatures of a quantum spin liquid in effective spin $\frac{1}{2}$ $\text{Ce}_2\text{Zr}_2\text{O}_7$ pyrochlore, submitted to *Nature Physics*. (2019) arXiv:1901.10092

***Acknowledgments.** — The neutron scattering work at Rice is supported US DOE BES DE-SC0012311 (P.D.). The single crystal growth work at Rice is supported by the Robert A. Welch Foundation under Grant No. C-1839 (P.D.). E.M. and C.L.H. acknowledge support from US DOE BES DE-SC0019503. A.H.N. acknowledges support of the Robert A. Welch Foundation Grant No. C-1818 and NSF CAREER Grant No. DMR-1350237. Research at UCSD was supported by the US DOE BES DE-FG02-04ER46105 (M.B.M.). The work of J.H.C. was supported by the National Research Foundation of Korea (NRF2017K1A3A7A09016303). This research used resources at the Spallation Neutron Source and High Flux Isotope Reactor, DOE Office of Science User Facilities operated by the ORNL. H.B.C. acknowledges support of US DOE BES Early Career Award KC0402010 under Contract DE-AC05-00OR22725. Crystal growth by B.G., X.X., and*

S.W.C. at Rutgers was supported by the visitor program at the center for Quantum Materials Synthesis (cQMS), funded by the Gordon and Betty Moore Foundation's EPiQS initiative through grant GBMF6402, and by Rutgers University. G.C. acknowledges support from the Ministry of Science and Technology of China with the Grant No. 2016YFA0301001 and 2016YFA0300500.

Chaowei Hu, Xiaoqing Zhou, Pengfei Liu, Jinyu Liu, Peipei Hao, Eve Emmanouilidou, Hongyi Sun, Yuntian Liu, Harlan Brawer, Arthur P. Ramirez, **Huibo Cao**, Qihang Liu, Dan Dessau, Ni Ni, A van der Waals antiferromagnetic topological insulator with weak interlayer magnetic coupling, submitted to *Nature Communications* (2019) [**arXiv:1905.02154**](https://arxiv.org/abs/1905.02154)

***Acknowledgments.** — We thank Paul C. Canfield, Dr. Quansheng Wu, Suyang Xu, Filip Ronning and Chris Regan for helpful discussions, and Chris Jozwiak and Roland Koch at the Advanced Light Source for experimental help. Work at UCLA, the University of Colorado and UCSC were supported by the U.S. Department of Energy (DOE), Office of Science, Office of Basic Energy Sciences under Award Number DE-SC0011978, DE-FG02-03ER46066 and DESC0017862, respectively. Work at SUSTech was supported by the NSFC under Grant No. 11874195. **HC acknowledges the support from US DOE BES Early Career Award KC0402010 under Contract DE-AC05-00OR22725.** This research used resources of the Advanced Light Source, which is a DOE Office of Science User Facility under contract no. DE-AC02-05CH11231.*

***In Operando* Neutron Diffraction Study of Phase Transitions in Si Electrode Morphologies Using a Novel Electrochemical Cell**

K. S. Ravi Chandran

Department of Metallurgical Engineering, University of Utah, SLC, UT 84112

Program Scope

The research focuses on the fundamental understanding of the phase transition and diffraction phenomena that occur in Si particle, Si nanowire and Si micro-columnar electrodes using an *in situ* cell that was developed in the previous project. Particle Si electrodes (micro- and nano-sized particles, nanowires created by CVD or etching) as well as Si columns with sizes ranging in size from mid-nano to micron scale and with varying wall and pore architectures are prepared for *in operando* experiments in Vulcan diffractometer at SNS, ORNL. Using the *in situ* electrochemical cell, the phase transitions and diffraction phenomena that occur during the reversible lithiation of Si are being investigated. The over-arching goal is to explore in detail the unexpected phenomena observed in our recent *in situ* experiments and develop a correlation to energy storage capacity of the electrodes. This will help to resolve many electrochemical limitations which are the stumbling blocks in the way to the realization of very high capacity energy storage Li-ion batteries. As in previous years, parts of this research will be done in collaboration with ORNL using neutron diffraction (Dr. Ke An)

The research also investigates the phase transitions in electrodes made of Si micro/nano particles, and their mixtures with conductive meso-C of various proportions. The experiments involve both Vulcan diffractometer and NOMAD diffractometer. The premise is that by understanding the particle size and composition effect, one can discover electrode microstructures that facilitate reversible phase transformations upon Li insertion and extraction in Si electrode. Going from micro-particles to nanoparticles is expected to vastly change the phase transition behavior of electrodes. The reduced dimensions in nanoparticles can (i) increase the rate of Li insertion and removal because diffusion scales as $t=L^2/D$ (L is diffusion length and D is diffusivity), (ii) enhance electron transport and phase transformation, (iii) provide high particle surface area/contact and (iv) better accommodate compositional extensions and volume changes during Li insertion. The research is planned for collaboration with NOMAD scientists at ORNL through beam time allocations.

Recent Progress

I. *In situ* cell for the study of phase transitions in microcolumnar Si (100) electrode using ND

The experimental approach uses the *in situ* electrochemical cell we designed and validated [1], which enables capturing of Rietveld-refinable neutron diffraction patterns in VULCAN neutron diffractometer, enabling the study of phase transitions in battery electrode materials. The cell was successfully demonstrated to track the phase transitions in standard small volume electrodes such as LiCoO₂/graphite. In the current work, the cell (Figure 1a & 1b) has been used to study the phase transitions in microcolumnar Si (100) electrodes. The cell containing microcolumnar Si (100) electrodes to be diffracted, is oriented at 45° (Figure 1c) to the VULCAN beam. This is

to enable Si (400) and Si (440)/(220) Bragg reflections to appear in the reflection bank and the transmission bank respectively. Some real time ND patterns collected during lithiation of Si are shown in Figure 2 and 3. The intensity of Si (400) (and also (440), (220), not shown here) can be seen to be increasing continuously, whereas that of Cu (200), acting as a standard, remains the same. The intensity development in ND is in contrast to XRD, which showed combined peak broadening and intensity decrease due to amorphization in, or phase transition of, Si.

Specifically, we are currently investigating if the increase in Si (hkl) intensity is due to mosaicity induced in Si (100) during lithiation. During lithiation, as Li diffuses in Si (100) along $\langle 110 \rangle$ direction, the Si-Si bonds across $\{111\}$ planes will be broken [2]. As a result, micro-cracks could form parallel to $\{111\}$ planes, causing the collapse of $\{111\}$ planes, possibly resulting in mosaicity.

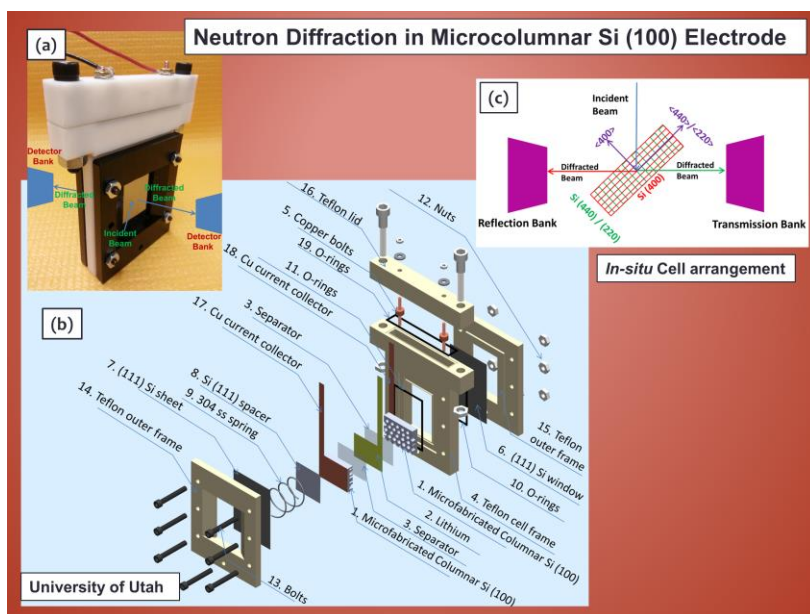


Figure 1(a) Photograph of the *in-situ* cell in the assembled form, (b) exploded view of the designed *in-situ* electrochemical cell, with Si (111) as casing, for ND studies with microcolumnar Si (100) electrodes and (c) *in-situ* cell at VULCAN diffractometer in Spallation Neutron Source, ORNL. In the preliminary experiments, the *in-situ* electrochemical cell was arranged such that the Si (100) electrode makes an angle of 44° with the incident beam (Figure 1(c)) in Vulcan diffractometer. As a result (400) and (440)/(220) planes in Si electrode were Bragg diffracted into the reflection bank and transmission bank, respectively.

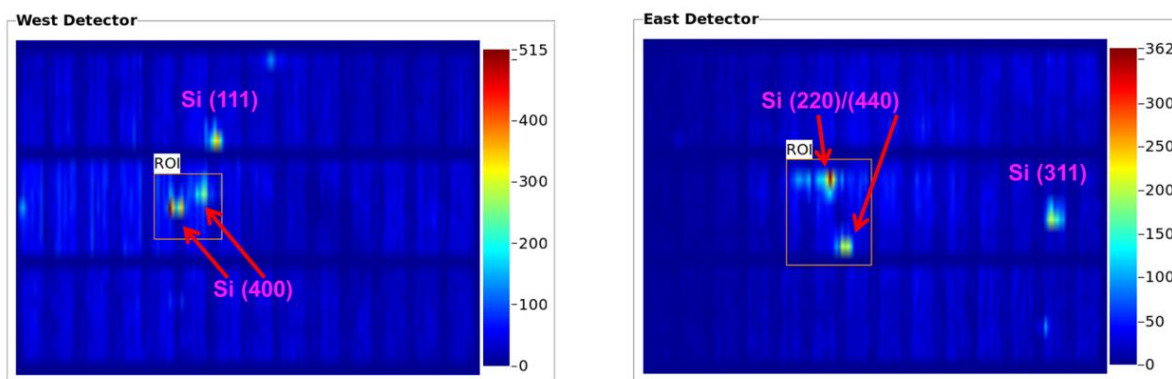


Figure 2. Diffraction signatures, during lithiation of PSI Si electrode, in east and west detectors in Vulcan.

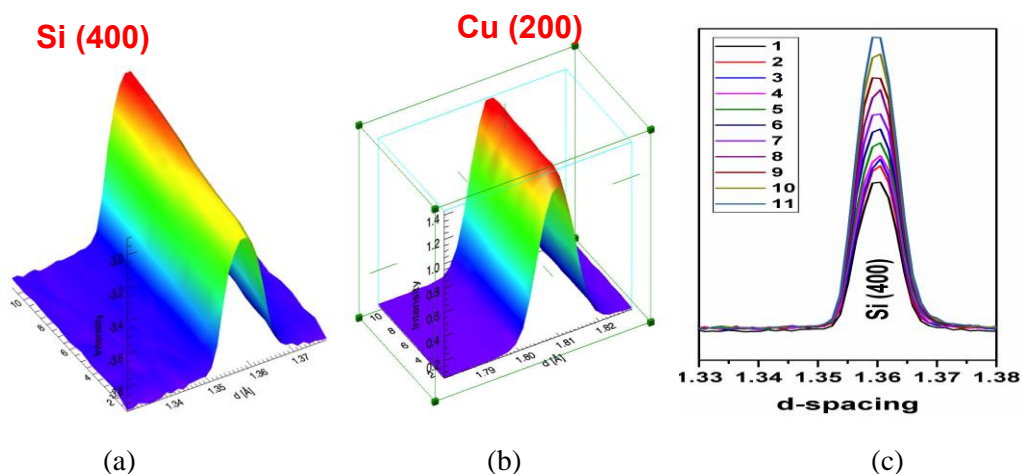
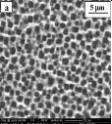
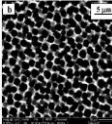
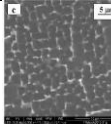
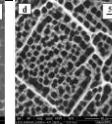


Figure 3. *In-situ* neutron data (extracted from the binned data) collected during the first lithiation cycle of PS1 Si, (a) the continuous change in Si(400) peak during lithiation; (b) showing Cu (200) peaks that do not change. (c) is a 2D plot of (a) showing an increase in intensity of Si (400), without a peak shift.

The diffraction signatures recorded in the east and west detectors are shown in Figure 2. The real time ND patterns collected during the 1st lithiation cycle of Si (100) electrode are shown in Figure 3. It can be seen that the intensities of the Si (400) reflections increase dramatically (Figure 3(a)). A similar pattern was observed for Si(220), but is not shown here. The intensity of Si(400) (and also that of Si(220)) reflection were found to nearly double towards end of lithiation (Figure 3(c)). Surprisingly, the d-spacing and FWHM of the (400) and (220) Si reflections remained the same through delithiation/lithiation. The intensity of the Cu (200) reflection (Figure 3(b)) in both the banks remained the same, which serves as a reference, indicating that the changes in intensities of (400) and (220) Si reflections are real and happened due to lithiation cycle in the *in situ* cell. This demonstrated the feasibility of in operando ND experiments. The question of if these are due to mosaic structure formation due to bond breaking [2] is being investigated.

II. Progress on the optimization of columnar Si electrodes for in operando neutron diffraction:

Our group have identified four different Si columnar structures (table below), which has different structural parameters and steady state cycling capacities. All the four structures have been cycled to 20 cycles in the preliminary evaluation. These samples were obtained from the optimization of experiments, which we have been performed and repeated over a period of five months. It can be

Sample	PS1	PS2	PS3	PS4
Average pore diameter(μm)	1	1.3	2	1
Average etched depth(μm)	8	7	9	8
Pore Fraction	0.52	0.63	0.75	0.49
Microstructure				
Average Capacity (mAh/g)	1500	1000	100	600

seen that the morphology of Si columns significantly impacts the total capacity. One of our primary objectives is to determine if any of these structures undergo mosaic pattern behavior, which may have a direct relation to the steady state capacity and cyclic performance of the battery.

III. Progress on the synthesis and in-situ cell Construction for PDF Analysis of nanocrystalline Si during lithiation/delithiation:

We have submitted a beam line proposal for neutron diffraction and PDF analysis of phase and local structure evolution during lithiation of nanoscale Si particle electrodes for Li-ion Batteries, using NOMAD diffractometer at SNS, Oak Ridge National Laboratory. In our recent work, it has been found that crystalline Si gets amorphized into Li_ySi phase during the first lithiation process. The amorphous Li_ySi phase is found to crystallize into $\text{Li}_{15}\text{Si}_4$ as the electrode approaches its maximum capacity. The voltage vs. capacity plot from our work, with the Si nanoparticle electrode, is shown in Figure 4.

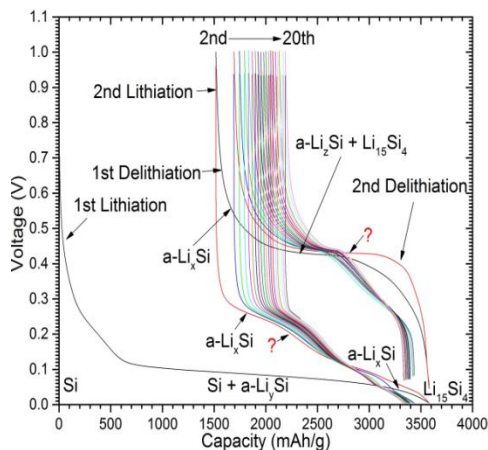


Figure 4: Voltage vs. Capacity plot of charge/discharge



Figure 5: XRD patterns after different cycles

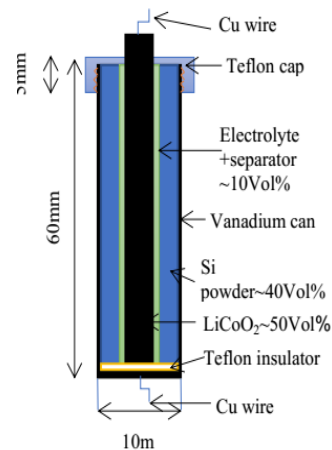


Figure 6 Si-LiCoO₂ cell

The XRD indicated that there is no presence of crystalline Si at both the plateaus from (Figure 5). Due to the inefficient scattering of Li phases by X-rays more detailed information is difficult to obtain. Hence we will perform these experiments, using the cell shown in Figure 6, under neutron diffraction to identify the diffracting phases.

Future Plans

The presence of mosaicity in crystal structure will be investigated in detail by studying the transmitted beam using the additional detector in Vulcan. Additionally, the effect of various pore morphologies on the performance of Li-ion batteries will be investigated. Electron microscopy of lithiated and delithiated microcolumnar Si (100) electrodes will be performed. We are starting the NOMAD experiments in Fall 2019. However, it may be necessary to do some PDF analysis using X-ray data. We hope to do this at the University of Utah before we do the NOMAD experiments/

References

1. B. Vadlamani, K. An, M. Jagannathan, K.S.Ravi Chandran, "A Novel In-situ Electrochemical Cell for Neutron Diffraction Studies of Phase Transitions in Small Volume Electrodes of Li-ion Batteries," *J. Electrochem. Soc.*, 161, A1731 (2014)
2. S.W. Lee, M.T. McDowell, J.W. Choi, Y. Cui, Anomalous shape changes of silicon nanopillars by electrochemical lithiation. *Nano Lett.* 11, 3034–3039 (2011)

Publications from this Project

1. Vadlamani, B. S., M. Jagannathan, and KS Ravi Chandran. "Silicon with Columnar Microporous Architecture for Ultrahigh Total Energy-Storage Capacity and with Highly Reversible Lithiation Performance." *ACS Applied Energy Materials* 1, no. 3 (2018): 993-1001.
2. J. Palmer, B. Vadlamani, and K.S. Ravi Chandran, "A Critical Review of Energy Storage Capacities and Cycling Performances of Various Columnar Silicon Electrode Structures in Li-ion Cells, Submitted to *J. Power Sources*, May 2019.
3. M. Jagannathan, B. Vadlamani, and K.S. Ravi Chandran, "Effect of the Morphology of Columnar Microporous Structure on the Lithiation and Delithiation Performance of Silicon Electrodes in Li-ion Cells, Submitted to *J. Electrochem. Soc.*, May 2019.

Early Career: Flow-through Neutron Reflectometry - An in Operando Sample Environment for Active Polymer Interface Studies

Steven C. DeCaluwe, Mechanical Engineering, Colorado School of Mines

Program Scope

There are two overarching goals for this project:

1. Design a porous support capable of "Flow-through" neutron reflectometry (NR). NR is a powerful technique for understanding the thickness and composition of layered thin-film samples in various relevant chemical environments. However, the technique is limited by the need for very flat samples, which typically results in samples deposited on thick, polished Si wafer supports. This prevents non-equilibrium measurements where there is a species flux across the sample, which are required to understand and quantify structure-property relationships to improve clean energy storage and conversion technologies. A primary goal of this project is to develop a porous "flow through" NR sample environment to support such measurements, as shown schematically in

Figure 1. Fabricating a support with the required properties (porous, flat, and structurally supportive) is challenging, but success will enable a wide range of novel and impactful measurements in a range of systems, ranging from biology to clean energy.

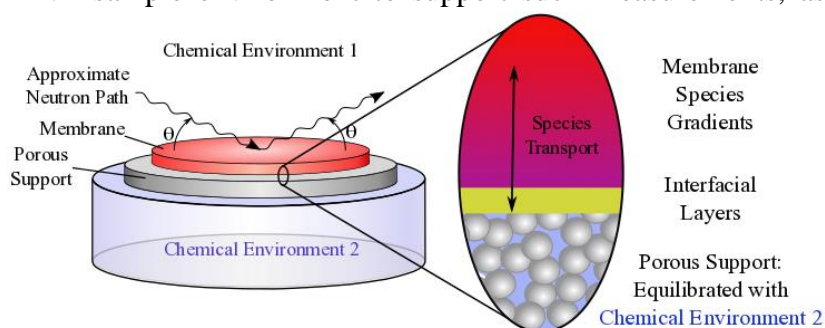


Figure 1. Conceptual illustration of flow-through neutron reflectometry. A porous support for thin-film membranes will allow for NR of non-equilibrium samples with species fluxes across the membrane thickness.

2. Understand the role of ion-conducting polymers in clean energy devices. Polymer Electrolyte Membrane Fuel Cells (PEMFCs) and Lithium-O₂ (Li-O₂) batteries require stable material interfaces with fast reaction rates and species transport. Measurement of active interfaces with species fluxes is therefore essential for fundamental insights and structure-property relationships. This second task will leverage flow-through NR, with complementary operando measurements, to advance the understanding of material interfaces in PEMFCs and Li-O₂ batteries. Multi-scale numerical simulations validated against the test suite will provide a framework to correlate, interpret, and quantify the information for a mechanistic description of device function. This, in turn, will provide the basis for predictive modeling tools to guide device design.

Recent Progress

1. *Porous supports for flow-through NR*: To support flow-through NR measurements, the first requirement is a support that is simultaneously porous, structurally supportive, and very very flat

(suitable for NR: RMS roughness = 2 nm). Toward this end, graduate research assistant C. Randall spent much of years 1 and 2 researching and assessing various methods for producing such a support. Three main techniques were evaluated: Deep Reactive Ion Etching (DRIE), Electrochemical Etching (E-Etch), and Metal-Assisted Chemical Etching (MAC-Etch). DRIE gives the lowest aspect ratio (pore width:pore depth) of the three, while MAC-Etch has the highest potential. However, while both DRIE and E-Etch have been demonstrated to etch pores through ~300 micron thick Si wafers, the MAC-Etch process would require significant development before possibly producing a suitable substrate. 2-inch Si wafer supports via DRIE and E-Etch have therefore been developed (DRIE) and procured (E-Etch). Both methods produce a regular array of micron-sized pores, with relatively flat substrate surfaces.

The primary challenge with these substrates is the size of the pores (2-10 micron diameter), which will require an intermediate microporous layer (MPL) to help the membranes under study (thicknesses 5-100 nm) span the membrane without collapsing into the pores. This MPL will also help promote a uniform gas composition and flux across the lateral span of the membranes studied. To optimize the MPL design, C. Randall wrote a simulation tool to predict the gas flux and composition throughout the layer, as a function of thickness, pore diameter and spacing, MPL porosity, and boundary flux (based on PEMFC current density). Using this tool, we identified support designs to provide uniform gas composition at the membrane interface. Based on these results, we have a deposited organosilicate spin-on glass MPL on a DRIE porous sample. Initial X-ray reflectometry (XRR) analysis in Figure 2 shows a fully dense layer with very low surface roughness (0.5 nm) and high-amplitude Keissig fringers out past 3.0 nm⁻¹. These results suggest that the porous support will be capable of high-resolution flow-through NR measurements for a range of thin-film membrane samples.

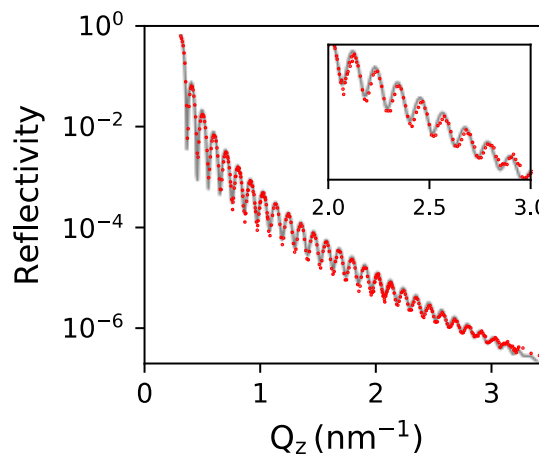


Figure 2. X-ray reflectometry of porous Si support with porous organosilicate spin-on glass. Accurate fits (grey line) to the data (red symbols) demonstrate a low-roughness substrate capable of high-quality reflectometry measurements out to high angles.

2. *Develop PEMFC simulation tools to test and validate process-structure-property relationships probed by the NR experiments.* The NR experiments described above are intended to elucidate and quantify structure-property relationships in thin-film conductive polymers: to understand how the polymer structure changes as a function of materials, fabrication, and operating conditions, and how in turn these structural changes influence properties that impact device performance. In order to fully leverage the insights from these experiments to understand the influence on PEMFC performance, C. Randall has developed a pseudo-2D PEMFC simulation tool which focuses on cathode catalyst layer processes (where limiting processes

typically occur when manufacturers attempt to reduce cost by lowering the Pt loading). The simulation tool implements various microstructure representations commonly employed in the literature and uses complex methods to evaluate Nafion polymer transport properties (proton conductivity, O₂ diffusivity and solubility) based on proposed polymer structures and structure-property relationships to demonstrate the interdependence between polymer properties, microstructure, and PEMFC performance. Two top-level conclusions are drawn: (i) For device-scale PEMFC simulations, careful thought must be given to develop "effective" microstructure representations which also capture important phenomena; and (ii) better estimates of thin-film Nafion transport properties in relevant PEMFC operating conditions are required. This modeling study therefore establishes the value of the flow-through NR experiments, provides a useful tool to incorporate and predict the impact of the properties measured by the NR experiments, and provides several important conclusions on its own, to be shared with the research community.

3. *Establish Li-O₂ battery fabrication and testing protocols.* In addition to PEMFCs, flow-through NR will provide new insight into the role and function of conductive polymers in Li-O₂ batteries. Toward this end, a second graduate research assistant (A. LeBar) was hired in grant year 2 to focus on building experimental infrastructure and protocols for Li-O₂ battery characterization. A. LeBar spent much of the year developing materials processing routines to prepare Li-O₂ battery cells for testing (the battery performance is incredibly sensitive to impurities, and so correctly processing the materials before assembling the battery is critical to getting even the most basic data). Procedures have now been developed for materials processing and assembly to obtain an accurate open circuit voltage and initial charge-discharge curves.

4. *Develop Li-O₂ simulation tools to interpret experimental results with and without functional binders.* Similar to the PEMFC research, new simulation tools will be required to interpret and understand the Li-O₂ battery experiments with varying binder type and binder loading. A. LeBar has developed a pseudo-2D Li-O₂ battery simulation tool, which she is using to explore how to model the Li₂O₂ precipitates that form in the cathode when the battery is discharged. We are currently in the process of verifying and validating the model, after which we will implement more sophisticated precipitation microstructures and implement binder effects in the model.

5. *Develop complimentary operando methods for quantifying layered structures.* The results from operando flow-through NR experiments will be strengthened by complementary operando measurements which can both verify and extend the NR results. We have developed and demonstrated operando quartz crystal microbalance (QCM) for high-resolution mass-uptake measurements in battery systems. This measurement is able to detect mass changes on the order of 2 ng/cm², with a time resolution of 100 Hz, and can therefore detect important reaction rates for batteries, including charge/discharge, solid electrolyte interphase (SEI) layer growth, or degradation/corrosion/removal of battery materials during operation. While simultaneously developing Li-O₂ battery protocols, we used QCM to measure SEI growth on a simple system (non-intercalating tungsten electrode with a Li counter electrode). The combined NR-QCM experiment was able to observe and quantify the chemical composition of the two-layer SEI.

Results were published in *J. Power Sources* (Lee, et al., 2019), and the protocols developed will be applied in the future to understand and identify reaction rates in Li-O₂ battery systems.

Future Plans

NR Flow-through: We have been awarded four days' beam time on the SNS liquids reflectometer for July – December 2019, and will test the viability of the DRIE and E-etch substrates. We will first verify the sample environment by recreating previous NR measurements of Nafion from standard (non flow-through) supports and comparing to these previous results. We will complement NR data with XRR, AFM, and SEM to fully understand the etched supports. The supports will be evaluated and compared, with a primary focus on suitable NR results, and a secondary focus on cost and ease of production. We will follow with initial flow-through NR, where the supported Nafion is suspended between two vapor environments: a dry air environment on one side, and a high-humidity air environment on the other.

PEMFCs: Research will focus on uncovering structure-property relationships for thin-film Nafion, including the impacts of film thickness, substrate, and PEMFC operation on Nafion structure (water and O₂ uptake) and properties (O₂, H₂O, and H⁺ transport rates). In the modeling realm, we will improve the pseudo-2D modeling tool, by adding detailed surface chemistry at the Pt catalyst surfaces, implementing water transport dynamics, and exploring new, efficient methods for representing catalyst layer microstructure, including multi-scale model approaches and non-spherical particles. Experimentally, we will use QCM to understand and quantify the difference between self-assembled Nafion (similar to operating PEMFCs) and spin-coated Nafion thin-films (used in NR). Initial flow-through NR experiments will explore the structural and transport properties of Nafion thin-films in the presence of species gradients.

Li-O₂ Batteries: Efforts will continue to quantify the electrochemical response of Li-O₂ batteries to conductive binders. As Li-O₂ batteries are at lower technology readiness than PEMFCs, the upcoming year will continue to focus on preliminary measurements and modeling efforts. Experimentally, we will test Li-O₂ coin-cell type batteries with traditional (Teflon) and conductive (Lithion) binders, looking at the influence of binder type and loading on battery performance and degradation over many cycles, for varying cycling rates. Simultaneous mass spectrometry will help analyze reaction pathways and identify/quantify any degradation reactions. We will also refine the pseudo-2D modeling tool, to include more sophisticated microstructural approaches to describe the impact of (i) the growth of Li₂O₂ particles during battery discharge, and (ii) conductive and non-conductive binders on electrochemical reactions and species transport through porous cathodes.

Publications

Lee, C.H., Dura, J.A., LeBar, A., DeCaluwe, S.C., "Direct, operando observation of the bilayer solid electrolyte interphase structure: Electrolyte reduction on a non-intercalating electrode," *J. Power Sources*, **412**, 2019, p. 725-735.

University of Minnesota Center for Quantum Materials (CQM): Superconductivity and Normal-State Transport in SrTiO₃

Rafael Fernandes¹, Martin Greven¹, Bharat Jalan² and Chris Leighton²

¹School of Physics and Astronomy, University of Minnesota

²Department of Chemical Engineering and Materials Science, University of Minnesota

Program Scope

The overarching goal of this specific CQM project is to further the understanding of the electronic phase behavior of doped strontium titanate (SrTiO₃, denoted STO hereafter). This system displays several phenomena that feature prominently in numerous quantum materials. For instance, a superconducting dome is observed as the doping concentration changes, and quantum fluctuations are widely believed to be the reason why the undoped compound is not a ferroelectric. The coupling between these paraelectric fluctuations and phonons offers an interesting route to probe their effects on normal-state and superconducting properties. Moreover, being one of the most dilute superconductors known, lightly-doped STO has a very small Fermi energy, raising unique challenges for a microscopic theory of superconductivity (and even metallicity), which has remained elusive for decades. The CQM at the University of Minnesota has shed new light on important open problems in this system through complementary theoretical and experimental efforts [1-4].

Recent Progress

Unconventional Superconductivity

An unresolved puzzle in the electronic phase diagram of STO has been the connection between its superconducting dome and Lifshitz transitions. As the carrier concentration increases, different electron-like bands cross the Fermi level in STO, marking the onset of two Lifshitz transitions. Recent experiments reveal that the superconducting dome is actually a double-hump dome, with the first maximum in the superconducting transition temperature T_c taking place at the first Lifshitz transition, whereas the second Lifshitz transition has no pronounced effect on T_c . The former behavior is very unexpected, since the additional electronic carriers provided by the band crossing the Fermi level should generally enhance T_c , at least according to the standard theory of clean multi-band superconductors. In back-to-back papers [1-2], CQM's *Fernandes* and his collaborators showed that this suppression of T_c across the first Lifshitz transition can be explained by the combination of disorder and inter-band repulsive pairing interaction. This is because in this case, across the Lifshitz transition, the pair-breaking effect due to the enhanced inter-band impurity scattering overcomes the positive effect due to the enhanced density of states, resulting in an overall suppression of T_c . Indirect evidence for inter-band repulsive pairing

interaction, and thus unconventional superconductivity, has been further provided by preliminary data on Nd-doped STO taken by CQM's *Jalan* and collaborators. This system shows a similar T_c dome to La-doped STO, despite the fact that Nd dopants should act as magnetic impurity scattering centers, which would have a strong pair-breaking effect for attractive inter-band pairing interaction.

In this context, a joint effort led by CQM's *Fernandes* and *Jalan* recently revealed an intriguing, and surprising, sharp drop of the residual resistivity across the second Lifshitz transition, indicative of weak inter-band impurity scattering. This is in qualitative agreement with the theoretical predictions of [1,2] that weak inter-band scattering has little effect on T_c . Temperature-dependent Hall measurements also showed an unusual dependence of the Hall coefficient, which reveals a surprising sensitivity of the carrier concentration on the antiferrodistortive phase transition that takes place at higher temperatures in STO.

Motivated by *Greven's* recent finding of highly unusual charge transport and diamagnetic behavior of cuprates at $T > T_c$, *Greven* and *Leighton* also performed measurements of the nonlinear, third-harmonic magnetic susceptibility above T_c in Nb-doped STO [5]. A compelling explanation for the observed exponential behavior is that inhomogeneities generate regions with a higher local T_c . Superconductivity then emerges in a percolative manner, with superconducting puddles that form already well above T_c in rare regions. The essential idea here was to test if the behavior observed in cuprates is in fact universal in perovskite-related oxides, which are known to exhibit structural inhomogeneity at various length scales. Remarkably, these measurements of superconducting STO revealed the same characteristic T dependence as in cuprates [3].

Unusual Normal State Properties

Besides unusual superconductivity, STO also displays puzzling normal state properties. Perhaps the most pronounced one is the persistence of a low-temperature T^2 resistivity even for very small doping concentrations. While at first sight this may seem to be the expected behavior of normal Fermi liquid metals, the fact that the Fermi surface of lightly-doped STO is very small precludes Umklapp processes from taking place, which are essential for standard T^2 resistivity. Moreover, the T^2 behavior continues up to temperatures of the order of the Fermi temperature of very diluted compositions. In [4], a joint experimental-theoretical effort led by CQM's *Leighton* and *Fernandes* revealed important properties of the normal state of STO. First, it was shown that the measured electronic contribution to the specific heat agrees very well with the theoretical one, based on tight-binding modeling of band structure, provided that a mass renormalization of 2 is included. Remarkably, this mass renormalization factor is constant over three decades of electron concentrations. This indicates that STO is a well-behaved, weakly-correlated Fermi liquid. The specific heat data then allowed us to test, for the first time, the Kadowaki-Woods scaling between the quadratic coefficient of the resistivity and the square of the linear coefficient of the specific heat (see Figure 1). Surprisingly, the standard Kadowaki-Woods scaling observed in transition metals and heavy fermion compounds is quantitatively and qualitatively violated in

STO, highlighting the unusual nature of the transport properties of this material. This result highlights the urgent need for a new theoretical description of the T^2 resistivity in doped STO.

Future Plans

To further elucidate the character of the multi-band superconducting state of STO, a detailed experimental comparison between the effects of La-doping (which presumably behave as non-magnetic impurity centers) and Nd-doping (which presumably behave as magnetic impurity centers) will be carried out, with support from theoretical calculations. Additionally, the CQM plans to control the ferroelectric fluctuations present in STO with the application of uniaxial strain, in order to reveal their impact on the normal state and superconducting properties. In this context, theory will focus on microscopic models for possible pairing mediated by the exchange of such fluctuations. Similarly, strain engineering of bulk crystals and thin films will be employed to better understand the unusual superconducting emergent behavior seen in the nonlinear susceptibility.

Publications (specific to this abstract)

- [1] *Unconventional multi-band superconductivity in bulk SrTiO3 and LaAlO3/SrTiO3 interfaces*, T. V. Trevisan, M. Schütt, and R. M. Fernandes, Phys. Rev. Lett. **121**, 127002 (2018).
- [2] *Impact of disorder on the superconducting transition temperature near a Lifshitz transition*, T. V. Trevisan, M. Schütt, and R. M. Fernandes, Phys. Rev. B **98**, 094514 (2018).
- [3] *Universal superconducting precursor in three classes of unconventional superconductors*, D. Pelc, Z. Anderson, B. Yu, C. Leighton, and M. Greven, Nat. Commun. in press (2019); [arXiv:1808.05763](https://arxiv.org/abs/1808.05763).
- [4] *Low temperature specific heat of doped SrTiO3: Doping dependence of the effective mass and Kadowaki-Woods scaling violation*, E. McCalla, M. N. Gastiasoro, G. Cassuto, R. M. Fernandes, and C. Leighton, Phys. Rev. Materials **3**, 022001 (2019).

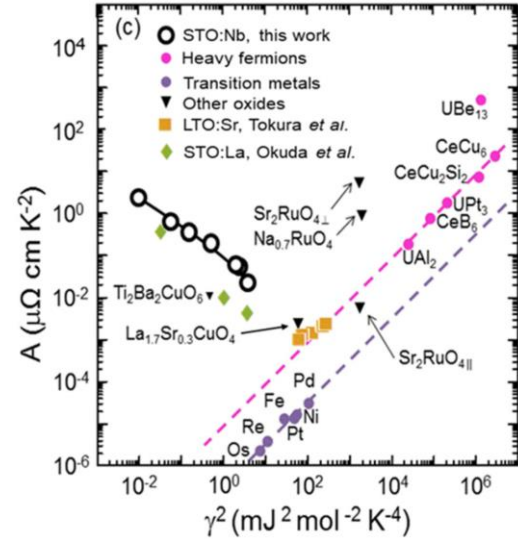


Figure 1: The Kadowaki-Woods scaling in STO deviates qualitatively from that of transition metals and heavy fermions [4].

University of Minnesota Center for Quantum Materials (CQM): Unusual Emergence of Superconductivity in Oxides

Martin Greven¹, with Rafael Fernandes¹, Bharat Jalan² and Chris Leighton²

¹School of Physics and Astronomy, University of Minnesota

²Department of Chemical Engineering and Materials Science, University of Minnesota

Program Scope

The overarching goal of this specific CQM project is to further the understanding of the emergence of superconductivity in complex oxides using novel approaches, and to explore the role of inhomogeneity. Superconductivity is one of the major research topics in materials physics, yet in many important materials this phenomenon is not well understood. Complex oxides are particularly interesting in this regard, because of the wide temperature and composition ranges where superconductivity occurs, and because the origin of superconductivity is thought to differ for different oxide families. In the context of the cuprates, two pivotal unresolved issues are the nature of the normal state and of the superconducting precursor above the macroscopic transition temperature T_c . Strontium ruthenate (SRO) and strontium titanate (STO) exhibit the same perovskite-based structure as the cuprates, and the superconducting precursor has not been thoroughly investigated in these oxides.

Recent Progress

Universal Emergence of Superconductivity

Greven and Leighton recently uncovered a remarkable universal feature shared by these distinct oxides [1]. The discovery was enabled by the development of a novel nonlinear magnetic response technique, an extremely sensitive probe of magnetism. Experiments on STO, SRO, and two cuprates (LSCO and Hg1201) revealed that upon cooling toward T_c , superconductivity emerges in a highly similar fashion (see Figure 1), despite dramatically different electronic properties and T_c values. The universal behavior in cuprates is further borne out in a separate set of experiments that covers a wide range of compounds [2,3]. Furthermore, the universal response follows highly unconventional, yet remarkably simple exponential behavior. We also uncovered that this behavior above T_c can be influenced by intentionally inducing structural

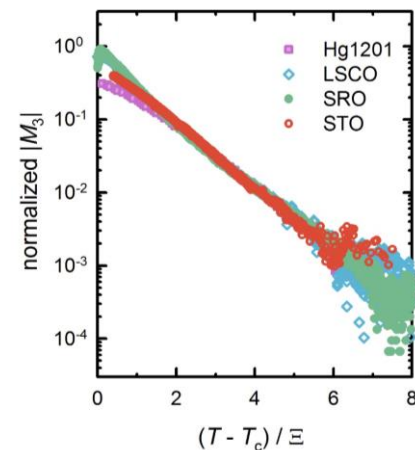


Figure 1: Universal superconducting fluctuations above T_c for four different unconventional superconductors, from nonlinear magnetic response [1].

inhomogeneity into the materials via plastic deformation. This suggests that the origin of the universal behavior is related to intrinsic structural inhomogeneity, which is therefore an essential ingredient in the unconventional physics of all the studied systems. In the case of the cuprates, Greven demonstrated that the paraconductivity follows percolation behavior quantitatively [4].

Phenomenological Model for the Cuprates

These insights were applied by Greven to gain new understanding into the physics of cuprate high-temperature superconductors. The cuprates are compounds with the highest T_c values at ambient pressure. Yet after more than three decades of truly remarkable research activity, the salient features of both the ‘normal’ state (above the superconducting transition temperature) and the superconductivity itself remain debated. We have developed a simple, yet powerful phenomenological model that resolves several major open questions [5]. Crucially, the model posits that the cuprates exhibit inherent inhomogeneity, as well as two co-existing electronic subsystems: localized and itinerant. These premises are strongly supported by a number of experiments, and naturally lead to a description of the normal state. Furthermore, the superconductivity is shown to arise from an interaction between the two subsystems, explaining the zero-temperature superfluid density (Figure 2). The model thus provides a clear framework for understanding the enigmatic cuprates.

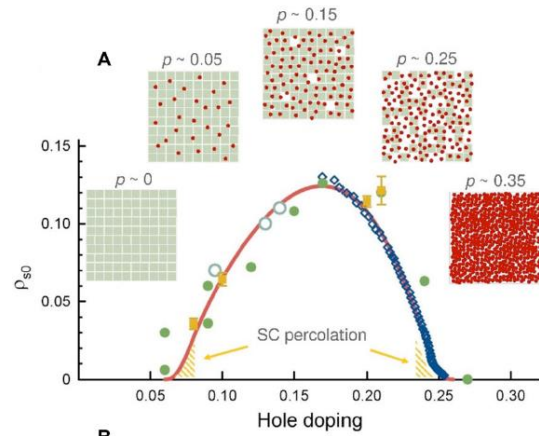


Figure 2: The zero-temperature superfluid density of the high- T_c cuprates in dependence on hole doping, from several experiments (points) compared to model calculations (line). The two electronic subsystems – localized (green) and itinerant (red) – are depicted schematically [5].

Future Plans

The overarching goal of our investigations of unconventional superconductors is twofold: to obtain a microscopic understanding of the universal intrinsic inhomogeneity that we have uncovered, and to influence and optimize it through strain engineering. Multiple complementary experimental approaches will be pursued to achieve these goals. In particular, state-of-the-art probes of local crystal structure will be employed, including neutron and X-ray diffuse scattering and neutron Larmor diffraction. Some of these experiments have already begun to yield promising results. Furthermore, we will combine these powerful structural probes with plastic deformation experiments to understand the microscopic effects of internal strain, with the aim to optimize the superconducting properties of strained samples. Specialized uniaxial pressure cells are under development, to enable *in situ* deformation at neutron and X-ray facilities. Other complex oxide superconductors, such as bismuthates, will also be included in future

experimental and theoretical studies, both in bulk-crystalline and thin-film form, which will provide a comprehensive picture of the local structure of this important class of materials.

Publications (specific to this abstract)

[1] *Universal superconducting precursor in three classes of unconventional superconductors*, D. Pelc, Z. Anderson, B. Yu, C. Leighton, and M. Greven, *Nat. Commun.* in press (2019); arXiv:1808:05763.

[2] D. Pelc, M. Vučković, M. S. Grbić, M. Požek, G. Yu, T. Sasagawa, M. Greven, and N. Barišić, *Nat. Commun.* **9**, 4327 (2018).

[3] *Universal precursor of superconductivity in the cuprates*, G. Yu, D.-D. Xia, D. Pelc, R.-H. He, N.-H. Kaneko, T. Sasagawa, Y. Li, X. Zhao, N. Barišić, A. Shekhter, and M. Greven, *Phys. Rev. B*, in press (2019); arXiv:1710:10957.

[4] *Percolative nature of the direct current paraconductivity in the cuprate superconductors*, P. Popčević, D. Pelc, Y. Tang, K. Velebit, Z. Anderson, V. Nagarajan, G. Yu, M. Požek, N. Barišić, and M. Greven, *npj Quant. Mat.* **3**, 42 (2018).

[5] *Unusual behavior of cuprates explained by heterogeneous charge localization*, D. Pelc, P. Popčević, M. Požek, M. Greven, and N. Barišić, *Sci. Adv.* **5**, eaau4538 (2019).

Long-Range Antiferromagnetic Order in an Entropy Stabilized Rocksalt Oxide

Raphaël P. Hermann

Materials Science & Technology, Oak Ridge National Laboratory, Oak Ridge, TN

Publication:

J. Zhang, J. Yan, S. Calder, Q. Zheng, M. A. McGuire, D. L. Abernathy, Y. Ren, S. H. Lapidus, K. Page, H. Zheng, J. W. Freeland, J. D. Budai, and R. P. Hermann, “Long-Range Antiferromagnetic Order in a Rocksalt High Entropy Oxide,” *Chem. Mater.* **31**, 3705 (2019).

High entropy oxides, solid solutions stabilized by high configurational entropy, have attracted much attention due to fundamental issues related to phase formation and materials design as well as properties that can emerge from their spin order and possible structural instability [1-17]. It has been reported that high entropy oxides exhibit colossal dielectric constants [17], superionic conductivity [8,16], and low thermal conductivity [10,13] in bulk samples, and antiferromagnetism in thin films [15]. In order to assess potential functionalities of this new class of materials, understanding the magnetic structure, magnetic and lattice dynamics bears significant importance.

We report the first observation of the long range magnetic structure and dynamics in the O rocksalt high entropy oxide ($\text{Mg}_{0.2}\text{Co}_{0.2}\text{Ni}_{0.2}\text{Cu}_{0.2}\text{Zn}_{0.2}$) by combining neutron diffraction and inelastic scattering with magnetometry and calorimetry. Neutron scattering reveals that long range magnetic order survives the configurational disorder and suggests that short range ordered domains persists even at room temperature. This work demonstrates potential functional magnetic properties in entropy-stabilized oxides that represent a novel platform to understand study how disorder impacts magnetic order and magnetic excitations.

We found that the long-range magnetic order of the rocksalt high entropy oxide cannot be well understood in the framework of the randomly diluted face-centered cubic system, including complicated spin

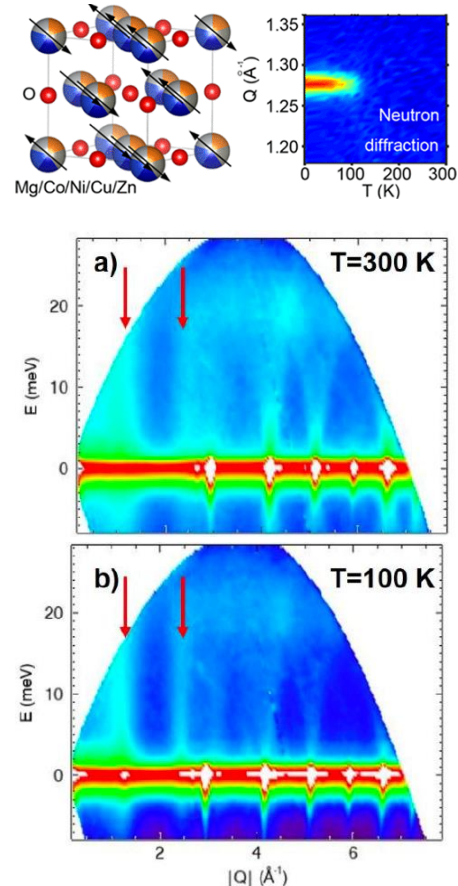


Fig. 1 Neutron diffraction (HB-2A, HFIR), top, reveals magnetic long range order below $T_N \sim 140$ K, with the NiO magnetic structure. Neutron spectroscopy (ARCS, SNS) reveals well-defined spin-waves 100 K, (a), and 300 K, (b), a temperature higher than twice the Neel temperature, which suggests that short range magnetism survives at ambient conditions.

exchange interactions, the lack of structural transition or deformation across the magnetic transition, and the absence of a lambda peak in heat capacity. Furthermore, our resonant ultrasound spectroscopy data reveals both anomalous behavior near the magnetic ordering temperature and strong hardening upon cooling down to 3 K. Hence, as an outlook we will investigate spin-lattice coupling by using polarized inelastic neutron scattering, develop a model for the spin-wave dispersions in these highly disordered materials, and carry out complementary muon spin-relaxation characterization (coll. Ben Frandsen, BYU).

References

1. C. M. Rost, *et al.*, Entropy-stabilized oxides. *Nat. Commun.* **6**, 8485 (2015).
2. A. Sarkar, *et al.*, High-Entropy Oxides: Fundamental Aspects and Electrochemical Properties. *Adv. Mater.* 1806236 (2019).
3. R. Witte, *et al.*, High-entropy oxides: An emerging prospect for magnetic rare-earth transition metal perovskites. *Phys. Rev. Mater.* **3**, 034406 (2019).
4. Q. Wang, *et al.*, High entropy oxides as anode material for Li-ion battery applications: A practical approach. *Electrochem. Commun.* **100**, 121 (2019).
5. M. P. Jimenez-Segura, *et al.*, Long-range magnetic ordering in rocksalt-type high-entropy oxides. *Appl. Phys. Lett.* **114**, 122401 (2019).
6. M. R. Chellali, *et al.*, On the homogeneity of high entropy oxides: An investigation at the atomic scale. *Scr. Mater.* **166**, 58 (2019).
7. Y. Sharma, B. L. Musico, X. Gao, C. Hua, A. F. May, A. Herklotz, A. Rastogi, D. Mandrus, J. Yan, H. N. Lee, M. F. Chisholm, V. Keppens, and T. Z. Ward, Single-crystal high entropy perovskite oxide epitaxial films. *Phys. Rev. Mater.* **2**, 060404 (2018).
8. A. Sarkar, *et al.*, High entropy oxides for reversible energy storage. *Nat. Commun.* **9**, 3400 (2018).
9. S. Jiang, *et al.*, A new class of high-entropy perovskite oxides. *Scr. Mater.* **142**, 116 (2018).
10. J. Gild, *et al.*, High-entropy fluorite oxides. *J. Eur. Ceram. Soc.* **38**, 3578 (2018).
11. J. Dąbrowa, *et al.*, Synthesis and microstructure of the (Co,Cr,Fe,Mn,Ni)₃O₄ high entropy oxide characterized by spinel structure. *Mater. Lett.* **216**, 32 (2018).
12. K. Chen, *et al.*, A five-component entropy-stabilized fluorite oxide. *J. Eur. Ceram. Soc.* **38**, 4161 (2018).
13. J. L. Braun, *et al.*, Charge-induced disorder controls the thermal conductivity of entropy-stabilized oxides. *Adv. Mater.* **30**, 1805004 (2018).
14. D. B. Miracle and O. N. Senkov, A critical review of high entropy alloys and related concepts. *Acta Mater.* **122**, 448 (2017).
15. P. B. Meisenheimer, T. J. Kratochvil, and J. T. Heron, Giant enhancement of exchange coupling in entropy-stabilized oxide heterostructures. *Sci. Rep.* **7**, 13344 (2017).
16. D. Bérardan, S. Franger, A. K. Meena, and N. Dragoe, Room temperature lithium superionic conductivity in high entropy oxides. *J. Mater. Chem. A* **4**, 9536 (2016).
17. D. Bérardan, S. Franger, D. Dragoe, A. K. Meena, and N. Dragoe, Colossal dielectric constant in high entropy oxides. *Phys. Status Solidi RRL* **10**, 328 (2016).

Field-induced quantum spin liquid in the Kitaev-Heisenberg model and its relation to α - RuCl_3

Hong-Chen Jiang, Yi-Fan Jiang, Thomas P. Devereaux, Chang-Yan Wang, Biao Huang, and Yuan-Ming Lu

Abstract: Recently considerable excitement has arisen due to the experimental observation of a field-induced spin liquid phase in the compound α - RuCl_3 , which is a promising Kitaev material consisting of effective spin-1/2s on distorted honeycomb layers. However, the nature of this putative spin liquid phase and the relevant microscopic model Hamiltonian remain still unclear. In this work, we address these questions by combining theoretical and large-scale numerical efforts of a generalized Kitaev-Heisenberg model proposed to describe the physics of α - RuCl_3 . Our results suggest that a stable spin liquid phase can be induced by out-of-plane magnetic fields, which is consistent with a $U(1)$ spin liquid possessing a spinon Fermi surface. The relevance of our results to α - RuCl_3 is also discussed.

Novel quantum phenomena in geometrically frustrated magnets near the metal-insulator phase boundary

Xianglin Ke, Department of Physics and Astronomy, Michigan State University, MI 48824

Program Scope

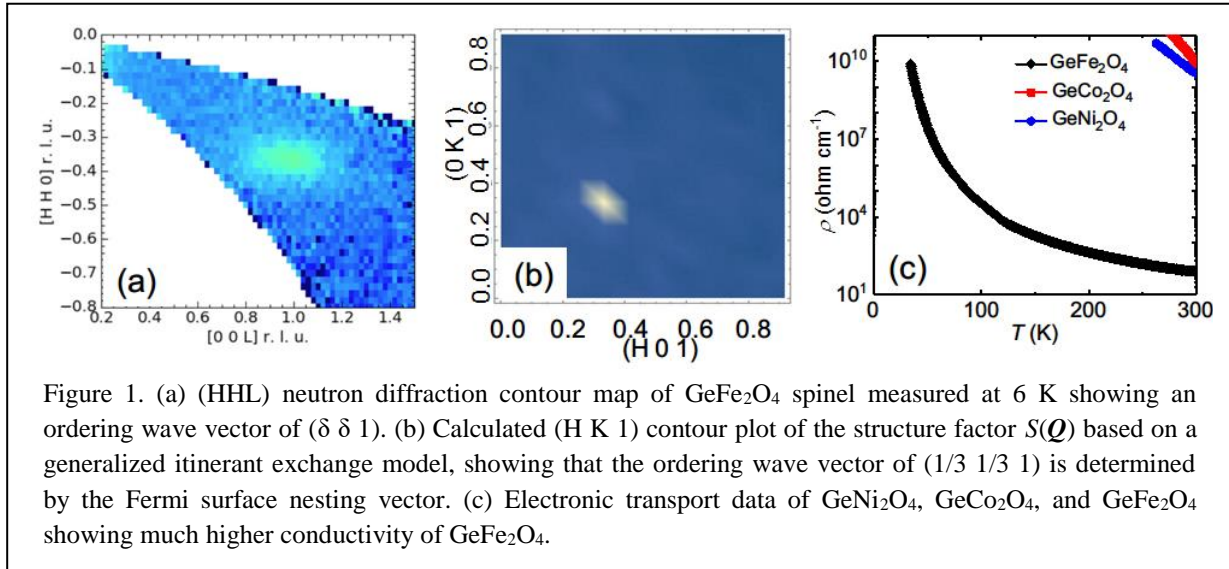
Geometric frustration, which arises from the competing interactions between magnetic ions placed on regular lattice sites, can often lead to a large degeneracy of spin states, giving rise to a rich variety of unconventional magnetic phases. To date, most of the research on frustrated magnets has focused on insulating materials, whose ground state properties are mainly determined by short-range interactions between localized spins. In contrast, fewer studies have been performed on metallic frustrated magnets, particularly on geometrically frustrated magnets in close proximity to a metal-insulator transition, i.e., proximate itinerant frustrated magnets. The primary objective of this proposal is to study novel quantum phenomena in geometrically frustrated magnets near the metal-insulator phase boundary and understand how the interplay and cooperation between electron itinerancy and magnetic frustration determines materials' physical properties.

Recent Progress

In the past 9 months since this program was awarded, we have been mainly working on two magnetically frustrated systems, GeFe_2O_4 spinel and $\text{Cu}_2(\text{OH})_3\text{Br}$ with a triangular lattice.

A. Unconventional magnetic ordering in GeFe_2O_4 . We have studied electronic and magnetic properties a spinel compound GeFe_2O_4 , where the magnetic Fe ions occupy a pyrochlore sublattice that is composed of a network of corner-sharing tetrahedral. Therefore, magnetic ions on this lattice geometry can give rise to strong competition of spin-spin interaction and naturally facilitate geometric magnetic frustration. In GeFe_2O_4 we have revealed an unusual magnetic ground state with an ordering wave vector of $\langle \delta \delta 1 \rangle$ with $\delta \approx 0.33$ for polycrystalline sample and $\delta \approx 0.36$ for single crystal sample (Fig. 1(a)), which is quite distinct from the magnetic ground state of its two sister compounds, GeNi_2O_4 and GeCo_2O_4 . The latter two compounds have an ordering wave vector of $(0.5 \ 0.5 \ 0.5)$ [1,2]. Interestingly, we also found that GeFe_2O_4 is much more (~ 7 orders of magnitude) conducting compared to GeNi_2O_4 and GeCo_2O_4 (Fig. 1(c)), which implies the impacts of itinerant carriers on the magnetic ordering of a frustrated lattice. This finding is corroborated by Monte Carlo simulation based on a generalized itinerant exchange model [3] via the collaboration with Prof. Gia-wei Chern in University of Virginia, which shows that the ordering wave vector of $\langle 1/3 \ 1/3 \ 1 \rangle$ is determined by the Fermi surface nesting vector (Fig. 1(b)). This study demonstrates a novel example showing the cooperative effects of enhanced electron itinerancy, magnetic frustration, and spin-

charge coupling in geometrically frustrated system. A manuscript on this study is currently in preparation.



B. Spin-magnon interaction in $\text{Cu}_2(\text{OH})_3\text{Br}$. We have also extended our research to $\text{Cu}_2(\text{OH})_3\text{Br}$ compound in which Cu^{2+} ions with $S = 1/2$ form a quasi-2D distorted triangular lattice. This material is an isomorphic compound to the parent compound of the Herbersmithite $\text{Cu}_3\text{Zn}(\text{OH})_6\text{Cl}_2$ which is a promising candidate showing quantum spin liquid [4]. This system shows an antiferromagnetic long range order below 9 K. Despite the quasi-2D triangular lattice of Cu^{2+} ions, very interestingly we find that the local coordinates of Cu ions relative to Br ions, combined with the magnetic frustration resulting from the triangular lattice geometry, leads to quasi-1D nature of magnetic exchange interaction between Cu ions. In another words, this system can be effectively treated as a unique quantum antiferromagnet consisting of nearly decoupled, alternating ferromagnetic and antiferromagnetic $S = 1/2$ chains. This is supported by our neutron scattering measurements and the first-principles density functional theory calculation via the collaboration with Prof. Turan Birol in University of Minnesota. Furthermore, we have observed for the first time, to our best knowledge, the coexistence of magnon and spinon continuum excitations which are associated with ferromagnetic and antiferromagnetic chains respectively. This study presents a new toy model which opens an unexplored paradigm where one can study the interaction between two different types of magnetic quasiparticles, magnons and spinons. We are currently working on a manuscript on this study.

Future Plans

Our initial study of GeFe_2O_4 suggests that there is indeed correlation between e electron itinerancy and magnetic ordering (i.e., ordering wave vector) in this system. In the next step, we will pursue to grow large enough GeFe_2O_4 single crystals for inelastic neutron scattering study to

investigate the competing exchange interactions and understand their effects on the unusual magnetic ground state of this system.

Currently, we are also growing $Y_{2-x}Bi_xRu_2O_7$ pyrochlore which shows insulator-metal transition with Bi substituted into Y sites [5]. We will perform neutron and synchrotron x-ray scattering studies to examine the effects of local atomic structure and Ru orbital occupancy on the insulator-metal transition, and to understand the correlation between electronic transition and magnetic ordering and spin dynamics of this system.

References

1. S. Diaz, S. de Brion, G. Chouteau, B. Canals, V. Simonet, and P. Strobel, *Magnetic frustration in the spinel compounds $GeCo_2O_4$ and $GeNi_2O_4$* , Physical Review B **74** (9), 092404 (2006).
2. M. Matsuda, J. H. Chung, S. Park, T. J. Sato, K. Matsuno, H. Aruga Katori, H. Takagi, K. Kakurai, K. Kamazawa, Y. Tsunoda, I. Kagomiya, C. L. Henley, and S. H. Lee, *Frustrated minority spins in $GeNi_2O_4$* , EPL (Europhysics Letters) **82** (3), 37006 (2008).
3. Gia-Wei Chern and Cristian D. Batista, *Spin Superstructure and Noncoplanar Ordering in Metallic Pyrochlore Magnets with Degenerate Orbitals*, Physical Review Letters **107** (18), 186403 (2011).
4. T.-H Han, J. S. Helton, S. Chu, D. G. Nocera, J. A. Rodriguez-Rivera, C. Broholm, and Y. S. Lee, *Fractionalized excitations in the spin-liquid state of a kagome-lattice antiferromagnet*, Nature **492**, 406 (2012).
5. Shunsuke Yoshii and Masatoshi Sato, *Studies on Metal-Insulator Transition of Pyrochlore Compound $Y_{2-x}Bi_xRu_2O_7$* , Journal of the Physical Society of Japan **68** (9), 3034 (1999).

Publications

University of Minnesota Center for Quantum Materials (CQM): Oxygen-Vacancy-Based Control of Perovskite Oxides

C. Leighton¹, with R. Fernandes² and M. Greven²

¹Department of Chemical Engineering and Materials Science, University of Minnesota

²School of Physics and Astronomy, University of Minnesota

Program Scope

The overarching goal of this specific CQM project is to further the understanding and capabilities of oxygen-vacancy-based control of complex oxides, particularly perovskites. Model systems such as cobaltites, stannates, and titanates are being employed, moving beyond conventional control of oxygen vacancy (V_O) *density*, to control of V_O *order*, and *in situ electrochemical* control. In perovskite cobaltites, for example, we have demonstrated extraordinary strain-based tuning of V_O ordering, enabling control of magnetism, electronic and thermal transport, dead layer thickness, and even advanced properties such as perpendicular magnetic anisotropy. Extension of these concepts to other perovskites is enabling further progress, such as V_O -based doping in the recently discovered high room temperature mobility stannates. Moreover, electrolyte gating methods based on ionic liquids and gels are also now being used for *in situ* electrochemical tuning of V_O density and order, using cobaltites as model systems. Powerful *operando* polarized neutron reflectometry (PNR) and synchrotron X-ray diffraction (SXRD) probes of ionic gating have been developed, yielding advances such as deconvolution of electrostatic and V_O -based gating mechanisms, and direct PNR-based confirmation of record-breaking electrical modulation of Curie temperature in ultrathin films.

Recent Progress

Due to the confluence of low V_O formation enthalpy and high V_O diffusivity, cobaltites are model systems for the exploration of V_O -based control concepts. In recent CQM work, tuning of not only V_O *density*, but also V_O *order*, has been used to control properties such as thermal conductivity [1], magnetic anisotropy, and interfacial dead layer thickness [2,3]. Collaborative time-domain thermoreflectance measurements, for example, were used to probe thermal conductivity in nanoscopic thin films of $\text{La}_{1-x}\text{Sr}_x\text{CoO}_{3-\delta}$ (LSCO), where both δ and the orientation of V_O order are strain-tunable [1-3]. Ultralow glass-like thermal conductivities were obtained, even in highly epitaxial single crystal films, ascribed primarily to the effects of high δ , with potential technological implications [1]. Studies of magnetic anisotropy provided another,

particularly striking example of V_O -based property tuning [2]. The magnetic anisotropy in ferromagnetic epitaxial LSCO was shown to flip from in-plane to perpendicular on moving from tensile to compressive strain. Of particular interest for applications, the achieved perpendicular magnetic anisotropy reaches almost 10^7 erg/cm^3 , comparable to values obtained in high spin-orbit coupling heterostructures such as those based on iridates. That such values can be strain-tuned in LSCO, *without* high Z elements, is remarkable. As shown in Fig. 1, clear correlations were uncovered between the spatial coherence of V_O order and the strength of the perpendicular magnetic anisotropy, clearly establishing that the anisotropy is controlled by the V_O -order-based symmetry lowering, *i.e.*, natural superlattice formation. More broadly, extensive measurements have also been made of magnetic and electronic transport properties *vs.* substrate-induced strain, establishing clear links between these properties and strain-tuned V_O order. As noted below, future work aims to forge direct links between V_O order and the important dead layer effects in oxide heterostructures, breaking new ground.

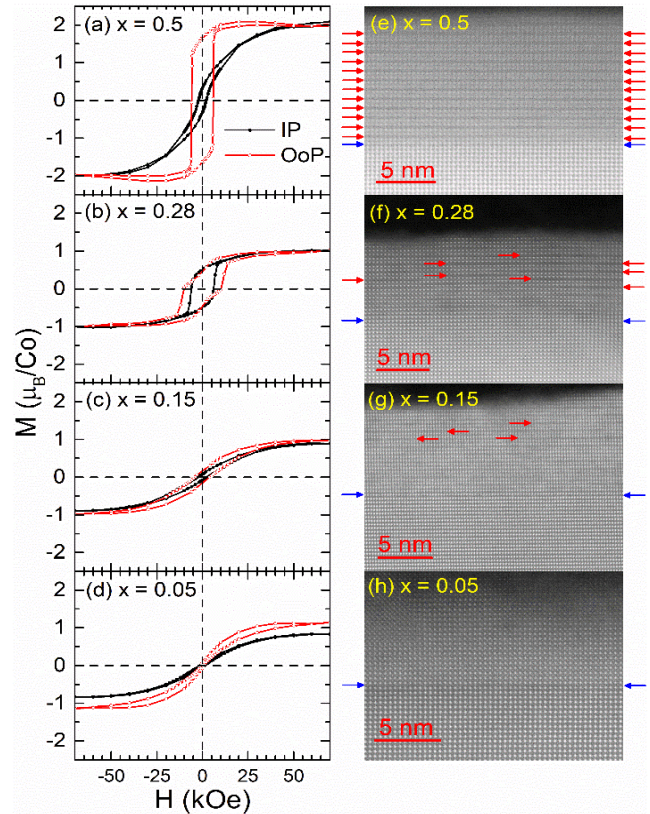


Figure 1: (a) In-Plane (IP) and Out-of-Plane (OoP) 5 K hysteresis loops *vs.* x in 100-Å-thick compressively-strained LSCO films on LaAlO_3 . (b) Corresponding Z -contrast cross-sectional transmission electron microscopy. Note the correlation between the extent of V_O ordering (dark stripes) and perpendicular magnetic anisotropy [2].

Extension of these capabilities and ideas to other systems is also underway in the CQM. V_O -based doping of the recently discovered high room temperature mobility semiconductor BaSnO_3 has been achieved, for example [4]. Significantly, this work resolved apparent discrepancies between single crystal and thin film results, which arise due to the extremely low V_O diffusivity in stannates. In the same work, magnetic rare-earth doping was also demonstrated, enabling precise quantification of doping densities and observation of crystal field effects [4].

Recent collaborative CQM research has extended this work to *electrochemical* fine-tuning of V_O density and order, enabling reversible, dynamic control of magnetism and transport. Scattering methods such as SXRD and PNR have been applied to electrolyte gating of complex oxides, using ionic liquids and gels. This CQM/MRSEC collaboration employs such scattering methods as powerful *operando* probes of ionic liquid/gel-gated complex oxides, particularly the highly electrochemically active cobaltites. Key advances include the application of SXRD (Fig.

2(a)) to directly distinguish V_O formation at positive gate voltage (*via* lattice expansion) from simple electrostatic gating at negative gate voltage (Fig. 2(b)) in LSCO [5]. This simply disentangles electrostatic and electrochemical gate responses, greatly clarifying a controversial issue in the field [6]. PNR (Fig. 2(c)) was then used to enable depth profiling of the magnetization, and thus V_O density, elucidating the process of electrochemical redox at positive bias [5].

Perhaps most significantly, with the simple division between electrostatic and electrochemical mechanisms understood, theory-guided experiment then demonstrated electrostatic control of ferromagnetism *via* gate-induced cluster percolation at negative bias [7]. Building on prior DOE-funded work understanding the nature of the phase-separated state at low x in LSCO, ultrathin sub-percolated films were gated across the percolation threshold to a metallic ferromagnetic state, establishing a record Curie temperature modulation of 150 K at only -4 V [7]. Critically, PNR was employed to directly verify electrically-induced long-range ferromagnetic order. Despite the 6 unit cell thickness, SNS PNR data at -3 V (Fig. 3(a,b)) clearly indicate spin asymmetry, the refined depth profile of the magnetization revealing a surprise. Specifically, the electrically induced magnetization is relatively uniform throughout the thickness (Fig. 3(c)), clearly distinguishable from the induced hole profile, which peaks sharply near the interface. This confirms a theoretical prediction that induced magnetization can penetrate far deeper than the electrostatic screening length due to surface-assisted connection of pre-formed magnetic clusters [7]. Importantly, subsequent to this work the capability to perform such *operando* PNR studies, accompanied by *in situ* electronic transport measurements, is now available at both the SNS and NCNR. Lateral scale-up challenges (the PNR measurements are performed on ~ 1 cm electrolyte-gate transistors) have been fully addressed.

Future Plans

As noted above, an immediate goal is to probe the influence of strain-tuned V_O order on thickness-dependent LSCO electronic/magnetic properties, seeking minimization of the well-known dead layer effects that pose such a challenge for heterostructured oxide devices. Other

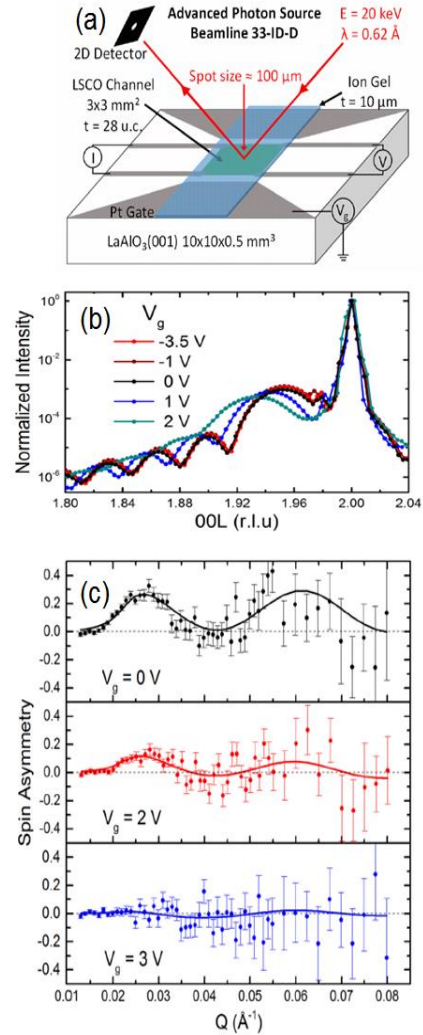


Figure 2: (a) Set-up for *operando* SXR of electrolyte-gated complex oxides. (b) Gate-voltage-dependent specular SXR data on epitaxial LSCO. (c) Gate-voltage-dependent PNR spin asymmetry from epitaxial LSCO. Note the damping of magnetization with increased positive voltage due to V_O formation [5].

unusual effects due to V_O -order-based symmetry lowering have also been detected, including giant AMR, and will be studied in full. Extension of *operando* probes of electrolyte-gated devices will also expand to other methods such as X-ray spectroscopy. Finally, the issue of the unexplained ferromagnetism in undoped LaCoO_3 , and the associated possibility to approach a spin-state quantum critical point, will be tackled by combining heterostructure growth with PNR.

Publications (specific to this abstract)

[1] *Glass-like through-plane thermal conductivity induced by oxygen vacancies in nanoscale epitaxial $\text{La}_{0.5}\text{Sr}_{0.5}\text{CoO}_{3-\delta}$* , X. Wu, J. Walter, T. Feng, J. Zhu, H. Zheng, J.F. Mitchell, N. Biskup, M. Varela, X. Ruan, C. Leighton and X. Wang, *Adv. Funct. Mater.* **27**, 170423 (2017).

[2] *Perpendicular magnetic anisotropy via strain-engineered oxygen vacancy ordering in epitaxial $\text{La}_{1-x}\text{Sr}_x\text{CoO}_3$* , J. Walter, M. Cabero Piris, B. Yu, G. Yu, M. Greven, M. Varela, and C. Leighton, *Phys. Rev. Materials (Rapid Comm.)* **2**, 111404(R) (2018).

[3] *Interface-induced phenomena in magnetism*, F. Hellman, A. Hoffmann, Y. Tserkovnyak, G.S.D. Beach, E.E. Fullerton, C. Leighton, A.H. MacDonald, D.C. Ralph, D.A. Arena, H.A. Durr, P. Fischer, J. Grollier, J.P. Heremans, T. Jungwirth, A.V. Kimel, B. Koopmans, I.N. Krivorotov, S.J. May, A.K. Petford-Long, J.M. Rondinelli, N. Samarth, I.K. Schuller, A.N. Slavin, M.D. Stiles, O. Tchernyshyov, A. Thiaville and B.L. Zink, *Rev. Mod. Phys.*, **89**, 025006 (2017).

[4] *Electrical transport, magnetic, and thermodynamic properties of La-, Pr- and Nd-doped $\text{BaSnO}_{3-\delta}$ single crystals*, E. McCalla, D. Phelan, M.J. Krogstad, B. Dabrowski and C. Leighton, *Phys. Rev. Materials* **2**, 084601 (2018).

[5] *Ion-Gel-Gating-Induced Oxygen Vacancy Formation in Epitaxial $\text{La}_{0.5}\text{Sr}_{0.5}\text{CoO}_{3-\delta}$ Films from in operando X-ray and Neutron Scattering*, J. Walter, G. Yu, B. Yu, A. Grutter, B. Kirby, J. Borchers, Z. Zhang, H. Zhou, T. Birol, M. Greven, and C. Leighton, *Phys. Rev. Materials (Rapid Comm.)* **1**, 071403(R) (2017).

[6] *Electrolyte-based control of functional materials: Electronics or ionics?*, C. Leighton, *Nat. Mater.* **18**, 13 (2019).

[7] *Giant electrostatic modification of magnetism via electrolyte-gate-induced cluster percolation in $\text{La}_{1-x}\text{Sr}_x\text{CoO}_{3-\delta}$* , J. Walter, T. Charlton, H. Ambaye, M. R. Fitzsimmons, P. P. Orth, R. M. Fernandes and C. Leighton, *Phys. Rev. Materials (Rapid Comm.)* **2**, 111406(R) (2018).

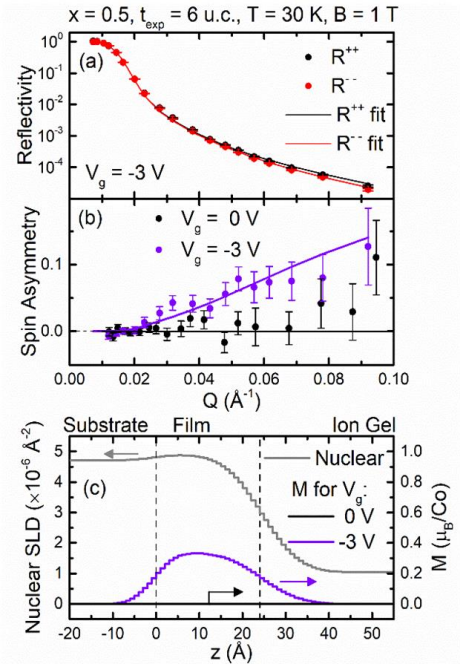


Figure 3: PNR (a) and spin asymmetry (b) data at 0 and -3 V gate voltage on a 6-unit-cell-thick LSCO film at 30 K and 1 T. (c) Refined magnetization depth profile [7].

Phason fast propagation and damping in ferroelectric materials

Michael E. Manley

Materials Science & Technology, Oak Ridge National Laboratory, Oak Ridge, TN

Publication:

M. E. Manley, P. J. Stonaha, D. L. Abernathy, S. Chi, R. Sahul, R. P. Hermann, J. D. Budai, “Supersonic propagation of lattice energy by phasons in fresnoite,” *Nature Commun.* **9**, 1823 (2018).

The existence of mutually incompatible elements of translational symmetry (i.e. incommensurate periodicities) introduces new quasiparticle excitations called phasons and amplitudons [1-5]. Phasons are acoustic-like excitations in the phase of the incommensurate modulation and amplitudons are optic-like excitations in the amplitude of the incommensurate modulation. In an inelastic neutron scattering spectrum phasons appear as gapless excitations emerging from the incommensurate reflections in a way similar to the acoustic phonons emerging from the primary Bragg reflections. However, phasons can have qualitatively different properties than acoustic phonons, including supersonic propagation velocities [4, 5], an intrinsic glass-like overdamping at long wavelengths, and low-energy gaps if the phase becomes pinned by imperfections in the incommensuration [6]. Glass-like overdamping originates with the viscosity of sliding the phase of an incommensurate modulation through the crystal [6]. These lattice excitations, which rearrange atoms rather than translate them as in phonons, are important because they contribute novel channels to bulk behavior including transport and thermodynamic properties.

Using neutron scattering, we made the first observations of the supersonic propagation of pure lattice energy (heat) in the piezoelectric fresnoite ($\text{Ba}_2\text{TiSi}_2\text{O}_8$) [4]. Our results show that energy moves at surprisingly high speeds of up to 4.3 times the speed of sound in the form of phasons. Phasons are usually overdamped and move diffusively. However, the phasons in fresnoite are found not to be overdamped owing to a characteristic rotation of the phasons away from the driving soft phonon, yielding the supersonic propagation. These supersonic phasons enhance thermal conductivity and propagate lattice energy at speeds well beyond the limits of phonons.

A comparison of the phason formation with the thermal transport properties indicate that these excitations make a significant, ~20%, positive contribution to in-plane thermal transport, and this

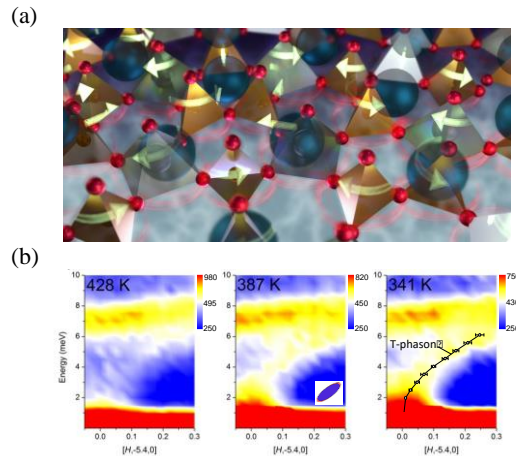


Fig. 1. (a) The twisting and sliding motion of corner-linked titanium pentahedra and pyrosilicate groups arranged in two-dimensional sheets within the structure of fresnoite enable supersonic propagation of the phasonic waves. (Image credit: ORNL/Jill Hemman) (b) Neutron scattering measurements of the phason emerging below a phonon on cooling (HB3 at HFIR).

is supported by simple arguments accounting for the high group velocities and the contribution to the vibrational density of states [4].

Existing inelastic neutron scattering data does not have high enough energy resolution to extract the phason lifetimes, which are critical to determining thermal conductivity, or determining whether there is any pinning gap. Based on an upturn in the low temperature heat capacity, any gap would have to be below about 0.2 meV, which was too small to be resolved using the thermal neutron measurements employed (HB3, HFIR and ARCS, SNS). Hence, as an outlook we plan to measure the phasons on a cold neutron instrument to extract the phason lifetimes and any pinning gap.

References

1. Bak, P. & von Boehm, J. Ising model with solitons, phasons, and “the devil’s staircase”. *Phys. Rev. B* **21**, 5297–5308 (1980).
2. Bak, P. Commensurate phases, incommensurate phases and the devil’s staircase. *Rep. Prog. Phys.* **45**, 587–629 (1981).
3. Axe, J. D. Incommensurate structures. *Philos. Trans. R. Soc. B* **290**, 593–603 (1980).
4. Manley, M. E., Stonaha, P. J., Abernathy, D. L., *et al.* Supersonic propagation of lattice energy by phasons in fresnoite. *Nat. Commun.* **9**, 1823 (2018).
5. Hennion, B., Pouget, J. P. & Sato, M. Charge-density-wave phase elasticity of the blue bronze. *Phys. Rev. Lett.* **68**, 2374–2377 (1992).
6. Cano, A. & Levanyuk, A. P. Explanation of the glass-like anomaly in the low-temperature specific heat of incommensurate phases. *Phys. Rev. Lett.* **93**, 245902 (2004).

Relating local disorder and short-range correlations to material properties using single crystal diffuse scattering

**M.J. Krogstad, R. Osborn, D. Phelan, S.G.E. te Velthuis, O. Chmaissem*, S. Rosenkranz
Argonne National Laboratory; *and Northern Illinois University**

Program Scope

Many material properties are shaped by short-range atomic correlations and local distortions embedded in an otherwise long-range ordered crystalline structure. Relaxor ferroelectrics are an example of such a class of materials that impact a wide range of applications including actuators, transducers, sonar, ultrasound, and energy harvesting. Other examples where ionic correlations and atomic disorder play a critical role include thermoelectrics and ionic conductors. Relaxor ferroelectrics exhibit behavior, *e.g.* a broad peak in the dielectric susceptibility coupled with strong piezoelectric properties, that have long been attributed to complex short-range disorder. But despite intense study of these technologically important materials, the nature of the local order and its relation to the material properties remains controversial, framed by many competing theories.

Obtaining a microscopic understanding of such disorder requires accurate measurements of the total scattering comprising both Bragg peaks from the long-range average order and diffuse scattering from deviations from that average, which includes short-range distortions as well as extended short-range order resulting from defect-defect interactions. Single-crystal diffuse scattering hence offers a powerful probe of the many unusual physical phenomena that are driven by complex disorder, but its use has been limited by the experimental challenge of collecting data over a sufficiently large volume of reciprocal space and the theoretical challenge of modeling the results.

In this program, we are developing methods for efficient measurements over large three-dimensional volumes of reciprocal space, with sufficient resolution to separate diffuse from Bragg scattering and sufficient dynamic range to include both contributions simultaneously, which is necessary to accurately test models of complex disorder. We also incorporate computational advances in order to rapidly transform the large data sets from detector to reciprocal space coordinates for real-time feedback during experimentation. For modeling the local disorder embedded in a crystalline lattice, we are developing novel techniques, such as the transformation of volumes of reciprocal space data into three-dimensional pair-distribution functions (3D-PDF), which provide model-independent images of nanoscale disorder in real space. These techniques are applied to systems in which ionic correlations and atomic distortions play critical roles in their functionalities and generally display strong diffuse scattering and 3D-PDF signatures, which simplify the development and refinement of our techniques. We can then incorporate these methods into our more challenging projects that study

electronic disorder induced by competing, coexisting, and intertwined order, as discussed in a separate abstract.

Recent Progress

We previously designed novel neutron scattering techniques, which led to the construction of *Corelli* at the Spallation Neutron Source. This instrument has the capability of measuring single crystal diffuse scattering over large volumes of reciprocal space with very good momentum resolution for crystals up to 1cm^3 in size, and utilizes the cross-correlation technique to separate elastic from inelastic scattering. The cross-correlation method allows the utilization of the full white beam spectrum, thereby providing two orders of magnitude improvement in measurement efficiency [see Publication 3]. We also developed highly efficient methods that exploit fast area detectors and high x-ray energies at synchrotron facilities to measure the diffuse scattering over large three-dimensional volumes and transform the measured data to physically meaningful coordinates in under 20 minutes, enabling parametric studies of the total scattering over a large range of temperature and doping.

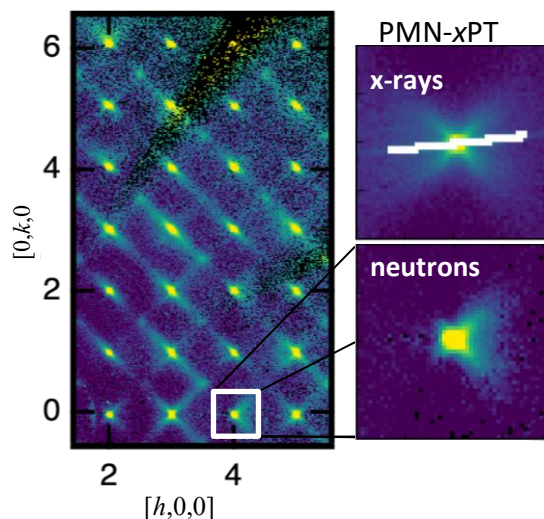


Fig. 1: Diffuse scattering from PMN-30%PT, revealing a strongly asymmetric butterfly shape with neutrons, which is symmetric with x-rays.

Our ability to efficiently measure the elastic scattering from the prototypical relaxor compounds $\text{PbMg}_{1/3}\text{Nb}_{2/3}\text{O}_{3-x}\text{PbTiO}_3$ (PMN-*x*PT) over a large volume of momentum transfer with fine wave-vector resolution allowed us to identify for the first time four distinct forms of local order (i) ferroelectric correlations giving rise to the well-known “butterfly” type scattering, (ii) antiferroelectric correlations, (iii) cation ordering, and (iv) distortions due to mismatched *B*-site radii. Measuring to much larger zones than was previously possible, it is immediately obvious that the “butterfly” type scattering is strongly asymmetric in certain zones when measured with neutrons, but symmetric in x-ray scattering (sig Fig. 1). The compositional dependence of this feature further revealed unambiguously that it is *not* correlated with relaxor behavior, as has been assumed in the majority of

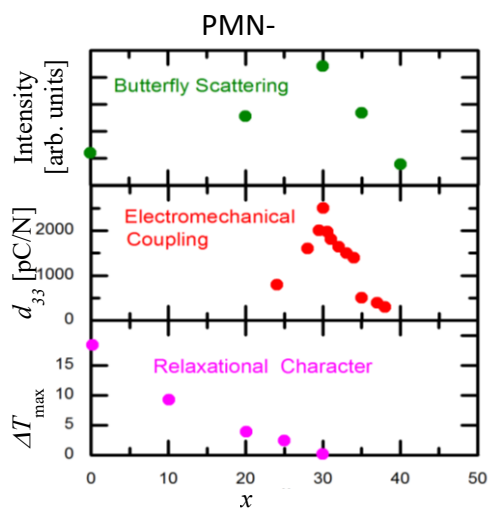


Fig. 2: Compositional dependence of the butterfly scattering intensity and physical properties in PMN-*x*PT.

Our ability to efficiently measure the elastic scattering from the prototypical relaxor compounds $\text{PbMg}_{1/3}\text{Nb}_{2/3}\text{O}_{3-x}\text{PbTiO}_3$ (PMN-*x*PT) over a large volume of momentum transfer with fine wave-vector resolution allowed us to identify for the first time four distinct forms of local order (i) ferroelectric correlations giving rise to the well-known “butterfly” type scattering, (ii) antiferroelectric correlations, (iii) cation ordering, and (iv) distortions due to mismatched *B*-site radii. Measuring to much larger zones than was previously possible, it is immediately obvious that the “butterfly” type scattering is strongly asymmetric in certain zones when measured with neutrons, but symmetric in x-ray scattering (sig Fig. 1). The compositional dependence of this feature further revealed unambiguously that it is *not* correlated with relaxor behavior, as has been assumed in the majority of

previous investigations of PMN-*x*PT. Rather, we find that it is strongly associated with piezoelectric properties (Fig. 2). Furthermore, by studying the same systems with both neutron and x-ray scattering, we showed that the local ordering must involve displacements of both heavy (Pb) and light (O) atoms. This finding demands a reworking of current theoretical models that assume light atom displacements are negligible. Our results further revealed that the relaxor behavior results from the frustration of both local antiferroelectric and ferroic order and that the butterfly-type scattering is strongly correlated with the electro-mechanical properties. Together, these findings provide a set of guidelines for developing and evaluating microscopic displacive models of the piezoelectric properties of other relaxor materials, including the next generation of efficient and Pb-free materials.

Future Plans

The ability to measure full volumes of scattering intensity enables novel avenues to resolve structures with complex disorder *via* transformation into three-dimensional pair-distribution-functions (PDFs). Transforming the entire measured scattering volume produces the total PDF of the structure, *i.e.*, the Patterson function, which includes the PDF of the average structure as well as any deviations from it. One of the unique advantages of single-crystal measurements, as compared to spherically averaged powder PDF or other methods, is that the average structure can be easily removed from the measured data before performing the PDF transformation, thereby providing a much deeper understanding of disorder and local ordering phenomena. The 3D- Δ PDF obtained this way only contains interatomic vectors whose probabilities deviate from the average structure, providing high sensitivity to very weak correlations, usually unobservable with powder diffraction, and also directly providing the morphology of the local order. We have recently started to develop methods to efficiently obtain the 3D- Δ PDF from measured volumes of diffuse scattering, and will further develop the algorithms in order to reduce artefacts induced by truncation and edge effects in the Fourier transforms. We will first apply, test, and develop these methods on systems in which the diffuse scattering is strong and the short-range correlation signatures are well separated from Bragg peaks. This is generally the case in systems with order-disorder transitions, which have a strong influence on phenomena such as ionic conductivity. For such systems, the 3D- Δ PDF will directly determine the length scale of ionic interactions, which are required to validate theoretical models.

Our preliminary experiments performed on $\text{Na}_x\text{V}_2\text{O}_5$ demonstrate how the 3D- Δ PDF can provide direct, model-free visualization of the real-space short-range ordering. In this compound, the Na ions occupy sites on two-leg ladders within

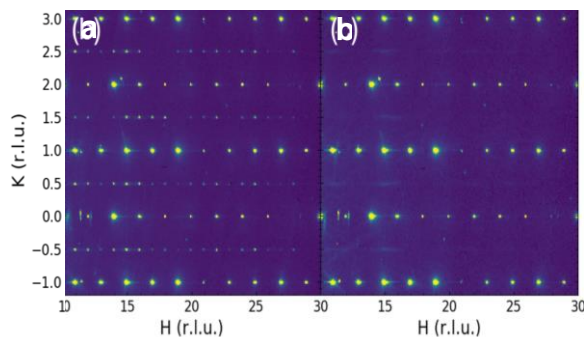


Fig. 3: Scattering from $\text{Na}_{0.45}\text{V}_2\text{O}_5$ in the (HK2) plane at (a) 150K and (b) 250K.

tunnels surrounded by edge-sharing vanadium oxide pyramids and octahedra. At room temperature, the diffuse scattering consists of highly structured rods, representing short-range-order within and between ladders in the same plane (Fig. 3b). However, below 200K, some of the diffuse intensity is transferred into sharp peaks (Fig. 3a) owing to sodium sublattice ordering. While it would be very difficult to directly model the disorder from the diffuse scattering data, the 3D- Δ PDF (Fig. 4) clearly shows without any modeling that the sodium ions tend to occupy alternate sites in a zig-zag configuration that is in phase with neighboring ladders. We plan to utilize and further develop the 3D- Δ PDF analysis to explore the phase diagrams of a range of intercalation compounds of interest, such as $\text{Na}_x\text{V}_2\text{O}_5$, $\text{Mg}_x\text{V}_2\text{O}_5$, and Mg_xTiSe_2 , as well as on other systems for which lattice disorder plays an important role in determining their properties, such as thermoelectrics.

We also plan further developments of the measurement and analysis technique to enable investigations of short-range order and disorder in thin films grown on substrates. The challenge here is to develop strategies to eliminate the normally dominant contributions from the substrate. If the lattice mismatch between substrate and film is sufficient, the 3D- Δ PDF will allow detailed investigations of the longrange structure of the film, but because many substrates exhibit diffuse scattering themselves, more sophisticated approaches may be needed. The 3D- Δ PDF however has great potential to provide novel insight into amorphous films deposited on single crystal substrates. This is a topic of great importance in particular for current research on solid-state electrolytes, where it was recently found that the interfacial reactivity strongly depends on the orientation and crystallinity of the electrolyte film. With nearly perfect single crystal substrates, the 3D- Δ PDF removes all but thermal diffuse scattering contributions from the substrate, such that the only spherically symmetric signal remaining will be from the amorphous film, which can then be analyzed as standard polycrystalline PDF.

We also plan to collaborate with other groups to incorporate our latest developments into their research projects, making this technique available to the wider community and spanning a wide range of fields including order-disorder transitions, lead-free relaxors, lattice disorder in solar perovskites, thermoelectrics, CDW and charge order correlations in a variety of systems, lattice distortions in topological compounds, frustrated magnets and frustrated ferroelectrics, and more.

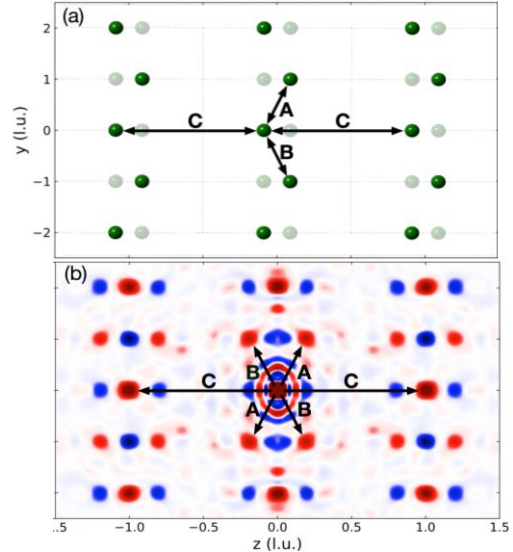


Fig. 4: Real space model of Na correlations in the $x=0$ plane (a) compared to the 3D- Δ PDF transform. The sodium sites form two-leg ladders and the zig-zag model in (a) is derived from (b) by connecting occupied sites with more probable (red) vectors, ignoring neighboring sites with less probable (blue) vectors.

Publications

- 1 M.J. Krogstad, S. Rosenkranz, J.M. Wozniak, G. Jennings, J.P.C. Ruff, J.T. Vaughey, R. Osborn, Reciprocal Space Imaging of Ionic Correlations in Intercalation Compounds, *Nature Materials* under review (2019).
- 2 M.J. Krogstad, P.M. Gehring, S. Rosenkranz, R. Osborn, Feng Ye, Yaohua Liu, J.P.C. Ruff, W. Chen, J.M. Wozniak, H. Luo, O. Chmaissem, Z.-G. Ye, and Daniel Phelan, The Relation of Local Order to Material Properties in Relaxor Ferroelectrics, *Nature Materials* **17**, 718 – 724 (2018).
- 3 Feng Ye, Yaohua Liu, Ross Whitfield Ray Osborn, Stephan Rosenkranz, Implementation of cross correlation for energy discrimination on the time-of-flight spectrometer CORELLI, *J. Appl. Cryst.* **51**, 315-322 (2018).

Exploiting Small Signatures: Quantifying Nanoscale Structure and Behavior

Katharine Page, Neutron Sciences Division, Oak Ridge National Laboratory

Program Scope

In catalysis, biomineralization and drug delivery, fuel cell and battery chemistry, geological processes, and a host of functional phenomena at the nanoscale, unique properties and material characteristics are governed by intricate structural details eluding current characterization methods. This program encompasses side-by-side development and application of neutron total scattering methods, aimed at uncovering the links in nanostructure between surface chemistry, particle morphology, and “internal” crystal structure. Scientific themes include: (1) unraveling the formation, transformation, and structure-property mechanisms in metastable oxide nanomaterials important in energy applications and the environment, including polymorph formation in hydrothermal and solvothermal environments; and (2) the distinct effects of particle shape and surface termination on the properties and structural phase transitions of ferroelectric oxide nanocrystals, including factors that stabilize polarization at smaller nanocrystal dimensions, across phase transitions, or under applied field. Concurrently, instrumentation, data collection, data reduction, and structure refinement methodologies will be advanced for *in situ* and stroboscopic neutron total scattering measurements. These investigations will set the stage for a broader approach to nanostructure and interface characterization that validates theory and simulation, evaluates synthesis and fabrication, and demonstrates enhanced performance in atomic- and nano-scale material processes.

Recent Progress

Over the reporting period we have addressed several outstanding materials challenges for which the advantages of neutron total scattering are essential: we explored the morphology-dependent catalytic properties of titanium and cerium oxide nanocrystals, the structure and electrochemical function of layered manganese oxide nanostructured materials, and a universal nanoscale cation ordered ground state in inverse spinel oxides. We have also examined the influence of size, shape, and ligand attachment on internal atomic structure in ferroelectric BaTiO₃ nanocrystals. Alongside these efforts we have made significant progress in developing and deploying tools and methods for improved quantification of nanoscale structure and behavior with diffraction and pair distribution function (PDF) techniques.

Nanostructured Polymorphs. Titania Nanocrystals. Anatase TiO₂ nanocrystals have attracted tremendous attention in recent years due to their excellent catalytic performance. Nanocrystals with dominant {001} facets present higher surface energy and (in theory) more active sites relative to other forms. Despite successes in synthesizing anatase TiO₂ nanocrystals with different {001} ratios, the impact of morphology on catalytic activity is still debated. We have carried out a

comprehensive structure study of anatase TiO₂ nanocrystals with different ratios of {101} and {001} facets. We have demonstrated that Differential Evolutionary fitting utilizing Debye scattering analysis of Bragg diffraction and PDF data can be used to obtain accurate atomistic structure and morphology information. The analysis of shape and size distribution agrees remarkably well with Transmission Electron Microscopy (TEM) and Small Angle Neutron Scattering (SANS) results. Our results on anatase TiO₂ nanocrystals with different {001} to {101} ratios demonstrates that samples with an intermediate amount of both {001} and {101} facets shows the best photocatalytic hydrogen evolution reaction (HER) activity [1]. We are currently applying similar methodology to quantify the effect of morphology and surface termination on the catalytic performance of various ceria nanoparticles. **Manganese Oxide Nanostructured Materials.** Considerable interest has been given to the electrochemical capacitance of manganese dioxide. It is well known that defects, microstructure, and crystalline polytype play critical roles in determining the specific capacitance and electrode cycling stability. Disentangling the influence of structural characteristics in poorly crystalline nanoscale manganates remains a significant challenge, while nanostructuring is a frequent strategy in device optimization. We have completed a comprehensive structure determination of Cu and vacancy rich layered δ -MnO₂ nanoflowers, determining a new synthesis route to large-scale volumes of the material (Figure 1) [2]. A second manuscript detailing electrochemical structure-property relationships in a series of MnO₂ polymorphs

resulting from dehydration of the parent (hydrated) phase is currently under preparation. Intriguing electrochemical behavior of the defect-rich layered oxide inspired us to explore cathode materials with appreciable vacancies on transition metal layers: Na₂Mn₃O₇ [3] and P3-type Na_{2/3}Mg_{1/3}Mn_{2/3}O₂ [4]. In these systems, vacancies on the MnO₂ layer are found to induce reversible lattice oxygen redox

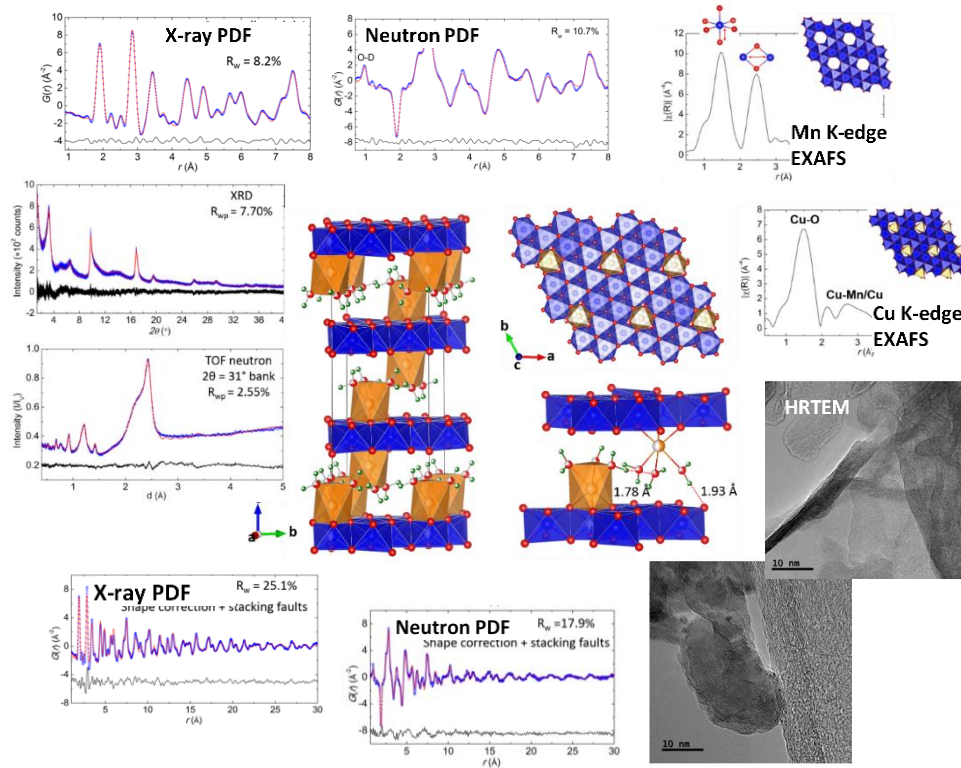


Figure 1. Comprehensive structural characterization of a heavily stacking faulted Cu-rich δ -MnO₂ nanoflower. Local x-ray and neutron PDF along with Cu K-edge and Mn K-edge EXAFS studies enable determination of the layer motif and the identification/quantification of interlayer Cu²⁺ and H₂O species. HRTEM, intermediate-range PDF, and x-ray and neutron diffraction approaches enable the determination of average stacking sequences and nanoparticle dimensions.

activity. Neutron total scattering is demonstrated as an ideal bulk characterization technique to investigate mechanisms for lattice oxygen redox and facilitate design and exploration of next generation battery cathode materials with potential superior energy densities.

Ferroelectric Nanocrystals. In this portion of the project, we are working towards *in situ* and stroboscopic studies of nanoscale ferroelectric spheres and cubes, examining the influence of size, surface and morphology on internal dipole-dipole correlations. These results will provide new information about the nature of ferroelectric materials at the limits of size reduction, offering guidance for the development of applications involving device miniaturization. **Nanospheres and Nanocubes:** We have completed detailed structural characterization of two series of nanocrystals; spheres ranging in diameter between 8 and 100 nm, and cubes ranging in diagonal dimension between 8 and 100 nanometers. We do not find significant differences in the internal dipole ordering of these nanocrystals, though we do find evidence for the presence of multi-domains in larger particles. A manuscript is currently in progress describing these findings.

Impurity Phases: Barium carbonate (BaCO_3) impurities are present in many published BaTiO_3 nanocrystal studies (and were present in our early studies). There are no detailed literature reports on the effect of the impurities, the process of removing them, and their impact on accurate determination of structure. We have now studied these effects with a set of seven nanocube samples of varying size, where half of each batch was treated to remove impurities. We find no significant changes to nanoparticle size or atomic structure after removal of the carbonate phase, and we provide evidence that it is a separate phase (not surface) impurity. We have submitted these results for publication.

Effect of Capping Ligands: We have investigated the internal dipole ordering of a series of BaTiO_3 nanocubes decorated with polar and nonpolar ligands utilizing neutron and x-ray total scattering approaches. We find that polar ligands at the surfaces of nanocubes stabilize internal dipoles. Neutron total scattering studies of the NOBF_4 (polar) capped nanoparticles reveals the nature of Ti-O pair-pair correlations at $\sim 2 \text{ \AA}$, as shown in **Figure 2**. The nanocubes are seen to exhibit the same type and degree of rhombohedral local distortion at room temperature as bulk BaTiO_3 , albeit with *increased* correlation length scale. We are preparing a manuscript describing our scientific findings.

New Tools and Methods for Quantification of Nanoscale Structure. Along the way to accomplishing the above studies, we are advancing neutron total scattering methods for nanoscale systems, producing new sample environment, data reduction, and data modeling tools for broad use. Several significant advancements in this arena include the following. **Nanocrystal Shape Functions:** In the structural refinement of nanoparticles, discrete atomistic modeling can be used for small nanocrystals ($< 15 \text{ nm}$), but becomes computationally unfeasible at larger sizes, where instead unit-cell based “small-box” modeling is usually employed. We have developed a method to derive numerical approximations of nanoparticle shape functions by fitting to a training set of discrete calculated shapes; the numerical approximations can then be implemented for larger

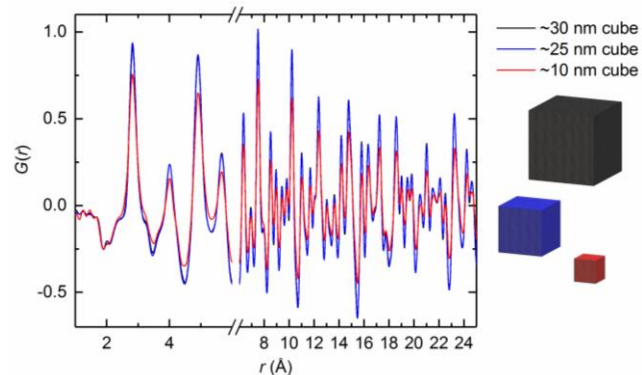


Figure 2: Neutron PDFs of three sizes of nanocubes with NOBF_4 capping ligands at room temperature. The local rhombohedral bonding environment (three short and three long Ti-O pair-pair correlations at $\sim 2 \text{ \AA}$) is observable in all three sizes.

nanocrystal sizes [5]. We are using this modeling approach in our quantitative nanostructure study of BaTiO₃ cubes, CeO₂ rods and cubes, as well as several others, and we are currently working on extensions to model polydispersity of nanostructures with this approach. ***Combinatorial Appraisal of Transition States (CATS) Software:*** *In situ* total scattering measurements are increasingly utilized to follow atomic and nano-scale structural details of phase transitions and other transient processes in materials. We have published a manuscript [6] and released associated software for an automated method to analyze series of diffraction and pair distribution function data with a linear combination of end-member states. CATS is useful in quantitative evaluation of many transient processes, including for *in situ* crystallization and growth. ***Implications of Time-of-flight Neutron Total Scattering:*** Our work explicitly exploring the effects of resolution, peak-shape, peak-asymmetry, inconsistent conversion of TOF-to-d spacing, and merging of multiple banks in neutron TOF data as they relate to accuracy in real-space neutron PDF analysis has been published as a feature article in *Acta Crystallographica Section A* [7]. The work discusses best practices for analysis of data from modern neutron TOF total scattering instruments when using available analysis programs and defines a roadmap for future instrumentation and data reduction/analysis advancements in the field.

Future Plans

We plan two tasks that build upon the scientific foundations above. The first involves the study of enhanced ferroelectric nanoparticle ensembles suspended in polymer matrices, including diffraction/PDF measurements under applied electric fields. Additional compositional spaces (NaNbO₃, PbTiO₃, BiFeO₃, SrTiO₃, mixtures, etc.) and a range of sizes/shapes (rods, cubes, plates, etc.) will be explored, determining whether enhancing effects found in BaTiO₃ are universal, and if internal order/response can be designed, predicted and controlled. The second will follow the nucleation, growth, and coarsening of nanocrystals *as they are formed* with neutron diffraction/PDF measurements. This will involve commissioning a null scattering sample environment currently under development for hydrothermal/solvothermal synthesis, following *in situ* the morphology / atomistic structure evolution of metal oxide particles (key to understanding, for example, the growth mechanisms and catalytic poisoning of specifically faceted nanocrystals). This foundational work will make full use of our previous developments in whole particle modeling, data stream monitoring algorithms, and sample environment developments, furnishing guidance for future studies in materials/properties areas of interest to the scientific community.

References

- [1] J. Liu et al., *Chem. Mater.* **29** (2017) 5591–5604.
- [2] J. Liu et al., *Inorg. Chem.* **57** (2018) 6873–6882.
- [3] B. Song et al., *Chem. Mater.* **311** (2019) 03756–3765.
- [4] B. Song et al., *J. Mater. Chem. A* **7** (2019) 1491–1498.
- [5] T.-M. Usher et al., *Acta Cryst. A* **74** (2018) 322–331.
- [6] D. Olds et al., *J. Appl. Cryst.* **50** (2017) 1744–1753.
- [7] D. Olds et al., *Acta Cryst. A* **74** (2018) 322–331.

Publications

1. Hsiu-Wen Wang*, Luke L. Daemen, Michael C. Cheshire, Michelle K. Kidder, Andrew G. Stack, L. F. Allard, Joerg Neufeind, D. Olds, J. Liu, and Katharine Page*, Synthesis and structure of synthetically pure and deuterated amorphous (basic) calcium carbonates, *Chemical Communications*, 53, 20, 2942-2945 (2017). <http://dx.doi.org/10.1039/C6CC08848A>
2. Daniel Olds, Katharine Page*, Arnold Paecklar, Peter F. Peterson, Jue Liu, Gerald Rucker, Mariano Ruiz-Rodriguez, Michael Olsen, Michelle Pawel, Steven H. Overbury, and James R. Neilson, A high precision gas flow cell for performing in situ neutron studies of local atomic structure in catalytic materials, *Review of Scientific Instruments*, **88**, 3, 034101 (2017). <http://dx.doi.org/10.1063/1.4978287>
3. Jue Liu*, Lei Yu, Daniel Olds, Guoshiou Foo, Zili Wu, Beth Guiton, and Katharine Page*, The morphology of {101} and {001} faceted anatase TiO₂ nanocrystals, *Chemistry of Materials* 29 (2017) 5591–5604. <https://dx.doi.org/10.1021/acs.chemmater.7b01172>
4. Shiliang Zhou, Erica S. Howard, Jue Liu, Nicholas Bashian, Kyle Nolan, Sankarganesh Krishnamoorthy, Geovanni M. Rangel, Moulay-Tahar Sougrati, G. K. Surya Prakash, Katharine Page, and Brent Melot*, Hydrothermal Preparation, Crystal Chemistry, and Redox Properties of Iron Muscovite Clay, *ACS Applied Materials & Interfaces*, 9 (2017) 34024-34032. <https://dx.doi.org/10.1021/acsami.7b08729>
5. Heinz Nakotte, Corinne Silkwood, Katharine Page, Hsiu-Wen Wang, Daniel Olds, Boris Kiefer, S. Manna, D. Karpov, Edwin Fohtung, and Eric E. Fullerton, Pair Distribution Function Analysis Applied to Decahedral Gold Nanoparticles, *Physica Scripta* 92 (2017) 114002. <http://dx.doi.org/10.1088/1402-4896/aa8afd>
6. Douglas H. Fabini, Ting Ann Siaw, Constantinos C. Stoumpos, Geneva Laurita, Daniel Olds, Katharine Page, Jerry G. Hu, Mercouri G. Kanatzidis, Songi Han, and Ram Seshadri*, Universal Dynamics of Molecular Reorientation in Hybrid Lead Iodide Perovskites, *Journal of the American Chemical Society*, 139 (2017) 16875-16884. <https://dx.doi.org/10.1021/jacs.7b09536>
7. Daniel Olds, Peter Peterson, Michael Crawford, James Neilson, Hsiu-Wen Wang, Pamela Whitfield and Katharine Page*, Combinatorial Appraisal of Transition States for in situ Pair Distribution Function Analysis, *Journal of Applied Crystallography* 50, (2017) 1744-1753. <https://doi.org/10.1107/S1600576717015163>
8. Daniel Olds, Keith V. Lawler, Arnold A. Paecklar, Jue Liu, Katharine Page*, Peter F. Peterson, Paul M. Forster, and James R. Neilson, Capturing the details of N₂ adsorption in zeolite X using stroboscopic isotope contrasted neutron total scattering, *Chemistry of Materials* 30 (2018) 296–302. <https://dx.doi.org/10.1021/acs.chemmater.7b04594>
9. Tedi-Marie Usher, Daniel Olds, Jue Liu, and Katharine Page*, A numerical method for deriving shape functions of nanoparticles for pair distribution function refinements, *Acta Crystallographica Section A* 74 (2018) 322-331. <https://doi.org/10.1107/S2053273318004977>

10. Daniel Olds, Claire N. Saunders, Megan Peters, Thomas Proffen, Joerg Neufeind and Katharine Page*, Precise implications on real-space PDF modeling from effects intrinsic to modern time of flight neutron diffractometers, *Acta Crystallographica Section A* 74 (2018) 293-307. <https://doi.org/10.1107/S2053273318003224>
11. Jue Liu, Lei Yu, Enyuan Hu, Beth S. Guiton, Xiao-Qing Yang, and Katharine Page*, Large scale synthesis and comprehensive structure study of δ -MnO₂, *Inorganic Chemistry*, 57 (2018) 6873-6882. <https://doi.org/10.1021/acs.inorgchem.8b00461>
12. Daniel Olds, Rebecca A. Mills, Marshall T. McDonnell, Jue Liu, Joshua R. Kim, Matthew T. Dunstan, Michael W. Gaultois, S. Michelle Everett, Matthew G. Tucker, and Katharine Page*, A high temperature gas flow environment for neutron total scattering studies of complex materials, *Review of Scientific Instruments*, **89** (2018) 092906. <https://doi.org/10.1063/1.5033464>
13. Tedi-Marie Usher, Jennifer S. Forrester, Marshall McDonnell, Joerg Neufeind, Katharine Page*, Peter Peterson, Igor Levin, and Jacob L. Jones, Time of flight neutron total scattering with applied electric field: ex situ studies of ferroelectric materials, *Review of Scientific Instruments* **89** (2018) 092905. <https://doi.org/10.1063/1.5037609>
14. Peter F. Peterson*, Daniel Olds, Andrei T. Savici, and Wenduo Zhou, Advances in utilizing event-based data structures for neutron scattering experiments, *Review of Scientific Instruments* **89** (2018) 093001. <https://doi.org/10.1063/1.5034782>
15. Lei Yu, Ruixin Han, Xiahan Sang, Jue Liu, Bethany M. Hudak, Amita Patel, Katharine Page, and Beth S. Guiton*, Independent Control of Structure, Composition, and Morphology in the Creation of Hollow Iron Oxide Nanocapsules, *ACS Nano* **12** (2018), 9051-9059. <https://doi.org/10.1021/acsnano.8b02946>
16. Bohang Song, Enyuan Hu, Jue Liu*, Yiman Zhang, Xiao-Qing Yang, Nanda Jagjit, Ashfia Huq*, and Katharine Page*, P3-type Na_{2/3}Mg_{1/3}Mn_{2/3}O₂ as a High Capacity and Low-Cost Sodium-Ion Cathode using Oxygen Redox Reaction, *Journal of Materials Chemistry A* **7** (2019) 1491-1498. <https://doi.org/10.1039/C8TA09422E>
17. Pinghui Zhanga, Jue Liu, Katharine Page, and Alexandra Navrotsky*, Calorimetric study of the thermodynamic properties of Mn₅O₈, *Journal of the American Ceramic Society*, **102** (2019) 1394-1401. <https://doi.org/10.1111/jace.15951>
18. Bohang Song, Mingxue Tang, Enyuan Hu, Olaf J. Borkiewicz, Kamila M. Wiaderek, Yiman Zhang, Nathan D. Phillip, Xiaoming Liu, Zulipiya Shadike, Cheng Li, Likai Song, Yan-Yan Hu, Miaofang Chi, Gabriel M. Veith, Xiao-Qing Yang, Jue Liu*, Jagjit Nanda*, Katharine Page*, and Ashfia Huq*, Understanding the low voltage hysteresis of anionic redox in Na₂Mn₃O₇, *Chemistry of Materials*, **311** (2019) 3756-3765. <https://doi.org/10.1021/acs.chemmater.9b00772>
19. Jue Liu*, Xuelong Wang, Olaf Borkiewicz, Enyuan Hu, R.-J. Xiao, L. Chen, and Katharine Page*, A unified view of the local cation ordered state in inverse spinel oxides, submitted.
20. Katharine Page*, Andrew G. Stack, and Hsiu-Wen Wang*, Nanopore facilitated monohydrocalcitic amorphous calcium carbonate precipitation, submitted.

21. Tedi-Marie Usher, Benard Kavey, Gabriel Caruntu, and Katharine Page*, The effect of BaCO₃ impurities on the structure of BaTiO₃ nanocrystals, submitted.

Ionic Polymers Under Dynamic Conditions: Shear and Electrical Field Response

Dvora Perahia, Clemson University, Clemson SC 29634-0973

Program Scope

Structure and dynamics results resolved from neutron techniques including small angle neutron scattering (SNS), neutron spin echo (NSE) and quasi elastic neutron scattering (QENS), accompanied by large scale molecular dynamics simulations (MD) studies on ionic polymers in their quiescent state and under fields, present a first comprehensive insight into the factors that control the delicate balance of van der Waals forces and electrostatic interactions in ionic polymers. With a distinctive goal of resolving the physics that underline the behavior of ionic polymers under shear and electric perturbation, the knowledge obtained will affect the energy-water nexus. In their many applications, such as clean energy, water purification, protective layers, memory shape material and a large variety of biotechnologies, ionic polymers function under shear and electric fields. In their quiescent state the segregation between ionic and non-ionic domains enables their function and stability. While the quiescent state has been thoroughly interrogated, the effects of shear and electrical fields on this class of macromolecules is yet to be resolved. The challenge lies in the need to probe inherently non-equilibrium systems, under changing conditions. Detailed neutron scattering studies including in situ measurements under fields, coupled with atomistic MD simulations and complimentary techniques, are used to derive quantitative structure-dynamics-forces correlations in model ionic polymers. The effects of fields on their structure and dynamics determines the performance-longevity-safety-cost foundation that underlines their uses.

A broad knowledge base points to the fact that the macroscopic properties of ionizable polymers immerge from coupling of nano aggregates of ionizable groups across length scales.¹⁻³

These ionizable groups tethered to the polymers act as “stickers” and assemble to form ionic domains, which drive the structure and dynamics of the macromolecules. An example of ionic domains in polystyrene sulfonate (PSS) as depicted by molecular dynamics (MD) simulations⁴ of an ionomer melt is shown in Figure 1.⁵ The program includes three major directions: a) understanding dynamics in the quiescent, non-perturbed state, b) resolving shear effects, b) following response to electric fields, as the cohesiveness of the ionic interactions are controlled. Through bridging across length, time and energy scales, we have obtained transformative fundamental knowledge that underline dynamic ionic assemblies under fields. This in turn will impact the design of new ionic polymers with controlled properties.

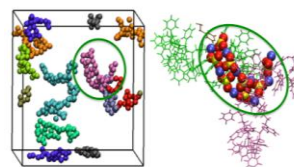


Figure 1 Distinctive ionic clusters in PSS-Na melts for $N=40$ at 10% random sulfonation at 600K. Right: zooming in on a cluster with a few chains shown. S-Yellow, Red-Oxygen, Blue sodium. (Agrawal et al., PRE 2015).

Recent Progress

SANS, QENS and NSE, coupled with MD simulations have been employed to determine the correlation of segmental dynamics of polystyrene sulfonic acid (PSS) in solution, whilst the cohesiveness of the ionic clusters is tuned by polar solvents. The molecular understanding attained by neutrons together with computational insight is discussed, focusing on multi-length scale dynamics. We find that driven by electrostatic forces, networks of polystyrene sulfonates are formed in solutions at extremely low ionic content of 3-9%mol (% of sulfonated aromatic groups) PSS. This sulfonation levels are well into the ionomer regime where both the inherent backbone conformation and the ionic charge affect the system.

SANS measurements presented in Figure 2 coupled with MD simulations, show that network is formed in toluene, even though only limited number of clusters are formed. Perturbing the electrostatic interactions through polar solvents results in breaking of ionic assemblies, and the long-range correlations captured at low q values diminish. The ionic groups remain segregated into ionic clouds that retain polar domains but allows dynamics within the network.

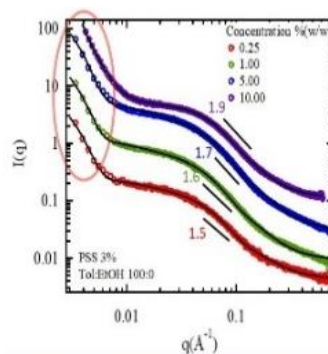


Figure 2. SANS patterns of PSS 3% sulfonation at the indicated concentrations of PSS in toluene.

Segmental dynamics measurements by QENS as solvent dielectrics is tuned by eloquent of ethanol added to 10%(w/w) PSS in cyclohexane captures the motion on the length scale of 0.5-2nm are shown in Figure 3. Cyclohexane is chosen to clearly distinguish the signal of the polymer from that of the solvent. A Kohlrausch -Williams -Watts (KWW) analysis provides characteristic relaxation times, and their distribution.⁶ Here we show for the first time that in hydrophobic solvents, the segmental dynamics, which is a relatively fast motion, is constrained in solutions on the length scale of the ionic interactions and clusters, depending on the ionic strength, as manifested at $q=0.3 \text{ \AA}^{-1}$. However segmental dynamics persists on the length scale of the smallest rigid segments. Addition of small amounts of ethanol enhances dynamics across the entire q range measured, however the effects become larger for larger q values. Overall, both ionic clusters and ionic

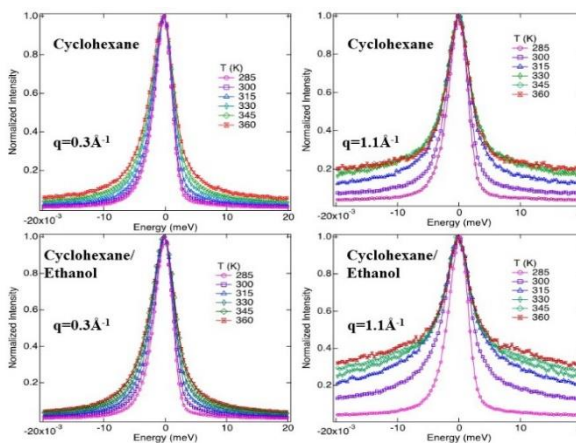


Figure 3. QENS data at two representative q values for PSS in cyclohexane and cyclohexane-ethanol at the indicated temperatures. Measured on BASIS at SNS. The lines correspond to KWW analysis.

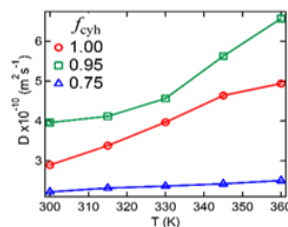


Figure 4. Effective diffusion extracted from fits to KWW model as a function of temperature.

clouds affect segmental motion on multiple length scales. MD simulations have shown that in low concentrations, the ethanol resides predominantly at the ionic groups. Studies of the degree of association are underway.

Increasing ethanol concentration further however, results in penetration of the solvent into the styrene matrix, resulting in tighter packing of the polymer backbone and constraints on the polymer motion, even though the polymers remain soluble. Effective diffusion constants extracted from these data are shown in Figure 5 as a function of temperature. For all networks, the dynamics increases with increasing temperature, where the theta temperature of PS in cyclohexane is marked by enhanced dynamics, for the pure solvent and small additions of ethanol. As the ethanol penetrates the styrene domain, the dynamics slows down significantly. An in-depth analysis coupling the QENS data with MD simulations are underway to define the actual atomistic level motion that controls the dynamics of the polymer.

The motion of the ionomer networks on the length scale of propagation of electrostatic interactions and that of the ionic clusters is captured by NSE. The time and length scales accessible to NSE cover molecular diffusion on the length scale where the nano-structures persist, and classical motion of polymer chains take place, as the ionic assemblies were tuned with polar solvent. The addition of ethanol perturbs the physical crosslinks of the PSS network. $S(q,t)$, the dynamic structure factor, measured across a broad temperature range, is analyzed first by KWW followed by a sum of two exponentials. Example of NSE spectra and their analysis are shown in Figure 5. We find that at length scales that correspond to the ionic domains, the motion is constrained in both solvents; however, ethanol enhances the dynamics. While the ionic domains expand, the dynamics remain restricted, pointing to formation of “ionic clouds” where the ionic clusters are swollen with alcohol, but remain segregated, retaining the physical crosslinks of the network. At smaller dimensions, the dynamics becomes significantly faster and no differences are observed as

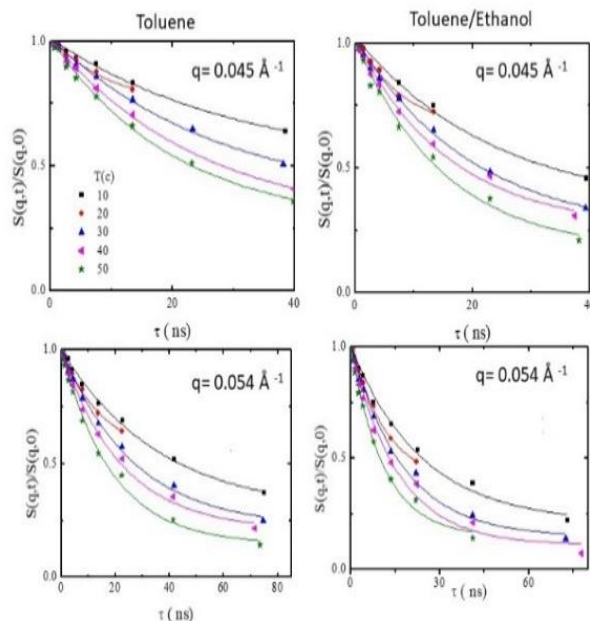


Figure 5. NSE measurements. Data were measured in SNS over three periods of 8 days each. The results for different q values are presented on different time scales since for the lower q the longer times become noisy. The solid lines correspond to KWW fits.

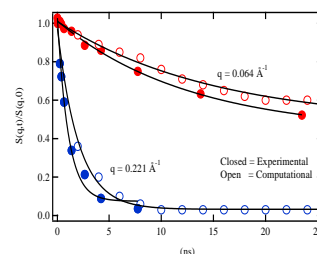


Figure 6: Experimental and computational $S(q,t)$. These are within the error of the measurements.

ethanol was added. Increasing the temperature results in equal acceleration of the motion across all q values, indicative of retaining the dynamic, swollen, physical crosslinks.

On the molecular level understanding of the dynamics will be attained from conjunction of NSE data and MD simulations. The excellent agreement between the experimental and computational $S(q,t)$ is demonstrated for two representative q values in Figure 6. This outstanding match will enable us to attain a direct observation of the dynamics on the length scale of the electrostatic interaction.

Future Plans

Following the study of the quiescent state of PSS in its sulfonic acid form, the effort will focus on two aspects, understanding the structure of ionic polymers under shear and commence the study under electrical fields. The effects of electrical fields on the ionic clusters are demonstrated through MD simulations in Figure 7. These preliminary results show that direct electric fields dissociate the clusters completely, in contrast to polar solvents that retain “ionic clouds”.

The efforts will concentrate of experiments on a) linear PSS with three different counterions: H^+ , Na^+ and Mg^{2+} followed by enhanced complexity. The next step in morphological complexity of ionic co-polymers are diblocks, where one block is ionizable and the other is neutral. Here we will study PS-PSS diblock co-polymers in their quiescent state and under shear.

References

1. Middleton, L. R.; Winey, K. I., Nanoscale Aggregation in Acid-and Ion-Containing Polymers. *Ann. Rev. Chem. Biomolecular Eng.* **2017**, *8*, 499-523.
2. Aryal, D.; Agrawal, A.; Perahia, D.; Grest, G. S., Structure and Dynamics of Ionic Block Copolymer Melts: Computational Study. *Macromolecules* **2017**, *50*, 7388-7398.
3. Ma, B.; Nguyen, T. D.; Pryamitsyn, V. A.; Olvera de la Cruz, M., Ionic correlations in random ionomers. *ACS nano* **2018**, *12*, 2311-2318.
4. Agrawal, A.; Perahia, D.; Grest, G. S., Cluster Morphology-Polymer Dynamics Correlations in Sulfonated Polystyrene Melts: Computational Study. *Phys. Rev. Lett.* **2016**, *116*, 158001.
5. Agrawal, A.; Perahia, D.; Grest, G. S., Clustering effects in ionic polymers: Molecular dynamics simulations. *Physical Review E* **2015**, *92*, 022601.
6. Osti, N.; Etampawala, T.; Shrestha, U.; Aryal, D.; Tyagi, M.; Diallo, S.; Mamontov, E.; Cornelius, C.; Perahia, D., Water dynamics in rigid ionomer networks. *J. Chem. Phys.* **2016**, *145*, 224901.

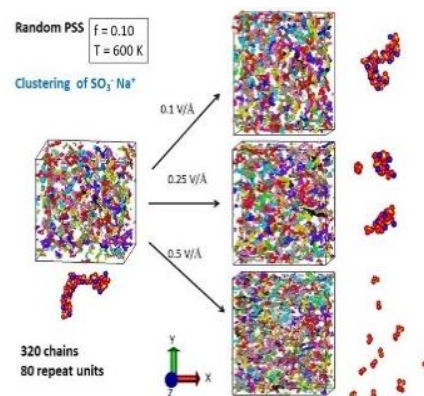


Figure 7. Computational insight into the effects of electric fields on ionic clusters in PSS. Different chains are marked in different colors.

Quantum Materials for Energy Science

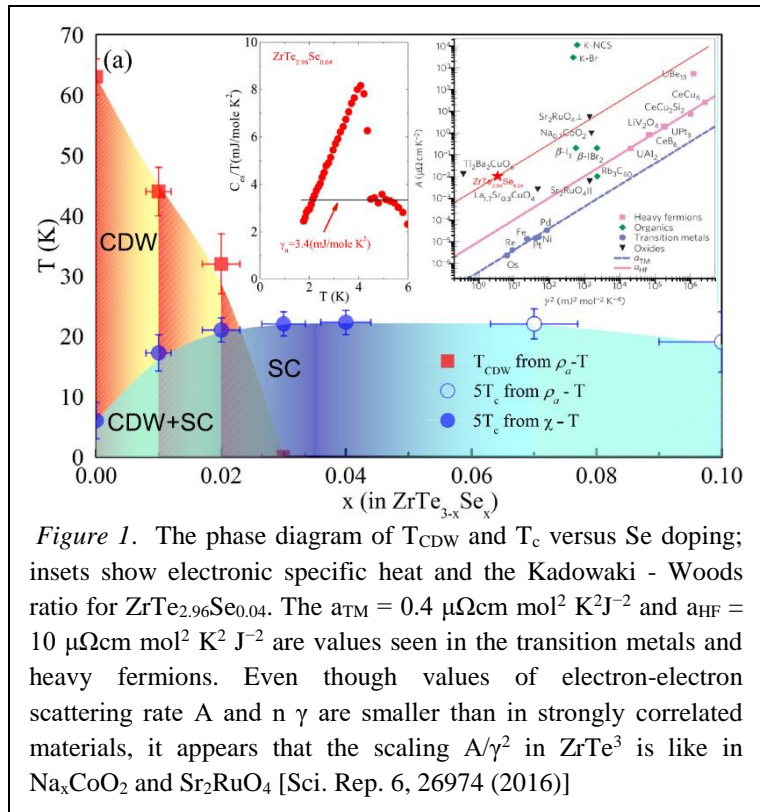
C. Petrovic (petrovic@bnl.gov), I Zaliznyak, Genda Gu and J. M. Tranquada

Condensed Matter Physics & Materials Science Department, Brookhaven National Laboratory, Upton, NY 11973-5000

Program Scope

Quantum fluctuations (QF) and topology have emerged as fundamental sources of new materials properties. QF near quantum critical point QCPs are not only believed to generate interactions responsible for pairing in high- T_c superconductors, but are also important in magnetocalorics, thermoelectrics, and topological Dirac materials. More generally, the interaction of itinerant charge carriers with the system of atomic magnetic moments in the proximity of a QCP is conducive to the emergence of novel phases, topological states and fractionalized excitations. The objective of this work is to create and evaluate new materials where the effects of either strong electronic correlations or topology, or both, in combination with enhanced QF result in properties and behaviors that are of interest for energy science.

The anchor of this program is the exploratory materials synthesis and characterization effort focused on design and discovery of Kondo lattices and strongly correlated topological (Dirac, Weyl) materials in single crystal form and their thermal, transport, magnetic and thermodynamic characterization. This is supplemented by studies of microscopic structure and dynamics using neutron scattering techniques. This approach is expected to contribute to better understanding of correlated quantum materials. We expect it to lead to discoveries of new materials with superior superconducting, spintronic or thermoelectric performance.



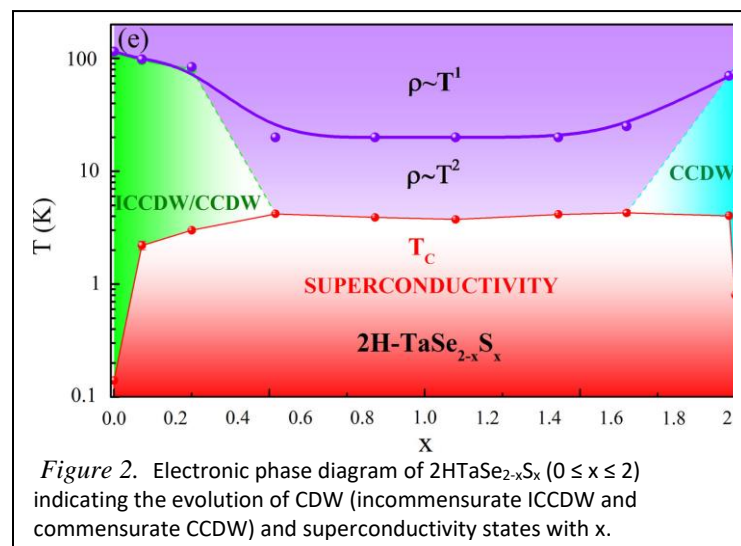
The program is organized in two focus questions.

Comparative studies of materials relevant for mechanism of high- T_c superconductivity. The first research trust aims to create new quantum materials in which interaction of Kondo moments or states in narrow bands with delocalized electrons results in ground phase diagrams with competing interactions, similar to copper-oxide materials. The properties of cuprate Mott-insulating ceramics are believed to be governed at least in part by strong fluctuations near QCP where high- T_c superconductivity arises in the presence of disorder and spin and charge fluctuations. This part of the program studies other superconductors where similar physics might also be present, but where lower energy scales and better control of disorder make it easier to explore entire phase diagrams and establish universal trends and behaviors.

Strongly correlated topological materials (TMs). The second research trust aims to manipulate states in TMs that have high mobility due to suppressed backscattering by coupling them to strongly correlated electron bands. We thus expect to be able to drive a TM towards a QCP, motivated by theoretical work that suggests an important role for QCPs due to disorder, electron-phonon, electron-electron, and spin-orbit interactions.

Recent Progress

Disorder quenching of the charge density wave in $ZrTe_3$. The charge density wave (CDW) in $ZrTe_3$ is quenched in samples with a small amount of Te isoelectronically substituted by Se (Fig. 1). Using angle-resolved photoemission spectroscopy we observed subtle changes in the electronic band dispersions and Fermi surfaces upon Se substitution [1]. The scattering rates are substantially increased, in particular for the large three-dimensional Fermi surface sheet. The quasi-one-dimensional band is unaffected by the substitution and still shows a gap at low temperature, which starts to open from room temperature. Long-range order is, however, absent



in the electronic states, as well as in the periodic lattice distortion. The emergence of superconductivity can thus be linked to the disorder-induced suppression of long-range order of the CDW.

Superconducting order from disorder in $2H-TaSe_{1-x}S_x$ crystals. In this work we report (Fig.2) on the emergence of robust superconducting order in single crystal alloys of $TaSe_{2-x}S_x$ ($0 \leq x \leq 2$) [2]. The critical temperature of the

alloy is surprisingly higher than that of the two end compounds $TaSe_2$ and TaS_2 . The evolution

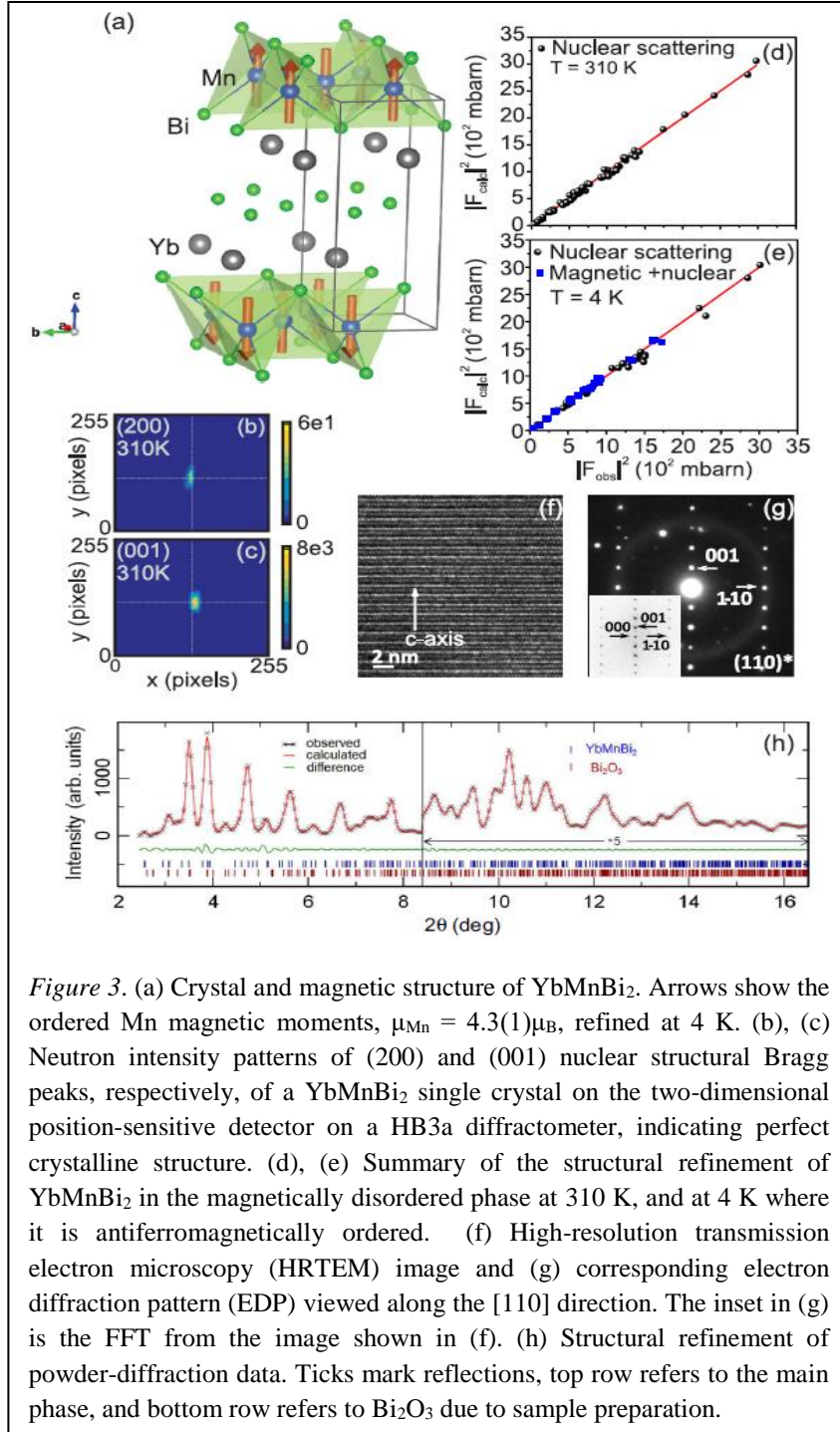


Figure 3. (a) Crystal and magnetic structure of YbMnBi_2 . Arrows show the ordered Mn magnetic moments, $\mu_{\text{Mn}} = 4.3(1)\mu_{\text{B}}$, refined at 4 K. (b), (c) Neutron intensity patterns of (200) and (001) nuclear structural Bragg peaks, respectively, of a YbMnBi_2 single crystal on the two-dimensional position-sensitive detector on a HB3a diffractometer, indicating perfect crystalline structure. (d), (e) Summary of the structural refinement of YbMnBi_2 in the magnetically disordered phase at 310 K, and at 4 K where it is antiferromagnetically ordered. (f) High-resolution transmission electron microscopy (HRTEM) image and (g) corresponding electron diffraction pattern (EDP) viewed along the [110] direction. The inset in (g) is the FFT from the image shown in (f). (h) Structural refinement of powder-diffraction data. Ticks mark reflections, top row refers to the main phase, and bottom row refers to Bi_2O_3 due to sample preparation.

of superconducting critical temperature $T_c(x)$ correlates with the full width at half maximum of the Bragg peaks and with the linear term of the high-temperature resistivity. The conductivity of the crystals near the middle of the alloy series is higher than that of either one of the end members, 2H-TaSe₂ and/or 2H-TaS₂. It is known that in these materials superconductivity is in close competition with charge density wave order. We interpret our experimental findings in a picture where disorder tilts this balance in favor of superconductivity by destroying the charge density wave.

Magnetotransport study of Dirac fermions in YbMnBi₂. In this work we reported quantum transport and Dirac fermions in YbMnBi_2 single crystals [3]. YbMnBi_2 is a layered material with anisotropic conductivity and magnetic order below 290 K. Magnetotransport properties, nonzero Berry phase, and small cyclotron mass

indicate the presence of Dirac fermions. Angular-dependent magnetoresistance indicates a possible quasi-two-dimensional Fermi surface, whereas the deviation from the nontrivial Berry phase expected for Dirac states suggests the contribution of parabolic bands at the Fermi level or spin-orbit coupling. The magnetic space group describing the collinear antiferromagnetic (AFM) order of Mn spins at 4 K (Fig. 3) has been refined in $P4/n'm'm$ ($3/4, 1/4, 0|0,0,mz$)($1/4,3/40,00,-mz$), ruling out weak antiferromagnetism stipulated in earlier ARPES work.

Future Plans

We will continue our work in the area of strongly correlated TMs in crystal structures with magnetic *4f* or *3d* atoms. Examples include:

Ca_{1-x}Sr_xMnSb₂ single crystal alloys. AMnBi₂ (A = Rare or alkaline earth) show quasi-2D quantum transport of Dirac fermions whereas the characteristics of Dirac cone is governed by spin-orbit coupling (SOC) and local arrangement of A atoms that surround the Bi square net. AMnSb₂ is far less explored; yet reduced SOC gap on 2D Sb square net and ferromagnetic state reported in off-stoichiometric Sr_{1-y}Mn_{1-z}Sb₂ offers an interesting opportunity to study the evolution of Dirac/Weyl states as Sr substitutes Ca in the lattice and as a function of alloying-induced defects by magneto- and thermal-transport, elastic and inelastic neutron scattering.

RAIGe (R=La,Ce,Pr) family. These materials feature Weyl semimetal state that breaks both time-reversal and inversion symmetry. Magnetic members of the family (R=Ce,Pr) break time reversal symmetry by Zeeman coupling, shifting Weyl nodes in *k*-space. LaAlGe features type-II Weyl nodes, however their signature in magnetotransport is absent and it is of interest since it has been proposed that the nature of chiral anomaly depends on the magnetic field direction. This will be supplemented by inelastic neutron scattering measurements in order to map the magnetic excitation spectrum.

Fe₃Sn₂. Ferromagnetic Fe₃Sn₂ with a geometrically frustrated kagome bilayer of Fe attracts considerable interest due to its magnetic structure, anomalous Hall effect (AHE) and Dirac electronic states. Previous studies show that Fe₃Sn₂ hosts massive Dirac fermions in the presence of metallic ferromagnetic order with a temperature-dependent noncollinear spin structure. The skyrmionic magnetic bubbles with variable topological spin textures form at room temperature and are sensitive to temperature and magnetic field. In Fe₃Sn₂ and in Fe_{3-x}T_xSn₂ (T=Mn,Cr,Co) we plan to look for the signatures of skyrmion lattice and for magnetic field-induced changes in local magnetism using thermal transport and neutron scattering methods.

References

1. Moritz Hoesch, Liam Gannon, Kenya Shimada, Benjamin J. Paret, Matthew D. Watson, Timur K. Kim, Xiangde Zhu and C. Petrovic. Disorder Quenching of the Charge Density Wave in ZrTe₃. Phys. Rev. Lett. 122, 017601 (2019).
2. Lijun Li, Xiaoyu Deng, Zhen Wang, Yu Liu, A. M. Milinda Abeykoon, E. Dooryhee, A. Tomic, Yanan Huang, J. B. Warren, E.S. Bozin, S. J. L. Billinge, Y. P. Sun, Yimei Zhu, G. Kotliar and C. Petrovic. Superconducting order from disorder in 2H-TaSe_{2-x}S_x. Nature Partner Journal Quantum Materials 2, 11 (2017).
3. Aifeng Wang, I. Zaliznyak, Weijun Ren, Lijun Wu, D. Graf, O. Garlea, J. B. Warren, Bozin, Yimei Zhu and C. Petrovic. Magnetotransport study of Dirac fermions in YbMnBi₂ antiferromagnet. Phys. Rev. B 94, 165161 (2016).

Full list of publication since the last PI meeting can be found in Publications document.

Inelastic Neutron and X-ray Scattering Investigation of Electron-Phonon Effects in Quantum Materials

Dmitry Reznik

Program Scope

Current research investigates Cu and Fe-based high temperature superconductors and related materials such as stripe-ordered nickelates and CMR manganites. Inelastic neutron scattering studies of electron-lattice effects in these materials aim to uncover different types of excitations of the atomic lattice that shed light on properties of electrons to which the atomic lattice is coupled. Phonons, dynamic charge stripes, and polaronic distortions have been discovered and investigated.

To be reported at the meeting:

1. Systematic investigation of $|\mathbf{q}|>0$ nematic fluctuations in Fe-based superconductors

Parent compounds of Fe-based superconductors undergo a structural phase transition from a tetragonal to an orthorhombic structure. Previously, we measured the temperature dependence of the frequencies of transverse acoustic (TA) phonons that extrapolate to the shear vibrational mode associated with this transition. It is typically detected by resonant ultrasound (RUS), which corresponds to the orthorhombic deformation of the structure at low temperatures in BaFe_2As_2 (Ba122) and SrFe_2As_2 . We found that acoustic phonons at small wavevectors soften gradually towards the transition from high temperatures, tracking the increase of the size of slowly fluctuating magnetic domains. On cooling below the transition the phonons harden following the square of the magnetic moment (which we find is proportional to the anisotropy gap).¹

Next we performed the same measurement in superconducting materials: Co-doped Ba122 and FeSe with the emphasis on nematic fluctuations. Nematic order is ubiquitous in liquid crystals and is characterized by a preferred direction in an otherwise uniform liquid. A similar symmetry breaking has been observed in some electronic phases in quantum materials related to high temperature superconductors.² We found that fluctuations at small momenta, which correspond to wavelengths of as much as 25 unit cells, do not compete with superconductivity. Instead they continue to grow below superconducting T_c .³ Our results imply the existence of a length scale larger than 25 unit cells that is important for understanding the interplay between nematicity and superconductivity.

2. Software to automate investigations of phonons in materials with large unit cells at the SNS: Phonon Explorer. We developed software for extracting phonon spectra from TOF

datasets obtained on materials with large unit cells (available at <https://github.com/dmitryr1234/phonon-Explorer>). A prototype version of the software has been written in the previous cycle and was successfully used on SrFe₂As₂.⁴ The current version of the software works well with data obtained on small samples, which have challenges of poor statistics and large background. We measured the phonon spectrum a copper oxide superconductor, HgBa₂CuO₄, and a prototypical stripe-ordered compound, La_{1.67}Sr_{0.33}NiO₄ on ARCS and used these datasets to successfully test the new code.

2. Search for signatures of incipient CDW in the phonon spectrum in HgBa₂CuO₄

We applied Phonon Explorer software to ARCS datasets taken on a small sample of HgBa₂CuO₄ cuprate 4 years ago. Previous attempts to extract useful information out of this dataset were unsuccessful because of large background and poor statistics. The new software allowed us to extract one-phonon spectra from the data for the majority of the most interesting optic phonon branches of oxygen character. We found that in strongly underdoped HgBa₂CuO₄ the bond-stretching phonon anomaly is significantly smaller than at optimal doping or in other cuprates such as La₂CuO₄. The dispersions of other phonons are qualitatively in line with DFT calculations.

3. Bond-Stretching phonon anomaly associated with dynamic charge stripes in La_{1.7}Sr_{0.3}NiO₄

Charge order manifesting as stripes in the nickelates La_{1.7}Sr_{0.3}NiO₄ has been at the center of research on correlated electrons. Owing to the similar structures of La₂CuO₄ and La₂NiO₄, they are of interest for comparing lattice dynamics that possibly couple to electronic order with the cuprates. As the Ni-O bond-stretching mode naturally has a polar effect, it should couple to charge dynamics. We completed comprehensive measurements of the bond-stretching branch at 6 temperatures between 10K and 600K. With the help of the Phonon explorer software we found previously unexplored Brillouin zones where the bond-stretching phonons are exceptionally strong. We found that the bond-stretching phonon dispersions have a large dip and broadening on approach to the zone boundary along both 100 and 110 directions. The strongest effect occurs at the charge-ordering temperature of 240K. It weakens as the temperature is raised.

Future Plans

We plan to continue investigating electron-phonon effects in select materials with orbital degrees of freedom: Fe-based superconductors, manganite perovskites and 4d/5d transition metal oxides. Scientific questions to be addressed are as follows:

What is the interplay between nematicity, orbital order, and superconductivity in both FeAs and FeSe-based superconductors with the emphasis on the latter? This work will address arguably the most important question in the field of Fe-based superconductors. On the theory side, we will perform DFT and molecular dynamics simulations.

How does short-range orbital order affect the lattice dynamical spectrum in quasicubic ferromagnetic manganites such as La_{1-x}Sr_xMnO₃? Optic phonons showed radical effects of short-

range orbital order and we now plan to understand these effects. This work will lead to a complete picture of the relationship between orbital ordering, lattice dynamics, and electrical transport.

What is the role of electron-phonon coupling in 4d and 5d transition metal oxides (TMOs) such as ruthenates and iridates? They received a lot of attention lately, because strong spin-orbit coupling is responsible for a rich and enigmatic phase diagram.⁵ It is generally recognized that spin-phonon coupling plays a big role, because orbital degrees of freedom entangled into magnetic moments couple them to the atomic lattice.^{6,7} We plan a comprehensive study of phonons in these compounds with the emphasis on rotational modes of the MO_6 (M-Ru, Ir) octahedra.

Methods: We will use IXS for measurements of phonons in Fe-based superconductors and iridates, INS for manganites, and both INS and IXS for ruthenates. Phonon explorer software developed by us will be used for data analysis.

Methods development: The current version of Phonon Explorer now works very well for in-house purposes. It is also fully compatible with the standards of the software group at the SNS, which requires all software to be written in Python and to work on top of Mantid, so we plan to work with the SNS staff to deploy it for users at ARCS and other similar instruments.

References

- ¹ D. Parshall et al., *Physical Review B* **91**, 134426 (2015).
- ² E. Fradkin, S. A. Kivelson, M. J. Lawler, J. P. Eisenstein, A. P. Mackenzie, *Annual Review of Condensed Matter Physics* **1**, 153-178 (2010).
- ³ F. Weber, D. Parshall, L. Pintschovius, J.-P. Castellan, M. Kauth, M. Merz, Th. Wolf, M. Schütt, J. Schmalian, R. M. Fernandes, and D. Reznik, *Phys. Rev. B* **98**, 014516 (2018)
- ⁴ D. Parshall, R. Heid, J. L. Niedziela, Th. Wolf, M. B. Stone, D. L. Abernathy, and D. Reznik, *Phys. Rev. B* **89**, 064310 (2014).
- ⁵ Jeffrey G. Rau, Eric Kin-Ho Lee, and Hae-Young Kee, *Annual Review of Condensed Matter Physics* **7**, 195 (2016).
- ⁶ J. C. Wang, J. Terzic, T. F. Qi, Feng Ye, J. Yuan, S. Aswartham, S. V. Streltsov, D. I. Khomskii, R. K. Kaul, and G. Cao, *Phys. Rev. B* **90**, 161110(R) (2014).
- ⁷ M. Ge, T. F. Qi, O. B. Korneta, D. E. De Long, P. Schlottmann, W. P. Crummett, and G. Cao, *Phys. Rev. B* **84**, 100402(R) (2011).

National School on Neutron and X-ray Scattering

Stephan Rosenkranz, Materials Science Division, Argonne National Laboratory
Bianca Haberl, Katharine Page, Neutron Sciences, Oak Ridge National Laboratory
Brian H. Toby, Uta Ruett, Advanced Photon Source, Argonne National Laboratory
Michael Manley, Materials Science and Technology Division, Oak Ridge National Laboratory

Program Scope

Since 1999, the National School on Neutron and X-ray Scattering has provided a comprehensive introduction to the underlying theory of neutron and x-ray scattering and related experimental techniques that are available at national facilities. The program includes both classroom lectures from experts in the field and hands-on experiments. The school plays an important strategic role in educating the United States scientific community in the capabilities of its national neutron and x-ray user facilities. While the two-week school was initially held at Argonne National Laboratory (ANL), starting in 2008 ANL partnered with Oak Ridge National Laboratory (ORNL), and participants now spend equal time at both sites.



Figure 1: Participants of the first 20 years of the NXSchool, 1999-2018.

Recent Progress

The 19th and 20th National School on Neutron and X-ray Scattering were held August 5-19, 2017 and July 22 – August 4, 2018, respectively. Interest from the scientific community in the school remains strong - the school has been consistently oversubscribed, by a factor of 3 or more. During the school, the participants (60 in 2017 and 2018) each performed a total of four neutron scattering experiments using ORNL's Spallation Neutron Source and High Flux Isotope Reactor beamlines. They also performed three to four x-ray experiments at ANL's Advanced Photon Source. The feedback from the students has been positive each year, and many of the students subsequently apply for postdoctoral positions at Argonne

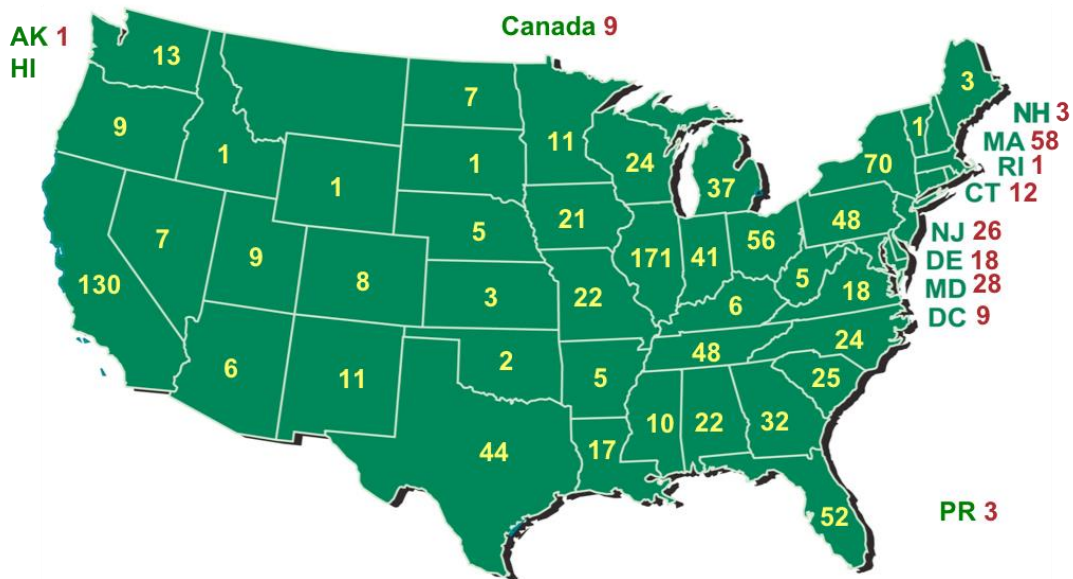
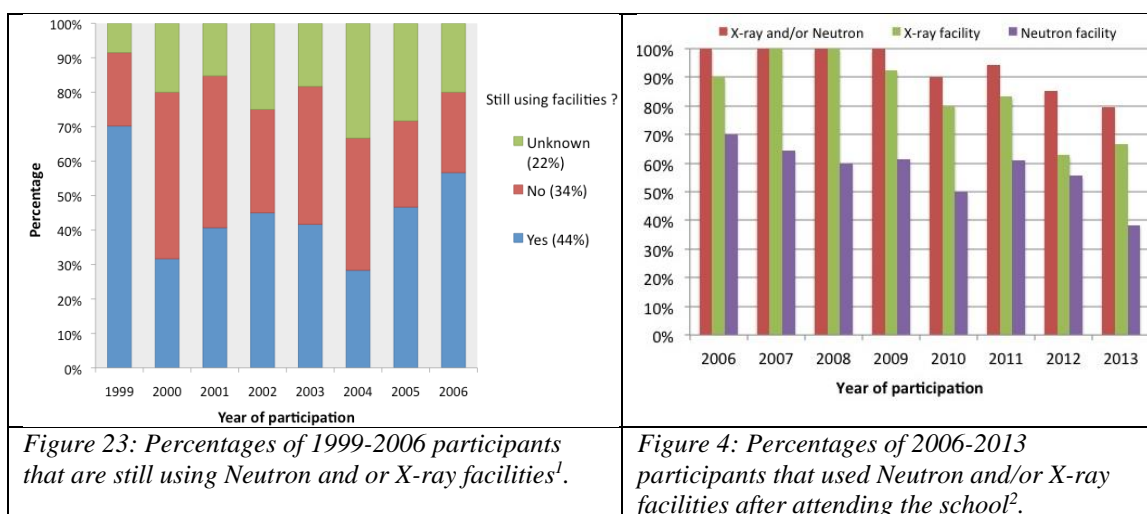


Figure 2: Geographic distribution of school participants from North America, 1999-2018.

or Oak Ridge National Laboratory as well as at other neutron and X-ray scattering facilities, or continue to use the facilities for their research.

To date, 1202 participants have attended the school. The national character of the school is reflected in the wide geographic distribution of the participants that have attended, as shown in Fig. 2. Participating students have represented 175 unique North American colleges and universities, spread over 48 different states, Washington DC, Puerto Rico, and Canada. About 18% of the participants were students at schools in EPSCoR states. The distribution of the participants over the different states or territories generally tracks the distribution of the applicants.



¹As determined by searches of the internet and facility user records between 2009-2011.

²Derived from a 2014 survey sent to participants from 2006-2013.

Most participants perform a neutron and/or X-ray experiment at a facility in the years directly following their attendance at the school (Figure 4). Additionally, many of the participants continued to utilize these sources well past their graduate studies in their post-doctoral research positions and beyond. In fact, 70% of the participants who attended the school in the first year (1999) are currently active facility users, while averaged over 1999-2006 this percentage is at least 44% (see Figure 3). To date, four of the school's alumni have been invited to return to the school as lecturers, as they have become recognized experts in the field.

Future Plans

The purpose of the school is to give the participants the opportunity to learn the fundamentals of the interaction of x-rays and neutrons with matter, as well as the methods of producing and detecting synchrotron radiation and neutrons. The school will dwell on the applications of these techniques to various scientific or technological areas, providing hands-on experience with instruments at neutron (HFIR, SNS) and x-ray (APS) facilities. The course, which will deal with all details of the interactions of x-rays and neutrons with matter, will be taught by leading experts in the field working at national facilities and universities and will represent a unique educational opportunity. The continuing participation of lecturers from outside the two organizing national laboratories is considered essential to preserving the national character of the school. The content of the lectures is also continually evolving as new facilities and techniques become available.

The school's directors will select at least 60 participants each year, consisting mainly of graduate students from North American universities. Occasionally the school is also attended by self-funded postdoctoral researchers, investigators from U.S. universities, national laboratories and industries. The primary audience for the school is graduate students from U.S. institutions near the beginning of their thesis studies. Therefore, graduate students early into their thesis research will make up at least 80% of each class. Due to capacity limitations, we restrict admission to no more than 60 students per year.

The National School on Neutron and X-ray Scattering will continue to be held for a period of two weeks, with dates chosen to minimize overlap with the academic year, other schools, and conferences, yet coinciding with the operation of the three facilities involved. The students will spend approximately one week at Argonne National Laboratory and one week at Oak Ridge National Laboratory, and if possible, the site at which the school starts is alternated each year. The 21th National School on Neutron and X-ray Scattering will be held June 16-29, 2019.

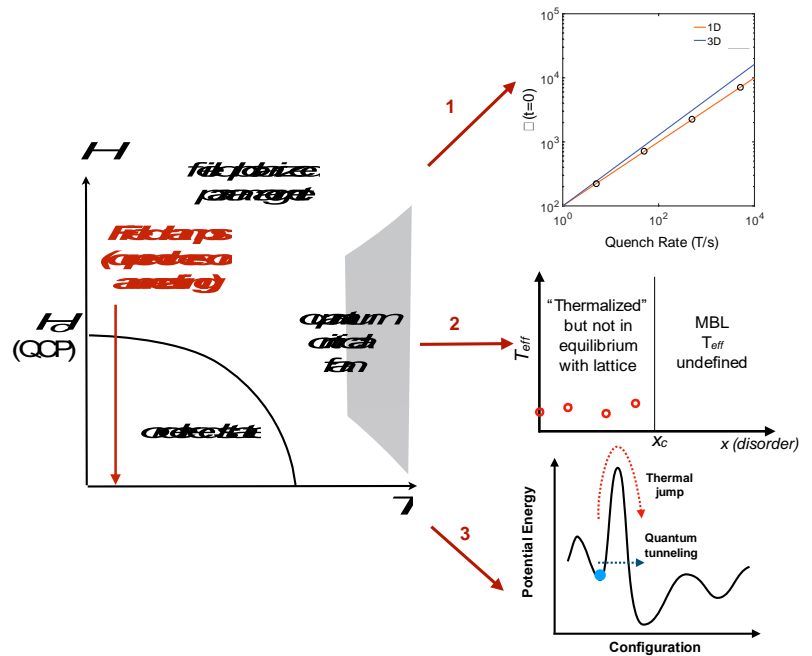
Non-Equilibrium Effects in Quantum Magnets

Kate A. Ross, (Assistant Professor in the Department of Physics at Colorado State University, Fellow of the CIFAR Quantum Materials Program)

Program Scope

The project aims to achieve non-equilibrium conditions in solid state quantum magnets, and measure the resulting properties *via* neutron scattering and ac magnetic susceptibility. The project is divided into three areas:

- 1) A measurement of *quantum* Kibble-Zurek scaling effect, which requires the measurement of correlation functions following quantum quenches (in this case, this means magnetic field ramps at low temperatures) with quench rates spanning several orders of magnitude. [1,2]
- 2) The creation and investigation of Many Body Localization [3] in a solid state material, which involves studying the thermalization (or lack thereof) after a quantum quench in a many-body system with disorder.
- 3) A study of the spin-spin correlations following a "quantum annealing" vs. "thermal annealing" protocol to optimize a glassy spin configuration [4].



General scope of the program: Neutron scattering signatures after field ramps through a quantum critical point will be used to investigate (1) Kibble-Zurek scaling, (2) Many Body Localization, and (3) quantum annealing.

For aims 1 and 2 above, we have begun to develop a pulsed magnet system for use at the Spallation Neutron Source that will enable fast (with *widely variable*) magnetic field ramp rates, but with a relatively low peak field (10 T). The idea is to use the magnet to generate the fast quenches and do elastic and inelastic neutron scattering measurements *after* the pulses (not at the peak field). This magnet must be able to operate at 3He temperatures and be compatible with neutron scattering experiments.

Recent Progress

We are in the beginning stages of designing the pulsed magnet system, which will enable variable ramp rates (“quantum quench rates”) of the magnetic field spanning several orders of magnitude. This system is different from conventional pulsed magnet setups, including the pulsed magnet already available at the SNS, in that it is not designed for measurement at the maximum field – our maximum field is only 10T, which is achievable with superconducting magnet technology. Because of this we are less constrained by magnet coil materials as well as generated heat loads.

In the lower quench rate regime (below 10T/min), we have already investigated the transverse field ramp rate dependence of the ac susceptibility in two quantum magnetic materials using the 35T resistive magnet at the National High Magnetic Field Laboratory (NHMFL). We have found a striking power law scaling of the susceptibility with quench rate, which is reminiscent of the Kibble-Zurek phenomenon, however the exponents are not as we initially expected. Both materials exhibit a glassy regime (slow relaxation), and our preliminary data raises questions about how the quantum Kibble-Zurek phenomenon applies to glassy phases.

Relating to aim 3) of the project, we have completed a preliminary neutron scattering experiment to measure the spin correlations following a quantum annealing and thermal annealing protocol in a glassy quantum magnet with a field tuned quantum critical point. The initial data are promising, however due to technical challenges during the experiment a follow up experiment is planned to rigorously compare the two protocols.

Future Plans

We plan to complete the design of the magnet system by the end of this summer and start building the system in the Fall. Once the magnet system is ready, we will use it to investigate aims 1) and 2) using neutron scattering.

We are also planning to follow up on the two preliminary experiments mentioned above to rule out systematic effects as well as resolve technical problems encountered in the first experiments.

References

[1] A Polkovnikov. Universal adiabatic dynamics in the vicinity of a quantum critical point. *Physical Review B*, 72(16), 2005

[2] WH Zurek, U Dorner, and P Zoller. Dynamics of a Quantum Phase Transition. *Physical Review Letters*, 95(10):105701, 2005.

[3] R Nandkishore, DA Huse. Many-body localization and thermalization in quantum statistical mechanics. *Annu. Rev. Condens. Matter Phys.*, (2015)

[4] J Brooke, D Bitko, G Aeppli, et al. Quantum annealing of a disordered magnet. *Science*, 284(5415):779–781, 1999.

Publications

No publications to report yet.

Fundamental Understanding of the Morphology and Dynamics of Bottlebrush Polymers

Gerald J. Schneider, Department of Chemistry and Department of Physics & Astronomy, Louisiana State University, Baton Rouge, LA 70803

Program Scope

This project explores the molecular structure and dynamics of bottlebrush polymers utilizing neutron scattering as the most advanced microscope. Bottlebrushes are very versatile macromolecules that combine polymeric and particulate features, with a broad spectrum of applications, ranging from epidermal electronics, mimicking biological tissue, to ultrasoft, ultratransparent, ultrastretchable and hyperelastic elastomers. As figure 1 illustrates, depending on their chemical composition, structure and dynamics they can be as soft as jelly fish, as transparent as eye lenses, as brittle as glass, as elastic as car tire or as light weight as plastics but even stronger than aluminum.

Bottlebrushes comprise of linear chains with bonded arms and are the microscopic analogue to the brushes used for the cleaning of baby bottles. This comparison illustrates the countless applications only depending on the number of arms and length of backbone and arms. As indicated by figure 2, bottlebrushes can be viewed as being a member of the family of comb polymers, with a very high grafting density, i.e., the number of grafted chains per backbone is high. The number of combinations between side chains and backbones is almost unlimited. The unprecedented flexibility of bottlebrushes opens the path to materials and technology with to-date unknown advantages, but the almost infinite number of combinations disables established design principles utilizing a systematic variation of

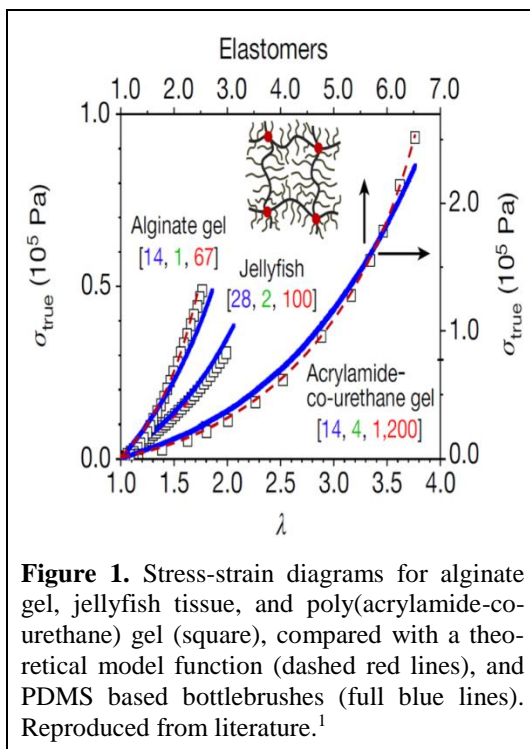


Figure 1. Stress-strain diagrams for alginate gel, jellyfish tissue, and poly(acrylamide-co-urethane) gel (square), compared with a theoretical model function (dashed red lines), and PDMS based bottlebrushes (full blue lines). Reproduced from literature.¹

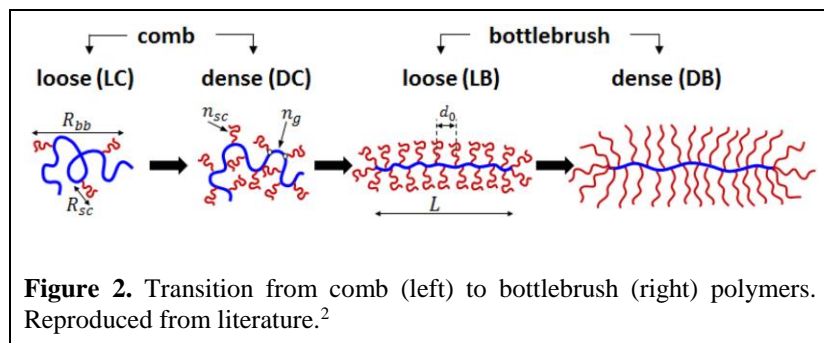


Figure 2. Transition from comb (left) to bottlebrush (right) polymers. Reproduced from literature.²

parameters. Understanding the microscopic structure and dynamics and their relationship to the materials behavior promises a much faster route. This project characterizes the molecular structure and dynamics by neutron scattering and the material behavior by electrical and mechanical testing. It explores the origin of the unprecedented flexibility at the molecular scale as

the indispensable prerequisite to derive constitutive equations that can be utilized to predict novel materials and technology with to-date unparalleled properties. Thus, the project will help to substitute the slow traditional test based material development by a novel construction kit design strategy that could boost the efficiency and discovery of objects.

Recent Progress

In a first step towards the understanding of polymer networks, we explored the conformation of polymer chains in solution and in melt. The morphology is important, because it is directly connected with the macroscopic mechanical behavior, which is often observed by stress strain experiments (figure 1). For that purpose, the polymers are synthesized in our own chemistry laboratory. Additionally, we synthesize the monomers, if these are not commercially available.

Figure 3 exemplifies those results on polydimethylsiloxane (PDMS) bottlebrushes (PDMS-g-PDMS) in solution. Changing the grafting density and the length of the backbone

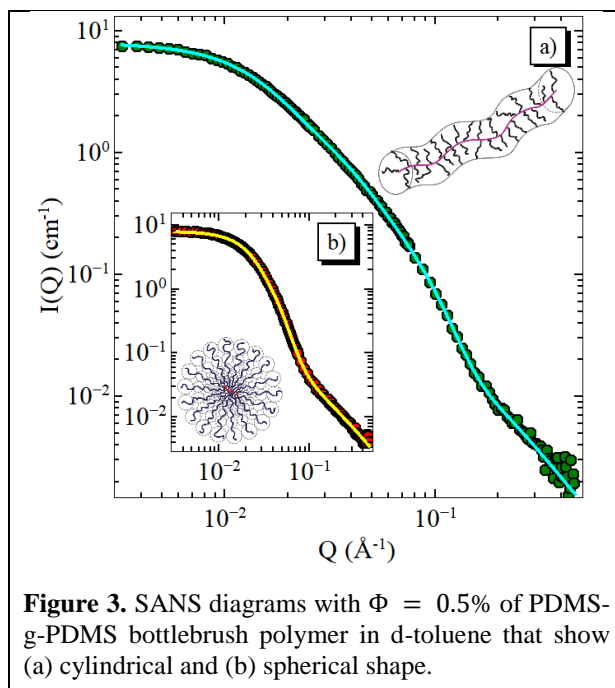


Figure 3. SANS diagrams with $\Phi = 0.5\%$ of PDMS-g-PDMS bottlebrush polymer in d-toluene that show (a) cylindrical and (b) spherical shape.

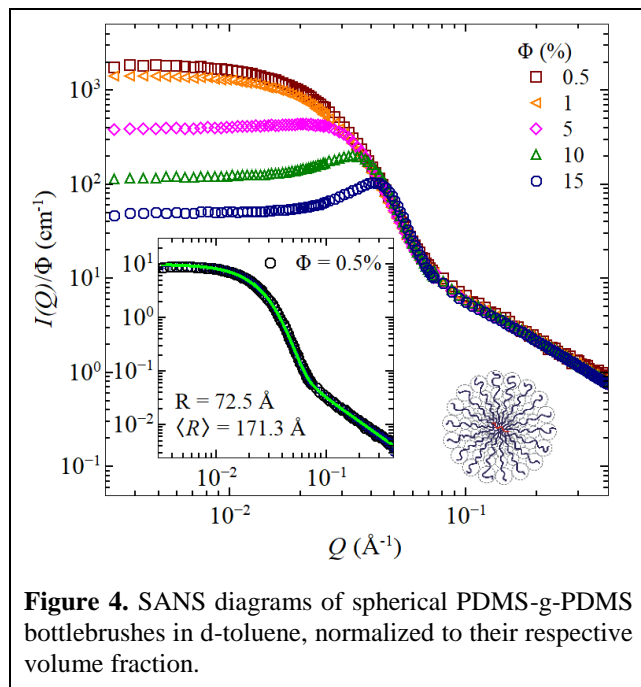
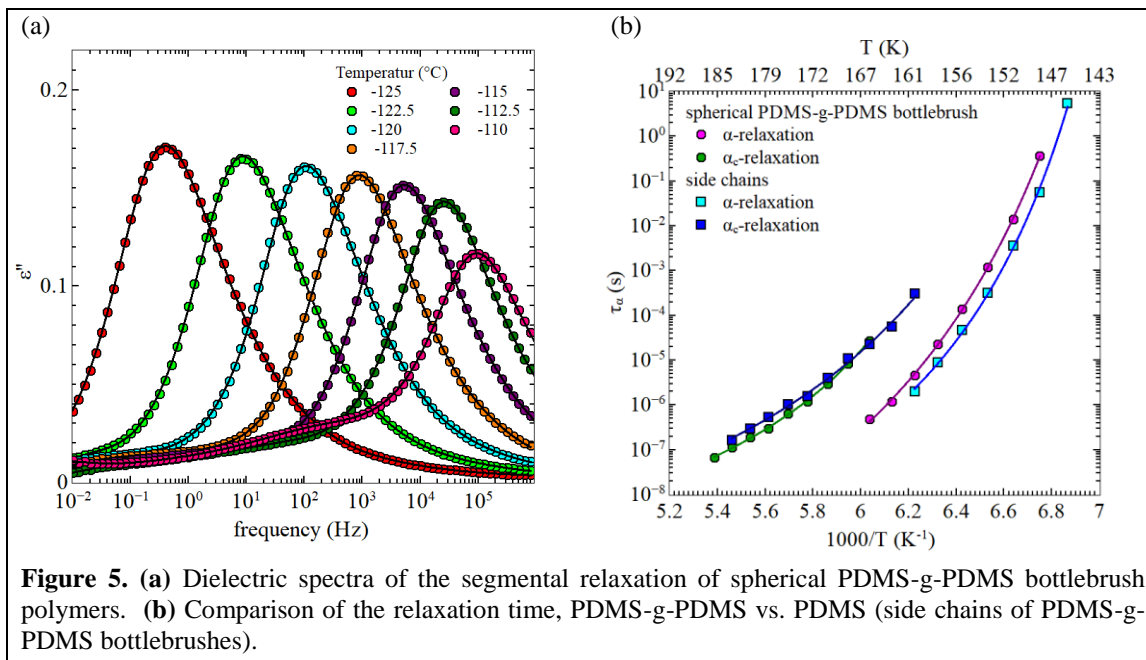


Figure 4. SANS diagrams of spherical PDMS-g-PDMS bottlebrushes in d-toluene, normalized to their respective volume fraction.

manifest themselves in a transition from a spherical to elongated structure. These morphologies are directly connected with the macroscopic material behavior. The observation in the melt is very similar.

The rheology of colloidal solutions is determined by the mutual interactions between the colloids. Therefore, in a next step, we explored the structure factor, as shown in figure 4. We see a very strong change from the low concentration, with no visible contribution by the structure factor to a forward scattering reduced by almost a factor of 100 in case of the high concentrations. This indicates very strong colloidal interactions.

In parallel to SANS, we are conducting experiments that represent the macroscopic mate-



rial behavior. Figure 5 illustrates the results of dielectric spectroscopy experiments on the bottlebrush melt. By applying an electrical periodic perturbation, we measure the complex dielectric permittivity, $\epsilon^* = \epsilon' + i\epsilon''$. The variables ϵ' , and ϵ'' describe the storage and the loss of energy, respectively. The peak position in figure 5 (a) represents the relaxation time of the segmental (or α -)relaxation. Its temperature dependence reflects a strong change of the relaxation time. Figure 5 (b) compares the segmental relaxation of the bottlebrush with the side chains in the melt. In this example there are much more side chain molecules than backbone monomers. Thus, it illustrates that the segmental relaxation time is not strongly changing from free to grafted chains. (Certain differences are existing, but the discussion is omitted here.) It is obvious that dielectric spectroscopy is capturing a change of relaxation time over almost 10 orders of magnitude. However, one objective of the project is to understand the fundamental principles behind, which includes a more detailed picture on the relaxation mechanism. Our scientific approach is outlined in our future plans.

Future Plans

In order to understand the α -relaxation more in detail, we are conducting quasi-elastic neutron spectroscopy (QENS) experiments at the moment (June 2019). These experiments will be continued by another QENS in September 2019. The combination of three spectrometers will capture a broad range of time-scales. In earlier work we demonstrated that selective deuteration and the time-dependence can be utilized to understand the dynamics more in detail.^{3,4} It permits to connect the monomer relaxation with the dielectric permittivity or the modulus from rheology. Therefore, we will also conduct rheology experiments.

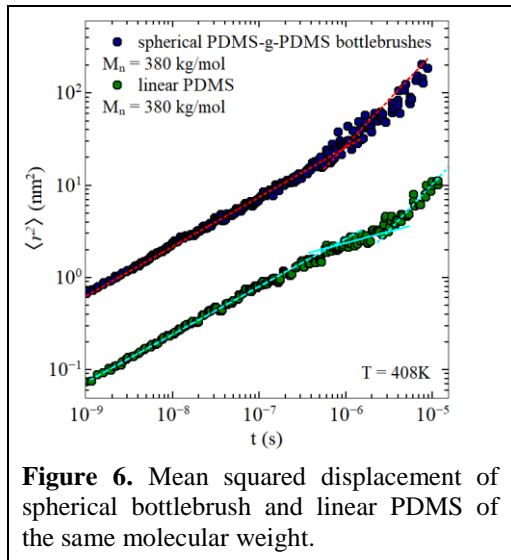


Figure 6. Mean squared displacement of spherical bottlebrush and linear PDMS of the same molecular weight.

While the linear polymer shows a typical behavior of an entangled polymer, the bottlebrush shows a simple Rouse behavior, i.e., the absence of entanglements.

The resolution of FFC is low, therefore it does not tell about the microscopic mechanism. Therefore, our ultimate experiment is neutron spin echo spectroscopy (NSE). The advantage of FFC is the projection of the results, by using $\langle r^2(t) \rangle$ and calculating the dynamic

structure factor, $S(Q, t)$, assuming Gaussian approximation. Once having the NSE experiments, we will be able to calculate FFC from NSE, which then represents the accurate picture.

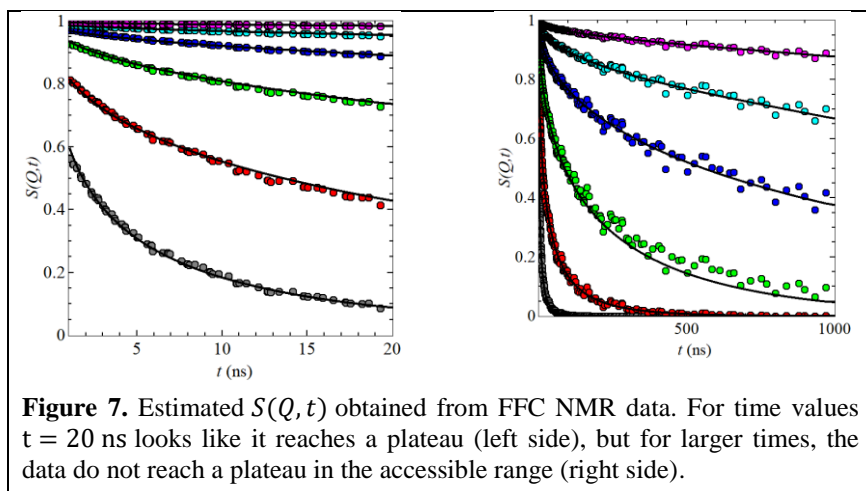


Figure 7. Estimated $S(Q, t)$ obtained from FFC NMR data. For time values $t = 20\text{ ns}$ looks like it reaches a plateau (left side), but for larger times, the data do not reach a plateau in the accessible range (right side).

References

1. M. Vatankhah-Varnosfaderani, W. F. Daniel, M. H. Everhart, A. A. Pandya, H. Liang, K. Matyjaszewski, A. V. Dobrynin and S. S. Sheiko, *Nature* **549** (7673), 497 (2017).
2. W. F. M. Daniel, J. Burdyńska, M. Vatankhah-Varnoosfaderani, K. Matyjaszewski, J. Paturej, M. Rubinstein, A. V. Dobrynin and S. S. Sheiko, *Nature Materials* **15**, 183 (2015).
3. C. Gerstl, G. J. Schneider, A. Fuxman, M. Zamponi, B. Frick, T. Seydel, M. Koza, A. C. Genix, J. Allgaier, D. Richter, J. Colmenero and A. Arbe, *Macromolecules* **45** (10), 4394-4405 (2012).
4. C. Gerstl, G. J. Schneider, W. Pyckhout-Hintzen, J. Allgaier, D. Richter, A. Alegría and J. Colmenero, *Macromolecules* **43** (11), 4968-4977 (2010).

Intertwined density waves and superconductivity in cuprate high temperature superconductors

Jiajia Wen¹, Young Lee^{1,2}

¹Stanford Institute for Materials and Energy Sciences, SLAC National Lab

²Department of Applied Physics, Stanford University

The discovery of charge- and spin-density-wave (CDW/SDW) orders in superconducting cuprates has altered our perspective on the nature of high-temperature superconductivity (SC). However, it has proven difficult to fully elucidate the relationship between the density wave orders and SC. Using resonant soft x-ray scattering we study the CDW in archetypal cuprate $\text{La}_{2-x}\text{Sr}_x\text{CuO}_4$ (LSCO) over a broad doping range. We discover two types of CDW, whose distinct behaviors below the superconducting transition temperature is strongly correlated with the strength of the SDW order. Such an intertwined relationship among density wave orders and SC is further revealed in oxygen-doped $\text{La}_2\text{CuO}_{4+y}$. Our results support an inhomogeneous low temperature electronic state in cuprate superconductors driven by competing ground states on the CuO_2 planes.

Polymer Conformations and Chain Dynamics under 1D and 2D Rigid Confinement

Karen I. Winey¹ and Robert A. Riggleman²

¹Department of Materials Science and Engineering and ²Department of Chemical and Biomolecular Engineering, University of Pennsylvania, Philadelphia, PA

Program Scope

Use molecular dynamics simulations and small angle neutron scattering methods to explore polymer conformations, segmental dynamics and chain-scale diffusion in rigid nanoscale confinement. Explore cylindrical, planar and diamond symmetries.

Recent Progress

Polymer diffusion is fastest at intermediate levels of cylindrical confinement.¹ The behavior of polymer melts under cylindrical confinement was investigated using molecular dynamics simulations, **Figure 1**. A range of polymer chains, from unentangled to highly entangled, were confined in cylindrical pores with radii ranging from much smaller to much larger than the polymer size. These simulations were used to measure polymer chain conformation, entanglement density, and center-of-mass diffusion. The conformational anisotropy is well-described by a confined random walk model, although excluded volume effects cause slight differences in the radius of gyration. The number of entanglements per chain in confinement is accurately described using a simple volume fraction model consisting of a zero-entanglement region near the pore wall and a bulklike entanglement region in the pore center. The size of the depletion region near the wall is chain length dependent. Finally, the diffusion along the pore axis exhibits nonmonotonic behavior with the pore radius. As the pore radius decreases, the diffusion coefficient, D , initially increases due to increasing chain disentanglement, though for small pores D eventually decreases as a result of confinement-induced chain segregation.

Polymer conformations and dynamics under confinement with two length scales² Although many studies have analyzed the behavior of polymers under 1-D thin film and 2-D cylindrical confinement, the knowledge about how confinement geometries with more than one length scale, such as random porous networks, impact polymers is yet to be fully explored, **Figure 2**. We simulate both entangled and unentangled polymer melts confined in a diamond network geometry with two characteristic length scales, where polymers are likely to inhabit multiple interconnected and neighboring channels. In all the confined systems with entangled polymer chains, the polymer radius of gyration and the number of polymer entanglements per chain are reduced compared to the bulk. We analyze the chain relaxation based on Rouse modes and show separate, competing effects between the local friction near the wall and chain disentanglement. The disentanglement of confined polymers increases diffusivity of entangled polymers along confined channels compared to the bulk after the confined diffusivities are corrected for the tortuosity of the confinement. We anticipate that the corrections due to

tortuosity could be important for properly characterizing the dynamics in complex geometries, including highly loaded nanocomposites.

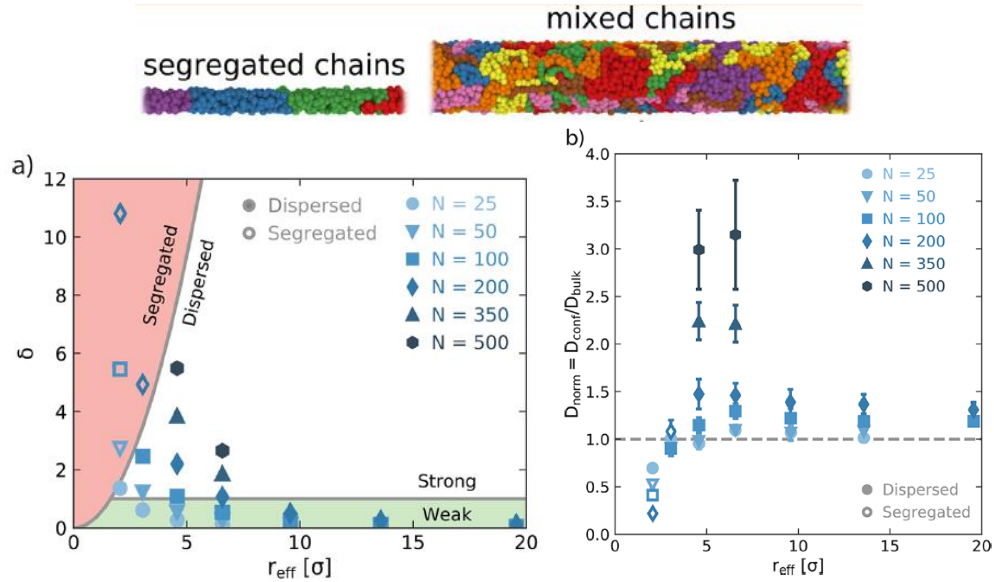


Figure 1: (top) Visualizations of polymer chains in confinement for a dispersed and a segregated chain system. (a) The confinement parameter, $\delta = Na^2/\pi r_{\text{eff}}^2$, as a function of the effective pore radius, r_{eff} . The colored domains indicate different confinement regimes. The systems examined span both the weak to strong confinement transition and the transition from dispersed chains (filled markers) to segregated chains (open markers). (b) Normalized diffusion coefficients plotted as a function of effective pore size. Filled and open markers indicate dispersed and segregated systems, respectively.

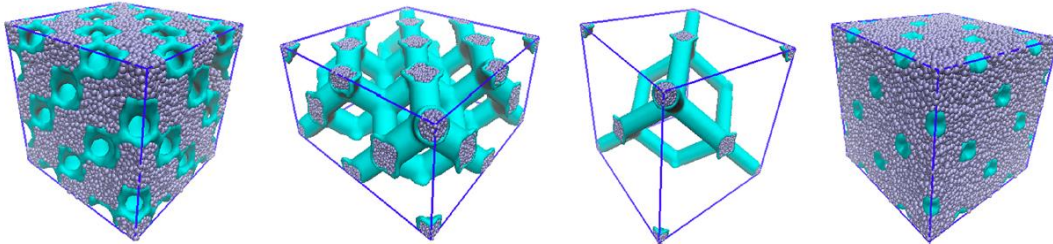


Figure 2: Diamond network confinement with two characteristic length scales of channel length and channel radius. The first three scaffolds of the confinement with channel length of $L = 10\sigma$, 20σ , and 40σ and radius of $R = 5\sigma$, respectively, are filled with polymer melt, and the last figure is the confinement with channel length of $L = 10\sigma$ and radius of $R = 7\sigma$, which has very little confining surfaces.

Increased Polymer Diffusivity in Thin Film Confinement³ The behavior of polymer melts under planar confinement was investigated using molecular dynamics simulations. A range of polymer chains, from unentangled to highly entangled ($N = 25$ – 400), were confined between two discrete-bead parallel walls to create thin films with thicknesses ranging from much larger to much smaller than the polymer size ($h = 3.5$ – 40σ), **Figure 3**. These simulations were used to measure polymer chain conformations, entanglement densities, and center-of-mass diffusion, and the results were compared with previous simulations of polymer melts under cylindrical confinement. Changes to the entanglement density and chain conformation in thin films follow

the same behavior as in cylindrical confinement, decreased entanglements per chain, decreased confined R_g , and increased unconfined R_g , though the deviations from bulk-like conformations are smaller. Despite similarities in conformation and entanglement behavior between thin film and cylindrical confinement, the diffusion behavior differs. Under planar confinement, the diffusion coefficient increases monotonically up to six times the bulk diffusivity with decreasing film thickness, while it behaves non-monotonically in cylinders. This is due to the increased degrees of freedom afforded to the polymer chains in a thin film compared to a cylinder, allowing chains to diffuse around one another rather than through as found in cylindrical confinement. Normalized diffusion coefficients, D_{norm} , can be well-described by a master curve with an exponential dependence on confinement after scaling D_{norm} by a thickness dependent term.

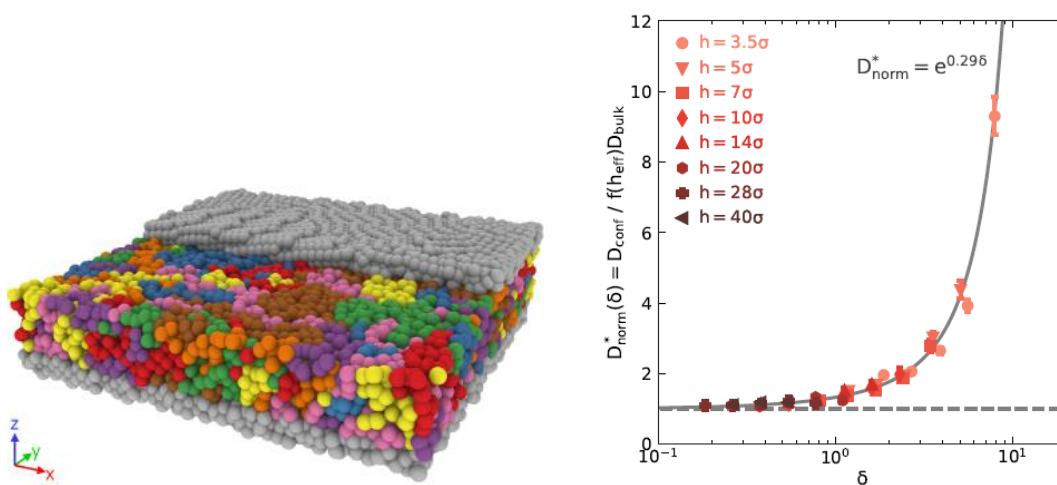


Figure 3: (left) A representative image showing a confined polymer simulation system ($h = 7\sigma$, $N = 200$, $L = 43.77\sigma$). The confining wall (gray beads) is partially cut away to expose the polymer. Different colors represent different polymer chains. (right) Normalized diffusion coefficients plotted as a function of $\delta = 2 R_{g,\text{bulk}}/h_{\text{eff}}$, the confinement parameters, showing that the diffusion coefficients can be shifted to a single curve described by an exponential function.

Determining the critical dimensions (profile features) of inhomogeneous nanostructures using dynamical theory and small angle neutron scattering⁴ The rapid development of the nanofabrication techniques for micro- and nanoscale gratings facilitate the progression of the semiconductor and flexible electronics industries, **Figure 4**. The complexity of the grating adds to the difficulty of precision in measuring the line shapes of the grating. To capture the irregular profiles a series of approaches have been explored. In this study, combined dynamical theory and covariance matrix adaptation evolution strategy (CMA-ES) allows good fit to the experimental data achieved from the small-angle neutron scattering (SANS) by automatically adjusting the structure profile of the sample. This method reproduces transmission data and retrieves the features of an alumina covered silicon grating with irregular shape (i.e. non-rectangular) profile. The codes underlying the fitting procedure will be posted on Github upon submission of this manuscript for publication.

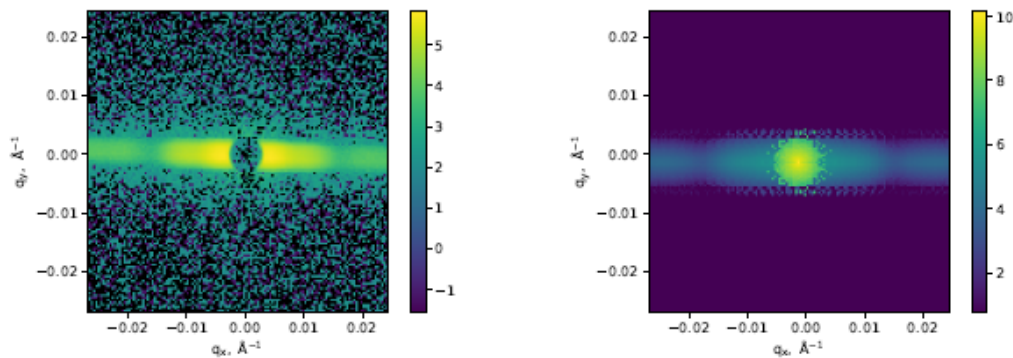


Figure 4: The 2D scattering patterns from the templates measured in SANS experiment on the left and those calculated in the DT model on the right. q_x corresponds to the direction perpendicular to the surface (confined) and q_y is the direction parallel to the surface (unconfined).

Future Plans

In the remaining few weeks of the project the last publication will be submitted and we expect to respond to review comments on the submitted manuscript. In addition, James Pressly will defend his dissertation.

References

1. “Polymer diffusion is fastest at intermediate levels of cylindrical confinement.” J. F. Pressly, R. A. Riggleman*, K. I. Winey*, *Macromolecules*, 51, 9789-9797, 2018.
2. “Polymer conformations and dynamics under confinement with two length scales.” T. Zhang, K. I. Winey*, R. A. Riggleman*, *Macromolecules*, 52, 217-226, 2019.
3. “Increased Polymer Diffusivity in Thin Film Confinement” J. F. Pressly, R. A. Riggleman*, K. I. Winey*, submitted to *Macromolecules*.
4. “Determining the critical dimensions (profile features) of inhomogeneous nanostructures using dynamical theory and small angle neutron scattering” T. Zhang, J. F. Pressly, R. A. Riggleman, R. Ashkar*, K. I. Winey*, to be submitted.

Publications

1. “Polymer diffusion is fastest at intermediate levels of cylindrical confinement.” J. F. Pressly, R. A. Riggleman*, K. I. Winey*, *Macromolecules*, 51, 9789-9797, 2018.
2. “Polymer conformations and dynamics under confinement with two length scales.” T. Zhang, K. I. Winey*, R. A. Riggleman*, *Macromolecules*, 52, 217-226, 2019.
3. “Segmental diffusion in attractive polymer nanocomposites: A quasi-elastic neutron scattering study.” E. J. Bailey, P. J. Griffin, M. Tyagi, K. I. Winey*, *Macromolecules*, **52**, 669-678, 2019.
4. “Increased Polymer Diffusivity in Thin Film Confinement” J. F. Pressly, R. A. Riggleman*, K. I. Winey*, submitted to *Macromolecules*.
5. “Determining the critical dimensions (profile features) of inhomogeneous nanostructures using dynamical theory and small angle neutron scattering” T. Zhang, J. F. Pressly, R. A. Riggleman, R. Ashkar*, K. I. Winey*, to be submitted.

Author Index

Allred, Jared M.....	157
Armitage, N. P.	7
Azoulay, Jason	68
Bates, F. S.	90
Bharti, B.	40
Bockstaller, Michael R.....	3
Broholm, C.....	7
Cao, Huibo	160
Cava, R. J.	7
Chandran, K. S. Ravi	167
Cheong, S.-W.	18
Chmaissem, O.	120, 194
Choi, Joshua J.	83
Christianson, A. D.....	25
Chubukov, Andrey	61
Dai, Pengcheng	30
DeCaluwe, Steven C.	172
Delaire, Olivier.....	35
Devereaux, Thomas P.	184
DiTusa, J. F.	40
Dorman, J. A.	40
Drichko, N.....	7
Eskildsen, Morten R.....	51
Fernandes, Rafael.....	61, 176, 179, 188
Fishman, R. S.	77
Fullerton, Eric	130
Fultz, Brent.....	56
Greven, Martin	61, 176, 179, 188
Gu, Genda	135, 210
Gu, Xiaodan	68
Haberl, Bianca.....	217
Helgeson, Matthew E.	73
Hermann, Raphaël P.....	77, 182
Huang, Biao	184
Jalan, Bharat.....	61, 176, 179
Jiang, Hongchen	86
Jiang, Hong-Chen.....	184
Jiang, Yi-Fan	184
Jin, R.	40
John, V. T.....	40
Karim, Alamgir	3
Ke, Xianglin	185
Khonsari, M.	40
Kiryukhin, V.	18
Koohpayeh, S. M.	7
Krogstad, M. J.....	194
Kumar, R.	40
Lee, Seung-Hun.....	83
Lee, Young.....	86, 227
Leighton, Chris.....	61, 176, 179, 188
Li, Yi	7
Lindsay, L. R.....	77
Lodge, T. P.....	90
Louca, Despina.....	96
Lu, Yuan-Ming.....	184
Mandrus, D.....	25
Manley, Michael E.	77, 192, 217
Mao, Z. Q.	40
Matyjaszewski, Krzysztof.....	3
May, A. F.	25
McQueen, T. M.	7
Moulé, Adam J.....	106
Mourigal, Martin.....	101
Nakatsuji, S.	7
Nesterov, E.....	40
Nikolic, P.	7
Olsen, Bradley D.....	111
Osborn, R.	120, 194
Page, Katharine	199, 217
Parker, D. S.	25
Perahia, Dvora.....	206
Petrovic, Cedomir	135, 210
Phelan, D.....	120, 194
Plummer, E. W.....	40
Reznik, Dmitry.....	214
Rick, S. W.	40
Riggleman, Robert A.	228
Rodriguez, Efrain E.....	117
Rosenkranz, Stephan.....	120, 194, 217
Ross, Kate A.	220
Ruett, Uta	217
Schneider, Gerald J.	40, 223
Shelton, W. A.....	40
Singh, Deepak Kumar	126
Sinha, Sunil K.	130
Sirenko, A.	18
Sun, J. W.	40
Tchernyshyov, O.	7
te Velthuis, S. G. E.....	120, 194
Toby, Brian H.	217
Tranquada, John M.....	135, 210
Vekhter, I.....	40

Wang, Chang-Yan.....	184
Wen, Jiajia.....	86, 227
Wilson, Stephen D.	147
Winey, Karen I.	228
Xei, W.	40
Young, D. P.....	40
Zaliznyak, Igor A.	135, 210
Zhang, D.....	40
Zhang, J.	40
Zhang, Yang.....	151

Participant List

Name	Organization
Allred, Jared	University of Alabama
Bates, Frank	University of Minnesota
Birol, Turan	University of Minnesota
Bockstaller, Michael	Carnegie Mellon University
Broholm, Collin	Johns Hopkins University
Cao, Huibo	Oak Ridge National Laboratory
Chandran, Ravi	University of Utah
Cheong, Sang-Wook	Rutgers University
Chmaissem, Omar	Northern Illinois University/Argonne National Laboratory
Choi, Joshua	University of Virginia
Christianson, Andrew	Oak Ridge National Laboratory
Dai, Pengcheng	Rice University
DeCaluwe, Steven	Colorado School of Mines
Delaire, Olivier	Duke University
DiTusa, John	Louisiana State University
Eskildsen, Morten	University of Notre Dame
Fernandes, Rafael	University of Minnesota
Fullerton, Eric	University of California, San Diego
Fultz, Brent	California Institute of Technology
Gu, Xiaodan	University of Southern Mississippi
Gu, Genda	Brookhaven National Laboratory
Helgeson, Matthew	University of California, Santa Barbara
Hermann, Raphael	Oak Ridge National Laboratory
Herwig, Kenneth	Oak Ridge National Laboratory
Jalan, Bharat	University of Minnesota
Jiang, Hong-Chen	SLAC National Accelerator Laboratory
Karim, Alamgir	University of Houston
Ke, Xianglin	Michigan State University
Kiryukhin, Valery	Rutgers University
Lee, Honyung	Oak Ridge National Laboratory
Lee, Seung-Hun	University of Virginia
Lee, Young	Stanford University/SLAC National Accelerator Laboratory
Leighton, Chris	University of Minnesota
Lodge, Timothy	University of Minnesota
Louca, Despina	University of Virginia
Manley, Michael	Oak Ridge National Laboratory
May, Andrew	Oak Ridge National Laboratory

Moule, Adam	University of California, Davis
Mourigal, Martin	Georgia Institute of Technology
Olsen, Bradley	Massachusetts Institute of Technology
Osborn, Raymond	Argonne National Laboratory
Page, Katharine	Oak Ridge National Laboratory
Perahia, Dvora	Clemson University
Petrovic, Cedomir	Brookhaven National Laboratory
Phelan, Daniel	Argonne National Laboratory
Reznik, Dmitry	University of Colorado, Boulder
Riggelman, Robert	University of Pennsylvania
Rodriguez, Efrain	University of Maryland
Rosenkranz, Stephan	Argonne National Laboratory
Ross, Kate	Colorado State University
Schneider, Gerald	Louisiana State University
Singh, Deepak	University of Missouri, Columbia
Sinha, Sunil	University of California, San Diego
Sirenko, Andrei	New Jersey Institute of Technology
Te Velthuis, Suzanne	Argonne National Laboratory
Thiyagarajan, Pappannan	US Department of Energy
Tranquada, John	Brookhaven National Laboratory
Wen, Jiajia	Stanford University
Wilson, Stephen	University of California, Santa Barbara
Winey, Karen	University of Pennsylvania
Zaliznyak, Igor	Brookhaven National Laboratory
Zhang, Yang	University of Illinois, Urbana-Champaign